Linear and nonlinear instability of shear driven liquid films

Paul Caporn

Ph. D. Thesis
1998

Department of Mathematics
University College London

Supervisor: Dr S.N. Timoshin. Dr R.I. Bowles

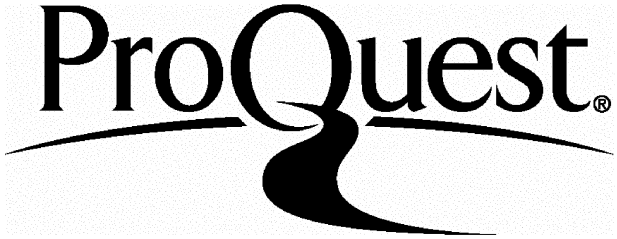

X2827185574

Acknowledgements

First and foremost I would like to express the deepest gratitude to the best Supervisors I could have wished for, Drs Sergei Timoshin and Robert Bowles. Without your time, patience and good humour none of this would have been possible. I would also like to thank Prof. Frank Smith for giving me the opportunity to do a Ph. D, Prof. Susan Brown and Dr Tom Allen for their interest in my work.

To all the mathematical support team, thank you, especially to Paul, Simon and Richard for keeping the computers at bay, and the basics backup boys in the postgrad room (you know who you are). To all the many friends who have been such good company over the last few years: Look what I've been up to!

Finally, Mum and Dad, THANK YOU. If it hadn't been for your constant support through everything I wouldn't be what I am today. I owe you everything.

Mathematickeskie osnovy zdorovy

Abstract

The governing equations for a high Reynolds number flow in a boundary layer over a film coated wall are derived from the full two dimensional Navier Stokes equations of motion for a two fluid flow. Numerical studies of the properties of the base flow and its stability are described for the case of the flow over an isolated surface roughness on an otherwise flat surface. Investigations of both short and long obstacles are undertaken in terms of the flow in a viscous-inviscid interaction region.

An investigation of strongly non-linear vortex wave interaction in a laminar boundary layer with two pairs of oblique waves is carried out. For a particular choice of flow parameters a resonance is found linking the two pairs of waves, and the governing amplitude equation for the leading order disturbance is derived and investigated.

Wave-amplitude equations are derived for the non-linear modulation of Tollmien-Schlichting (TS) type disturbances at high Reynolds numbers. An investigation of the instability of Reynolds-stress generated mean flow to short wavelength secondary disturbances is carried out. A regime with linear TS/capillary wave resonance is examined and the governing amplitude equation for non-linear wave interaction is derived. Two intermediary regimes are also studied.

The linear instability of high Reynolds number boundary layer flow over a film-coated wall is studied both numerically and analytically for the practically important limit of high film viscosity. We examine the various instabilities present and relate them to the instability classifications of Benjamin (1963) and Landahl (1962).

The work presented in Chapter 4 represents a joint investigation undertaken with Dr S.N. Timoshin and Dr R.I. Bowles and forms the basis of a paper to be published in Proceedings of the Royal Society.

Contents

Chapter 1

Introduction

The effect of thin liquid film coatings in a high Reynolds number boundary layer flow on both separation and transition to turbulence is a problem of great practical importance in many real life situations. These include the flow over rain wetted planes and cars, the de-icing of plane wings and the use of lubricants in many engineering applications. We begin this Thesis with a brief review of some of the developments in the relevant theories for homogeneous flows before examining the specific role of a film and the alterations its presence entails.

Boundary-layer separation and the transition from laminar to turbulent flow are two major phenomena typical for high Reynolds numbers. Both can be tackled using asymptotic methods. We begin with separation, starting with the classical boundary-layer theory as proposed by Prandtl in 1904. He introduced the idea of a thin viscous layer on the surface of solid bodies, driven by a prescribed pressure gradient and satisfying the condition of no slip on the solid boundary. In 1908 Blasius obtained a similarity solution for the flow over an aligned flat plate in a uniform stream, which held over its entire length, with the exception of the singularities in the solution at the leading and trailing edges and the wake behind the plate. An analysis of the 'near wake' behind the plate by Goldstein (1930) showed the wake splitting into two separate layers and his order of magnitude balances paved the way for the later triple-deck theory. The classical theory however was shown to fail

for almost all applications, by Goldstein (1948), at the point of flow reversal, and hence separation, via what became known as a Goldstein singularity in the slope of both the skin friction on the body surface and the boundary layer displacement. A new theory was required to cope with separation. This was provided by a triple-deck scheme, a viscous/inviscid interaction theory which allowed for an unspecified pressure gradient, as developed by Stewartson & Williams (1969), Neiland (1969), Messiter (1970), Stewartson (1970). The theory split the boundary layer into two so-called decks with a nonlinear viscous lower deck on the body surface driven by an external induced pressure and a rotational inviscid main deck, which remains largely passive, shifted via the displacement caused by the lower deck. A third 'potential-flow' upper deck completed the description, with the local displacement from the lower deck affecting the induced local pressure, of the order of the slope of the streamlines in the boundary layer, and hence affecting the lower deck. This 'interactive' approach avoids the failure of the classical theory due to the unspecified pressure gradient, and hence unknown displacement. The theory also does not depend on a particular set of wall boundary conditions, which makes it applicable to a wide range of different problems e.g. flows over bluff bodies, plates with a local wall roughness or flows with walls containing fluid injections. For weak distortions, flow separation leads to a fully viscous eddy and re-attachment further downstream within the triple-deck region. Larger distortions lead to global (breakaway) separation with the viscous shear layer centering around an algebraic curve of increasing distance from the body downstream of the separation point, see Sychev (1972), Messiter (1975), Smith (1977). There are however some particular cases in which classical boundary layer theory is still applicable, as in the marginal separation regime examined in Ruban (1981), complemented by a local interactive structure in Ruban (1982) and Stewartson, Smith & Kaups (1982) or in the condensed flow of Smith & Daniels (1981). A detailed review of these issues can be found in Messiter (1979) and Smith (1982).

In this Thesis a study is made of the effects of a liquid film coating within boundary layers on both the classical and triple-deck scales.

The second important topic of research relevant to this Thesis is on the instability of fluid flows to infinitesimal disturbances and the transition of laminar flow to turbulence. Instability theory developed from a need to understand why most high speed flows are of a turbulent rather then laminar nature. With all the early works based on an inviscid treatment, it has its beginnings in the analytical studies of Helmholtz, Kelvin and Lord Rayleigh and in the experimental work of Reynolds. This instability theory for inviscid waves was extended to include the effects of viscosity in the works of Orr, Sommerfeld, Taylor, Prandtl, Tollmien and Schlichting. The reader is referred to Drazin & Reid (1981) for a review of the early theory. Tollmien and Schlichting showed that viscous effects could provide the mechanism for instability, an essentially counter intuitive effect. All these theories were based on linear approximations, and it was not until Landau (1944), in a quite general postulation, that a nonlinear theory, now termed weakly nonlinear, was proposed. Landau's ideas were confirmed in an examination of plane parallel flows by Stuart (1960) and Watson (1960), and these first three authors lend their name to the typical Landau-Stuart-Watson amplitude equation governing weakly nonlinear instability waves. Itoh (1974), who derived the same form of equation for the Blasius layer, and many subsequent works were all applied to flows at finite Reynolds numbers where the effects of the flow non-parallelism are non-negligible. Smith (1979a,b) began more rigorous investigations of the linear and nonlinear instability of boundary-layer flows, at large Reynolds numbers, by placing the base flow and disturbances within the triple-deck scalings (an account of earlier asymptotic approaches to the viscous-flow instability is given in Lin (1955)). Many other high Reynolds number studies followed, examining a wide variety of instability mechanisms and disturbance scalings (see review articles by Smith (1993), Hall (1990), Cowley & Wu (1993)).

A novel nonlinear mechanism for the transition of laminar to turbulent flow was developed initially by Hall & Smith (1988) which modelled the spatial development of three-dimensional vortices and their interaction with relatively short wavelength neutral waves. The theory divides into numerous categories depending on the size of

the wave disturbance and the proportion of the 3D vortex in the mean flow. When the vortex part of the flow was simply a small correction to the mean profile the interactions with the disturbances were termed weakly nonlinear, whilst those where the vortex comprised the entire mean flow were termed strongly nonlinear. Interactions with small disturbances of the minimum magnitude to instigate non-linear interactions, were investigated for both inviscid Rayleigh and viscous Tollmien-Schlichting (TS) waves by Hall & Smith (1988, 1989, 1990), Smith & Walton (1989), Blackaby (1991), Smith & Blennerhassett (1992) for 'weakly' non-linear interactions, and by Smith & Walton (1989) Walton & Smith (1992), Hall & Smith (1991), Seddougui & Bassom (1991) for 'strongly' non-linear interactions. The work of Hall & Smith (1991), a study of both compressible and incompressible flows, relied on the existence of a saturated neutral wave at some upstream position, at which the interaction was initiated with the vortex then developing downstream in order to keep the wave neutral. Brown *et al.* (1993) studied shorter scale events for the initiation of this behaviour in the incompressible case for Rayleigh waves, although still with an abrupt start to the interaction. Smith, Brown & Brown (1993) examined even shorter scale events, with the vortex/wave interaction occurring chiefly through the jump in transverse shear stress across a critical layer. They derived a wave-amplitude equation governing the wave disturbance and found various solutions for the downstream behaviour including wave decay, a finite-distance wave-amplitude blow-up and periodic solutions, which they conjectured were more likely to occur than the downstream match to a constant wave amplitude required by Brown *et al.* (1993), Hall & Smith (1991).

Much of this basic knowledge can be applied to the high Reynolds number two-fluid problems studied in this Thesis. In addition to the behaviours noted in the above works, the presence of an interface greatly influences the flow development. With regard to the base flow profiles Nelson *et al.* (1995) examined the boundary-layer flow development of air blowing over a film of water on a flat plate and showed that whilst the non-parallel boundary layer growth is of $O(x^{1/2})$, where x is the streamwise coordinate, the film grows like $O(x^{1/4})$. They constructed non-similar

analytic solutions and showed that a linear profile in the water and Blasius profile in the air are reasonable base-flow profiles for instability calculations. Coward & Hall (1996), in a study of the stability of thin coatings of water on a porous wall in air flow, constructed similarity solutions for the base profiles, made possible through the wall condition. We could not find other works which examined the form of base profiles for boundary layers with thin liquid film coatings, and in Chapter 1 we aim to shed some light, computationally, on the behaviour and shape of possible base flows.

The instabilities present for two-fluid flows in a boundary layer, on the other hand, have received more attention, both experimentally and theoretically. Experimental investigations have been performed by, amongst others, Hanratty & Engen (1957), Kao & Park (1972), Charles & Lilleleht (1965), Andreussi *et al.* (1985) and Ludwieg & Hornung (1989). For two fluids of comparable depths Kao & Park (1972) found no interfacial modes with the surface distortion being a manifestation of the shear (TS) waves and concluded that the presence of an interface enhanced transition. The investigation of Ludwieg & Hornung (1989), for air flow over a thin film of oil, showed the appearance of visible waves on the interface occuring at different stages in the transition from laminar to turbulent air boundary layers depending on the film thickness. The properties of the second fluid, including its depth, density and viscosity all appear to be important. In the 1950s much theoretical work was carried out trying to explain the phenomena of water waves generated by wind, with a variety of mechanisms proposed, initially through the work of Lock (1954), Feldman (1957) and later by Miles (1957 ,1959, 1960, 1962). Miles (1957) studied the instigation of waves on deep water by wind, based on a basic solution of near-neutral gravity waves. He showed that the instability of a unidirectional air flow to inviscid Rayleigh-scale disturbances was dependent on a negative curvature of the mean flow profile at the height where the wave speed was equal to the streamwise velocity (the critical level), thus showing that non-inflexional profiles were unstable to these Rayleigh disturbances, in contrast with the requirement in homogeneous flow of an inflexional profile. A classification of the various instabilities present in two-fluid

problems was given by Benjamin (1960, 1963) and Landahl (1962) who attempted a physical explanation of instabilities based on energy levels. They categorized three different instabilities appearing in flows with flexible boundaries referring to these as Class A, Class B and Kelvin-Helmholtz (K-H) waves. The first of these, the Class A instability, which includes Tollmien-Schlichting waves modified by the flexible boundary, is destabilized by dissipative forces. They demonstrated, via the energy considerations, that an essentially counter intuitive destabilization, with the wave growth accompanied by a transfer of energy from the wave to the main flow, is present in the system. The Class B instability on the other hand is stabilized by the dissipative forces and grows via an energy transfer from the mean flow to the wave, a more intuitive mechanism. The final class, the K-H instability is driven by velocity discontinuities. Classification in these papers is based upon near-neutral calculations and we aim in this Thesis to verify the general classifications by direct computation of the instabilities.

More recent instability studies involving two phase flows include those made by Hooper & Boyd (1986), Morland & Saffman & Yuen (1991), Shrira (1993), Morland & Saffman (1993), Coward & Hall (1996) and Timoshin (1997). Shrira (1993) examined instabilities of disturbances found in deep water with a current and a free surface, whilst Morland & Saffman (1993) carried out linear stability analysis of an inviscid parallel air flow over water and made numerical comparisons, finding fair agreement with the analytic solution of Miles (1957). Coward & Hall (1996) studied the three-dimensional flow over a porous flat plate, with suction or blowing chosen to maintain a constant lower fluid depth. Their stability analysis showed, as in Hooper and Boyd (1986), that discontinuities in the viscosity and/or density of the two immiscible fluids greatly enhanced instability. Timoshin (1997) examined linear instabilities within the triple-deck formulation of a two-fluid flow including the case of a very viscous film and derived growth rates for TS and interfacial waves.

The inclusion of a second fluid in nonlinear stability problems leads to an enhanced mean flow generated by the Reynolds stresses at the fluid/fluid interface, as first studied by Longuet-Higgins (1953) and subsequently by Dore (1970, 1976,

1977). This effect is due to the jump in shears across the viscous layers surrounding the interface as opposed to a shift in velocities due to viscous layers on solid boundaries. Dore (1976, 1977) incorporated outer viscous layers about the interfacial layers, based on the double boundary layer theories developed by Riley (1965) and Stuart (1966), through which the induced mean flow is diffused. The effect of this stronger mean flow on the wave instability is felt through interactions at a lower order than those with wall induced mean flow. A second fluid also allows for resonant interactions between the various instabilities that may be present such as those classified by Benjamin-Landahl, outlined above. One such case is studied in Akylas (1982), Akylas & Benney (1982) who identify a resonance between 'air' (Class A) and 'water' (Class B) modes in the case of wind on deep water.

We see then that the study of boundary layers with thin films is a complex and fascinating field, with very little known about the effect of films on separation, along with the apparently strong effect on stability provoked by the presence of an interface.

For the majority of this study we simplify our analysis by assuming piecewise constant-shear base profiles in the regions on either side of the interface with a thickness comparable to that of the film. However we must begin by examining if these are satisfactory base profiles, and this justification is undertaken in Chapter 2, where we investigate the boundary layer flow over a film-coated wall with a surface obstacle of prescribed magnitude. The first part of this chapter deals with the base flow development from the source of the film generation. We then proceed to the flow over a surface roughness, with the choice of scalings and the 'long' and 'short' obstacle classification used within this chapter following those given by Smith *et al* (1981) in their investigation of homogeneous flow development. We then examine the flow over 'long' obstacles on the triple-deck length scale, with a prescribed pressure gradient dependent on the obstacle shape. Computations, both numerical and analytic, are undertaken to calculate the flow development and its stability to Rayleigh-like disturbances. In the second part of Chapter 2 we examine 'short' obstacles within a condensed flow formulation, again with a numerical treatment of the

base flow development. This provides an important insight into the role of a film in the onset of separation, an area which up to now has received scant attention to this author's best knowledge. A stability analysis is then carried out on the calculated profiles.

In Chapter 3 we investigate weakly-nonlinear vortex/inviscid wave interactions, in the early stages of transition for a two fluid flow, based on the single fluid study of Smith, Brown & Brown (1993). By utilizing the assumptions of a parallel flow and a base profile consisting of two constant shears in our region of study, we obtain wave-amplitude equations governing the evolution of two pairs of oblique waves travelling with identical phase speed. We show that the nonlinear development of this flow can lead to finite-distance blow-up of the wave disturbances. In the case of non-resonant waves we show that the amplitude equations simplify to those derived in Smith, Brown & Brown (1993).

The stability of nonlinear Tollmien-Schlichting (TS) waves is studied within a triple-deck framework in Chapter 4, an extension of the linear analysis of Timoshin (1997). In a weakly non-linear analysis, the temporal evolution of two dimensional disturbances is modelled via an amplitude evolution equation coupled with equations governing the Reynolds stress induced mean flow. A twofold investigation of both the stability of the much altered mean flow to Rayleigh scale disturbances and the development of the wave disturbance is carried out. The amplitude equation is found to contain a singularity centered around a specific combination of the surface tension, gravity, density ratios and film thickness. A close analysis is performed within this parameter space and a resonant structure found with magnified disturbance amplitudes. This non-linear resonance is directly related to the linear resonance between growing TS and decaying capillary waves outlined in Timoshin (1997). A full investigation of the properties of the governing amplitude equation is carried out, with the nonlinearity appearing in an unusual differentiated form. The properties of the amplitude equations are quite disparate and two further intermediate regimes are studied, giving a full account of the possible disturbance development schemes.

A classical boundary-layer base flow structure is used to examine the Rayleigh-

scale stability properties of flow over a very viscous film in Chapter 5. The different classes of instability suggested by Benjamin (1960,1963) and Landahl (1962) are shown to be present as different limits of our general formulation, and we demonstrate that various cases studied previously, (e.g. Kelvin-Helmholtz, Tollmien-Schlichting, Miles, capillary/TS wave resonance) are all continuously linked in the parameter space studied here.

We begin our investigation by outlining the dimensional governing equations and boundary conditions for two-fluid flows which we will use throughout this study with the specific non-dimensionalizations given at the start of each chapter.

1.1 The dimensional governing equations

The two fluid flows studied in this thesis are governed by the incompressible Navier-Stokes equations. We define x_*, y_* to be the dimensional coordinates parallel and normal to the flow direction and z_* to be the spanwise coordinate perpendicular to x_* in the plane $y_* = 0$. Then $u_*^{\pm}$, $v_*^{\pm}$, $w_*^{=}$, $p_*^{\pm}$ represent the streamwise, normal and cross-flow velocities and the pressure respectively, with the superscripts $+/-$ denoting the regions above or below the interface separating the two fluids at $y_* = f_*(x_*, z_*, t_*)$. All the flows studied take place within a boundary layer which develops over a surface defined by $y_* = h_*(x_*)$, placed in the flow. The density and viscosity of the fluid in the film are denoted by ρ_*^-, μ_*^- and in the main boundary layer fluid by ρ_*^+, μ_*^+. With g_* representing the dimensional gravitational acceleration, the governing equations are

$$\frac{Du_*^{\pm}}{Dt_*} = \frac{-1}{\rho_*^{\pm}}\frac{\partial p_*^{\pm}}{\partial x_*} + \frac{\mu_*^{\pm}}{\rho_*^{\pm}}\left(\frac{\partial^2 u_*^{\pm}}{\partial x_*^2} + \frac{\partial^2 u_*^{\pm}}{\partial y_*^2} + \frac{\partial^2 u_*^{\pm}}{\partial z_*^2}\right), \tag{1.1.1a}$$

$$\frac{Dv_*^{\pm}}{Dt_*} = \frac{-1}{\rho_*^{\pm}}\frac{\partial p_*^{\pm}}{\partial y_*} - g_* + \frac{\mu_*^{\pm}}{\rho_*^{\pm}}\left(\frac{\partial^2 v_*^{\pm}}{\partial x_*^2} + \frac{\partial^2 v_*^{\pm}}{\partial y_*^2} + \frac{\partial^2 v_*^{\pm}}{\partial z_*^2}\right), \tag{1.1.1b}$$

$$\frac{Dw_*^{\pm}}{Dt_*} = \frac{-1}{\rho_*^{\pm}}\frac{\partial p_*^{\pm}}{\partial z_*} + \frac{\mu_*^{\pm}}{\rho_*^{\pm}}\left(\frac{\partial^2 w_*^{\pm}}{\partial x_*^2} + \frac{\partial^2 w_*^{\pm}}{\partial y_*^2} + \frac{\partial^2 w_*^{\pm}}{\partial z_*^2}\right), \tag{1.1.1c}$$

$$\frac{\partial u_*^{\pm}}{\partial x_*} + \frac{\partial v_*^{\pm}}{\partial y_*} + \frac{\partial w_*^{\pm}}{\partial z_*} = 0. \tag{1.1.1d}$$

The boundary conditions for these equations are firstly those of no slip on the surface, continuity in the streamwise and spanwise velocities at the interface and the kinematic condition at the interface

$$u_*^- = v_*^- = 0, \text{at } y_* = h_*(x_*), \tag{1.1.2}$$

$$v_*^+ = v_*^- = \frac{Df_*}{Dt}, \; u_*^- = u_*^+, \; w_*^- = w_*^+, \text{ at } y_* = f_*(x_*, z_*, t_*), \tag{1.1.3}$$

where the material derivative is defined by $D/Dt_* = \partial/\partial t_* + u_*^{\pm}\partial/\partial x_* + v_*^{\pm}\partial/\partial y_* + w_*^{\pm}\partial/\partial z_*$. Secondly, at the interface, defined by $y_* = f_*$, between the two fluids the equation

$$[\underline{\sigma}.\mathrm{n}]_-^+ - \mathrm{n}\gamma_* \left(\frac{1}{R_1} + \frac{1}{R_2}\right) = 0 \text{ at } y_* = f_* \tag{1.1.4}$$

must be satisfied, where $\underline{\sigma}$ is the stress tensor, γ_* is the surface tension, the square brackets [] denote a jump across the interface,

$$\frac{1}{R_1} = \frac{\partial^2 f_*/\partial x_*^2}{(1 + (\partial f_*/\partial x_*)^2)^{3/2}}, \quad \frac{1}{R_2} = \frac{\partial^2 f_*/\partial z_*^2}{(1 + (\partial f_*/\partial z_*)^2)^{3/2}}, \tag{1.1.5}$$

are the radii of curvature, and $\mathbf{n}$ is the unit normal to the interface given by

$$\mathbf{n} = \frac{1}{\sqrt{(\partial f_*/\partial x_*)^2 + 1 + (\partial f_*/\partial z_*)^2}}(-\partial f_*/\partial x_*, 1, -\partial f_*/\partial z_*). \tag{1.1.6}$$

We write the unit tangent vectors to $\mathbf{n}$ as

$$\mathrm{t}_{x_*} = \frac{1}{\sqrt{1 + (\partial f_*/\partial x_*)^2}} \left(1, \frac{\partial f_*}{\partial x_*}, 0\right), \tag{1.1.7}$$

$$\mathrm{t}_{z_*} = \frac{1}{\sqrt{1 + (\partial f_*/\partial z_*)^2}} \left(0, \frac{\partial f_*}{\partial z_*}, 1\right), \tag{1.1.8}$$

and, taking the dot product of (1.1.4) with $\mathbf{t}_{x_*}$, $\mathbf{t}_{z_*}$ $\mathbf{n}$, respectively we obtain three interfacial jump conditions

$$\left[\mu_* \left(\begin{array}{l} \dfrac{\partial f_*}{\partial x_*}\left(\dfrac{\partial v_*}{\partial y_*} - \dfrac{\partial u_*}{\partial x_*}\right) + A_*\left(1 - \left(\dfrac{\partial f_*}{\partial x_*}\right)^2\right) \\ -B_*\dfrac{\partial f_*}{\partial z_*}\dfrac{\partial f_*}{\partial x_*} - C_*\dfrac{\partial f_*}{\partial z_*} \end{array} \right)\right]_-^+ = 0 \quad (1.1.9)$$

$$\left[\mu_* \left(\begin{array}{l} \dfrac{\partial f_*}{\partial z_*}\left(\dfrac{\partial v_*}{\partial y_*} - \dfrac{\partial w_*}{\partial z_*}\right) + A_*\dfrac{\partial f_*}{\partial z_*}\dfrac{\partial f_*}{\partial x_*} \\ -B_*\left(1 - \left(\dfrac{\partial f_*}{\partial z_*}\right)^2\right) - C_*\dfrac{\partial f_*}{\partial x_*} \end{array} \right)\right]_-^+ = 0 \quad (1.1.10)$$

$$\left[-p_* + 2\mu_* \left(\begin{array}{l} \dfrac{\partial u_*}{\partial x_*}\left(\dfrac{\partial f_*}{\partial x_*}\right)^2 + \dfrac{\partial v_*}{\partial y_*} + \dfrac{\partial w_*}{\partial z_*}\left(\dfrac{\partial f_*}{\partial z_*}\right)^2 - 2\dfrac{\partial f_*}{\partial x_*}A_* \\ -2\dfrac{\partial f_*}{\partial z_*}B_* + 2\dfrac{\partial f_*}{\partial x_*}\dfrac{\partial f_*}{\partial z_*}C_* \end{array} \right)\right]_-^+$$
$$+\gamma_*\left(\frac{\partial^2 f_*/\partial {x_*}^2}{(1+(\partial f_*/\partial x_*)^2)^{3/2}} + \frac{\partial^2 f_*/\partial {z_*}^2}{(1+(\partial f_*/\partial z_*)^2)^{3/2}}\right) = 0 \quad (1.1.11)$$

where square brackets indicate a jump across the interface, parameters in the boundary layer and film are denoted by $+/-$ respectively (a different notation is used in chapter 2 for these layers) and

$$A_* = \frac{1}{2}\left(\frac{\partial u_*}{\partial y_*} + \frac{\partial v_*}{\partial x_*}\right),\ B_* = \frac{1}{2}\left(\frac{\partial v_*}{\partial z_*} + \frac{\partial w_*}{\partial y_*}\right),\ C_* = \frac{1}{2}\left(\frac{\partial u_*}{\partial z_*} + \frac{\partial w_*}{\partial x_*}\right). \quad (1.1.12)$$

where A_*, B_*, C_* are represent elements of the rate of strain tensor E_{ij}.

Chapter 2

Flow over a surface mounted obstacle

In this chapter we numerically tackle the flow within a boundary layer on a wall, for homogeneous flows and for those with a thin film coating on the wall. The aims here are to prepare the ground for examination of film coated flows in the subsequent chapters. First and foremost we provide a realistic model for the base flow, which we will use for all the subsequent work. Secondly we investigate the effects of a certain prescribed wall roughness on the base flow, and the form of the singularities which we expect to find in the boundary layer solution when the pressure on the boundary layer and in the film is given. We show that for all cases considered the singularities are always due to zero wall shear, as found in the works of Goldstein (1948), Stewartson, Smith & Kaups (1982), Ruban (1981,1982) rather than to flow reversal in the middle of the flow region as in Sychev (1980), Elliott, Smith & Cowley (1983), Timoshin (1996). Our final aim in this chapter is to investigate the destabilizing effect of the wall roughness, or indeed of any other mechanism which affects constant shear profiles in thin films. We find inviscid instability which is strongly influenced by the properties of the interface.

In this work hump flows are treated as limiting cases of the triple-deck formulation with the film placed in the near-wall viscous zone. Prescribed-pressure regimes

arise when the wall roughness is long compared to the triple deck. In §2.5 we also examine the opposite limiting case of shorter obstacles, leading to a condensed flow formulation. The second regime is irrelevant to the base flow investigation, which is one of the primary interests in this chapter, but is a logical analytic compliment to the solution we derive for the longer obstacle, requiring only a straightforward change in the problem formulation. An analysis of the single-fluid triple-deck problem for obstacles in both these limits and of those on the triple-deck scale is given by, for example, Smith, Brighton, Jackson, Hunt (1981); see also a review article by Smith (1982).

2.1 Blasius boundary layer on a film-coated wall

In the following chapters the investigations utilize an initial unperturbed upstream flow consisting of piecewise linear profiles in the near-wall part of the boundary layer. In this section we outline the general assumptions and scalings we will use for tackling film coated flows, including the base flow profiles. Once the form of base flow has been verified, the following subsection outlines the triple-deck scalings used to examine flow over a wall mounted obstacle.

We assume the flow to be two-dimensional and, further, that at the leading edge of a flat plate in a uniform stream a boundary layer on a surface is generated in which we have steady, incompressible planar flow. Downstream of the leading edge we have a film generated by a slot, in the form of a jet; see fig 2:1(a). Gravity and surface tension are included in the problem formulation for the base flow calculations, although they are discarded in the numerical investigation later as in a related work by Nelson *et al.* (1995).

The governing Navier-Stokes equations, (1.1.1), are non-dimensionalized using the distance between the leading edge of the plate and the slot $\breve{L}_*$, the free stream speed U_*, the viscosity ν_*^+ and the density ρ_*^+ in the upper fluid. The typical pressure is $\rho_* U_*^2$, and we use standard notation for the Reynolds number $\breve{R}e = \rho_*^+ U_* \breve{L}_* / \mu_*^+$ ($\gg 1$), the Froude number $\breve{F}r = U_*^2 / g_* \breve{L}_*$ and surface tension coef-

ficient $\breve{\gamma} = \gamma_*/\rho_*^+ U_*^2 \breve{L}_*$. The non-dimensionalized streamwise and normal velocity components are $\breve{u}$, $\breve{v}$, we take $\breve{x}$, $\breve{y}$ as the boundary layer coordinates parallel and normal to the flow, with $x_* = \breve{L}_*(\breve{x}+1)$, $y_* = \breve{L}_* \breve{R}e^{-1/2}\breve{y}$. With $\breve{p}$ the non-dimensional pressure and $\breve{f}$ the interface position between the two fluids, taken initially to be $\breve{a}$, the height of the slot, the governing equations become

$$\frac{\partial \breve{u}^{\pm}}{\partial \breve{t}} + \breve{u}^{\pm}\frac{\partial \breve{u}^{\pm}}{\partial \breve{x}} + \breve{v}^{\pm}\frac{\partial \breve{u}^{\pm}}{\partial \breve{y}} = -\frac{1}{\rho^{\pm}}\frac{\partial \breve{p}^{\pm}}{\partial \breve{x}} + \nu^{\pm}\frac{\partial^2 \breve{u}^{\pm}}{\partial \breve{y}^2}, \tag{2.1.1}$$

$$\frac{\partial \breve{p}^{\pm}}{\partial \breve{y}} = 0. \quad \frac{\partial \breve{u}^{\pm}}{\partial \breve{x}} + \frac{\partial \breve{v}^{\pm}}{\partial \breve{y}} = 0, \tag{2.1.2}$$

where we define $\rho^+ = 1$, $\nu^+ = 1$, $\rho^- = \rho_*{}^-/\rho_*{}^+$, $\nu^- = \nu_*{}^-/\nu_*{}^+$. The appropriate boundary conditions are

$$\breve{y} \to \infty \qquad \breve{u}^+ = 1, \tag{2.1.3}$$

$$\breve{y} = \breve{f}: \qquad \breve{u}^+ = \breve{u}^-, \quad \breve{v}^+ = \breve{v}^- = \frac{D\breve{f}}{D\breve{t}}, \quad \frac{\partial \breve{u}^+}{\partial \breve{y}} = \mu^- \frac{\partial \breve{u}^-}{\partial \breve{y}}, \tag{2.1.4}$$

$$\breve{p}^+ - \breve{p}^- = \breve{\gamma}\breve{f}_{\breve{x}\breve{x}} - (\rho^- - 1)\breve{f}/\breve{F}r,$$

$$\breve{y} = 0: \qquad \breve{u}^- = 0, \ \breve{v}^- = 0, \tag{2.1.5}$$

$$x = 0: \qquad \breve{u}^+ = U_B, \ \breve{u}^- = \breve{J}\breve{y}(\breve{a} - \breve{y}), \ ; \ \breve{f} = \breve{a} \tag{2.1.6}$$

where $U_B = U_B(\breve{y} - \breve{a})$ is the Blasius profile, $\breve{J}$ is a constant measuring the strength of the jet and the shape of the interface is described by $\breve{y} = \breve{f}(x)$.

Using the numerical method outlined below, in §2.3.1, a number of different profiles were placed at the initial station and the profiles calculated for the flow downstream. We were looking for these test profiles to quickly form two linear profiles, one in the film and the other in the boundary layer. A model of the case with a Blasius profile in the boundary-layer fluid and a jet flow from the slot is shown in fig 2:1(b). We see that the profiles in the near-wall region reach a limiting piecewise linear form over the distance $\mid X \mid = 10$, where $X = \breve{x}$, see also fig 2:1(c). Many different initial profiles were run and all of them eventually formed two constant shear profiles. Nelson *et al.* (1995) established the limiting behaviour as $\breve{x} \to \infty$ for a film within a Blasius boundary layer on a flat plate. The film thickens like

$\breve{x}^{1/4}$, with the main boundary layer growing like $\breve{x}^{1/2}$, and the interfacial shear in the boundary layer decreasing like $\breve{x}^{-1/2}$ with the film flow driven by the applied interfacial shear. If Ψ_0^- is the mass flux at the slot, given by the value of the stream function Ψ at the interface, so that $\breve{u}^- = \partial\Psi/\partial\breve{y}$, then the streamwise velocities and interface position in the region $\breve{y} \sim O(\breve{x}^{1/4})$ are given by

$$\breve{u}^- = \frac{\lambda_b}{\mu^-\sqrt{\breve{x}}}\breve{y}, \quad u^+ = (1-\mu^-)\sqrt{\frac{2\Psi_0^-\lambda_b}{\mu^-\breve{x}^{1/2}}} + \frac{\lambda_b\breve{y}}{\sqrt{\breve{x}}}, \quad \breve{f} = \sqrt{\frac{2\Psi_0^-\mu^-\breve{x}^{1/2}}{\lambda_b}}, \qquad (2.1.7)$$

where $\lambda_b = \partial U_B/\partial\breve{y}(0)$, and the boundary layer flow approaches the Blasius profile downstream in the region $\breve{y}\breve{x}^{-1/2} \sim 1$. By altering Ψ_0^-, either via the size of the injection slot or the speed of the jet, we can set the film thickness downstream. At $\breve{x} \gg 1$ the film forgets about the specific source. This allows us to perform the triple-deck analysis at a station L_* downstream in the next section, which requires a film of thickness $O(Re^{-5/8})$, in terms of the local Reynolds number (see fig 2:1(a)), if we have a flux of $O(\breve{R}e^{-1/8}L_*^{3/8}\breve{L}_*^{-3/8})$. Hence we may assume for all our subsequent analysis that our predetermined initial local base profile consisting of two constant shears can be obtained, or is indeed typical, in a two fluid system. Other mechanisms can be treated in a similar fashion, for example injection through a porous wall, cf Coward & Hall (1996).

2.2 Triple deck on a wall mounted obstacle

In this subsection we outline the scalings used to investigate the flow within a boundary layer which develops over a local surface roughness defined by $y_* = h_*(x_*)$, see fig 2:2(a). We quote the rescalings used for a short-scale analysis of flow over a flat plate, which lead to the triple-deck equations for film coated flows, as derived by Timoshin (1997), Tsao *et al.* (1996) from the full Navier-Stokes equations. After non-dimensionalizing we perform a Prandtl shift, introducing the surface shape into the problem.

The governing Navier-Stokes equations are non-dimensionalized as in §2.1, but here we take the characteristic length L_* to be from the leading edge of the plate

to the local point of investigation (taken to be the centre of an obstacle on the wall later in this section), with corresponding Reynolds number $Re = \rho_*^+ U_* L_* / \mu_*^+$ ($\gg 1$), Froude number $\hat{Fr} = U_*^2 / g_* L_*$ and surface tension coefficient $\hat{\gamma} = \gamma_* / \rho_*^+ U_*^2 L_*$. The non-dimensionalized temporal and spatial co-ordinates, velocities, pressures and interface shape are denoted by $\hat{t}$, $\hat{x}$, $\hat{y}$, $\hat{u}$, $\hat{v}$, $\hat{p}$ and $\hat{f}$. With $\hat{a}$ denoting the unperturbed interface position upstream from the area under investigation, we rescale to the triple-deck variables in the viscous sublayer (zone I in fig 2:1(a))

$$\left[\hat{u},\hat{v},\hat{p},\hat{x},\hat{y},\hat{t},\hat{a},\hat{f}\right] = \left[\epsilon_0\lambda^{+3/4}u, \epsilon_0^3\lambda^{+3/4}v, \epsilon_0^2\lambda^{+1/2}p, \epsilon_0^3(\lambda^+)^{-5/4}x, \right.$$
$$\left. \epsilon_0^5(\lambda^+)^{-3/4}y, \epsilon_0^2(\lambda^+)^{-3/2}t, \epsilon_0^5(\lambda^+)^{-3/4}a, \epsilon_0^5(\lambda^+)^{-3/4}f\right] \qquad (2.2.1)$$

with $\epsilon_0 = Re^{-1/8}$, y representing the local normal coordinate in the viscous sublayer, and λ^+ denoting the shear of the upper profile. We write $\rho^+ = 1$, $\nu^+ = 1$, $\rho^- = \rho_*^-/\rho_*^+$, $\nu^- = \nu_*^-/\nu_*^+$ and defining $y = h(x)$ to be the non-dimensional wall shape apply a Prandtl shift to the triple-deck equations,

$$y = Y + h(x), \quad v = V + u\frac{\partial h}{\partial x}. \qquad (2.2.2)$$

This leaves us with

$$\frac{\partial u^\pm}{\partial t} + u^\pm\frac{\partial u^\pm}{\partial x} + V^\pm\frac{\partial u^\pm}{\partial Y} = -\frac{1}{\rho^\pm}\frac{\partial p^\pm}{\partial x} + \nu^\pm\frac{\partial^2 u^\pm}{\partial Y^2}, \qquad (2.2.3)$$

$$\frac{\partial u^\pm}{\partial x} + \frac{\partial V^\pm}{\partial Y} = 0, \qquad (2.2.4)$$

and the appropriate boundary conditions are

$$Y \to \infty \quad u^+ = Y + a(\frac{1}{\rho^-\nu^-} - 1) + A(x) + h(x) + o(1), \qquad (2.2.5)$$

$$Y = 0 \qquad u^- = 0,\ v^- = 0, \qquad (2.2.6)$$

$$x \to -\infty \qquad \begin{cases} u^+ = Y - a + U_s, \\ u^- = \lambda^- Y \end{cases}, \qquad (2.2.7)$$

where $\lambda^- = 1/\rho^-\nu^-$, $U_s = a\lambda^-$ and the shape of the interface is described by $Y = f(x,t)$ with $a = f(x = -\infty)$ denoting the film thickness upstream from the roughness. The interfacial conditions become

$$u^+ = u^-, \quad V^+ = V^- = \frac{\partial f}{\partial t} + u^\pm\frac{\partial f}{\partial x}, \quad \frac{\partial u^+}{\partial Y} = \mu^-\frac{\partial u^-}{\partial Y}, \qquad (2.2.8)$$

$$p^+ - p^- = \gamma(f_{xx} + h_{xx}) - (\rho^- - 1)(f + h)/Fr \tag{2.2.9}$$

where $\gamma = \hat{\gamma}\epsilon_0^3(\lambda^+)^{-5/4}$, $Fr = \hat{Fr}\epsilon_0^3(\lambda^+)^{-5/4}$ are the rescaled surface tension coefficient and Froude number respectively. Finally the interaction condition for subsonic flows completes the triple deck formulation,

$$p^+ = \frac{1}{\pi}\int_{-\infty}^{\infty} \frac{\partial A/\partial s(s,t)}{x - s} ds. \tag{2.2.10}$$

2.3 Boundary layer on elongated obstacles

From now one in this Chapter we examine the steady case, $\partial/\partial t = 0$. The first step now is to rescale the problem taking the length of the hump L as our typical length scale. We consider long humps with $L \gg 1$ on the triple deck scale. The procedure is similar to that used in Smith, Brighton, Jackson, Hunt (1981). We take

$$Y \sim L^{\frac{1}{3}}, \quad x \sim L, \quad u \sim Y \sim L^{\frac{1}{3}},$$

Then from the balance $u^{\pm}u_x^{\pm} \sim p_x^{\pm}$ and, from (2.2.10) we know $A \sim xp^+$, we have

$$p^{\pm} \sim L^{\frac{2}{3}}, \quad A \sim L^{\frac{5}{3}}.$$

We examine now humps with a height scale $h \sim L^{\frac{5}{3}}$, as we want a contribution $(A+h) \sim O(L^{\frac{1}{3}})$ i.e. $A = -h + O(L^{\frac{1}{3}})$. This height produces a nonlinear response in the viscous layer with the induced pressure proportional to the slope of the obstacle h/L.

To keep the interfacial effects in the analysis we must ensure that the film remains within the viscous sublayer so we take

$$a \sim f \sim L^{\frac{1}{3}} \quad \Rightarrow \quad f \ll h. \tag{2.3.1}$$

Finally in order to keep surface tension and gravitational effects in the problem formulation we take

$$L^{\frac{2}{3}} \sim \gamma(L^{-1/3}) \sim (L^{5/3})/Fr \quad \Rightarrow \quad \gamma \sim O(L),\ Fr \sim O(L). \tag{2.3.2}$$

In accordance with the estimates above we introduce new variables,

$$\begin{aligned} Y &= L^{1/3}\bar{y}, \qquad x = L\bar{x}, \\ V^{\pm} &= L^{-1/3}\bar{v}^{\pm}, \quad p^{\pm} = L^{2/3}\bar{p}^{\pm}, \quad u^{\pm} = L^{1/3}\bar{u}^{\pm}, \\ f &= L^{1/3}\bar{f}, \quad h = L^{5/3}\bar{h}, \quad a = L^{1/3}\bar{a}, \\ \gamma &= L\bar{\gamma}, \quad Fr = \frac{\bar{F}r}{L}, \quad A = -L^{\frac{5}{3}}\bar{h}(\bar{x}) + L^{\frac{1}{3}}\bar{A}(\bar{x}). \end{aligned} \tag{2.3.3}$$

The flow scheme is shown in fig2:2(a) and the governing equations expressed in the new variables are

$$\bar{u}^{\pm}\frac{\partial \bar{u}^{\pm}}{\partial \bar{x}} + \bar{v}^{\pm}\frac{\partial \bar{u}^{\pm}}{\partial \bar{y}} = -\frac{1}{\rho^{\pm}}\frac{\partial \bar{p}^{\pm}}{\partial \bar{x}} + \nu^{\pm}\frac{\partial^2 \bar{u}^{\pm}}{\partial \bar{y}^2}, \tag{2.3.4}$$

$$\frac{\partial \bar{u}^{\pm}}{\partial \bar{x}} + \frac{\partial \bar{v}^{\pm}}{\partial \bar{y}} = 0, \tag{2.3.5}$$

with the boundary conditions

$$\bar{y} \to \infty : \quad \bar{u}^{+} = \bar{y} - \bar{a} + U_s + \bar{A}(\bar{x}) + o(1), \tag{2.3.6}$$

$$\bar{y} = 0 : \qquad \bar{u}^{-} = 0, \ \bar{v}^{-} = 0, \tag{2.3.7}$$

$$x \to -\infty \qquad \begin{cases} \bar{u}^{+} = \bar{y} - \bar{a} + U_s, \\ u^{-} = \lambda^{-}\bar{y}, \end{cases} \tag{2.3.8}$$

and also at $\bar{y} = \bar{f}(\bar{x})$

$$\bar{u}^{+} = \bar{u}^{-}, \ \bar{v}^{+} = \bar{v}^{-} = \bar{u}^{\pm}\bar{f}_{\bar{x}}(\bar{x}), \ \frac{\partial \bar{u}^{+}}{\partial \bar{y}} = \mu^{-}\frac{\partial \bar{u}^{-}}{\partial \bar{y}}, \tag{2.3.9}$$

$$\bar{p}^{+} - \bar{p}^{-} = \bar{\gamma}\bar{h}_{\bar{x}\bar{x}} - \bar{h}(\rho^{-} - 1)/\bar{F}r, \tag{2.3.10}$$

$$\bar{p}^{+} = -\frac{1}{\pi}\int_{-\infty}^{\infty} \frac{\partial \bar{h}/\partial s(s)}{\bar{x} - s} ds. \tag{2.3.11}$$

There is no pressure/displacement relation now with the interaction condition replaced by a given pressure related to the surface roughness.

For computational purposes the pressure-hump shape relation (2.3.11) is rewritten taking Fourier transforms,

$$\mathcal{F}(\bar{p}^{+}) = \int_{-\infty}^{\infty} e^{-ik\bar{x}}\bar{p}^{+}(\bar{x})d\bar{x}, \ \mathcal{F}(\bar{p}^{+}) = -\mid k \mid \mathcal{F}(\bar{h}(\bar{x})), \tag{2.3.12}$$

so that

$$\frac{d\bar{p}^+}{d\bar{x}} = \frac{1}{2\pi}\int_{-\infty}^{\infty} e^{ik\bar{x}}\left[-ik \mid k \mid \mathcal{F}(\bar{h}(\bar{x}))\right] dk. \tag{2.3.13}$$

For the pressure gradient in the film the relation (2.3.10) can be differentiated and the derivatives of $\bar{h}$ calculated explicitly for a chosen roughness.

2.3.1 The numerical method

Numerical solutions are obtained to the problems setup in §2.1 and §2.3, by marching in the appropriate co-ordinate $\check{x}$ or $\bar{x}$, using iterations at each streamwise station. We outline the numerical method in terms of the variables in §2.3, however the rescalings take the same form for both problems, replacing all variables $\bar{x}, \ldots$ with $\check{x}, \ldots$ and setting $\bar{h} = 0$, with the only difference in numerical representations being the far-field boundary conditions.

To construct the actual solution we rescale the normal coordinate in the film and make a further Prandtl shift in the boundary layer with respect to the unknown interface position. In the boundary-layer equations (2.3.4), (2.3.5) we write

$$U^+ = \bar{u}^+, \quad V^+ = \bar{v}^+ - \bar{u}^+\bar{f}_{\bar{x}}(\bar{x}), \quad X = \bar{x}, \tag{2.3.1.1a}$$

$$P^+ = \bar{p}^+, \qquad Y^+ = \bar{y} - \bar{f}(\bar{x}), \qquad F = \bar{f}, \tag{2.3.1.1b}$$

which yields the equations, valid for $Y^+ \geq 0$,

$$U^+\frac{\partial U^+}{\partial X} + V^+\frac{\partial U^+}{\partial Y^+} = -\frac{\partial P^+}{\partial X} + \frac{\partial^2 U^+}{\partial {Y^+}^2} \tag{2.3.1.2}$$

$$\frac{\partial U^+}{\partial X} + \frac{\partial V^+}{\partial Y^+} = 0 \tag{2.3.1.3}$$

with boundary conditions

$$Y^+ \to \infty: \quad U^+ = Y^+ + U_s - \bar{a} + \bar{A}(X) + F(X) + o(1) \tag{2.3.1.4}$$

$$Y^+ = 0: \qquad V^+ = 0 \tag{2.3.1.5}$$

$$X \to -\infty: \qquad U^+ = Y^+ + U_s, \ F \to \bar{a} \tag{2.3.1.6}$$

where our initial interfacial speed is $U_s = \bar{a}/\rho^-\nu^-$.

The film region is mapped onto the finite strip $0 \leq Y^- \leq 1$ using a change of variables suggested by Dr J. W. Elliott (private communication). We write

$$Y^- = \frac{\bar{y}}{\bar{f}(\bar{x})}, \quad X = \bar{x}, \quad U^- = \bar{u}^-, \tag{2.3.1.7a}$$

$$V^- = \bar{v}^- - Y^- \frac{\partial \bar{f}}{\partial \bar{x}} \bar{u}^-, \quad P^- = \bar{p}^-, \quad F = \bar{f}, \tag{2.3.1.7b}$$

which give the equations

$$U^- \frac{\partial U^-}{\partial X} + \frac{V^-}{F} \frac{\partial U^-}{\partial Y^-} = -\frac{1}{\rho^-} \frac{\partial P^-}{\partial X} + \frac{\nu^-}{F^2} \frac{\partial^2 U^-}{\partial Y^{-2}}, \tag{2.3.1.8}$$

$$\frac{\partial (U^- F)}{\partial X} + \frac{\partial V^-}{\partial Y^-} = 0, \tag{2.3.1.9}$$

and boundary conditions

$$Y^- = 0: \quad U^- = V^- = 0, \tag{2.3.1.10}$$

$$Y^- = 1: \quad V^- = 0, \tag{2.3.1.11}$$

$$X \to -\infty: \quad U = U_s Y^-. \tag{2.3.1.12}$$

The interfacial conditions of continuity of tangential velocity and normal velocity, the jump in pressures and shears and the viscous-inviscid interaction condition, which becomes a given pressure relation, are then expressed as

$$U^+(Y^+ = 0) = U^-(Y^- = 1), \quad \frac{\partial U^+}{\partial Y^+}(Y^+ = 0) = \frac{\mu^-}{F} \frac{\partial U^-}{\partial Y^-}(Y^- = 1), \tag{2.3.1.13}$$

$$V^+(Y^+ = 0) = V^-(Y^- = 1) = 0, \tag{2.3.1.14}$$

$$\frac{dP^+}{dX} - \frac{dP^-}{dX} = \bar{\gamma} \frac{d^3 H}{dX^3} - \frac{(\rho^- - 1)}{\bar{F}r} \frac{dH}{dX}, \tag{2.3.1.15}$$

$$P^+ = -\frac{1}{\pi} \int_{-\infty}^{\infty} \frac{\partial H / \partial s(s)}{X - s} ds, \tag{2.3.1.16}$$

where $\bar{h}(\bar{x}) = H(X)$.

The problem in §2.1 can also be represented by the same transformations (2.3.1.1), (2.3.1.7) (with all variables $\bar{x}, \ldots$ replaced by $\breve{x}, \ldots$) and the obstacle removed, $H(X) =$

0. The only differences, for numerical purposes, are the boundary conditions, (2.1.3), (2.1.6), which become

$$Y^+ \to \infty : \qquad U^+ \to 1, \tag{2.3.1.17}$$

$$X = 0 : \quad U^+ = U_B(Y^+), \quad U^- = JY^-(1 - Y-), \quad F = \breve{a} \tag{2.3.1.18}$$

where $J = \breve{a}^2 \breve{J}$.

A three-point backward difference is used for X-derivatives and a two-point central difference for the normal direction:

$$\frac{\partial \xi(X)}{\partial X} = \frac{3\xi(X) - 4\xi(X - \Delta X) + \xi(X - 2\Delta X)}{2\Delta X}, \tag{2.3.1.19}$$

$$\frac{\partial \xi(Y^\pm)}{\partial Y^\pm} = \frac{\xi(Y^\pm + \Delta Y^\pm) - \xi(Y^\pm - \Delta Y^\pm)}{2\Delta Y^\pm}, \tag{2.3.1.20}$$

where ξ is a representative function.

Provided the solution is known at $X - 2\Delta X$ and $X - \Delta X$ the momentum equations at the next X-station are written in the form

$$a_j^\pm U_{j+1}^{\pm c} + b_j^\pm U_j^{c\pm} + c_j^\pm U_{j-1}^{c\pm} = d_j^\pm \tag{2.3.1.21}$$

with the coefficients given by

$$a_j^- = \frac{V_j^{-p}\Delta Y^-}{2F^p} - \frac{\nu^-}{(F^p)^2}, \quad b_j^- = \frac{3U_j^{-p}\Delta Y^-}{2\Delta X} + \frac{2\nu^-}{(F^p)^2}, \tag{2.3.1.22a}$$

$$c_j^- = -\frac{V_j^{-p}\Delta Y^-}{2F^p} - \frac{\nu^-}{(F^p)^2}, \tag{2.3.1.22b}$$

$$d_j^- = (\Delta Y^-)^2 \left(-\frac{1}{\rho^-}\frac{dP^-}{dX} + \frac{U_j^{-p}}{2\Delta X}\left(\frac{4U_j^{-2} - U_j^{-1}}{2\Delta X}\right)\right), \tag{2.3.1.22c}$$

$$a_j^+ = \frac{V_j^{+p}\Delta Y^+}{2} - 1, \qquad b_j^+ = \frac{3U_j^{+p}\Delta Y^{+2}}{2\Delta X} + 2,$$

$$c_j^+ = -\frac{V_j^{+p}\Delta Y^+}{2} - 1, \quad d_j^+ = (\Delta Y^+)^2 \left(-\frac{dP^+}{dX} + \frac{U_j^{+p}}{2\Delta X}\left(\frac{4U_j^{+2} + U_j^{+1}}{2\Delta X}\right)\right), \tag{2.3.1.22d}$$

where the superscripts $p, 2, 1$ and subscript j represent, respectively, the predictor value for the current X- station, the value at the $X - \Delta X$ and at $X - 2\Delta X$ and the $Y^{\pm}$ position. Omitting references to the specific fluid layer, to calculate the new values for U, V, F, the function U^c is written in the form

$$U^c_{j+1} = p_j U^c_j + q_j \tag{2.3.1.23}$$

which upon substitution into (2.3.1.21) gives

$$p_{j-1} = \frac{-c_j}{a_j p_j + b_j} \quad q_{j-1} = \frac{d_j - a_j q_j}{a_j p_j + b_j} \tag{2.3.1.24}$$

From the boundary conditions, (2.3.1.10), (2.3.1.4), along with the condition of continuity in $U^{\pm}$ at the interface we find

$$p^-_{jmax^- - 1} = 0, \quad q^-_{jmax^- - 1} = U^c_{int}, \quad U^-_1 = 0, \quad U^+_1 = U^c_{int}. \tag{2.3.1.25}$$

For the problem in boundary layer flow in §2.1 the far-field conditions require

$$p^+_{jmax^+ - 1} = 0, \quad q^+_{jmax^+ - 1} = 1, \tag{2.3.1.26a}$$

and for the triple deck problem described in §2.3 we have

$$p^+_{jmax^+ - 1} = 1, \quad q^+_{jmax^+ - 1} = \Delta Y^+, \tag{2.3.1.26b}$$

where the subscripts $jmax^+, jmax^-, int$ refer to values being taken at the final points in Y^+, Y^- and at the interface, respectively. V^c is then found using the incompressibility conditions (2.3.1.9), (2.3.1.3) which have also been discretized using the two- and three-point difference forms (2.3.1.19), (2.3.1.20).

To begin the solution procedure, guesses are made for the interfacial velocity and position U_{int}, F at the new $X-$station, together with a predicted velocity distribution $U^{\pm p}$, $V^{\pm p}$ across the flow. Then the relations (2.3.1.21) -(2.3.1.25) with the appropriate far-field condition, (2.3.1.26a) or (2.3.1.26b) are used to calculate the 'corrector' velocities $U^{\pm c}$, $V^{\pm c}$. This procedure is carried out with three pairs of initial guesses for the interfacial speeds and positions. Two functions representing interfacial boundary conditions, A and B defined as

$$A(U_{int}, F) = U^c_{int} F^c_X - V^c_{int}, \quad B(U_{int}, F) = \mu^-(U^-_{Y-})_{int} - (U^+_{Y+})_{int} \tag{2.3.1.27}$$

are used to calculate corrector values for U_{int}, F with two-point Newton iterations aimed at satisfying the conditions $A = 0$, $B = 0$ and the whole procedure is iterated until a convergence criterion,

$$\Delta U \ll \epsilon_1 \quad \Delta F \ll \epsilon_1, \tag{2.3.1.28}$$

is satisfied, where ϵ_1 is a chosen tolerance, typically of $O(10^{-6})$.

2.3.2 Results

Having established a credible model for the two-fluid flow, within the film and for a comparable depth within the boundary layer fluid, we look at the various parameters which influence the onset of the Goldstein singularity/flow breakdown for flow over an obstacle. For the purposes of the numerical calculations the obstacle was defined to be

$$H(X) = h_0 e^{-X^2}, \quad -\infty < X < \infty. \tag{2.3.2.1}$$

The first and most obvious parameter is h_0, the hump size coefficient. The velocity profile in the film can be written in the form

$$U^- = \lambda^- Y^- + h_0 \bar{U}^-, \tag{2.3.2.2}$$

and since the flow breaks down where $\partial U^-/\partial Y^- \to 0$, we expect the height h_0 to be important, especially close to the wall where the correction $\bar{U}^-$ is likely to have its greatest influence. Looking at our figures 2:2 and 2:3 we see that the slope of the skin friction approaches the Goldstein singularity, through the marginal singularity where $\partial U^-/\partial Y^-(0) \to 0$, as the obstacle height, $|h_0|$, is increased. Graphs of the comparative hump effects are shown in figs 2:2(b)-(e), for a system of water in the film and an equal mixture of silicone oil V2 and 1-2-3-4-tetrahydronaphtalene in the boundary layer, with the parameters taken from Pouliquen, Chomaz & Huerre (1994) as an example of a real dynamical system, and in Figs 2:3(a),(b) for a homogeneous system. The other factors which can affect the onset of the marginal singularity are, ρ^-, ν^-, $\bar{\gamma}$, $\bar{Fr}$ and $\bar{a}$, and Table 2:1 shows how the variation of these parameters affects flow breakdown within the obstacle range $-0.5 < h_0 < 0.5$.

Starting with the effect of the density ratios on flow separation, it was found that if the film fluid is less dense than that in the boundary layer then separation is retarded, whilst denser films cause separation for smaller obstacles. This is because the shear is reduced in a denser film fluid and vice versa and so a film coating of a less dense fluid will cause an otherwise separating flow to remain attached.

Introduction of surface tension into the system appears to enhance flow reversal as does an increased gravitational influence, $\bar{Fr} \neq \infty$. As with density, less viscous fluids in the film do not cause separated flows for the same obstacle height as the equivalent homogeneous system, whilst more viscous fluids in the film have the opposite effect, enhancing separation.

The final parameter, the non-dimensional film thickness, does not appear to affect the behaviour of the system in terms of flow reversal, at least not for the chosen values of $\bar{a}$, although it must be remembered that the assumption has been made in the scaling of the problem that the film thickness remains within the viscous sublayer of the triple deck formulation. No internal separation of the type found in Sychev (1980), Elliott, Smith, Cowley (1993), Timoshin (1996) was encountered in the cases studied here, with all failures of the numerical method, i.e. the occurrence of singularities, being caused by zero wall shear.

Leaving separation aside, and concentrating on flows whose streamwise velocity profiles return to their original linear form far downstream, we turn to the graphs of the displacement function $\bar{A}(\bar{x})$ and the skin friction for a given obstacle and two fluid system. Figs 2:2(b),(e) and 2:3(a),(b) show intervals of x with decreasing wall shear but increased displacement and hence the likelihood of inflexion points developing in the velocity profiles fig 2:4(a),(b), which will facilitate Rayleigh instability. This will be examined in the next section.

2.4 Inviscid instabilities in film-coated flows

It was noted in §2.3.2 that the flow may become unstable to inviscid shorter-scale Rayleigh-like instabilities. If we write $\bar{L} = LRe^{-\frac{3}{8}}$ as the lengthscale of the boundary

layer flow over an obstacle on the triple-deck scale, with L representing the obstacle length, then the new disturbance lengthscale scale L_w is taken as

$$\bar{L}^{1/3}Re^{-\frac{1}{4}} \leq L_w \ll \bar{L}^{1/3} \tag{2.4.1}$$

i.e. short compared to the triple deck scale but at least as long as the characteristic Rayleigh scale $O(Re^{-5/8})$. First we examine the case $Re^{-\frac{1}{4}}\bar{L}^{1/3} \ll L_w$, from which we obtain a long-wave (in terms of the film thickness) integral condition for the disturbance phase speed c. We then examine disturbances with $L_w = Re^{-\frac{1}{4}}\bar{L}^{1/3}$, variations of the pressure term in y then affect the flow and instability is governed by the full inviscid Rayleigh equation.

We begin with an analytical examination of both regimes, solving for a slightly perturbed two shear streamwise linear velocity profile, such as that generated by the flow over a shallow obstacle, to obtain the disturbance growth rate explicitly. The results are then compared with those obtained numerically using a discrete iterative method for the full Rayleigh problem, as outlined in a subsequent section, on the profiles calculated in §2.3.2.

2.4.1 The long-wave instability

We introduce small temporal and spatial wave perturburbations, $O(\delta)$, to the velocities and pressure fields and define the wave as

$$E = \exp\left[ik\left(\frac{1}{L_w}\bar{x} - \frac{c}{L_w}\bar{t}\right)\right]. \tag{2.4.1.1}$$

With the governing equations given by (2.3.4)-(2.3.11) we write the velocities and pressure as

$$\bar{u}^{\pm} = U^{\pm}(\bar{y}) + \delta(\bar{u}_1^{\pm}E + c.c.) + ... \tag{2.4.1.2}$$

$$\bar{v}^{\pm} = ... + \frac{\delta}{L_w}(\bar{v}_1^{\pm}E + c.c.) + ... \tag{2.4.1.3}$$

$$\bar{p}^{\pm} = ... + \delta(\bar{p}_1^{\pm}E + c.c.) + ... \tag{2.4.1.4}$$

which lead to the relation

$$(U^{\pm} - c)\bar{v}_{1\bar{y}\bar{y}}^{\pm} = U_{\bar{y}\bar{y}}^{\pm}\bar{v}_1^{\pm}. \tag{2.4.1.5}$$

The boundary conditions at the wall, infinity and an interfacial condition relating the normal velocity and pressure in the film to that in the boundary layer complete the problem formulation:

$$\bar{v}^-(\bar{y}=0)=0\,,\ \frac{\partial \bar{v}^+}{\partial \bar{y}}(\bar{y}=\infty)=0 \tag{2.4.1.6}$$

and at $\bar{y}=\bar{f}$

$$(U^{\pm}-c)\begin{pmatrix}(\bar{v}_1^+U_{\bar{y}}{}^+-(U^+-c)\bar{v}_{1\bar{y}}^+)\\ -\rho^-((\bar{v}_1^-U_{\bar{y}}{}^--(U^--c)\bar{v}_{1\bar{y}}^-))\end{pmatrix}=\hat{\gamma}k^2\bar{v}_1^{\pm} \tag{2.4.1.7}$$

where $\hat{\gamma}=\gamma/L_w^2$. We solve this and find a general solution in the form

$$\bar{v}_1^+=Q_1^+(U^+-c)\int_{\infty}^{\bar{y}}\frac{1}{(U^+-c)^2}d\bar{y}+Q_2^+(U^+-c) \tag{2.4.1.8}$$

$$\bar{v}_1^-=Q_1^-(U^--c)\int_0^{\bar{f}}\frac{1}{(U^--c)^2}d\bar{y}+Q_2^-(U^--c) \tag{2.4.1.9}$$

The boundary conditions (2.4.1.6) force $Q_2^-=0$, $Q_2^+=0$, from the interfacial condition (2.4.1.7) we obtain the relation

$$Q_1^+=\rho^-Q_1^--\frac{\hat{\gamma}k^2}{U_s-c}, \tag{2.4.1.10}$$

and the normalization condition $\bar{v}_1(\bar{f})=1$ gives

$$Q_1^-=\left((U_s-c)\int_0^{\bar{f}}\frac{1}{(U^--c)^2}d\bar{y}\right)^{-1}. \tag{2.4.1.11}$$

Continuity of $\bar{v}$ at the interface then gives the dispersion relation

$$\rho^-\left(1-\frac{\hat{\gamma}k^2}{\rho^-}\int_0^{\bar{f}}\frac{1}{(U^--c)^2}d\bar{y}\right)\int_{\bar{f}}^{\infty}\frac{1}{(U^+-c)^2}d\bar{y}+\int_0^{\bar{f}}\frac{1}{(U^--c)^2}d\bar{y}=0. \tag{2.4.1.12}$$

2.4.2 Rayleigh-wave instability

In this subsection we attain an asymptotic approximation to the disturbance phase speed c from the inviscid Rayleigh equation for disturbances with wavelength $L_w=Re^{-1/4}\bar{L}^{1/3}$.

We start by taking an analytic approximation to the streamwise base velocity profiles $U(\bar{y})$ in (2.4.1.2), writing them as piecewise-linear profiles with a small correction $O(\epsilon)$, here proportional to base flow departure from linearity and hence the hump size h_0, where $\delta \ll \epsilon \ll 1$. A similar analysis applies to the enhanced mean flow profiles examined in Chapter 4. We also expand the interfacial position in powers of ϵ, and write

$$U^+ = \bar{y} - \bar{a} + U_s + \epsilon G^+(\bar{y}), \tag{2.4.2.1}$$

$$U^- = \lambda^- \bar{y} + \epsilon G^-(\bar{y}), \tag{2.4.2.2}$$

$$\bar{f} = \bar{a} + \epsilon f_1. \tag{2.4.2.3}$$

Here $\bar{a}$ is the unperturbed interface position, $\lambda^- = 1/\mu^-$, $U_s = \lambda^- \bar{a}$ and we normalize the flow such that at the interface $\bar{u}^{\pm}(\bar{y} = \bar{f}) = U_s + \epsilon$.

The shortened lengthscale, compared with that of §2.4.1, leads to the full inviscid Rayleigh equation for the normal velocities $\bar{v}_1^{\pm}$,

$$(U^{\pm} - c)(\bar{v}_{1\bar{y}\bar{y}}^{\pm} - k^2 \bar{v}_1^{\pm}) = U_{\bar{y}\bar{y}}{}^{\pm} \bar{v}_1^{\pm} \tag{2.4.2.4}$$

with boundary conditions

$$\bar{v}^-(\bar{y} = 0) = 0\,, \; \bar{v}^+(\bar{y} = \infty) = 0. \tag{2.4.2.5}$$

Expanding $\bar{v}_1$ and c in powers of ϵ

$$\bar{v}_1 = V_0 + \epsilon V_1 + ..., \;\; c = c_0 + \epsilon c_1 + ..., \tag{2.4.2.6}$$

and, substituting into (2.4.2.4), we find the solutions

$$V_0^+ = e^{k(\bar{a} - \bar{y})}, \;\; V_0^- = \frac{\sinh k\bar{y}}{\sinh k\bar{a}}. \tag{2.4.2.7}$$

We take these solutions, which satisfy the boundary conditions (2.4.2.5) and put them into the interfacial condition (2.4.1.7). Linearizing and taking terms $O(1)$ gives a dispersion relation for the leading order phase speed c_0,

$$(U_s - c_0)\left(1 + k(U_s - c_0) - \rho^-(\lambda^- - (U_s - c_0)k \coth k\bar{a})\right) = \hat{\gamma}k^2, \tag{2.4.2.8}$$

which has the solution

$$c_0 = U_s + \frac{1-\rho^-\lambda^- \pm \sqrt{(1-\rho^-\lambda^-)^2 + 4\hat{\gamma}k^3(1+\rho^-\coth k\bar{a})}}{2k(1+\rho^-\coth k\bar{a})}. \qquad (2.4.2.9)$$

We note that, for all positive wavenumbers k, c_0 is real. In particular in the case of no surface tension

$$c_0 = U_s \text{ or } c_0 = U_s + \frac{1-\rho^-\lambda^-}{k(1+\rho^-\coth k\bar{a})}. \qquad (2.4.2.10)$$

The growth rate will be found from c_1. The next order terms, $O(\epsilon)$, in (2.4.2.4) give

$$(U^\pm - c_0)(V_{1\bar{y}\bar{y}}^\pm - k^2 V_1^\pm) = G_{\bar{y}\bar{y}}^\pm V_0^\pm, \qquad (2.4.2.11)$$

and we look for a solution of the form $V_1^\pm(\bar{y}) = F^\pm(\bar{y})V_0^\pm(\bar{y})$. The solution now depends on the position of a critical layer which forms at $\bar{y} = \bar{y}_c$ where $U(\bar{y}_c) = c_0$. We will first pursue the case of a critical layer in the film. We have

for $\bar{y} < \bar{y}_c$,

$$V_1^- = V_0^- \int_0^{\bar{y}} \frac{1}{V_0^{-2}} \left\{ \int_0^{\hat{s}} \frac{G_{ss}^- V_0^{-2}}{\lambda^- s - c_0} ds \right\} d\hat{s} + b_1 V_0^-; \qquad (2.4.2.12)$$

for $\bar{y} > \bar{y}_c$,

$$V_1^- = V_0^- \int_{\bar{y}_c}^{\bar{y}} \frac{1}{V_0^{-2}} \left\{ \int_{\bar{y}_c}^{\hat{s}} \frac{G_{ss}^- V_0^{-2}}{\lambda^- s - c_0} ds \right\} d\hat{s} + V_0^- \int_{\bar{y}_c}^{\bar{y}} \frac{b_2}{V_0^{-2}} dy + b_3 V_0^-, \qquad (2.4.2.13)$$

$$V_1^+ = V_0^+ \int_{\bar{a}}^{\bar{y}} \frac{1}{V_0^{+2}} \left\{ \int_{\bar{a}}^{\hat{s}} \frac{G_{ss}^+ V_0^{+2}}{\bar{y} - \bar{a} + U_s - c_0} ds \right\} d\hat{s} + V_0^+ \int_{\bar{a}}^{\bar{y}} \frac{b_4}{V_0^{+2}} dy + b_5 V_0^+, \qquad (2.4.2.14)$$

where the b_i's are constants of integration. The solution for V_1^- contains a term of the form

$$V_1^- = B(\bar{y} - \bar{y}_c)\ln|\bar{y} - \bar{y}_c| + ..., \qquad (2.4.2.15)$$

and as $\bar{y} \to \bar{y}_c$

$$V_{1\bar{y}\bar{y}}^- = \frac{B}{\bar{y} - \bar{y}_c} + ... = \frac{(G_{\bar{y}\bar{y}}^- V_0^-)_{\bar{y}=\bar{y}_c}}{\lambda^-(\bar{y} - c_0/\lambda^-)}, \qquad (2.4.2.16)$$

so $B = G^-_{\bar{y}\bar{y}}(\bar{y}_c)V_0^-(\bar{y}_c)/\lambda^-$ and $\bar{y}_c = c_0/\lambda^-$. The jump in the derivative of the normal velocity across the critical layer is proportional to the logarithmic term in (2.4.2.15),

$$V^-_{1\bar{y}}(\bar{y}_c^+) - V^-_{1\bar{y}}(\bar{y}_c^-) = i\pi B = \frac{i\pi G^-_{\bar{y}\bar{y}}(\bar{y}_c)V_0^-(\bar{y}_c)}{\lambda^-}, \tag{2.4.2.17}$$

where $\bar{y}_c^{\pm}$ denotes the limit value taken as $y \to \bar{y}_c$ above or below the critical layer. The remaining boundary conditions are the normalization (2.4.1.6) at the interface, the continuity in the normal velocity across the critical layer, i.e.

$$V_1^{\pm}(\bar{a}) = -f_1 V^{\pm}_{0\bar{y}}(\bar{a}), \;\; V_1^-(\bar{y}_c^+) = V_1^-(\bar{y}_c^-), \tag{2.4.2.18}$$

and the pressure jump across the interface written as (2.4.1.7).

Our aim is to find the imaginary part of c_1 so we need concentrate only on the imaginary parts of the relations (2.4.2.18). Solving for V_{1i} using the boundary conditions (2.4.2.17), (2.4.2.18), substituting into (2.4.1.7), and taking the imaginary terms $O(\epsilon)$ we find

$$c_{1i} = \frac{\rho^-(U_s - c_0)^3\pi G^-_{\bar{y}\bar{y}}(\bar{y}_c)\sinh^2 k\bar{y}_c}{\lambda^- \sinh k\bar{a}((U_s - c_0)^2 k(\sinh k\bar{a} + \rho^- \cosh k\bar{a}) - \hat{\gamma}k^2 \sinh k\bar{a})} \tag{2.4.2.19}$$

In the case of the critical layer occurring in the boundary layer we find

$$c_{1i} = \frac{(U_s - c_0)^3\pi G^+_{\bar{y}\bar{y}}(\bar{y}_c)e^{k(\bar{a}-\bar{y}_c)}}{(\sinh k(\bar{y}_c - \bar{a}) + \cosh k(\bar{y}_c - \bar{a}))(k(1 + \rho^- \coth ka)(U_s - c_0)^2 - \hat{\gamma}k^2)}. \tag{2.4.2.20}$$

Taking the long wave limit $k \to 0$, the imaginary part of the complex wave speed is given by the formula

$$c_{1i} \to \frac{G^-_{\bar{y}\bar{y}}(\bar{y}_c)\pi(U_s - c_0)\bar{y}_c^2}{\lambda^-\bar{a}} \text{ if } \bar{y}_c < \bar{a}, \tag{2.4.2.21}$$

$$c_{1i} \to \frac{G^+_{\bar{y}\bar{y}}(\bar{y}_c)\pi(U_s - c_0)}{\rho^-\bar{a}^{-1}} \text{ if } \bar{y}_c > \bar{a}. \tag{2.4.2.22}$$

We see that positive curvature at the critical height $\bar{y} = \bar{y}_c$ provokes instability if $\bar{y}_c < \bar{a}$, and conversely negative curvature is destabilizing if $\bar{y}_c > \bar{a}$.

We also examine the short wave limit $k \to \infty$ of (2.4.2.19), (2.4.2.20) to see if instability persists. For both the case of the critical layer in the film and the critical layer in the boundary layer flow we see that surface tension becomes the dominant effect for short waves and the disturbance is strongly stabilized. If there is no surface tension $c_{1i} \to 0^+$ as $k \to \infty$.

2.4.3 The numerical Rayleigh instability calculation

Here we solve the problem numerically for the boundary layer and film flows with boundary conditions (2.4.1.6), (2.4.1.7) with the velocity profile, $\bar{u}^{\pm}$, and interfacial position $\bar{f}$ calculated using the numerical method of §2.3.1. Our numerical method uses the inviscid Rayleigh equation (2.4.2.4) rewritten with the second order derivative in the normal velocity $V^{\pm}$ in a central difference form,

$$V^{\pm}_{j+1} + a_j V^{\pm}_j + V^{\pm}_{j-1} = 0, \tag{2.4.3.1}$$

where

$$a_j = -\left(2 + k^2(\Delta\bar{y}^{\pm})^2 + \frac{U''_j(\Delta\bar{y}^{\pm})^2}{U_j - c}\right), \tag{2.4.3.2}$$

with the base velocity profiles written in terms of the original vertical co-ordinate $\bar{y}$, subscripts j corresponding to the discrete $\bar{y}$ position and primes denoting differentiation with respect to $\bar{y}$. We write

$$V^{\pm}_{j-1} = p^{\pm}_j V^{\pm}_j + q^{\pm}_j, \tag{2.4.3.3}$$

which, upon substitution into (2.4.3.1), gives us the formulae

$$p^{\pm}_{j+1} = -\frac{1}{p^{\pm}_j + a^{\pm}_j}, \quad q^{\pm}_{j+1} = -\frac{q^{\pm}_j}{p^{\pm}_j + a^{\pm}_j}, \tag{2.4.3.4}$$

with the boundary conditions (2.4.1.6), (2.4.1.7) requiring

$$q^+_2 = 1, \quad p^+_2 = 0, \quad V^+_{jmax^+} = 0, \tag{2.4.3.5}$$

$$q^-_2 = 0, \quad p^-_2 = 0, \quad V^-_{jmax^-} = 1. \tag{2.4.3.6}$$

For any given k we make a guess on c, calculate the appropriate normal velocity profile as above, and perform Newton iterations to satisfy the interfacial condition (2.4.1.7).

It is important to note that there are three constraints on the effectiveness of this method, numerically speaking. The first is due to the normalization in V at the interface. If the non-dimensional initial film thickness, $\bar{a}$, is too large then the numerical method for the film will struggle, as the solution decays away from the wall. This in effect means the entire solution is being distorted to satisfy our condition $V^{\pm} = 1$ at the interface.

The film thickness also affects the size of the phase speed c which, as was seen in the analytic approximation where $c_i = c_i(c_0)$, affects the magnitude of the instability. Further, the method is unable to detect weak instabilities, $c_i = O(10^{-4})$, as these would require a grid size smaller than our minimum computationally reasonable stepsize, 2.5×10^{-3}.

The final constraint is the value for the numerical far field. In the numerical solution for the viscous sublayer flow over an obstacle, a value of $\bar{y}_\infty = \bar{y}_i + 10$ was used since, at this point, the gradient of the profile was always unaffected by the obstacle (i.e. it remained constant). This was sufficient then for a calculation of the profiles over the length of the obstacle, a more distant far field would have just increased calculation time unnecessarily. However for the instability calculations, especially at small wavenumbers, the numerical method requires a more distant far field such that a smooth and natural decay of the normal velocity can occur. To overcome this problem the profiles calculated for the flow over the hump were linearly extended such that the far field became $\bar{y}_\infty = \bar{y}_i + 80$. This number was reached upon comparison of values calculated for the phase speed c for different values of $\bar{y}_\infty$. At this distance our solutions did not alter before the third decimal place, an accuracy we were willing to accept in return for a realistic computational time.

2.4.4 Numerical results for instability

We examine the case of non-separating flows which remain attached over the entire obstacle. We will compare the instabilities of two fluid flows over a given obstacle with those of its homogeneous counterpart.

We start by examining the displacement function $\bar{A}(\bar{x})$ and the skin friction for a given obstacle and two fluid flow, figs 2:2(a),(d), and 2:3(a),(b). We observe intervals of x with decreasing wall shear but increased displacement and hence the likelihood of inflexion points , see figs 2:4(a),(b), developing in our velocity profiles, which will facilitate Rayleigh instability.

We discovered, as in Bodonyi & Smith (1985), Tutty & Cowley (1986), that for homogeneous flow inflexional profiles are not necessarily sufficient for instability. We examined an obstacle of a slightly different form but, as was seen in Bodonyi & Smith, there appears to be a minimum obstacle height required to instigate instability. In the next section we will examine the stability of a flow with parameters based on two realistic fluids but first we compare the stability of a two fluid system with its homogeneous counterpart taking into account the effect of varying parameters in the two fluid system. We look for instabilities in the flow over an obstacle of height $h = 0.35$, close to the greatest common obstacle height for which both flows remain attached. When the skin friction $(\partial U^-/\partial \bar{y}(\bar{y} = 0))$ becomes zero a singularity occurs in the slope of the skin friction and displacement and the flow scheme breaksdown, indicating a strong effect of the obstacle on the flow development. Using the size of the skin friction as an indication of the effect on flow development we compared a variety of homogeneous and two fluid systems. Even for two fluid systems with a larger skin friction than the homogeneous counterpart we find instabilities where none could be found for the single fluid case. When we examine the hump size $(h_0 = 0.42)$ which causes the minimum non-zero, i.e. calculable, skin friction for a homogeneous system, we did eventually find a small pocket of instability for the single fluid system, fig 2:5, but this was still much smaller than that of a two fluid counterpart with $\rho^- = 2$, $\nu^- = 0.5$, $a = 2$ which had much larger minimum skin

friction.

These instabilities, which we found analytically in equations (2.4.2.20), (2.4.2.19), appear to be present for many non-homogeneous flows. We can have confidence in the validity of the asymptotic approximation to the growth rate when we see how well it correlates with our numerical solution, see figs 2:6(e). We will show that the presence of a film significantly enhances the instabilities present in homogeneous flows over an obstacle, with instability found for arbritrarily shallow obstacles in two-fluid flow.

2.4.5 A particular two-fluid flow

In this subsection we examine the instabilities present for a particular two fluid flow, that of water in the film and an equal mixture of silicone oil V2 and 1-2-3-4-tetrahydronaphtalene in the boundary layer, as used in §2.3.2, and compare the results with its homogeneous counterpart over an obstacle of height $h_0 = 0.35$. In the two fluid case strong instabilities were discovered at the x-stations before and after the hump maximum, in the areas of greatest velocity variation, as the flow first accelerates and later deccelerates. With a film thickness $a = 2$, we discover, in the area leading up to the hump, that the profiles are unstable to long waves which decay in strength and become much shorter as the hump is approached (figs 2:6(a),(b)). At the crest of the hump no instabilities could be found. Soon after the crest the profiles again become susceptible to long wave instabilities, and the strength of these instabilities decreases and their wavelengths become shorter, until eventually no unstable waves were detected for profiles further downstream (figs 2:6(c),(d)). Comparison of the numerical calculations, using the full numerical solution, for long waves $k \to 0$ is favourable with the numerical solutions calculated using the integral condition (2.4.1.12). Further comparisons were made with the analytic main approximation to the growth rate (2.4.2.19) and, as shown in fig 2:6(e), there appears to be a fair degree of correlation.

For homogeneous flow over the same obstacle height no instabilities could be found. It was unclear however if this lack of instability in the homogeneous flow was

realistic or simply a failing in the numerical method to detect small instabilities. To establish which of these eventualities was more likely we devised a 'merged' profile, where the two calculated profiles for each distinct station were combined in the ratio

$$U = (1-\lambda)U_{\mathrm{w/oil}} + \lambda U_{\mathrm{hg}},\ 0 \leq \lambda \leq 1, \tag{2.4.5.1}$$

where the subscripts 'w/oil' and 'hg' refer to water/oil, and homogeneous flows respectively. As can be seen in figs 2.7 (a)-(c), there do not appear to be any significant instabilities in the homogeneous flow. Fig 2:7(c) shows the value for the growth rate calculated using the integral condition (2.4.1.12), for varying values of λ.

2.5 The condensed flow problem

In this section we consider a different regime of the previous problem, that of condensed flow over a short surface mounted hump on a film coated wall, of length $L \ll 1$ on the triple deck scale. The formulation is exactly the same as §2.3 but with the hump size and displacement written as

$$h \sim L^{\frac{1}{3}},\ A \sim L^{5/3}. \tag{2.5.1}$$

The obstacle size is the minimum required to illicit a non-linear response from the viscous layer, and now the far field boundary condition for the viscous sublayer, (2.2.5), is replaced by

$$\bar{u}^{+} = \bar{y} + \bar{h}(\bar{x}) - \bar{a} + U_s, \quad \text{as } \bar{y} \to \infty \tag{2.5.2}$$

The problem is rescaled as in §2.3.1, using (2.3.1.1), (2.3.1.7) and we obtain the governing equations (2.3.1.2), (2.3.1.3) and (2.3.1.8), (2.3.1.9). Taking the derivative

with respect to $Y^{\pm}$ of these equations we find

$$U^{+}\frac{\partial W^{+}}{\partial X}+V^{+}\frac{\partial W^{+}}{\partial Y^{+}} = \frac{\partial^{2}W^{+}}{\partial Y^{+2}}, \tag{2.5.3}$$

$$\frac{\partial U^{+}}{\partial X}+\frac{\partial V^{+}}{\partial Y^{+}} = 0, \tag{2.5.4}$$

$$U^{-}\frac{\partial W^{-}}{\partial X}+\frac{V^{-}}{F}\frac{\partial W^{-}}{\partial Y^{-}}-U^{-}\frac{W^{-}}{F}\frac{\partial F}{\delta X} = \frac{\nu^{-}}{F^{2}}\frac{\partial^{2}W^{-}}{\partial Y^{-2}}, \tag{2.5.5}$$

$$\frac{\partial FU^{-}}{\partial X}+\frac{\partial V^{-}}{\partial Y^{-}} = 0, \tag{2.5.6}$$

where $W^{\pm}=\partial U^{\pm}/\partial Y^{\pm}$, and the boundary conditions are

$$W^{+}\rightarrow 1 \text{ as } Y^{+}\rightarrow\infty, \tag{2.5.7}$$

and, at the interface $Y^{+}=0, Y^{-}=1$

$$\mu^{-}W^{-}/F=W^{+}, \tag{2.5.8}$$

$$\frac{F^{2}}{\nu^{-}\rho^{-}}\left((\rho^{-}-1)U^{+}\frac{\partial U^{+}}{\partial X}+\frac{\partial W^{+}}{\partial Y^{+}}+\frac{(\rho^{-}-1)}{\bar{F}r}\frac{\partial F}{\partial X}-\bar{\gamma}\frac{\partial^{3}F}{\partial X^{3}}\right)=\frac{\partial W^{-}}{\partial Y^{-}}. \tag{2.5.9}$$

The last of these conditions comes from the equations (2.5.3), (2.5.5) at the interface at $Y^{+}=0$, $Y^{-}=1$ where

$$V^{\pm}=0,\quad \frac{\partial P^{+}}{\partial X}-\frac{\partial P^{-}}{\partial X}=\bar{\gamma}\frac{\partial^{3}F}{\partial X^{3}}+\frac{(1-\rho^{-})}{\bar{F}r}\frac{\partial F}{\partial X}, \tag{2.5.10}$$

$$U^{+}=U^{-},\quad \frac{\partial U^{+}}{\partial X}=\frac{\partial U^{-}}{\partial X} \tag{2.5.11}$$

and is required to fully specify the problem.

2.5.1 The numerical method

Exactly as before we discretize (2.5.3)-(2.5.9), writing derivatives with respect to X in a three point backward difference form and those in Y in a central difference form. In the same manner as in §2.3.1, $W^{\pm}$ is written as

$$W^{+}_{j+1,i}=P^{+}_{j}W^{+}_{j,i}+Q^{+}_{j},\quad W^{-}_{j-1,i}=P^{-}_{j}W^{-}_{j,i}+Q^{-}_{j}, \tag{2.5.1.1}$$

and the governing equations (2.5.3), (2.5.5) are written as

$$a_j^{\pm} W_{j+1,i} + b_j^{\pm} W_{j,i}^{\pm} + c_j^{\pm} W_{j-1,i}^{\pm} = d_j^{\pm}, \tag{2.5.1.2}$$

with the index i, j indicating the discretized $X, Y^{\pm}$ positions respectively and the constants $a_j^{\pm}, b_j^{\pm}, c_j^{\pm}, d_j^{\pm}$, when $U_{j,i}^{\pm} > 0$, given by

$$a_j^+ = 1 - \frac{V_{j,i}^+ \Delta Y^+}{2}, \quad b_j^+ = -2 - \frac{3U_{j,i}^+ \Delta Y^{+2}}{2\Delta X}, \quad c_j^+ = 2 + \frac{V_{j,i}^+ \Delta Y^+}{2} \tag{2.5.1.3}$$

$$d_j^+ = \frac{(W_{j,i-2}^+ - 4W_{j,i-1}^+)\Delta Y^{+2} U_{j,i}^+}{2\Delta X}, \quad a_j^- = 1 - \frac{V_{j,i}^- \Delta Y^- F_i}{2\nu^-}, \tag{2.5.1.4}$$

$$b_j^- = -2 - \frac{3U_{j,i}^- \Delta Y^{-2} F_i^2}{2\Delta X \nu^-} + \frac{(3F_i - 4F_{i-1} + F_{i-2})\Delta Y^{-2} F_i}{2\Delta X \nu^-}, \tag{2.5.1.5}$$

$$c_j^- = 1 + \frac{V_{j,i}^- \Delta Y^- F_i}{2\nu^-}, \quad d_j^- = \frac{(W_{j,i-2}^- - 4W_{j,i-1}^-)\Delta Y^{-2} F_i^2 U_{j,i}^-}{2\Delta X \nu^-}, \tag{2.5.1.6}$$

with $\Delta X, \Delta Y^{\pm}$ representing the stepsize in the $X, Y^{\pm}$ directions. In the regions of reversed flow then the backward difference for X-derivatives is exchanged for a three-point forward difference, i.e. if $U_{j,i}^- < 0$ then

$$b_j^- = -2 + \frac{3\Delta Y^{-2} F_i^2 U_{j,i}^-}{2\Delta \nu^-} + \frac{(3F_i - 4F_{i-1} + F_{i-2})\Delta Y^{-2} F_i}{2\Delta X \nu^-}, \tag{2.5.1.7}$$

$$d_j^- = \frac{(W_{j,i+1}^- - (W_{j,i+2}^-)\Delta Y^{-2} F_i^2 U_{j,i}^-)}{2\Delta X \nu^-}, \tag{2.5.1.8}$$

and similarly if $U_{j,i}^+ < 0$,

$$b_j^+ = -2 + \frac{3U_{j,i}^+}{\Delta Y^{+2}}, \quad d_j^+ = \frac{(4W_{j,i+1}^+ - W_{j,i+2}^+)\Delta Y^{+2} U_{j,i}^+}{2\Delta X}. \tag{2.5.1.9}$$

The difference representations of the momentum equations, (2.5.1.2) along with (2.5.1.1) give the relations

$$P_{j+1}^- = \frac{-a_j^-}{c_j^- P_j^- + b_j^-}, \quad Q_{j+1}^- = \frac{d_j^- - c_j^- Q_j^-}{c_j^- P_j^- + b_j^-}, \tag{2.5.1.10}$$

$$P_{j-1}^+ = \frac{-c_j^+}{a_j^+ P_j^+ + b_j^+}, \quad Q_{j-1}^+ = \frac{d_j^+ - a_j^+ Q_j^+}{a_j^+ P_j^+ + b_j^+}, \tag{2.5.1.11}$$

and so the boundary conditions become

$$U_{max,i}^- = Y - \bar{a} + U_s + F_i + H_i, \quad V_{1,i}^+ = V_{max,i}^- = 0, \tag{2.5.1.12}$$

$$\frac{\mu^-}{F_i} W_{max,i}^+ = W_{1,i}^+, \quad W_{max}^- = \frac{W_{\text{num}}^-}{W_{\text{denom}}^-}, \tag{2.5.1.13}$$

where

$$W^-_{\rm num} = \frac{F_i^2 Q_1^+}{\mu^- \Delta Y^+} + \frac{Q^-_{max}}{\Delta Y^-} + \frac{F_i^2(\rho^- - 1)U^+_{1,i}(3U^+_{1,i} - 4U^+_{1,i-1} + U^+_{1,i-2})}{2\mu^- \Delta X} + \frac{(\rho^- - 1)(3F_i - 4F_{i-1} + F_{i-2})}{2Fr\Delta X} - \frac{\gamma(3F_{i-2} - 3F_{i-1} - F_{i-3} - F_i)}{(\Delta X)^3} \quad (2.5.1.14)$$

$$W^-_{\rm denom} = \frac{1 - P^-_{max}}{\Delta Y^-} - \frac{F_i(P_1^+ - 1)}{\Delta Y^+}. \quad (2.5.1.15)$$

We define $P^+_{max-1} = 0$, $Q^+_{max-1} = 1$ and $P_2^- = 0$, $Q_2^- = W^-_{1c,i}$ where $W^-_{1c,i}$ is the guess for $W^-_{1,i}$, initially taken to be the value at the previous X station. The same approach is taken with the problem formulation now as in §2.3.1, and we apply Newtons method, using two functions

$$A(W^-_{1,i}, F_i) = U^+_{max,i} - (Y - \bar{a} + U_s + F_i + H_i), \quad B(W^-_{1,i}, F_i) = V^+_{1,i}, \quad (2.5.1.16)$$

to satisfy $A = 0$, $B = 0$. The solution is then marched in X and for areas of reversed flow two approaches were used. The first was to make the downstream profiles $U^{\pm}$ all zero as a first guess, the FLARE approximation (Reyhner & Flügge-Lotz (1968), Smith (1982)) and then iterate globally. The second involved using downstream profiles calculated previously for an obstacle of height $h_0 - \delta h$ where h_0 is the obstacle height under investigation, with $\delta h \ll 1$, again see Smith (1982).

2.5.2 Results for condensed flow

In this subsection we examine how the different flow parameters ρ^-, μ^-, a influence the flow development. Table 2:2 shows the obstacle heights, with an error $O(0.2)$ at which the flow reversed. We see that denser fluids in the film retard flow separation due to the implicit decrease in adverse pressure gradient in the momentum equations. Stronger viscosity in the film has a similar effect, whilst the film thickness does not appear to affect the flow structure on these scales. The effects of gravity and surface tension on the hump flow were neglected. We present the profile curvatures for both a homogeneous and the two fluid flow of water and oil examined in §2.4.4 in figs 2:8(a) & (b) , over the maximum obstacle height at which we could obtain good

results for the homogeneous case, before making a stability analysis of these profiles. The regions of reversed flow ($U_{ij}^{\pm} < 0$) can be seen more clearly on a contour plot of the streamfunction ψ, where $\bar{u} = \partial\psi/\partial\bar{y}$, shown in fig 2:8c for the water/oil flow over a hump of height 2. As an accuracy test for this method, a comparison was made of our results with those calculated by F.T.Smith (1977), (for an obstacle defined by $H(X) = h_0(1-X^2)$ for the region $\mid X \mid < 1$ and zero elsewhere) and Tutty & Cowley (1986) (for an exponential profile similar to our own, $H(X) = h_0 \exp[-10X^2]$). Good agreement was found with the single fluid solutions, although our method fails for strong regions of reversed flow. We performed a stability analysis on the profiles calculated for a hump size $h_0 = 2.0$ to see their susceptibility to Rayleigh type disturbances and both long and short wave instability. Profiles at x-stations upstream of the obstacle maxima $h = h_0$, which have negative curvature (see fig 2:8a,b), were stable at all wavenumbers whilst those downstream of the obstacle maxima, where curvatures are positive, were found to be unstable. It would appear from a comparison of figs 2:9(a),(b) with figs 2:9(c),(d) that the short wave instability found in the water/oil case may be due to the presence of an interface. As for the case of long obstacles calculated previously, the instabilities found were stronger in the two fluid flow examined than in the homogeneous flow over similar obstacles. We conclude that even for short scale surface roughness the presence of a film can dramatically affect the stability and development of the flow.

2.6 Tables and figures

ρ^-	ν^-	$\overline{a}$	$\overline{\gamma}$	$\overline{g} = 1/\overline{Fr}$	Obstacle height
1.00	0.51	1.00	0	0	-
1.00	0.51	1.00	0	0	-
1.00	1.01	1.00	0	0	0.5
1.00	1.01	1.00	0	0	-0.4
1.00	1.51	1.00	0	0	0.4
1.00	1.51	1.00	0	0	-0.3
0.51	1.00	1.00	0	0	-
0.51	1.00	1.00	0	0	-0.5
1.01	1.00	1.00	0	0	0.5
1.01	1.00	1.00	0	0	-0.4
1.51	1.00	1.00	0	0	0.4
1.51	1.00	1.00	0	0	-0.3
2.00	2.00	2.00	0	0	0.2
2.00	2.00	2.00	0	0	-0.2
2.00	2.00	2.00	2	0	0.1
2.00	2.00	2.00	2	0	-0.1
2.00	2.00	2.00	0	2	–0.1
2.00	2.00	2.00	0	2	-0.1
1.20	1.20	1.01	0	0	0.4
1.20	1.20	1.01	0	0	-0.3
1.20	1.20	0.51	0	0	0.4
1.20	1.20	0.51	0	0	-0.3
1.20	1.20	0.01	0	0	0.5
1.20	1.20	0.01	0	0	-0.4

Table 2:1 A table of initial obstacle heights at which the flow scheme in §2.3 failed, i.e. where $F^{-1}\partial U^-/\partial Y^- \to 0$. The flow was calculated for obstacles in the region $|h_0| \leq 0.5$, initially for $h_0 = 0$, with a stepsize $dh = |0.1|$. A bar indicates no failure.

ν^-	ρ^-	$\bar{a}$	Obstacle separation height
1.0	0.1	5.0	1.00
1.0	0.1	5.0	-1.00
1.0	0.575	5.0	2.00
1.0	0.575	5.0	-1.60
1.0	1.05	5.0	2.40
1.0	1.05	5.0	-1.80
1.0	1.525	5.0	2.60
1.0	1.525	5.0	-2.00
0.1	1.0	5.0	1.00
0.1	1.0	5.0	-1.00
0.575	1.0	5.0	1.80
0.575	1.0	5.0	-1.40
1.05	1.0	5.0	2.40
1.05	1.0	5.0	-1.80
1.525	1.0	5.0	3.00
1.525	1.0	5.0	-2.40
2.0	1.0	5.0	3.40
2.0	1.0	5.0	-2.60
2.0	1.0	2.75	3.20
2.0	1.0	2.75	-2.40
2.0	1.0	0.5	2.40
2.0	1.0	0.5	-1.80

Table 2:2 Neglecting surface tension and gravity, values of the obstacle height h_0 at which flow reversal first occurs in the condensed flow scheme of §2.5, for various combinations of ρ^-, ν^-, $\bar{a}$.

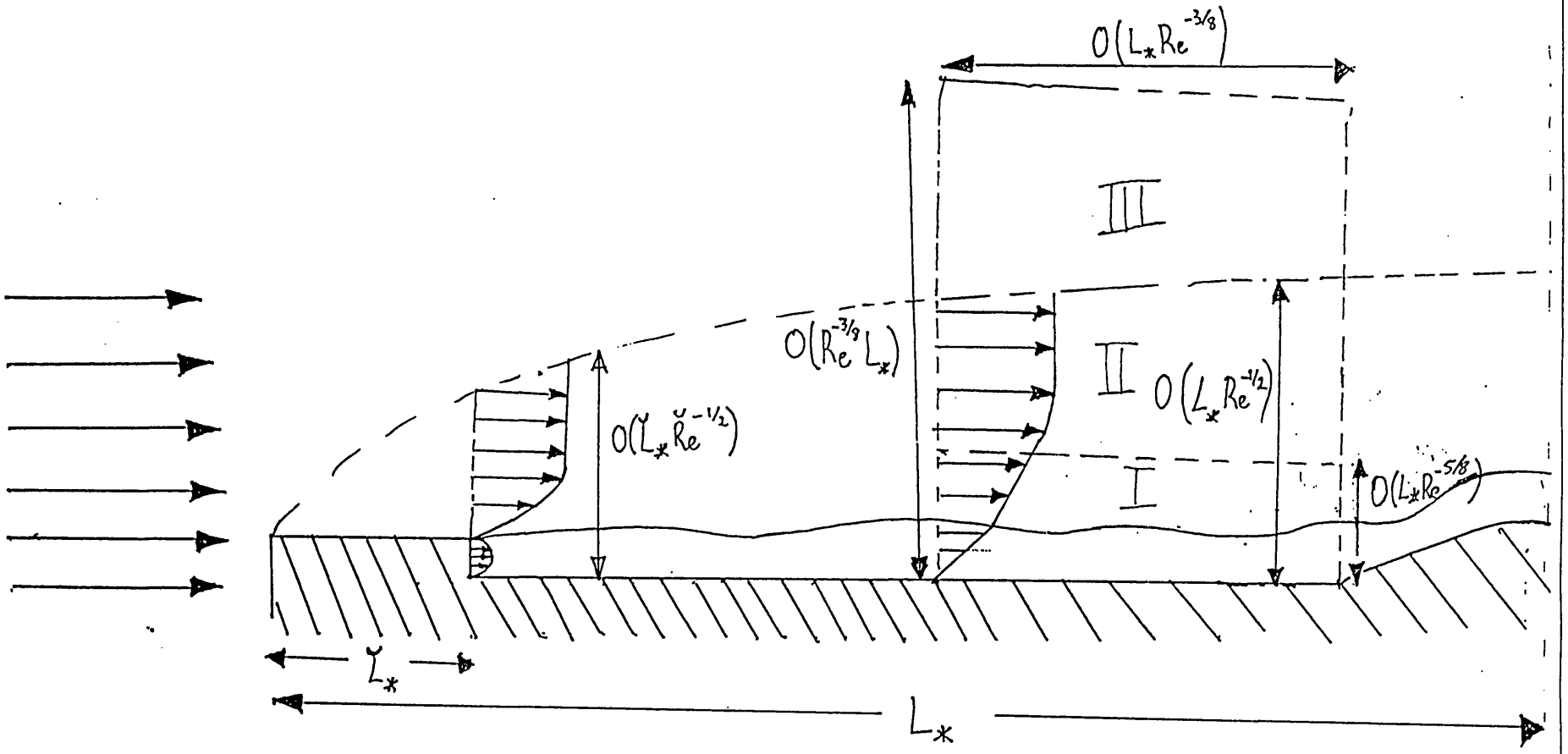

Figure 2:1. (a) The flow structure for film generation via a jet from a slot inside the boundary layer on a plate with an obstacle downstream.

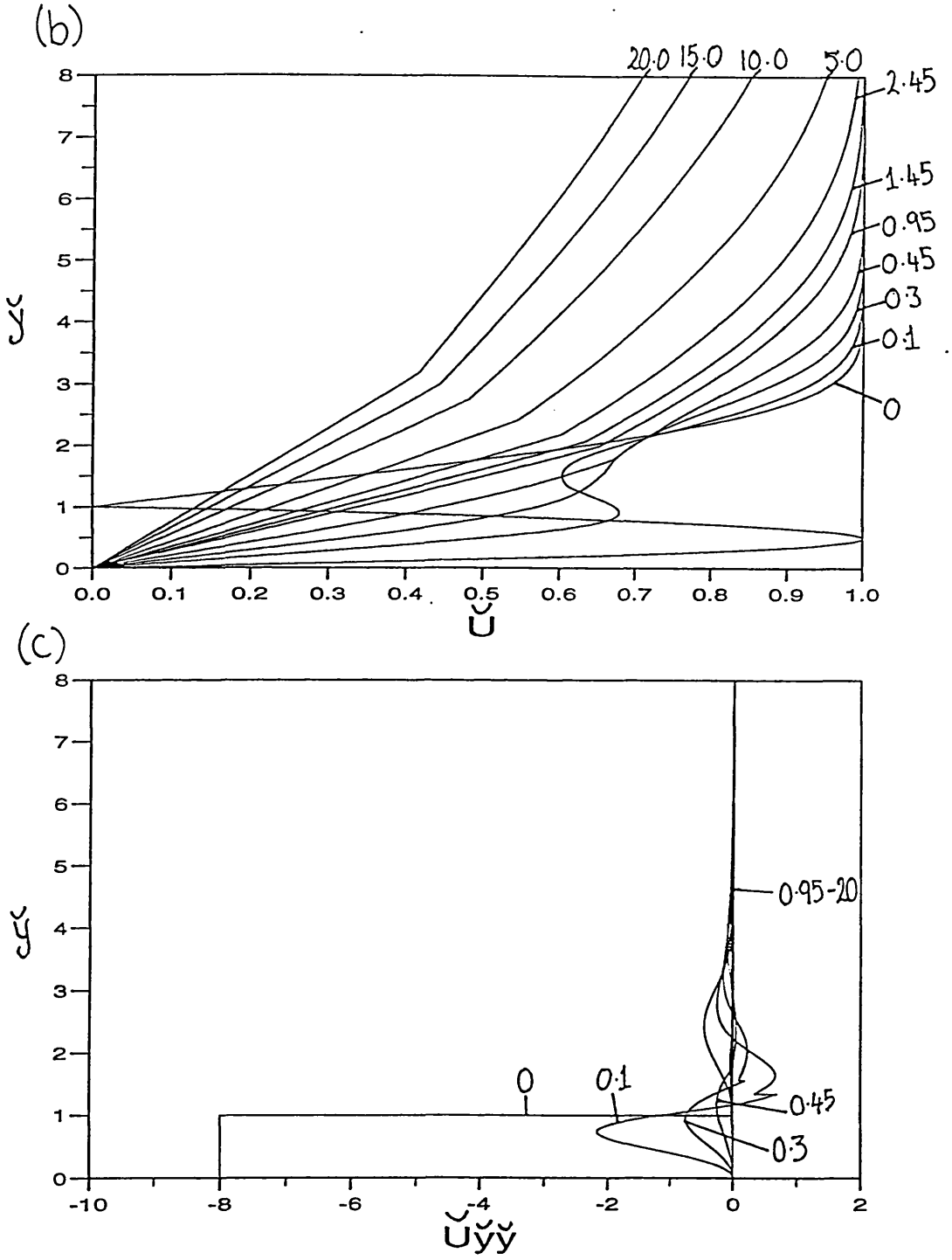

Figure2:1(b) The velocity profiles at various X-stations calculated numerically for (2.3.1.2)-(2.3.1.3), (2.3.1.8)-(2.3.1.9) with upstream profiles $U^- = 4Y(1-Y)$, in the film, and the Blasius profile, in the boundary layer fluid, with boundary conditions (2.3.1.4), (2.3.1.13) (2.3.1.16) for $\check{a} = 2$, $\rho^- = 1.087$, $\nu^- = 0.484$, $\check{\gamma} = 0$, $\check{F}r = \infty$, $h_0 = 0$ (c) The velocity profile curvature $\partial^2\check{u}/\partial\check{y}^2$ for (a)

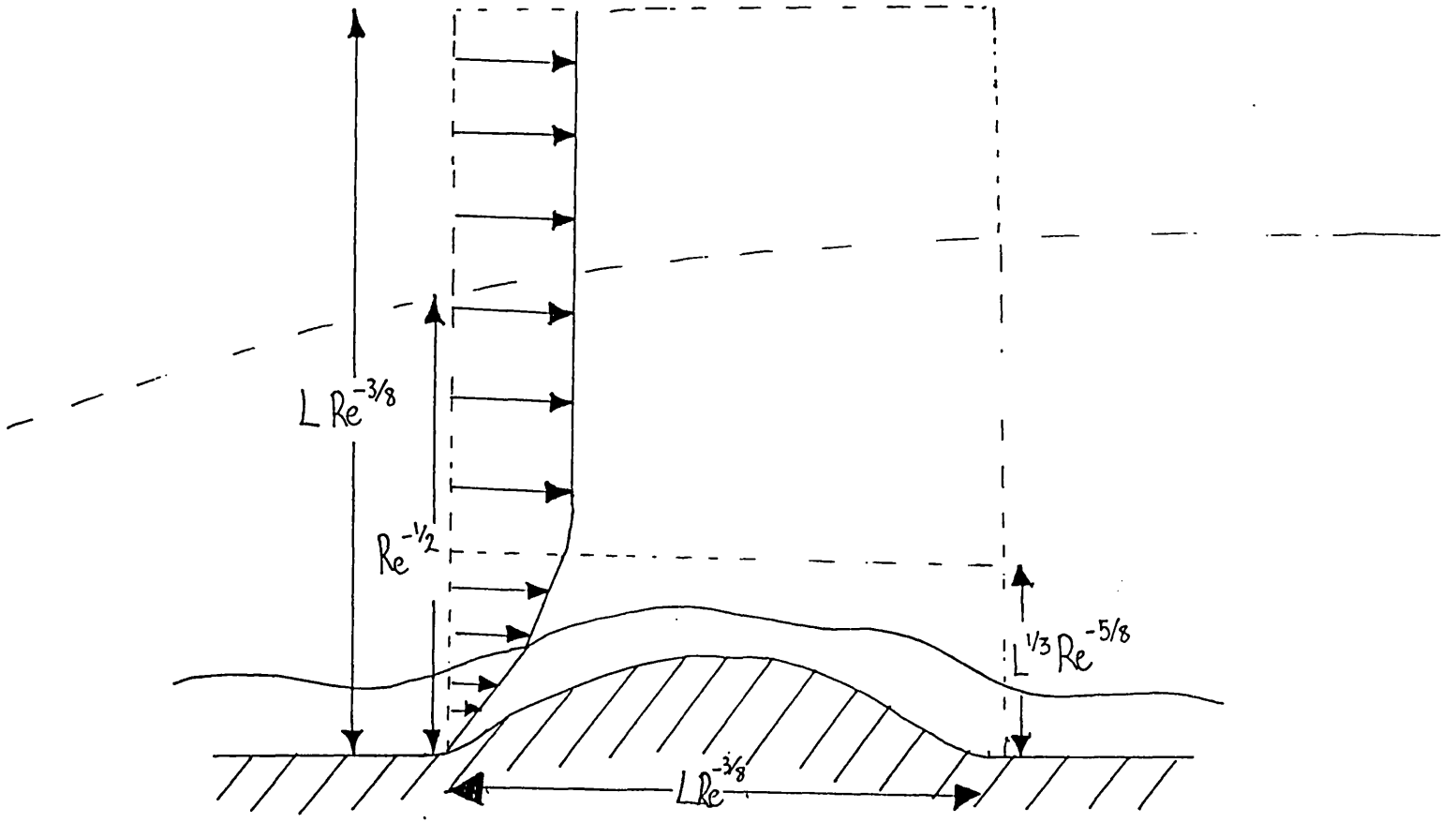

Figure 2:2. (a) The Triple-deck structure for the boundary layer flow on a film coated wall over an obstacle of nondimensional length L.

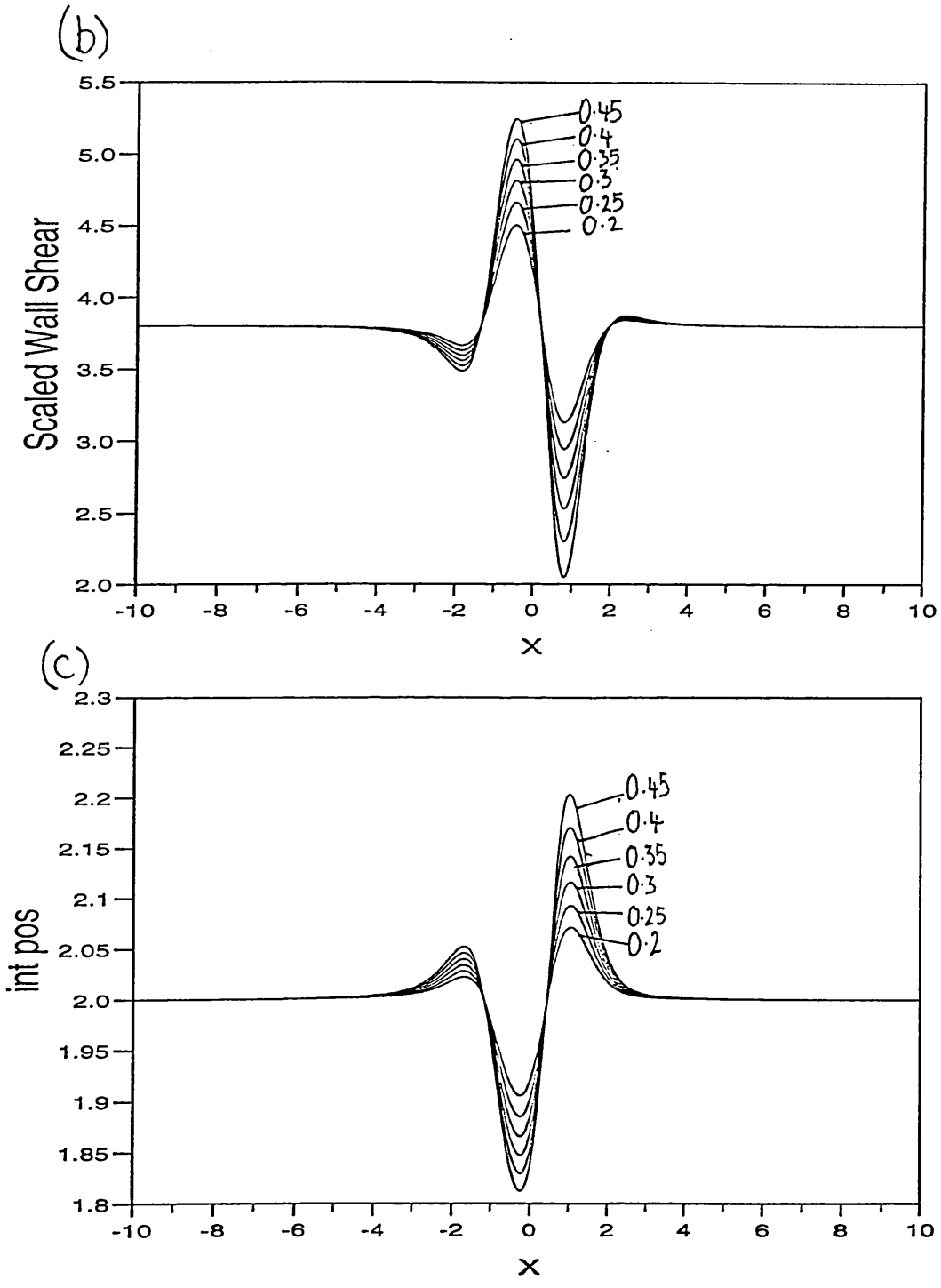

Figure 2:2 Numerical solutions for the flow scheme in (a), with initial base flow profileas given by (2.3.1.6), (2.3.1.12) and parameters $\bar{a} = 2$, $\rho^- = 1.087$, $\nu^- = 0.484$, $\bar{\gamma} = 0$, $\bar{Fr} = \infty$, for various obstacle heights:(b) The scaled wall shear $F^{-1}dU^-/dY^-(0)$ against X-station, (c) The interfacial position F against X-station.

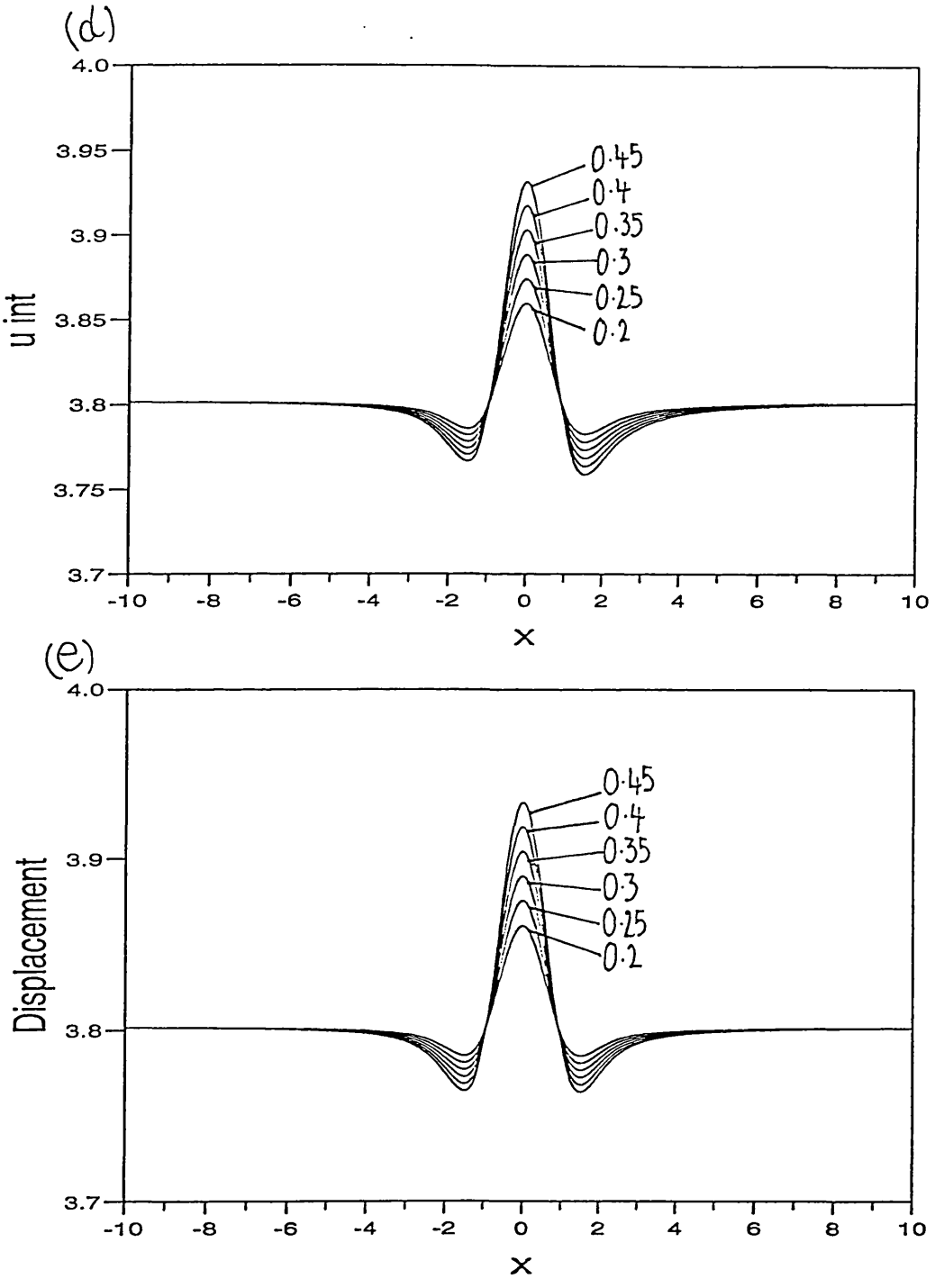

Figure 2:2. As before. (d) The interfacial speed $U^+(0)$ against X-station, (e) The displacement $\bar{A}$ against X-station.

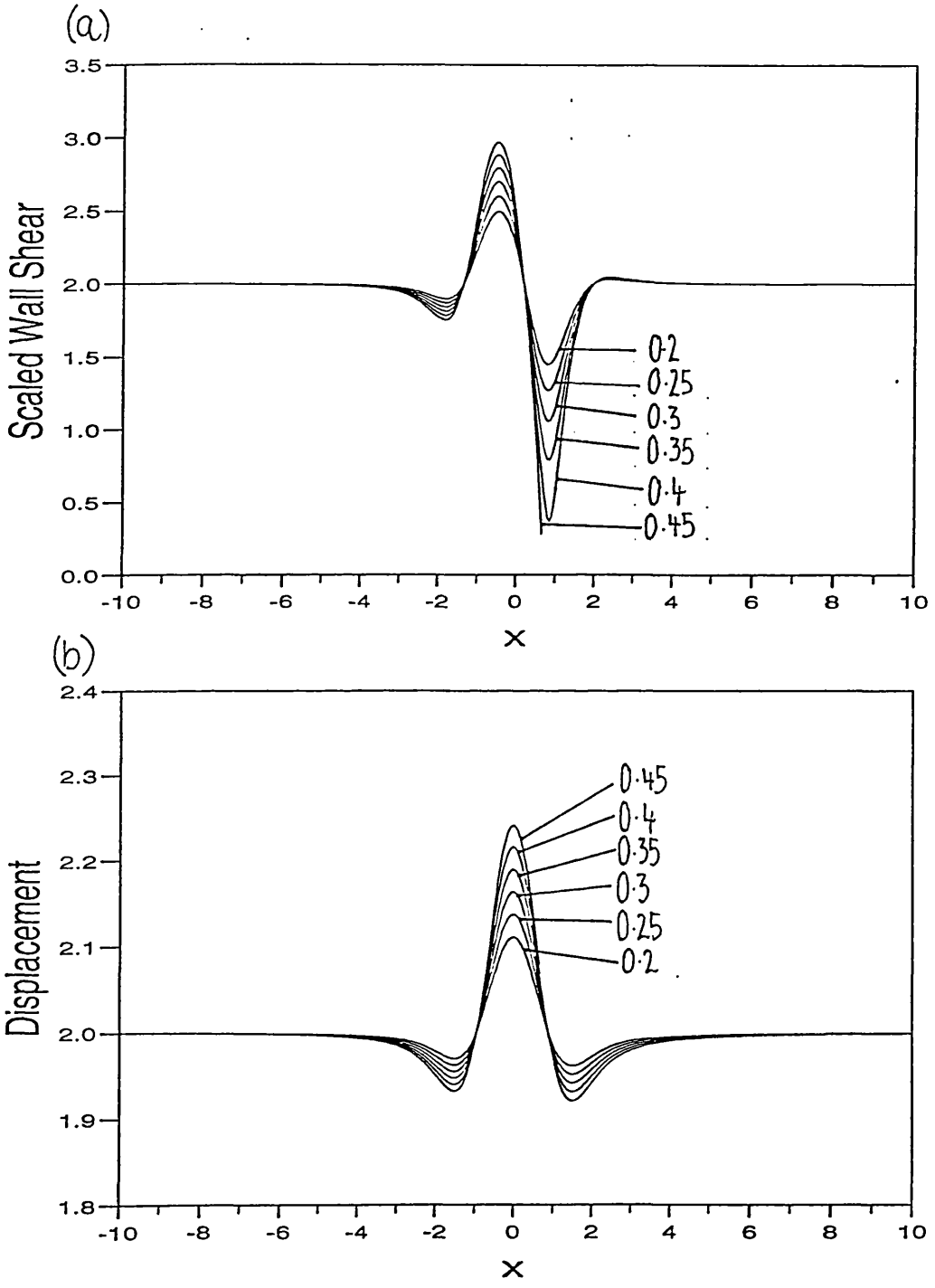

Figure 2:3. Numerical solutions as in fig 2:2 for homogeneous flow with parameters $a = 2$, $\rho^- = 1.0$, $\nu^- = 1.0$, $\bar{\gamma} = 0$, $\bar{Fr} = \infty$ for various h_0. (a) The scaled wall shear $F^{-1}dU^-/dY^-(0)$ against X-station, (b) The displacement $\bar{A}$ against X-station.

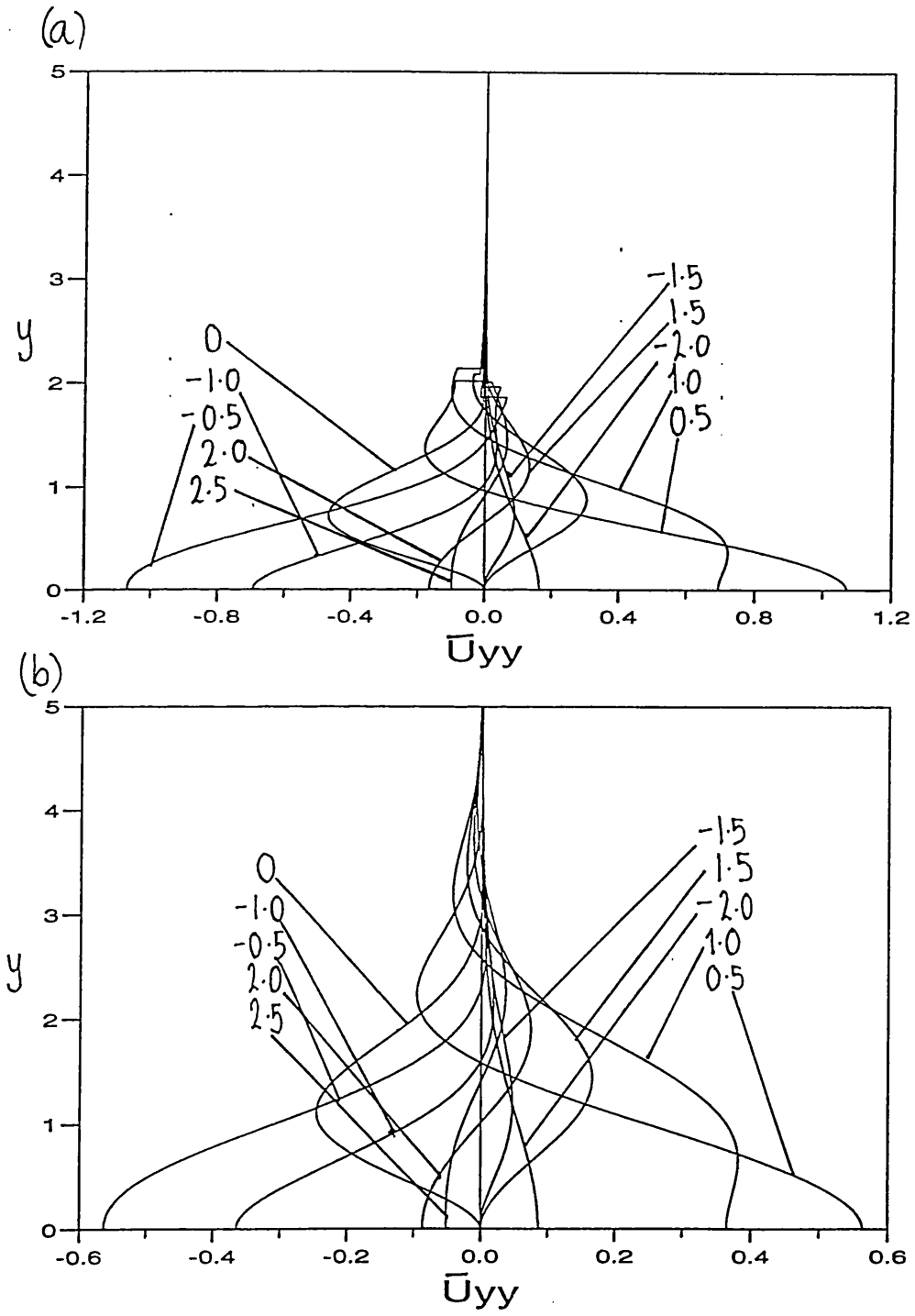

Figure 2:4. The cuvature of the velocity profiles $\bar{u}^{\pm}$ at various X-stations, $h_0 = 0.35$, $\bar{\gamma} = 0$, $\bar{Fr} = \infty$ (a) For the water/oil system $\rho^- = 1.087$, $\nu^- = 0.484$. (b) For the homogeneous system $\rho^- = \nu^- = 1$.

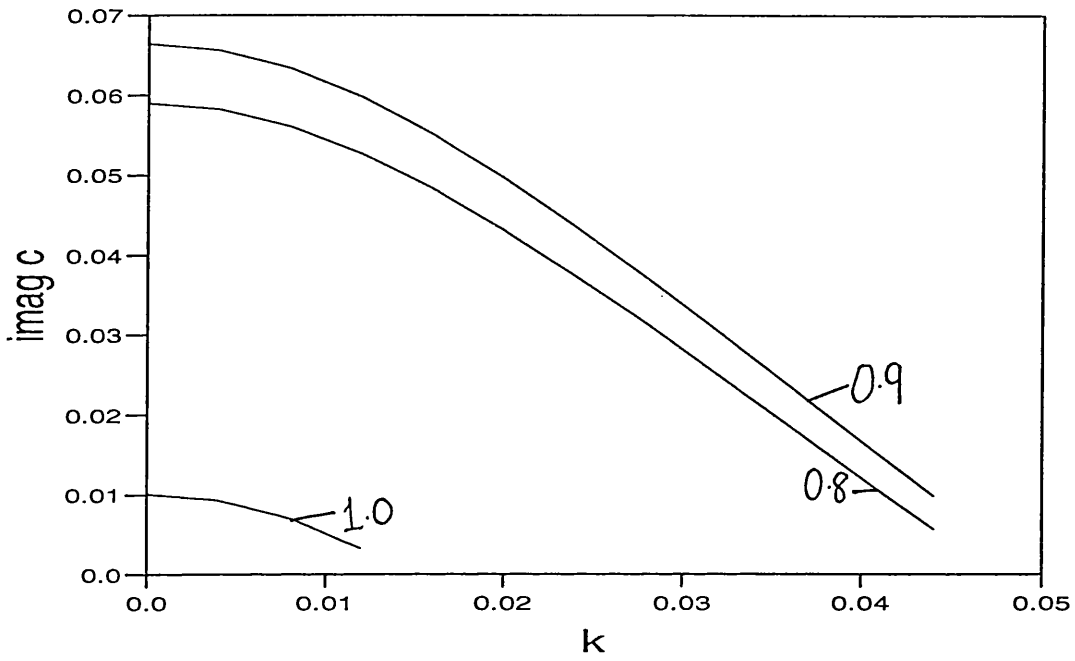

Figure 2:5. The unstable eigenvalues of (2.4.2.4), with boundary conditions (2.4.2.5), (2.4.1.7), and velocity profiles of the homogeneous flow over an obstacle height $h_0 = 0.42$, with, $\rho^- = 1.0$, $\nu^- = 1.0$, $\bar{\gamma} = 0$, $\bar{Fr} = 0$, $\bar{a} = 2.0$. Imaginary wave speed c_i versus k for profiles at various X-stations.

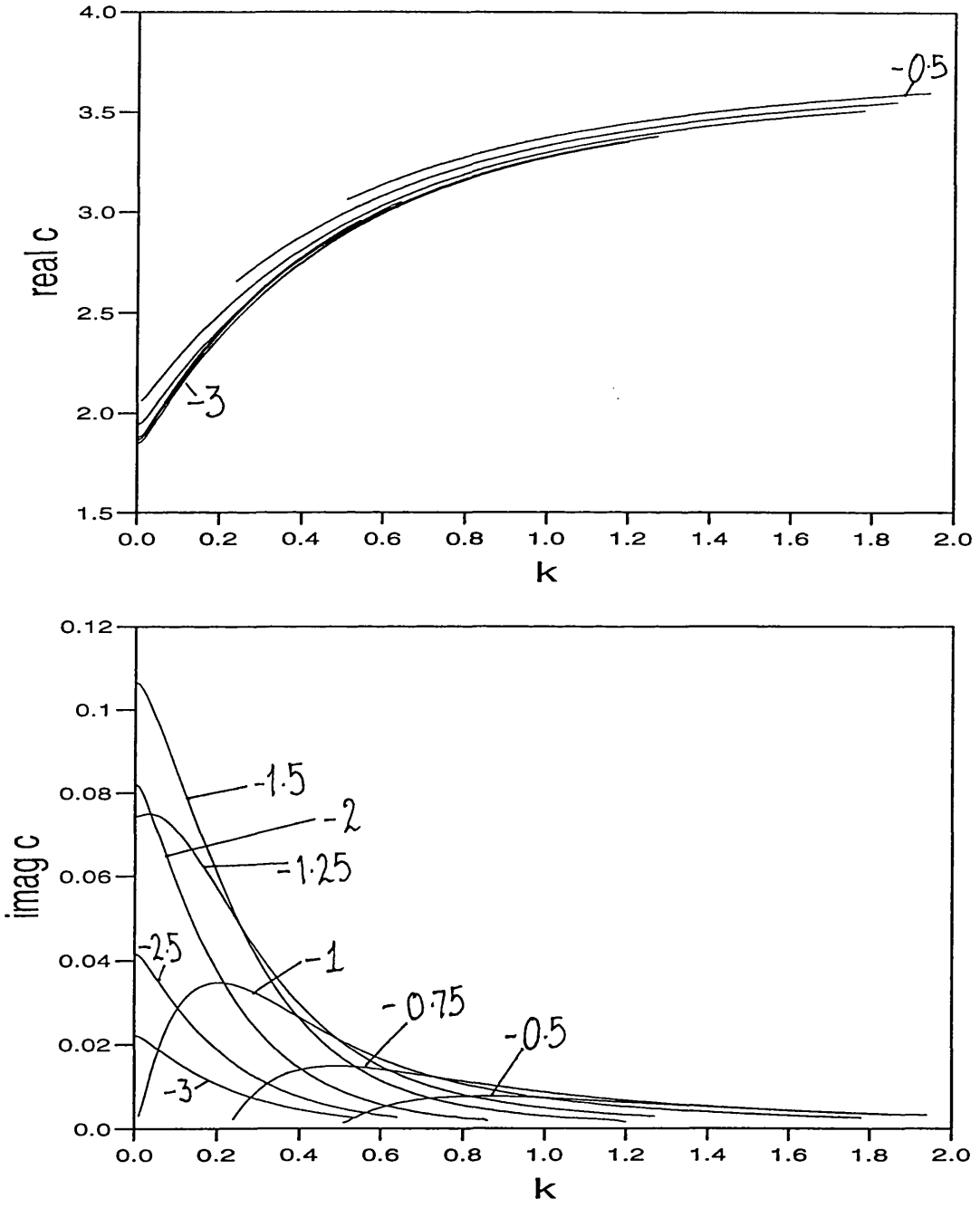

Figure 2:6. The Rayleigh instability of velocity profiles taken from flow over a hump, with $\rho^- = 1.087$, $\nu^- = 0.484$, $\bar{a} = 2.0$, $h_0 = 0.35$, $\bar{\gamma} = 0$, $\bar{Fr} = \infty$. **(a)** real phase speed c_r against k for various X-stations upstream of hump peak, **(b)** imaginary phase speed c_i with X-stations as (a)

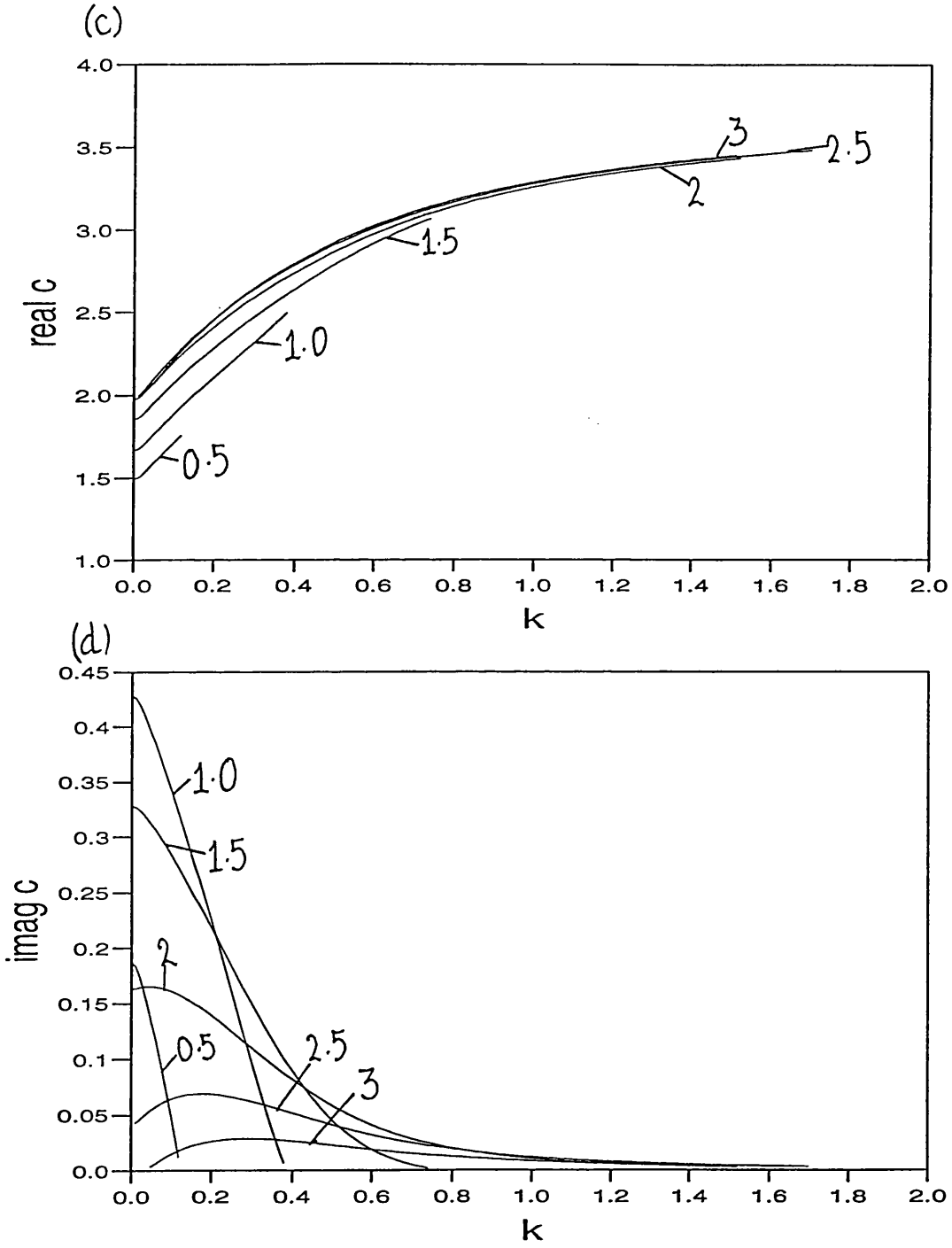

Figure 2:6. As before, (c) real phase speed c_r against k, for various X-stations downstream of hump peak, (d) imaginary phase speed c_i against k.

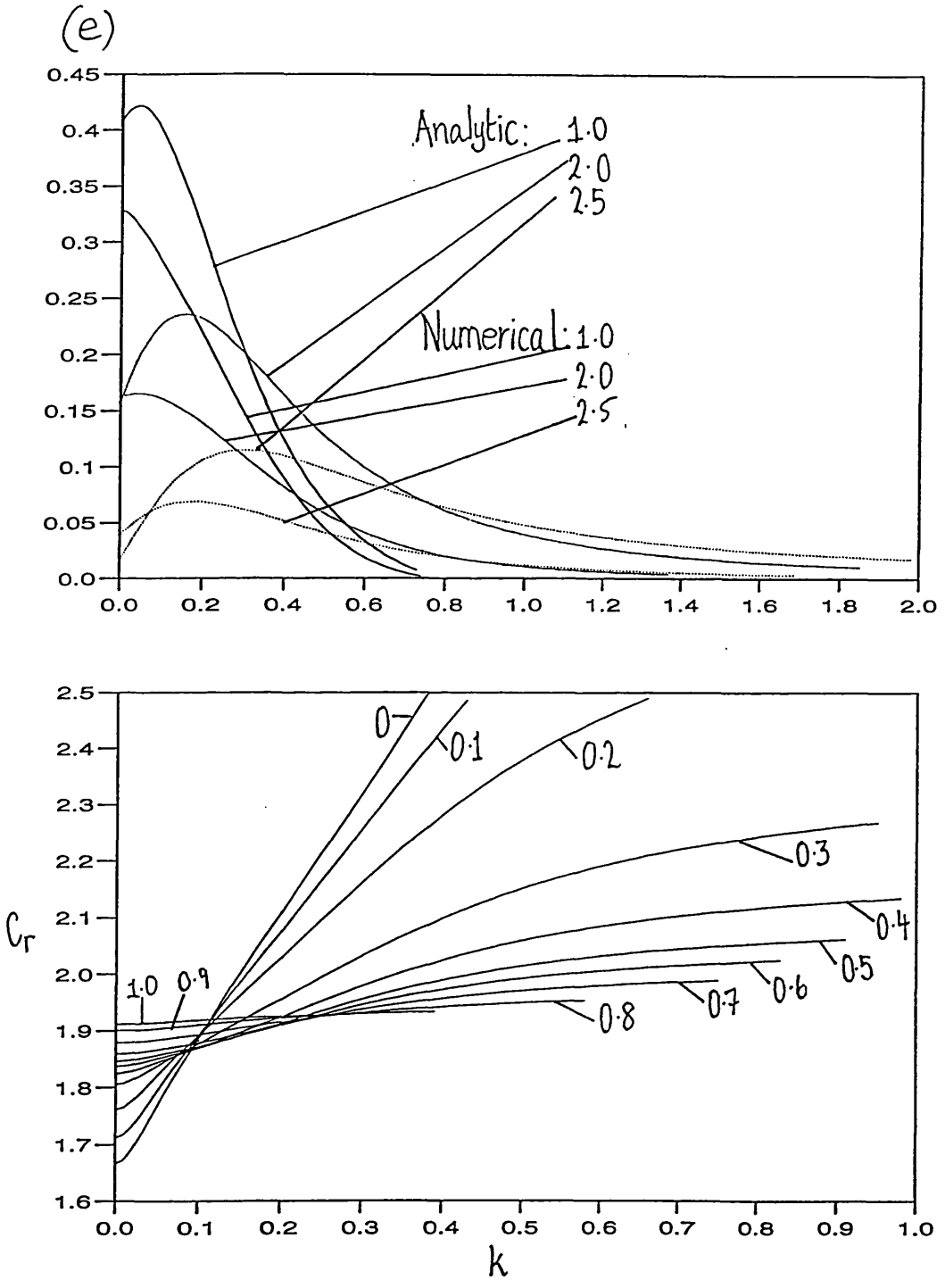

Figure 2:6. (e) Comparison of analytic solution for c_i from (2.4.2.19) with the numerical solution, for various X-stations.

Figure 2:7. The Rayleigh instability of the combined profiles in (2.4.5.1) for an obstacle of height $h_0 = 0.35$, at $X = 1$ with $\bar{\gamma} = 0$, $\bar{Fr} = \infty$, $\bar{a} = 2.0$. (a) Phase speed c_r against wavenumber k for various λ.

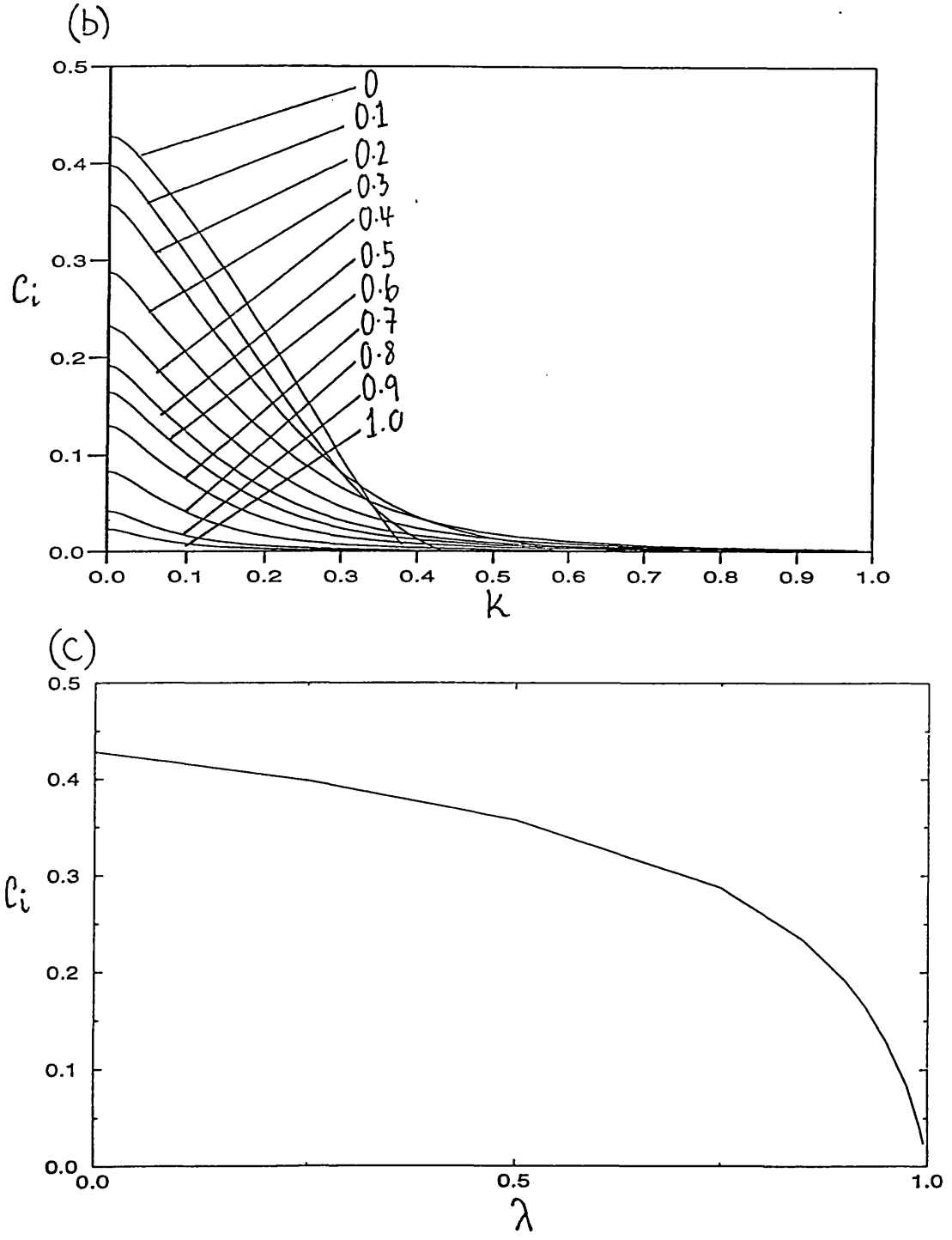

Figure 2:7. As before (b) imaginary phase speed c_i agianst k. (c) c_i against λ for $\hat{k} = 0$ calculated using (2.4.1.12).

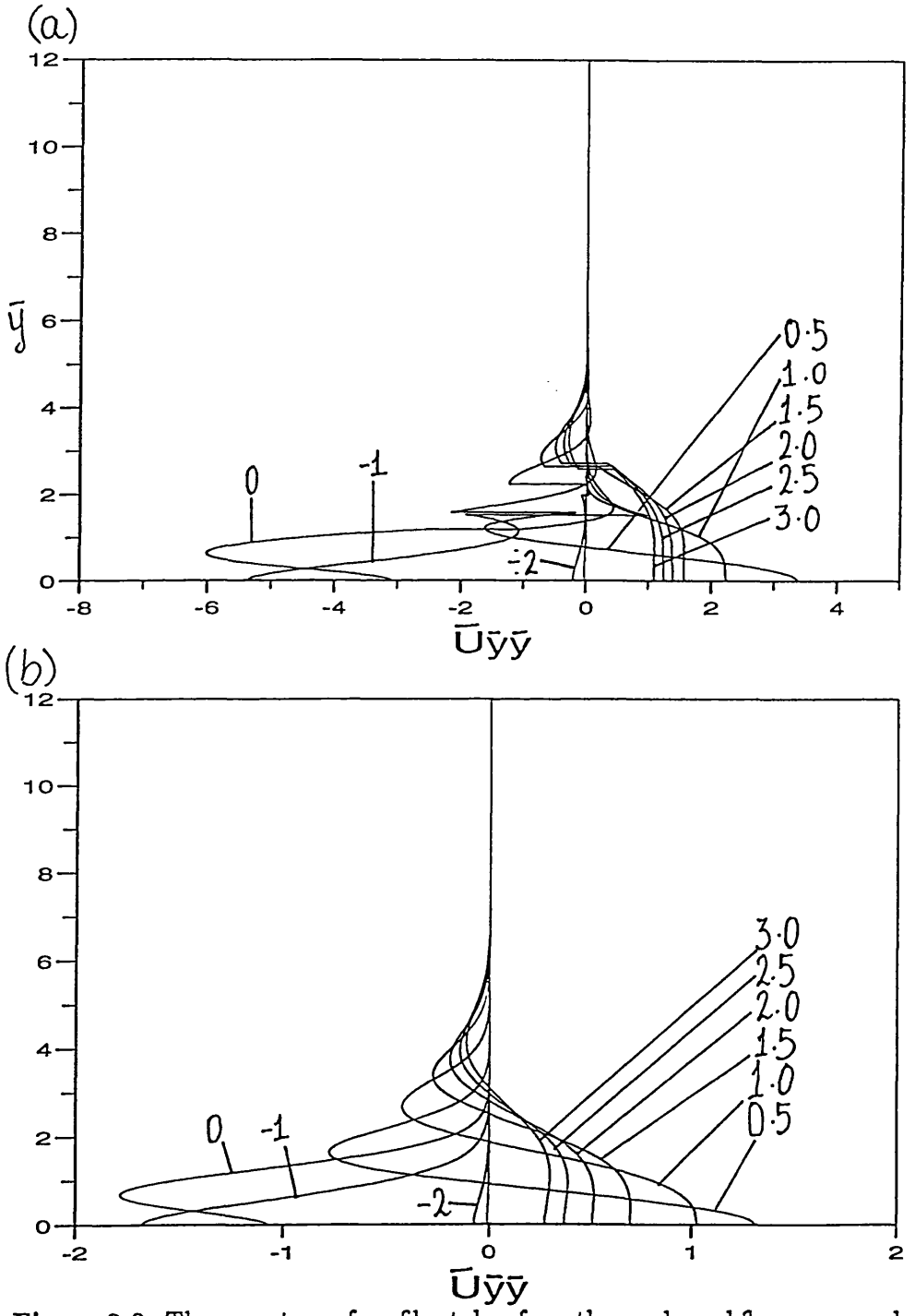

Figure 2:8. The curvature of profiles taken from the condensed flow over an obstacle of height $h_0 = 2.0$, with $\bar{\gamma} = 0$, $\bar{Fr} = \infty$, $\bar{a} = 2$. (a) for $\rho^- = 1.087$, $\nu^- = 0.484$, with $\bar{y}$ plotted against $\partial^2\bar{u}/\partial\bar{y}^2$. (b) $\bar{y}$ plotted against $\partial^2\bar{u}/\partial\bar{y}^2$ for $\rho^- = 1.0$, $\nu^- = 1.0$.

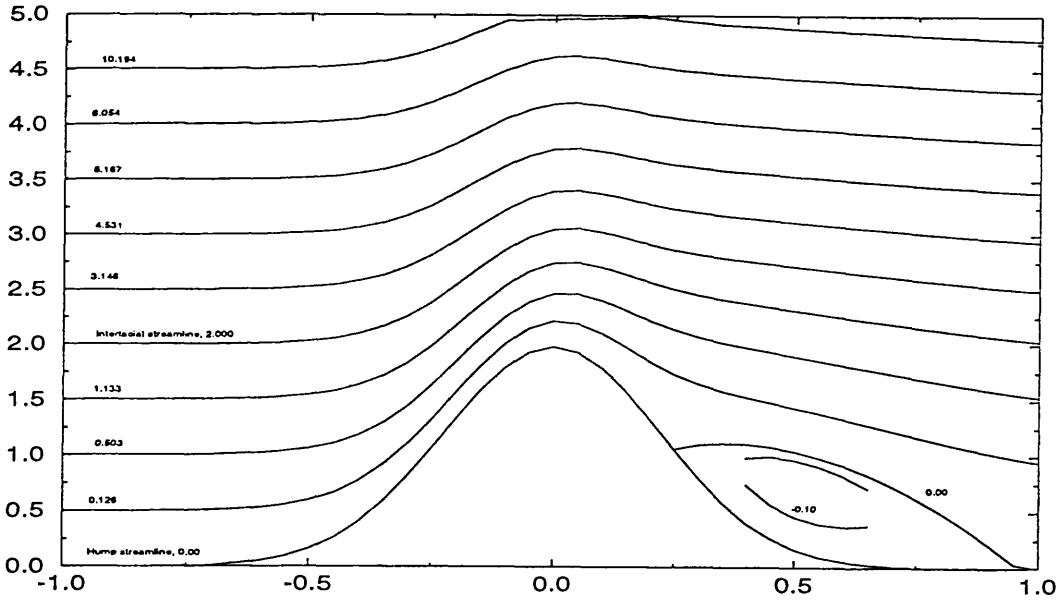

Figure 2:8 As before, (c) Contour plot of the flow in (a) for various constant values of the streamfunction ψ, indicated next to each streamline.

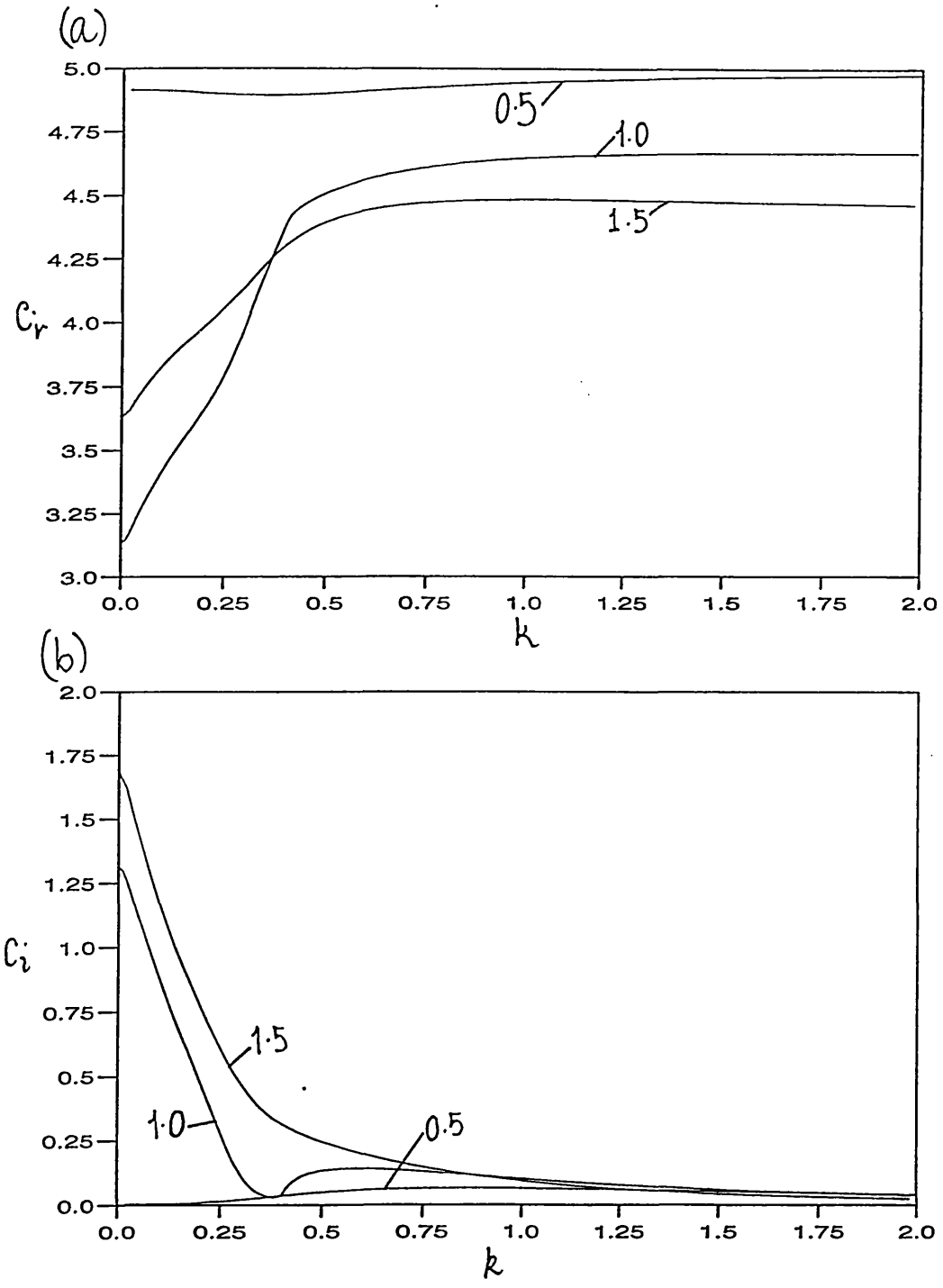

Figure 2:9. The unstable eigenvalues of (2.4.2.4), with boundary conditions (2.4.2.5), (2.4.1.7), and velocity profiles taken at various X-stations for the condensed flow over an obtacle with $h_0 = 2.0$, $\bar{a} = 2$ (a) $\rho^- = 1.087$, $\nu^- = 0.484$, real phase speed c_r against wavenumber k. (b) as (a), imaginary phase speed c_i against wavenumber k

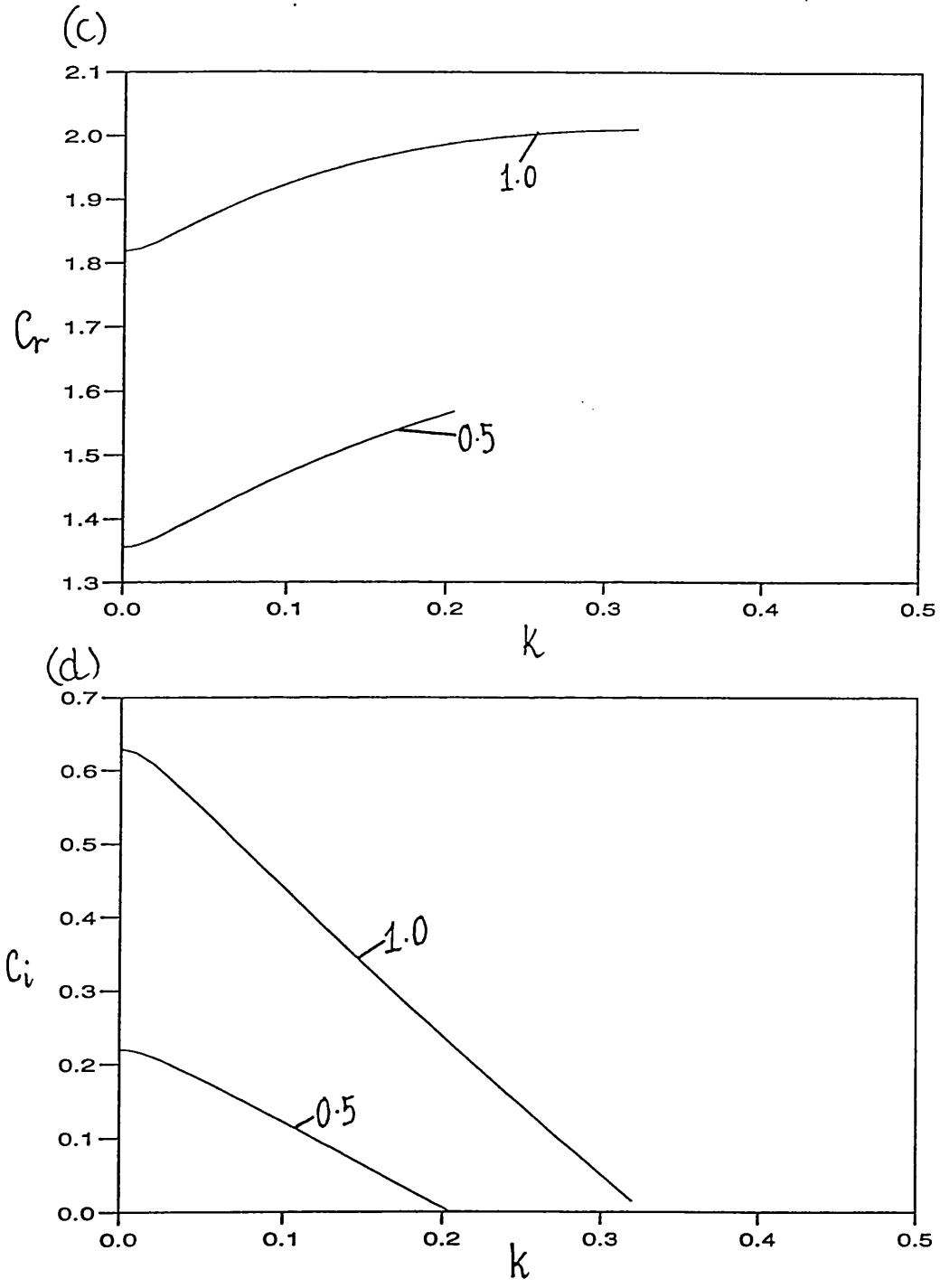

Figure 2:9. As before, (c) $\rho^- = 1.0$, $\nu^- = 1.0$, c_r against wavenumber k. (d) as (c), c_i against wavenumber k

Chapter 3

Vortex-wave interaction in a two-fluid flow

3.1 Introduction

As outlined in the literature review in the general Introduction, vortex-wave interaction (VWI) theory involves the coupling of a steady three-dimensional vortex with oblique short scale waves in a boundary-layer flow and attempts to track the development of both vortex and wave downstream of the wave source. It is thought that these type of interactions may provide a mechanism for the transition to turbulence in a boundary layer. In this Chapter we develop the weakly nonlinear vortex/inviscid wave theory for the case of two-fluid flow in a linear shearing motion. To start with, a pair of oblique waves are assumed to be imposed on the base flow as in the related work of Brown (1993), Brown *et al* (1993) Smith, Brown, Brown (1993) (hereafter referred to as SBB). However due to the specific role of the interface and the zero curvature of the base profile, we find that, firstly, all oblique waves are neutral in the leading inviscid flow approximation (and therefore can produce VWI) and, secondly, for some choices of the film parameters two pairs of oblique waves with the cross-wavenumbers β and 3β can have equal phase speeds and streamwise wavenumbers. The second property means that the two pairs will interact between themselves via

the contributions to the wave induced vortex which is generated around the critical layer in the manner described in SBB. The precise mechanism of the resonance will become clear from the form of the amplitude equations. We add this second pair of waves to the problem formulation and, using an asymptotic flow structure similar to that developed in SBB, we find equations governing the wave amplitudes.

The chapter is organized as follows. In §3.1.1 we establish a dispersion relation, through which we show the possibility of a resonance between pairs of waves, in the sense described above. A numerical analysis of the dispersion relation is followed by some analytic work which verifies the existence of resonant modes. In §3.2 we use the asymptotic structure developed in Brown *et al* (1993) and SBB to introduce the second pair of oblique waves and in the subsequent sections obtain solutions in the various flow regions, shown in fig 3:1(a)(b) . Matching the various solutions we obtain four wave-amplitude evolution equations and some solutions for various initial conditions are then calculated, with the effects of nonlinearity shown.

Our approach to the flow is similar to that taken in SBB, although we make a slightly different non-dimensionalization to suit our problem. At a set point the streamwise velocity profile is perturbed by means of a vibrating ribbon or some other device, generating a pair of oblique waves, periodic in the span-wise direction. The equations of motion (1.1.1) are non-dimensionalized taking the interfacial speed U_*, the undisturbed film thickness h_*, the time h_*/U_*, the film viscosity μ_*^- and density ρ_*^- and the pressure $\rho_*^- g_* h_*$ as reference parameters, g_* being the gravitational acceleration. This gives the Navier-Stokes equations for a three-dimensional (3-D) flow in the form

$$\frac{Du}{Dt} = \frac{-1}{Fr\rho^{\pm}}\frac{\partial p}{\partial x} + \frac{\mu^{\pm}}{\rho^{\pm} Re}\nabla^2 u, \tag{3.1.1a}$$

$$\frac{Dv}{Dt} = \frac{-1}{Fr\rho^{\pm}}\left(\frac{\partial p}{\partial y} - \rho^{\pm}\right) + \frac{\mu^{\pm}}{\rho^{\pm} Re}\nabla^2 v, \tag{3.1.1b}$$

$$\frac{Dw}{Dt} = \frac{-1}{Fr\rho^{\pm}}\frac{\partial p}{\partial z} + \frac{\mu^{\pm}}{\rho^{\pm} Re}\nabla^2 w, \tag{3.1.1c}$$

$$\frac{\partial u}{\partial x} + \frac{\partial v}{\partial y} + \frac{\partial w}{\partial z} = 0. \tag{3.1.1d}$$

Here $Fr = U_*^2/g_*h_*$, $Re = \rho_*^- U_* h_*/\mu_*^-$, are the Froude number and Reynolds number respectively, the $+/-$ signs refer to the flow above and below the interface, $\rho^- = \mu^- = 1$, $\rho^+ = \rho, \mu^+ = \mu$, where $\mu = \mu_*^+/\mu_*^-$ and $\rho = \rho_*^+/\rho_*^-$ denote the viscosity and density ratios in the fluids. Also $D = \partial/\partial t + u\partial/\partial x + v\partial/\partial y + w\partial/\partial z$ and $\nabla^2 = \partial^2/\partial x^2 + \partial^2/\partial y^2 + \partial^2/\partial z^2$. The base flow solution of these equations is taken as

$$u = U_0(y), \;\; p = P_0(y), \;\; v = 0, \;\; w = 0, \tag{3.1.2}$$

where

$$P_0 = -y, \;\; U_0 = y, \;\; \text{for } 0 \leq y \leq 1, \tag{3.1.3}$$

$$P_0 = -(\rho(y-1)+1), \;\; U_0 = \lambda^+(y-1)+1, \;\; \text{for } y \geq 1, \tag{3.1.4}$$

and $\lambda^+ = 1/\mu$.

3.1.1 Linear inviscid disturbances

For large Reynolds numbers a monochromatic disturbance to the base flow in the form

$$(u, v, w, p) = (U_0, 0, 0, P_0) + (\bar{u}, \bar{v}, \bar{w}, \bar{p})E + c.c. \tag{3.1.1.1}$$

where $E = \exp[i(\alpha x + \beta z - \omega t)]$, $c = \omega/\alpha$, and $\bar{u}, \bar{v}, \bar{w}, \bar{p}$ are small, is governed by the equations

$$i\alpha(U_0 - c)\bar{u} + U_0'(y)\bar{v} = \frac{-1}{Fr\rho^{\pm}} i\alpha\bar{p}, \tag{3.1.1.2}$$

$$i\alpha(U_0 - c)\bar{v} = \frac{-1}{Fr\rho^{\pm}} \frac{\partial\bar{p}}{\partial y}, \tag{3.1.1.3}$$

$$i\alpha(U_0 - c)\bar{w} = \frac{-1}{Fr\rho^{\pm}} i\beta\bar{p}, \tag{3.1.1.4}$$

$$i\alpha\bar{u} + \frac{\partial\bar{v}}{\partial y} + i\beta\bar{w} = 0, \tag{3.1.1.5}$$

which, for the constant-shear base profile, combine into a simplified Rayleigh equation,

$$\bar{v}_{yy} - (\alpha^2 + \beta^2)\bar{v} = 0. \tag{3.1.1.6}$$

The solution of the latter must be continuous at the interface and vanish at $y = 0$ and as $y \to \infty$, hence we can take

$$\bar{v} = A \sinh \gamma y, \text{ when } 0 \leq y \leq 1, \tag{3.1.1.7}$$

$$\bar{v} = A \sinh \gamma \exp[\gamma(1 - y)], \text{ when } y \geq 1, \tag{3.1.1.8}$$

where $\gamma^2 = \alpha^2 + \beta^2$. For the effectively inviscid perturbed motion the interfacial kinematic and pressure-jump conditions can be combined to give

$$[\bar{p}(y = 1)]^+_- = -(B\gamma^2 + (1 - \rho))\frac{\bar{v}}{i\alpha(1 - c)} \tag{3.1.1.9}$$

where $B = \gamma_*/\rho_*^- g_* h_*^2$ is the Bond number and the square brackets indicate the jump value across the interface. Using (3.1.1.2), (3.1.1.4), (3.1.1.5) and (3.1.1.7), (3.1.1.8) the explicit solution for $\bar{v}$, the interfacial condition (3.1.1.9) gives the following expression for the disturbance phase speed

$$\begin{aligned} c &= 1 - \frac{(\nu - 1)\tanh\gamma}{2\nu(1 + \rho\tanh\gamma)\gamma} \\ &\quad \pm\sqrt{\left(\frac{(\nu - 1)\tanh\gamma}{2\nu(1 + \rho\tanh\gamma)\gamma}\right)^2 + \frac{\gamma\tanh\gamma(1 - \rho + \gamma^2 B)}{\alpha^2 Fr(1 + \rho\tanh\gamma)}} \end{aligned} \tag{3.1.1.10}$$

and we have used $\lambda^+ = 1/\mu$. Examples of the phase speed dependence on the flow parameters are shown in figures 3:2(a)-(e). The nonlinear theory presented later in this chapter relies on the assumption that the oblique waves with the spanwise wavenumbers β and 3β have the same phase speed and wavenumber α. Figs 3:3 (a),(b) show this type of resonance for some choices of the parameters λ^+ and ρ, and in Table 3:1 we show a few examples of the many sets of parameters for which $c(\beta) = c(3\beta)$. Below we establish certain sufficient conditions for the resonance.

3.1.2 A sufficient condition for resonance

Assuming that β is small we expand $\hat{c} = 1 - c$ as a Taylor series in β^2

$$\hat{c} = \hat{c_0}(\alpha) + \beta^2 \hat{c_1}(\alpha) + \frac{\beta^4}{2!}\hat{c_2}(\alpha) + ..., \tag{3.1.2.1}$$

where $\hat{c_1} = \partial\hat{c}/\partial(\beta^2)(\beta = 0)$, $\hat{c_2} = \partial^2\hat{c}/\partial(\beta^2)^2(\beta = 0)$. For the resonance condition $\hat{c}(\alpha,\beta) = \hat{c}(\alpha, 3\beta)$ to be satisfied it is sufficient to have $\hat{c_1}(\alpha) = 0$ at some $\alpha = \alpha_0$. Indeed, in this case we can take

$$\alpha = \alpha_0 + \epsilon\bar{\alpha}, \;\; \beta = \epsilon^{1/2}\bar{\beta}, \tag{3.1.2.2}$$

with small ϵ, so that the resonance condition can be written as

$$9\bar{\beta}^2\epsilon^2\bar{\alpha}\frac{\partial\hat{c_1}}{\partial\alpha}(\alpha_0) + \frac{81}{2}\epsilon^2\bar{\beta}^4\hat{c_2}(\alpha_0) = \bar{\beta}^2\epsilon^2\bar{\alpha}\frac{\partial\hat{c_1}}{\partial\alpha}(\alpha_0) + \frac{\epsilon^2\bar{\beta}^4}{2}\hat{c_2}(\alpha_0) + ... \tag{3.1.2.3}$$

Hence

$$\bar{\beta}^2 = -\frac{\bar{\alpha}}{5\hat{c_2}(\alpha_0)}\frac{d\hat{c_1}}{d\alpha}(\alpha_0) + ... \tag{3.1.2.4}$$

The right-hand side of (3.1.2.4) can always be made positive by choosing $\bar{\alpha}$ with the appropriate sign. Further, we can show that the sufficient condition $\hat{c_1} = 0$ will be satisfied, at least for small $\bar{\alpha}$, provided the kinematic viscosity of the upper fluid is small. Suppose that

$$\alpha^* = {h_0}^*\alpha, \;\; \beta^* = {h_0}^*\beta, \;\; B^* = {h_0}^{*2}B, \;\; Fr^* = Fr/h_0^*, \;\; \rho^* = \rho, \;\; \mu^* = \mu \tag{3.1.2.5}$$

with ${h_0}^* \to \infty$ and the scaled variables $\alpha^*, \beta^*, ...$ of $O(1)$. We find that if ${h_0}^* \to \infty$, then

$$\left.\frac{\partial\hat{c}}{\partial(\beta^{*2})}\right|_{\beta^{*2}=0} \to \frac{(1-\rho^*\lambda^+)}{4\alpha^{*3}(1+\rho^*)} \pm \left(\frac{-2(\rho^*\lambda^+ - 1)^2}{4\alpha^{*3}(1+\rho^*)^2} + \frac{(1-\rho^* + 3\alpha^{*2}B^*)}{\alpha^{*2}Fr^*(1+\rho^*)}\right) \times \left(4\alpha^*\sqrt{\frac{(\rho^*\lambda^+ - 1)^2}{4(1+\rho^*)^2\alpha^{*2}} + \frac{(1-\rho^* + \alpha^{*2}B^*)}{\alpha^* Fr^*(1+\rho^*)}}\right)^{-1} \tag{3.1.2.6}$$

The condition $\partial\hat{c}/\partial(\beta^{*2}) = 0$ can now be written as

$$2D_1\sqrt{{D_1}^2 + D_2\alpha^* + D_3\alpha^{*3}} = -2{D_1}^2 + D_2\alpha^* + 3D_3\alpha^{*3} \tag{3.1.2.7}$$

where $D_1 = (\rho^\star\lambda^+ - 1)/(2(1+\rho^\star))$, $D_2 = (1-\rho^\star)/(Fr^\star(1+\rho^\star))$, $D_3 = B^\star/(Fr^\star(1+\rho^\star))$. We find that $D_1 > 0$ when $1/\nu^\star = \rho^\star/\mu^\star > 1$ and $D_1 < 0$ for $1/\nu^\star < 1$, $D_2 > 0$ for all values of $\rho^\star$ as long as the lower liquid is denser then the upper liquid, and D_3 is always positive. The sketch of the left-hand side and right-hand side of (3.1.2.7) in fig 3:4 shows that the required $\alpha^\star$ exists when $D_1 > 0$ i.e. when $\nu^\star < 1$.

3.2 VWI with two pairs of waves.

In the previous section we established the possibility of co-existence of two pairs of oblique waves having the same values of the phase speed and streamwise wavenumber and with the cross-wavenumbers β and 3β. Here we consider nonlinear interactions between such waves. The starting equations are taken in the non-dimensional form (3.1.1).

3.2.1 The core flow.

The inviscid core flow regions are those marked 1,2,3 in fig 3:1 and have scalings $y = O(1)$ and $x = O(1)$. For the velocity and pressure we make the following expansions:

$$u = U_0(y) + \epsilon^7 \begin{pmatrix} (\bar{u}_1 e^{i\beta z} + \bar{u}_1^* e^{-i\beta z} + \bar{u}_2 e^{i3\beta z} + \bar{u}_2^* e^{-i3\beta z})E + \\ \epsilon^3(\bar{u}_3 e^{i\beta z} + \bar{u}_3^* e^{-i\beta z} + \bar{u}_4 e^{i3\beta z} + \bar{u}_4^* e^{-i3\beta z})E + \\ +\ldots + c.c. \end{pmatrix} \qquad (3.2.1.1a)$$

$$v = \epsilon^7 \begin{pmatrix} (\bar{v}_1 e^{i\beta z} + \bar{v}_1^* e^{-i\beta z} + \bar{v}_2 e^{i3\beta z} + \bar{v}_2^* e^{-i3\beta z})E + \\ \epsilon^3(\bar{v}_3 e^{i\beta z} + \bar{v}_3^* e^{-i\beta z} + \bar{v}_4 e^{i3\beta z} + \bar{v}_4^* e^{-i3\beta z})E + \\ +\ldots + c.c. \end{pmatrix} \qquad (3.2.1.1b)$$

$$w = \epsilon^7 \begin{pmatrix} (\bar{w}_1 e^{i\beta z} + \bar{w}_1^* e^{-i\beta z} + \bar{w}_2 e^{i3\beta z} + \bar{w}_2^* e^{-i3\beta z})E + \\ \epsilon^3(\bar{w}_3 e^{i\beta z} + \bar{w}_3^* e^{-i\beta z} + \bar{w}_4 e^{i3\beta z} + \bar{w}_4^* e^{-i3\beta z})E + \\ +\ldots + c.c. \end{pmatrix} \qquad (3.2.1.1c)$$

$$p = P_0(y) + \epsilon^7 \begin{pmatrix} (\bar{p}_1 e^{i\beta z} + \bar{p}_1^* e^{-i\beta z} + \bar{p}_2 e^{i3\beta z} + \bar{p}_2^* e^{-i3\beta z})E + \\ \epsilon^3(\bar{p}_3 e^{i\beta z} + \bar{p}_3^* e^{-i\beta z} + \bar{p}_4 e^{i3\beta z} + \bar{p}_4^* e^{-i3\beta z})E + \\ +\ldots + c.c. \end{pmatrix} \qquad (3.2.1.1d)$$

where $E = \exp[i\alpha(x - ct)]$, $\epsilon = Re^{-1/6}$, *c.c.* stands for the complex conjugate and terms in E^2 and E^3 have been ignored since they do not affect the VWI. NOTE: the superscript $*$ does NOT denote the complex conjugate in this context.

A explanation of notation is required before we proceed. We will be using the superscript [*] to indicate the result for the second (asterisked) wave as the same as that for the first wave with any sign changes for the second wave indicated by $[\mp]$ in front of the corresponding expression. We will be adding a second subscript where necessary to differentiate between core solutions in regions 1,2 and 3 of figures 3:1(a), 3:1(b) where the precise domain of the solution is important.

For the leading normal-velocity terms the solution can be written in the form

$$\bar{v}_1(x_1,y) = V_1(y)A_1(x_1), \quad \bar{v}_1^*(x_1,y) = V_1{}^*(y)A_1{}^*(x_1), \tag{3.2.1.2}$$

$$\bar{v}_2(x_1,y) = V_2(y)A_2(x_1), \quad \bar{v}_2^*(x_1,y) = V_2{}^*(y)A_2{}^*(x_1), \tag{3.2.1.3}$$

and we aim to obtain amplitude equations for the functions A_i. The y-dependent coefficients, for the case of the critical layer in the lower fluid are

$$V_{11}^{[*]} = V_{12}^{[*]} = \frac{\sinh\gamma_1 y}{\sinh\gamma_1 y_c}, \quad V_{13}^{[*]} = \frac{\sinh\gamma_1}{\sinh\gamma_1 y_c}e^{\gamma_1(1-y)}, \tag{3.2.1.4a}$$

$$V_{21}^{[*]} = V_{22}^{[*]} = \frac{\sinh\gamma_2 y}{\sinh\gamma_2 y_c}, \quad V_{23}^{[*]} = \frac{\sinh\gamma_2}{\sinh\gamma_2 y_c}e^{\gamma_2(1-y)}, \tag{3.2.1.4b}$$

where $x_1 = \epsilon^3 x$ is the slow streamwise coordinate and $\gamma_1^2 = \alpha^2+\beta^2$, $\gamma_2^2 = \alpha^2+9\beta^2$. The wave amplitudes are hence defined by the magnitude of the normal velocity oscillation at the critical layer. For the case of the critical layer in the upper fluid we have

$$V_{11}^{[*]} = \frac{\sinh\gamma_1 y}{\sinh\gamma_1}e^{\gamma_1(y_c-1)}, \quad V_{12}^{[*]} = V_{13}^{[*]} = e^{\gamma_1(y_c-y)}, \tag{3.2.1.5a}$$

$$V_{21}^{[*]} = \frac{\sinh\gamma_2 y}{\sinh\gamma_2}e^{\gamma_2(y_c-1)}, \quad V_{22}^{[*]} = V_{23}^{[*]} = e^{\gamma_2(y_c-y)}. \tag{3.2.1.5b}$$

We now use these solutions to solve for the next-order wave perturbations. For the critical layer in the lower flow we get the general solutions

$$\bar{v}_{31}^{[*]} = F_{31}^{[*]-}\sinh\gamma_1 y + G_{31}^{[*]-}\cosh\gamma_1 y - \frac{i\alpha\cosh\gamma_1 y}{\gamma_1\sinh\gamma_1 y_c}yA_1^{[*]\prime}(x_1), \tag{3.2.1.6a}$$

$$\bar{v}_{32}^{[*]} = F_{32}^{[*]-}\sinh\gamma_1 y + G_{32}^{[*]-}\cosh\gamma_1 y - \frac{i\alpha\cosh\gamma_1 y}{\gamma_1\sinh\gamma_1 y_c} y A_1^{[*]'}(x_1), \qquad (3.2.1.6b)$$

$$\bar{v}_{33}^{[*]} = F_{33}^{[*]-}e^{-\gamma_1 y} - \frac{i\alpha\sinh\gamma_1}{\gamma_1\sinh\gamma_1 y_c} y e^{\gamma_1(1-y)} A_1^{[*]'}(x_1), \qquad (3.2.1.6c)$$

and, for the case of the critical layer in the upper fluid,

$$\bar{v}_{31}^{[*]} = F_{31}^{[*]+}\sinh\gamma_1 y + G_{31}^{[*]+}\cosh\gamma_1 y - \frac{i\alpha\cosh\gamma_1 y}{\gamma_1\sinh\gamma_1} y e^{\gamma_1(y_c-1)} A_1^{[*]'}(x_1), \qquad (3.2.1.7a)$$

$$\bar{v}_{32}^{[*]} = F_{32}^{[*]+}\sinh\gamma_1 y + G_{32}^{[*]+}\cosh\gamma_1 y + \frac{i\alpha}{\gamma_1} y e^{\gamma_1(y_c-y)} A_1^{[*]'}(x_1), \qquad (3.2.1.7b)$$

$$\bar{v}_{33}^{[*]} = F_{33}^{[*]+}e^{-\gamma_1 y} + \frac{i\alpha}{\gamma_1} y e^{\gamma_1(y_c-y)} A_1^{[*]'}(x_1). \qquad (3.2.1.7c)$$

Similar results are derived for $\bar{v}_4$,$\bar{v}_4^*$.

The undetermined constants F, G will be deduced in §3.3 where matches are made to the Stokes layer at the wall, and to the buffer and interfacial boundary layers. The superscripts $+/-$ used here refer to the critical layer occurring above or below the interface.

3.2.2 The buffer layer.

The buffer, zones 4 in fig 3:1(a),(b), acts as a viscous, diffusive layer which smoothes the discontinuities in the mean velocity field generated by the waves and supplies the main vortex corrections to the wave. We introduce a new variable $Y = O(1)$ such that $y - y_c = \epsilon^{3/2}Y$ and expand the solution in the form

$$\begin{aligned} u &= U_0(y_c) + \epsilon^{3/2} Y U_0{}'(y_c) + \epsilon^6 \tilde{u}_m + \\ &\quad \epsilon^{11/2}\left(\sum_{n=1}^{4} \epsilon^{\frac{3(n-1)}{2}} \begin{pmatrix} \tilde{u}_{2n-1}e^{i\beta z} & + & \tilde{u}_{2n-1}^* e^{-i\beta z} \\ +\tilde{u}_{2n}e^{3i\beta z} & + & \tilde{u}_{2n}^* e^{-3i\beta z} \end{pmatrix} E \right. \\ &\quad \left. + h.o.t. + c.c. \right) \end{aligned} \qquad (3.2.2.1)$$

$$\begin{aligned} v &= \epsilon^9 \tilde{v}_m + \\ &\quad \epsilon^7\left(\sum_{n=1}^{4} \epsilon^{\frac{3(n-1)}{2}} \begin{pmatrix} \tilde{v}_{2n-1}e^{i\beta z} & + & \tilde{v}_{2n-1}^* e^{-i\beta z} \\ +\tilde{v}_{2n}e^{3i\beta z} & + & \tilde{v}_{2n}^* e^{-3i\beta z} \end{pmatrix} E \right. \\ &\quad \left. + h.o.t. + c.c. \right) \end{aligned} \qquad (3.2.2.2)$$

$$w = \epsilon^{15/2}\tilde{w}_m + \epsilon^{11/2}\left(\sum_{n=1}^{4} \epsilon^{\frac{3(n-1)}{2}} \begin{pmatrix} \tilde{w}_{2n-1}e^{i\beta z} & + & \tilde{w}^*_{2n-1}e^{-i\beta z} \\ +\tilde{w}_{2n}e^{3i\beta z} & + & \tilde{w}^*_{2n}e^{-3i\beta z} \end{pmatrix} E + h.o.t. + c.c. \right) \quad (3.2.2.3)$$

$$p = P_0(y_c) + \epsilon^{3/2} Y P_0{}'(y_c) + ... + \epsilon^{7}\left(\sum_{n=1}^{4} \epsilon^{\frac{3(n-1)}{2}} \begin{pmatrix} \tilde{p}_{2n-1}e^{i\beta z} & + & \tilde{p}^*_{2n-1}e^{-i\beta z} \\ +\tilde{p}_{2n}e^{3i\beta z} & + & \tilde{p}^*_{2n}e^{-3i\beta z} \end{pmatrix} E + h.o.t. + c.c. \right) \quad (3.2.2.4)$$

where $\tilde{u}_m$, $\tilde{v}_m$ and $\tilde{w}_m$ are the mean-flow corrections which can be written in the form,

$$\tilde{\mathbf{u}}_\mathbf{m} = \tilde{\mathbf{u}}_{\mathbf{2m}}e^{2i\beta z} + \tilde{\mathbf{u}}^*_{\mathbf{2m}}e^{-2i\beta z} + \tilde{\mathbf{u}}_{\mathbf{4m}}e^{4i\beta z} + \tilde{\mathbf{u}}^*_{\mathbf{4m}}e^{-4i\beta z} + \tilde{\mathbf{u}}_{\mathbf{6m}}e^{6i\beta z} + \tilde{\mathbf{u}}^*_{\mathbf{6m}}e^{-6i\beta z}. \quad (3.2.2.5)$$

Here $\tilde{\mathbf{u}}_\mathbf{m} = (\tilde{u}_m, \tilde{v}_m, \tilde{w}_m)$ and the coefficients $\tilde{\mathbf{u}}^{[*]}_{\mathbf{im}}$ are z-independent.

Upon substitution into equations (3.1.1) we obtain relations similar to those in SBB for the first few wave terms, in particular matching to the core flow we find

$$\tilde{v}_1 = A_1(x_1), \qquad \tilde{v}_2 = A_2(x_1), \quad (3.2.2.6)$$

$$\tilde{p}_1 = \frac{Fr\rho^{\pm}U_{0y}(y_c)}{i\alpha}A_1^{[*]}(x_1), \quad \tilde{p}_2 = \frac{Fr\rho^{\pm}U_{0y}(y_c)}{i\alpha}A_2^{[*]}(x_1). \quad (3.2.2.7)$$

The density and shear here are assumed to be chosen according to the position of the critical layer. The solutions to the leading wave terms, in a similar manner to those in Brown (1993), are all manifestations of the external core behaviour. Solutions for the $e^{\pm 3i\beta z}$ harmonics are of an equivalent form to those for $e^{\pm i\beta z}$ with all parameters β replaced with 3β, and γ_1 with γ_2.

The first significant change from the theory in Brown (1993) is when we examine the terms of $O(\epsilon^{23/2})$ in the $x-$ and $z-$ momentum and continuity equations. For

example, for the terms with $e^{i\beta z}$ harmonic we have the governing equations

$$\begin{aligned} U_0{}'(y_c)Y(i\alpha\tilde{u}_7+\tilde{u}_{3x_1})+c\tilde{u}_{5x_1}+i\alpha\tilde{u}_1^*\tilde{u}_{2m}+i\alpha\tilde{u}_2\tilde{u}_{2m}^* \\ +i\alpha\tilde{u}_2^*\tilde{u}_{4m}+\tilde{u}_{2mY}\tilde{v}_1^*+\tilde{u}_{2mY}^*\tilde{v}_2+\tilde{u}_{4mY}\tilde{v}_2^* \\ +U_0{}'(y_c)\tilde{v}_7+i\beta(2\tilde{w}_1^*\tilde{u}_{2m}-2\tilde{w}_2\tilde{u}_{2m}^*+4\tilde{w}_2^*\tilde{u}_{4m}) \\ =-\frac{i\alpha}{Fr\rho^{\pm}}\tilde{p}_7+\frac{\mu^{\pm}}{\rho^{\pm}}(\tilde{u}_{5YY}-{\gamma_1}^2\tilde{u}_1), \end{aligned} \tag{3.2.2.8}$$

and

$$\begin{aligned} U_0{}'(y_c)Y(i\alpha\tilde{w}_7+\tilde{w}_{3x_1})+i\alpha(\tilde{u}_{2m}\tilde{w}_1^*+\tilde{u}_{2m}^*\tilde{w}_2+\tilde{u}_{4m}\tilde{w}_2^*) \\ =-\frac{i\beta}{Fr\rho^{\pm}}\tilde{p}_7+\frac{\mu^{\pm}}{\rho^{\pm}}(\tilde{w}_{5YY}-{\gamma_1}^2\tilde{w}_1), \end{aligned} \tag{3.2.2.9}$$

$$i\alpha\tilde{u}_7+\tilde{u}_{3x_1}+i\beta\tilde{w}_7+\tilde{v}_{7Y}=0. \tag{3.2.2.10}$$

Manipulating these relations using solutions for the previous terms we find that

$$\begin{aligned} \tilde{v}_{7YY}=\frac{Y}{2}{\gamma_1}^2V_{12}A_1(x_1)+\frac{4i\beta}{U_y(y_c)Y}(\tilde{u}_{2m}\tilde{w}_1^*-\tilde{u}_{2m}^*\tilde{w}_2+2\tilde{u}_{4m}\tilde{w}_2^*)_Y \\ +\frac{1}{U_y(y_c)Y}(\tilde{v}_1^*\tilde{u}_{2mYY}+\tilde{v}_2\tilde{u}_{2mYY}^*+\tilde{v}_2^*\tilde{u}_{4mYY}) \end{aligned} \tag{3.2.2.11}$$

where we have expanded $V_1^{[*]}, V_2^{[*]}$ in the core flow about the critical layer in the form

$$V_1^{[*]}=1+\sum_{n=1}^{\infty}\frac{V_{1n}^{[*]}(y-y_c)^n}{n!},$$

$$V_2^{[*]}=1+\sum_{n=1}^{\infty}\frac{V_{2n}^{[*]}(y-y_c)^n}{n!},$$

and matched to the buffer. The relation (3.2.2.11) shows that the $e^{i\beta z}$-component of the wave is affected by mean-flow corrections proportional to $\cos(2\beta z)$ and $\cos(4\beta z)$. These corrections are calculated next. For the vortex components in the buffer, given by (3.2.2.5), the continuity equation reduces to

$$\frac{\partial\tilde{v}_{nm}}{\partial Y}=-ni\beta\tilde{w}_{nm},\quad \frac{\partial\tilde{v}_{nm}^*}{\partial Y}=ni\beta\tilde{w}_{nm}^* \text{ where } n=2,4,6, \tag{3.2.2.12}$$

and the x- and z-momentum equations are, respectively,

$$\frac{\partial^2\tilde{u}_{nm}^{[*]}}{\partial Y^2}-\frac{\rho^{\pm}c}{\mu^{\pm}}\frac{\partial\tilde{u}_{nm}^{[*]}}{\partial x_1}=U_y(y_c)\frac{\rho^{\pm}}{\mu^{\pm}}\tilde{v}_{nm}^{[*]}, \tag{3.2.2.13}$$

$$c\frac{\partial \tilde{w}_{nm}^{[*]}}{\partial x_1} = \frac{\mu^{\pm}}{\rho^{\pm}}\frac{\partial^2 \tilde{w}_{nm}^{[*]}}{\partial Y^2}. \tag{3.2.2.14}$$

Again the viscosity and density are chosen according to the critical layer position. Except for differences in notation, analysis of (3.2.2.12)-(3.2.2.14) proceeds exactly as in Brown (1993) by taking Fourier transforms, of equation (3.2.2.14) first, writing the jump value for the nth z-harmonic of the mean vortex as

$$[\tilde{w}_{nmY}^{[*]}]_{0^-}^{0^+} = [\breve{w}_{nmY}^{[*]}]_{-\infty}^{\infty} = J_n^{[*]}, \tag{3.2.2.15}$$

where $[\breve{w}_{nmY}]_{-\infty}^{\infty}$ is found in the critical layer analysis in the Appendix to this Chapter, and defining the Fourier transform of a function g to be

$$\mathcal{F}(g) = \frac{1}{\sqrt{2\pi}}\int_{-\infty}^{\infty} g(x_1, Y)e^{-i\omega x_1}dx_1. \tag{3.2.2.16}$$

Performing the transform and solving for $\mathcal{F}(\tilde{w}_{nm})$ we obtain the solution

$$\mathcal{F}(\tilde{w}_{nm}^{[*]}) = \frac{\mathcal{F}(J_n^{[*]})}{2\sigma}e^{-\sigma|Y|}, \tag{3.2.2.17}$$

where $\sigma^2 = ikc\rho^{\pm}/\mu^{\pm}$ and $Real(\sigma) > 0$. We then substitute (3.2.2.17), along with (3.2.2.12), into (3.2.2.13) to obtain an equation for $\tilde{u}_{nm}^{[*]}$

$$\mathcal{F}(\tilde{u}_{nmYY}^{[*]}) - \sigma^2\mathcal{F}(\tilde{u}_{nm}^{[*]}) = \frac{[-]U_y(y_c)ni\beta\rho^{\pm}}{\mu^{\pm}}\int_0^Y \frac{\mathcal{F}(J_n^{[*]})}{2\sigma}e^{-\sigma|Y|}dY_1. \tag{3.2.2.18}$$

Integrating the right hand side for $Y > 0$, $Y < 0$ and solving, we establish that

$$\mathcal{F}(\tilde{u}_{nm}^{[*]}) = +\frac{[-]ni\beta U_y(y_c)\rho^{\pm}}{2\mu^{\pm}\sigma^4}\mathcal{F}(J_n^{[*]})(1 - e^{-\sigma|Y|}(\frac{\sigma|Y|}{2} + 1)), \tag{3.2.2.19a}$$

$$\mathcal{F}(\tilde{u}_{nm}^{[*]}) = -\frac{[-]ni\beta U_y(y_c)\rho^{\pm}}{2\mu^{\pm}\sigma^4}\mathcal{F}(J_n^{[*]})(1 - e^{-\sigma|Y|}(\frac{\sigma|Y|}{2} + 1)), \tag{3.2.2.19b}$$

for $Y > 0$ and $Y < 0$, respectively. We substitute this form into equation (3.2.2.18) to obtain the relation

$$\int_0^{\infty}\frac{1}{Y}\frac{\partial^2\mathcal{F}(\tilde{u}_{nm})}{\partial Y^2}dY = \frac{[-]U_y(y_c)ni\beta}{4ikc}\mathcal{F}(J_n^{[*]}), \text{ for } Y > 0, \tag{3.2.2.20}$$

which we can invert using the convolution theorem. Coupled with the corresponding result for $Y < 0$ this leaves us with

$$\int_{-\infty}^{\infty}\frac{1}{Y}\frac{\partial^2\tilde{u}_{nm}^{[*]}}{\partial Y^2}dY = \frac{[-]U_y(y_c)ni\beta}{2c}\int_{-\infty}^{x_1} J_n^{[*]}(s)ds. \tag{3.2.2.21}$$

We can now use this relation to integrate (3.2.2.11) across the buffer layer. This is done, in a similar fashion to the approach in Brown (1993), by using

$$\tilde{w}_1^{[*]} = -\frac{[-]i\beta\tilde{p}_1^{[*]}}{Fr\rho^{\pm}i\alpha U_0'(y_c)Y}, \quad \tilde{w}_2^{[*]} = -\frac{[-]3i\beta\tilde{p}_2^{[*]}}{Fr\rho^{\pm}i\alpha U_0'(y_c)Y}, \tag{3.2.2.22}$$

to establish a relation of the form

$$\int_0^{\infty} \frac{(\tilde{u}_{2m}\tilde{w}_1)_Y}{U_y(y_c)Y}dY = -\frac{i\beta\tilde{p}_1}{2Fr\rho^{\pm}i\alpha U_y(y_c)}\int_0^{\infty}\frac{\tilde{u}_{2mYY}}{Y}dY \tag{3.2.2.23}$$

which, along with similar expressions for the other terms in (3.2.2.11), reduces all integrals to the form (3.2.2.21).

As a result we obtain

$$\begin{aligned}[\tilde{v}_{7Y}]_{-\infty}^{\infty} = B_7^+ - B_7^- &+ \left(\frac{\tilde{v}_1^*}{U_y(y_c)} - \frac{2\beta^2\tilde{p}_1^*}{Fr\rho^{\pm}i\alpha U_y(y_c)^2}\right)\int_{-\infty}^{\infty}\frac{\tilde{u}_{2mYY}}{Y}dY \\ &+ \left(\frac{\tilde{v}_2}{U_y(y_c)} - \frac{6\beta^2\tilde{p}_2}{Fr\rho^{\pm}i\alpha U_y(y_c)^2}\right)\int_{-\infty}^{\infty}\frac{\tilde{u}_{2mYY}^*}{Y}dY \\ &+ \left(\frac{\tilde{v}_2^*}{U_y(y_c)} - \frac{12\beta^2\tilde{p}_2^*}{Fr\rho^{\pm}i\alpha U_y(y_c)^2}\right)\int_{-\infty}^{\infty}\frac{\tilde{u}_{4mYY}}{Y}dY.\end{aligned} \tag{3.2.2.24a}$$

For the other three wave terms of this magnitude in ϵ, upon similar manipulation, we have

$$\begin{aligned}[\tilde{v}_{7Y}^*]_{-\infty}^{\infty} = B_7^{*+} - B_7^{*-} &+ \left(\frac{\tilde{v}_1}{U_y(y_c)} - \frac{2\beta^2\tilde{p}_1}{Fr\rho^{\pm}i\alpha U_y(y_c)^2}\right)\int_{-\infty}^{\infty}\frac{\tilde{u}_{2mYY}^*}{Y}dY \\ &+ \left(\frac{\tilde{v}_2}{U_y(y_c)} - \frac{12\beta^2\tilde{p}_2}{Fr\rho^{\pm}i\alpha U_y(y_c)^2}\right)\int_{-\infty}^{\infty}\frac{\tilde{u}_{4mYY}^*}{Y}dY \\ &+ \left(\frac{\tilde{v}_2^*}{U_y(y_c)} - \frac{6\beta^2\tilde{p}_2^*}{Fr\rho^{\pm}i\alpha U_y(y_c)^2}\right)\int_{-\infty}^{\infty}\frac{\tilde{u}_{2mYY}}{Y}dY,\end{aligned} \tag{3.2.2.24b}$$

$$\begin{aligned}[\tilde{v}_{8Y}]_{-\infty}^{\infty} = B_8^+ - B_8^- &+ \left(\frac{\tilde{v}_1}{U_y(y_c)} + \frac{2\beta^2\tilde{p}_1}{Fr\rho^{\pm}i\alpha U_y(y_c)^2}\right)\int_{-\infty}^{\infty}\frac{\tilde{u}_{2mYY}}{Y}dY \\ &+ \left(\frac{\tilde{v}_1^*}{U_y(y_c)} - \frac{4\beta^2\tilde{p}_1^*}{Fr\rho^{\pm}i\alpha U_y(y_c)^2}\right)\int_{-\infty}^{\infty}\frac{\tilde{u}_{4mYY}}{Y}dY \\ &+ \left(\frac{\tilde{v}_2^*}{U_y(y_c)} - \frac{18\beta^2\tilde{p}_2^*}{Fr\rho^{\pm}i\alpha U_y(y_c)^2}\right)\int_{-\infty}^{\infty}\frac{\tilde{u}_{6mYY}}{Y}dY,\end{aligned} \tag{3.2.2.24c}$$

$$\begin{aligned}[\tilde{v}_{8Y}^*]_{-\infty}^{\infty} = B_8^{*+} - B_8^{*-} &+ \left(\frac{\tilde{v}_1}{U_y(y_c)} - \frac{4\beta^2\tilde{p}_1}{Fr\rho^{\pm}i\alpha U_y(y_c)^2}\right)\int_{-\infty}^{\infty}\frac{\tilde{u}_{4mYY}^*}{Y}dY \\ &+ \left(\frac{\tilde{v}_1^*}{U_y(y_c)} + \frac{2\beta^2\tilde{p}_1^*}{Fr\rho^{\pm}i\alpha U_y(y_c)^2}\right)\int_{-\infty}^{\infty}\frac{\tilde{u}_{2mYY}^*}{Y}dY \\ &+ \left(\frac{\tilde{v}_2}{U_y(y_c)} - \frac{18\beta^2\tilde{p}_2}{Fr\rho^{\pm}i\alpha U_y(y_c)^2}\right)\int_{-\infty}^{\infty}\frac{\tilde{u}_{6mYY}^*}{Y}dY.\end{aligned} \tag{3.2.2.24d}$$

Here $B_7^{[*]}, B_8^{[*]}$ are constants which will be discussed in §3.3.

3.2.3 The viscous interfacial layers

The shape of the interface is taken in the form

$$y = y_i = 1 + \epsilon^7 \left(\begin{array}{l} (\eta_1 e^{i\beta z} + \eta_1{}^* e^{-i\beta z} + \eta_2 e^{3i\beta z} + \eta_2{}^* e^{-3i\beta z})E \\ +\epsilon^3(\eta_3 e^{i\beta z} + ...)E + ... + c.c. \end{array} \right)$$

and we write the new vertical coordinate as

$$\hat{y} = \epsilon^{-3}(y - y_i) = O(1). \tag{3.2.3.1}$$

As in the other layers of the flow we expand the velocities and pressures as

$$\begin{aligned} u &= U_0(1) + \epsilon^3 U_0{}'(1)\hat{y} + \epsilon^7 \left((\hat{u}_1 + \eta_1 U_0{}'(1))e^{i\beta z} + (\hat{u}_2 + \eta_2 U_0{}'(1))\epsilon^{3i\beta z} \right) E \\ &\quad +\epsilon^{10}((\hat{u}_3 + \eta_3 U_0{}'(1))e^{i\beta z} + ...)E + ... + c.c. \end{aligned} \tag{3.2.3.2}$$

$$\begin{aligned} v &= \epsilon^7 \left(\hat{v}_1 e^{i\beta z} + \hat{v}_1^* \epsilon^{-i\beta z} + \hat{v}_2 \epsilon^{3i\beta z} + \hat{v}_2^* \epsilon^{-3i\beta z} \right) E + \epsilon^{10}(\hat{v}_3 e^{i\beta z} + ...)E \\ &\quad +... + c.c. \end{aligned} \tag{3.2.3.3}$$

$$\begin{aligned} w &= \epsilon^7 \left(\hat{w}_1 e^{i\beta z} + \hat{w}_1^* \epsilon^{-i\beta z} + \hat{w}_2 \epsilon^{3i\beta z} + \hat{w}_2^* \epsilon^{-3i\beta z} \right) E + \epsilon^{10}(\hat{w}_3 e^{i\beta z} + ...)E \\ &\quad +... + c.c. \end{aligned} \tag{3.2.3.4}$$

$$\begin{aligned} p &= P_0(1) + \epsilon^3 P_0{}'(1)\hat{y} + \epsilon^7 \left((\hat{p}_1 + \eta_1 P_0{}'(1))e^{i\beta z} + +(\hat{p}_2 + \eta_2 P_0{}'(1))\epsilon^{3i\beta z} + ... \right) E \\ &\quad +\epsilon^{10}((\hat{p}_3 + \eta_3 P_0{}'(1))e^{i\beta z} + ...)E + c.c. \end{aligned} \tag{3.2.3.5}$$

For the $e^{i\beta z}$ terms, the governing equations to the order required here are

$$\hat{v}_{1\hat{y}} = 0, \;\; \hat{p}_{1\hat{y}} = 0, \tag{3.2.3.6}$$

and

$$i\alpha U_s \hat{u}_1 + U_0{}'(1)\hat{v}_1 = -\frac{i\alpha}{Fr\rho^{\pm}}\hat{p}_1 + \frac{\mu^{\pm}}{\rho^{\pm}}\hat{u}_{1\hat{y}\hat{y}}, \tag{3.2.3.7a}$$

$$i\alpha U_s \hat{v}_1 = -\frac{1}{Fr\rho^{\pm}}\hat{p}_{3\hat{y}}, \tag{3.2.3.7b}$$

$$i\alpha U_s \hat{w}_1 = -\frac{i\beta}{Fr\rho^{\pm}}\hat{p}_1 + \frac{\mu^{\pm}}{\rho^{\pm}}\hat{w}_{1\hat{y}\hat{y}}, \tag{3.2.3.7c}$$

$$i\alpha\hat{u}_1 + \hat{v}_{3\hat{y}} + i\beta\hat{w}_1 = 0, \tag{3.2.3.7d}$$

where $U_s = 1 - c$. From these equations, observing the invariance of $\hat{v}_1$ and $\hat{p}_1$ with respect to $\hat{y}$, we establish that

$$\hat{p}_3^{\pm} = -Fr\rho^{\pm}i\alpha U_s\hat{v}_1\hat{y} + P_{3c}^{\pm}, \tag{3.2.3.8}$$

$$\hat{u}_1^{\pm} = -\frac{\hat{v}_1^{\pm}U_0{}'(1)}{i\alpha U_s} - \frac{i\alpha\hat{p}_1^{\pm}}{Fr\mu^{\pm}(\sigma^{\pm})^2} + A_1^{\pm}\cosh\sigma^{\pm}\hat{y} + B_1^{\pm}\sinh\sigma^{\pm}\hat{y}, \tag{3.2.3.9}$$

where $\sigma^{\pm} = \sqrt{i\alpha U_s\rho^{\pm}/\mu^{\pm}}$ with $\sigma^{\pm} = \sigma_r^{\pm} + i\sigma_i^{\pm}$ and $\sigma_r^{\pm} > 0$. Again the superscripts $+/-$ indicate whether we are examining the parameters above or below the interface and $P_{3c}^{\pm}$ is a constant of integration to be calculated later. We apply the boundary conditions of no exponential growth as $|\hat{y}| \to \infty$ and find

$$A_1^{+} = -B_1^{+}, \quad A_1^{-} = B_1^{-}. \tag{3.2.3.10}$$

Using similar arguments we find, from (3.2.3.7c), that

$$\hat{w}_1^{\pm} = -\frac{i\beta\hat{p}_1^{\pm}}{Fr\mu^{\pm}(\sigma^{\pm})^2} + C_1^{\pm}(\cosh\sigma^{\pm}\hat{y} \mp \sinh\sigma^{\pm}\hat{y}), \tag{3.2.3.11}$$

and substituting (3.2.3.9), (3.2.3.11) into equation (3.2.3.7d) we obtain

$$\hat{v}_3^{\pm} = -\frac{{\gamma_1}^2\hat{p}_1^{\pm}}{Fr\mu^{\pm}(\sigma^{\pm})^2}\hat{y} + \frac{\hat{v}_1^{\pm}U_0{}'(1)}{U_s}\hat{y} + \frac{E_3^{\pm}}{\sigma^{\pm}}(\sinh\sigma^{\pm}\hat{y} \mp \cosh\sigma^{\pm}\hat{y}) + V_{3c}^{\pm}, \tag{3.2.3.12}$$

where $V_{3c}^{\pm}$ are constants of integration, which will be determined from matching, and $E_3^{\pm} = -i\alpha A_1^{\pm} - i\beta C_1^{\pm}$. Using the conditions at the interface,

$$[\mu^{\pm}\hat{u}_{1\hat{y}}]_{-}^{+} = 0, \quad [\mu^{\pm}\hat{w}_{1\hat{y}}]_{-}^{+} = 0, \quad \hat{v}_1^{+} = \hat{v}_1^{-}, \tag{3.2.3.13}$$

the constants $A_1^{\pm}, C_1^{\pm}$ and $E_3^{\pm}$ can be expressed in terms of the pressure component $\hat{p}_1^{\pm}$ and the interface shift η_1 in the following form:

$$C_1^{+} = \left(\hat{p}_1^{+}(\frac{1}{\rho} - 1) + \eta_1(1 - \rho + {\gamma_1}^2 B)\right)\frac{\beta}{Fr\alpha U_s(1 + \sqrt{\rho\mu})}, \tag{3.2.3.14}$$

$$A_1^+ = \frac{\alpha}{\beta}C_1^+, \quad A_1^- = -\sqrt{\rho\mu}\frac{\alpha}{\beta}C_1^+, \tag{3.2.3.15}$$

$$E_3^+ = -\frac{i{\gamma_1}^2}{\beta}C_1^+, \quad E_3^- = \frac{i{\gamma_1}^2\sqrt{\rho\mu}}{\beta}C_1^+. \tag{3.2.3.16}$$

Then, application of the kinematic condition to (3.2.3.12) shows that

$$\eta_3 = \frac{-E_3^\pm/\sigma^\pm + V_{3c}^\pm}{i\alpha U_s} + \frac{\hat{v}_{1x_1}^\pm}{\alpha^2{U_s}^2}. \tag{3.2.3.17}$$

We can now express the jump value $[P_{3c}]_-^+$, which we will require for matching to the core flow, in terms of known constants and V_{3c}^+. From the interfacial jump requirement

$$[\hat{p}_3 + \eta_3 P_{0\hat{y}}]_{0^-}^{0^+} = -{\gamma_1}^2 B\eta_3, \tag{3.2.3.18}$$

we then find that

$$[\hat{p}_3]_{-\infty}^{+\infty} = -\left({\gamma_1}^2 B + 1 - \rho\right)\left(\frac{-E_3^+/\sigma^+ + V_{3c}^+}{i\alpha U_s} + \frac{\hat{v}_{1x_1}}{\alpha^2{U_s}^2}\right), \tag{3.2.3.19}$$

and similar results are obtained for the jumps in $\hat{p}_3^*$, $\hat{p}_4$, and $\hat{p}_4^*$.

3.2.4 The viscous Stokes layer on the wall

The viscous Stokes layer on the wall behaves exactly as in Brown (1993). It has a stretched vertical co-ordinate $\bar{Y} = \epsilon^{-3}y = O(1)$, and the expansions

$$u = \epsilon^3\bar{Y} + \epsilon^7(\bar{\bar{u}}_1 e^{i\beta z} + ...)E + ...) + c.c., \tag{3.2.4.1}$$

$$v = \epsilon^{10}(\bar{\bar{v}}_1 e^{i\beta z}E + ...) + c.c., \tag{3.2.4.2}$$

$$w = \epsilon^7(\bar{\bar{w}}_1 e^{i\beta z}E + ...) + c.c., \tag{3.2.4.3}$$

$$p = -\epsilon^3\bar{Y} + \epsilon^7(\bar{\bar{p}}_1 e^{i\beta z}E + ...) + c.c. \tag{3.2.4.4}$$

We obtain, on substitution into the governing equations (3.1.1), the solutions

$$\bar{\bar{v}}_1^{[*]} = -\frac{i{\gamma_1}^2\bar{\bar{p}}_1^{[*]}}{\alpha cFr}\left(\bar{Y} + \frac{1}{\bar{\sigma}}(e^{-\bar{\sigma}\bar{Y}} - 1)\right), \tag{3.2.4.5a}$$

$$\bar{\bar{v}}_2^{[*]} = -\frac{i{\gamma_2}^2\bar{\bar{p}}_2^{[*]}}{\alpha cFr}\left(\bar{Y} + \frac{1}{\bar{\sigma}}(e^{-\bar{\sigma}\bar{Y}} - 1)\right), \tag{3.2.4.5b}$$

where $\bar{\sigma} = \sqrt{-i\alpha c}$, $\mathrm{Real}(\bar{\sigma}) > 0$ and we will match these solutions to the core flow in the next section.

3.3 The amplitude equations

In this section we derive the controlling wave-amplitude equations for $A_1^{[*]}, A_2^{[*]}$ by establishing the jump in the fundamental correction to the leading disturbances in the core flow, $\bar{v}_3^{[*]}$, and its derivative, $\partial\bar{v}_3^{[*]}/\partial y$, across the critical and interfacial boundary layers. We do this by matching the solutions in the buffer, the core flow, the Stokes wall layer and the critical layer. Due to the linearity of the base profile the logarithmic singularity in the wave solution at the critical layer present in SBB, Brown *et al* (1993), Brown (1993) is absent therefore

$$B_i^{(*)+} - B_i^{(*)-} = 0 \text{ for } i = 7, 8. \tag{3.3.1}$$

The constants of integration, $F_{31}^{\pm}$, $F_{32}^{\pm}$, $G_{31}^{\pm}$, $G_{32}^{\pm}$, in (3.2.1.6), (3.2.1.7) can now be calculated. Recall, when the critical layer occured in the lower fluid the solutions for $\bar{v}_3^*$ (and similarly $\bar{v}_4$, $\bar{v}_4^*$) were

$$\bar{v}_{31}^{[*]-} = F_{31}^{[*]-}\sinh\gamma_1 y + G_{31}^{[*]-}\cosh\gamma_1 y + T_{31}^{[*]-}(y), \tag{3.3.2a}$$

$$\bar{v}_{32}^{[*]-} = F_{32}^{[*]-}\sinh\gamma_1 y + G_{32}^{[*]-}\cosh\gamma_1 y + T_{31}^{[*]-}(y), \tag{3.3.2b}$$

$$\bar{v}_{33}^{[*]-} = F_{33}^{[*]-}e^{-\gamma_1 y} + T_{32}^{[*]-}(y), \tag{3.3.2c}$$

and for the case of the critical layer in the upper fluid

$$\bar{v}_{31}^{[*]+} = F_{31}^{[*]+}\sinh\gamma_1 y + G_{31}^{[*]+}\cosh\gamma_1 y + T_{31}^{[*]+}(y), \tag{3.3.3a}$$

$$\bar{v}_{32}^{[*]+} = F_{32}^{[*]+}\sinh\gamma_1 y + G_{32}^{[*]+}\cosh\gamma_1 y + T_{32}^{[*]+}(y), \tag{3.3.3b}$$

$$\bar{v}_{33}^{[*]+} = F_{33}^{[*]+}e^{-\gamma_1 y} + T_{32}^{[*]+}(y), \tag{3.3.3c}$$

where we have defined $T_{3i}^{*\pm}$ as

$$T_{31}^{[*]-} = -\frac{i\alpha\cosh\gamma_1 y}{\gamma_1\sinh\gamma_1 y_c}yA_1^{[*]\prime}(x_1),\ T_{32}^{[*]-} = -\frac{i\alpha\sinh\gamma_1}{\gamma_1\sinh\gamma_1 y_c}ye^{\gamma_1(1-y)}A_1^{[*]\prime}(x_1), \tag{3.3.4a}$$

$$T_{31}^{[*]+} = -\frac{i\alpha\cosh\gamma_1 y}{\gamma_1\sinh\gamma_1}ye^{\gamma_1(y_c-1)}A_1^{[*]\prime}(x_1),\ T_{32}^{[*]+} = \frac{i\alpha}{\gamma_1}ye^{\gamma_1(y_c-y)}A_1^{[*]\prime}(x_1) \tag{3.3.4b}$$

Matching to the Stokes layer at the wall we find, from (3.2.4.5),

$$G_{31}^{[*]\pm} = \frac{i{\gamma_1}^2}{\alpha c Fr\sqrt{-i\alpha c}}\bar{p}_{11}^{[*]}(0), \tag{3.3.5}$$

and we can express $\bar{p}_{11}^{[*]}(0)$, using the solutions (3.2.1.4), (3.2.1.5), (3.2.1.3) to show that,

$$\begin{aligned}\bar{p}_{11}^{[*]}(0) &= \frac{i\alpha Fr}{{\gamma_1}^2}\left(U_0'(0)\bar{v}_{11}^{[*]}(0) - (U_0(0)-c)\bar{v}_{11y}^{[*]}(0)\right)\\ &= \begin{cases} \dfrac{ci\alpha Fr}{\gamma_1 \sinh\gamma_1 y_c}A_1^{[*]}(x_1) \text{ for } y_c < 1 \\ \dfrac{ci\alpha Fr}{\gamma_1 \sinh\gamma_1}e^{\gamma_1(y_c-1)}A_1^{[*]}(x_1) \text{ for } y_c > 1 \end{cases}\end{aligned} \tag{3.3.6}$$

and again similar results hold, with γ_1 replaced by γ_2, for $\bar{v}_4$,$\bar{v}_4^*$. To find the values of the other unknowns we must use relations found from matching to the buffer and viscous interfacial layers. For clarity we will concentrate on the case of the wave $\bar{v}_3$ only. First, matching to the buffer layer yields the relations

$$[\bar{v}_3]_{y=y_c^-}^{y=y_c^+} = 0, \tag{3.3.7a}$$

$$\begin{aligned}[\bar{v}_{3y}]_{y=y_c^-}^{y=y_c^+} &= \left(\frac{\tilde{v}_1^*}{U_y(y_c)} - \frac{2\beta^2\tilde{p}_1^*}{Fr\rho^{\pm}i\alpha U_y(y_c)^2}\right)\int_{-\infty}^{\infty}\frac{\tilde{u}_{2mYY}}{Y}dY\\ &\quad +\left(\frac{\tilde{v}_2}{U_y(y_c)} - \frac{6\beta^2\tilde{p}_2}{Fr\rho^{\pm}i\alpha U_y(y_c)^2}\right)\int_{-\infty}^{\infty}\frac{\tilde{u}_{2mYY}^*}{Y}dY\\ &\quad +\left(\frac{\tilde{v}_2^*}{U_y(y_c)} - \frac{12\beta^2\tilde{p}_2^*}{Fr\rho^{\pm}i\alpha U_y(y_c)^2}\right)\int_{-\infty}^{\infty}\frac{\tilde{u}_{4mYY}}{Y}dY\\ &= K_1,\end{aligned} \tag{3.3.7b}$$

and then matching between the core flow and the viscous interfacial boundary layer we find

$$\bar{v}_3(y=1^+) = V_{3c}^+,\ \bar{v}_3(y=1^-) = V_{3c}^-, \tag{3.3.8}$$

$$\bar{p}_3(y=1^+) = P_{3c}^+,\ \bar{p}_3(y=1^-) = P_{3c}^-, \tag{3.3.9}$$

where $V_{3c}^{\pm}$,$P_{3c}^{\pm}$ are unknown constants of integration. Although we do not know anything about the precise values of these constants all that is required is the difference between them, which we find from (3.2.3.16) with (3.2.3.17). Hence

$$[\bar{v}_3]_{y=1^-}^{y=1^+} = V_{3c}^+ - V_{3c}^- = \frac{E_3^+}{\sigma^+}(1-\rho), \tag{3.3.10}$$

and E_3^+ is given by (3.2.3.14)-(3.2.3.16), with

$$\hat{p}_1^+ = \bar{p}_{1j}(1) = \frac{Fr\rho i\alpha}{{\gamma_1}^2}\left(U_{0j}'(1)\bar{v}_1(1) - (U_0(1)-c)\bar{v}_{1jy}(1)\right), \tag{3.3.11}$$

where $j = 2$ or $j = 3$ depending on whether $y_c < 1$ or $y_c > 1$ respectively. We need one further relation, and we find this in the core flow from a coupling of the $x-, z-$momentum equations with the incompressibility condition to get

$$[\rho^{\pm} i\alpha U_s \bar{v}_{3y}]_{1^-}^{1^+} = \left[\begin{array}{l} \rho^{\pm} i\alpha \bar{v}_3 {U_0}'(1) - \rho^{\pm} U_0(1)\bar{v}_{1yx_1} - \rho^{\pm} i\alpha U_s \bar{u}_{1x_1} \\ +\dfrac{i\alpha}{Fr}\bar{p}_{1x_1} - \dfrac{{\gamma_1}^2}{Fr}\bar{p}_3 \end{array}\right]_{1^-}^{1^+} \tag{3.3.12}$$

or, using the result from the interfacial layer (3.2.3.19), with (3.3.10) and (3.2.3.13)

$$[\rho^{\pm} i\alpha U_s \bar{v}_{3y}]_{1^-}^{1^+} = P_3\hat{v}_{1x_1}(1) + Q_3\bar{v}_{3j}(1) + R_3, \tag{3.3.13}$$

where $j = 3$ if $y_c < 1$, $j = 2$ if $y_c > 1$, and

$$\begin{aligned} P_3 &= 2\left(\frac{{\gamma_1}^2}{Fr\alpha^2 {U_s}^2} - \frac{1}{FrU_s}\right)(1 - \rho + {\gamma_1}^2 B) \\ &\quad + \left(1 - \frac{1}{U_s}\right)(\rho\lambda^+ - 1), \end{aligned}$$

$$Q_3 = \frac{{\gamma_1}^2}{i\alpha U_s Fr}(1 - \rho + {\gamma_1}^2 B) + i\alpha(\rho\lambda^+ - 1),$$

$$R_3 = \left(\frac{{\gamma_1}^2}{i\alpha U_s Fr}(1 - \rho + {\gamma_1}^2 B) - i\alpha(1-\rho)\right)\frac{E_3^+}{\sigma^+}.$$

We can now determine the unknown constants, in the expressions for $\bar{v}_{3i}$, (3.3.3). On substitution into the two interfacial jump conditions (3.3.13), (3.3.10) we find

$$F_{33}^- = e^{\gamma_1}\left(\frac{E_3^+}{\sigma^+}(1-\rho) + T_{31}^-(1) - T_{32}^-(1) + F_{32}^- \sinh\gamma_1 + G_{32}^- \cosh\gamma_1\right) \tag{3.3.14}$$

Applying relation (3.3.7a) we obtain

$$F_{31}^- = F_{32}^- + \frac{(G_{32}^- - G_{31}^-)}{\tanh\gamma_1 y_c}, \tag{3.3.15}$$

and then using the latter and substituting into the relation (3.3.7b) we get

$$G_{32}^- = G_{31}^- + \frac{K_1 \sinh\gamma_1}{\gamma_1\left(\sinh {\gamma_1}^2 - \cosh {\gamma_1}^2\right)}. \tag{3.3.16}$$

Substitution for F_{33}^-, G_{32}^- into the interfacial jump condition (3.3.13) gives the relation

$$\begin{aligned} F_{32}^-(-i\alpha U_s\gamma_1(\rho\sinh\gamma_1+\cosh\gamma_1)-Q_3\sinh\gamma_1) = \\ -i\alpha U_s\left(\rho T_{32y}^-(1)-T_{31y}^-(1)\right)+\left(G_{31}^-+\frac{K_1\sinh\gamma_1}{\gamma_1\left(\sinh^2\gamma_1-\cosh^2\gamma_1\right)}\right) \\ \times(i\alpha U_s\gamma_1(\rho\cosh\gamma_1+\sinh\gamma_1)+Q_3\cosh\gamma_1) \\ +P_3\bar{v}_{1x_1}(1)+R_3+Q_3\left(\frac{E_3^+}{\sigma^+}(1-\rho)+T_{31}^-(1)\right) \\ +i\alpha U_s\gamma_1\rho\left(\frac{E_3^+}{\sigma^+}(1-\rho)+T_{31}^-(1)-T_{32}^-(1)\right) \end{aligned} \tag{3.3.17}$$

and we note that

$$(-i\alpha U_s\gamma_1(\rho\sinh\gamma_1+\cosh\gamma_1)-Q_3\sinh\gamma_1)=0$$

is equivalent to the dispersion relation for the phase speed (3.1.1.10) and so the left hand side of (3.3.17) is zero, which gives the basis equation governing the amplitude function A_1. All that is to be done now is write all the various components in terms of A_1.

For the case of the critical layer in the upper fluid we find

$$\begin{aligned} F_{31}^+ = \left(\frac{E_3^+}{\sigma^+}(\rho-1)+(T_{32}^+(1)-T_{31}^+(1))+(G_{32}^+-G_{31}^+)\cosh\gamma_1\right) \\ \times\frac{1}{\sinh\gamma_1}+F_{32}^+, \end{aligned} \tag{3.3.18}$$

$$F_{33}^+ = e^{\gamma_1 y_c}\left(F_{32}^+\sinh\gamma_1 y_c+G_{32}^+\cosh\gamma_1 y_c\right), \tag{3.3.19}$$

$$G_{32}^+ = -F_{32}^+-\frac{K_1}{\gamma_1\sinh\gamma_1 y_c+\gamma_1\cosh\gamma_1 y_c}, \tag{3.3.20}$$

$$\begin{aligned} F_{32}^+(Q_3\sinh\gamma_1+i\alpha U_s\gamma_1(\rho\sinh\gamma_1+\cosh\gamma_1)(1+\frac{\cosh\gamma_1}{\sinh\gamma_1}) = \\ K_1\left(i\alpha U_s\left(\rho\gamma_1\sinh\gamma_1-\gamma_1\frac{\cosh{\gamma_1}^2}{\sinh\gamma_1}\right)-Q_3\cosh\gamma_1\right) \\ \times(\gamma_1\sinh\gamma_1 y_c+\gamma_1\cosh\gamma_1 y_c)^{-1} \\ -i\alpha U_s(\rho T_{32y}^+(1)-T_{31y}^+(1))+i\alpha U_s G_{31}^+\gamma_1\sinh\gamma_1 \\ -\frac{i\alpha U_s\cosh\gamma_1}{\sinh\gamma_1}\left(\frac{E_3^+}{\sigma^+}(1-\rho)+T_{31}^+(1)-T_{32}^+(1)+G_{31}^+\cosh\gamma_1\right) \\ +P_3\bar{v}_{1x_1}(1)+R_3+Q_3T_{32}^+(1). \end{aligned} \tag{3.3.21}$$

Again the left hand side of equation (3.3.21) is zero as it has a factor which is the dispersion relation and again we may form an amplitude equation for A_1. With similar results holding for $\bar{v}_3^*$, $\bar{v}_4$, $\bar{v}_4^*$ the problem is now fully described.

Next we write the pressures and normal velocity components in terms of the amplitudes $A_i^{[*]}$ and match the solutions of the core flow as $y \to y_c$ with those of the buffer layer as $|Y| \to \infty$.

From matching, via the buffer layer, to the core flow, the leading order normal velocity perturbations $\check{v}_{1,2}$ in the critical layer are

$$\check{v}_j^{[*]} = \bar{v}_j^{[*]}(y_c) \text{ for } j = 1, 2, \tag{3.3.22}$$

and so in conjunction with equation (A.8) from the Appendix we find

$$\check{p}_j^{[*]} = \frac{Fr\rho^{\pm}U_y(y_c)i\alpha}{{\gamma_j}^2} A_j^{[*]}(x_1) \text{ for } j = 1, 2. \tag{3.3.23}$$

We substitute for $\int_{-\infty}^{\infty} \tilde{u}_{nmYY}/Y dY$ in (3.2.2.24) using equations (A.19), (3.2.2.21) and change the notation to explicitly show the $A_1^{[*]}$-dependence writing

$$E_3^{+[*]} = \hat{E}_3^{+[*]} A_1^{[*]}(x_1), \qquad R_3 = \hat{R}_3^{[*]} A_1^{[*]}(x_1), \qquad T_{3i}^{\pm[*]} = \hat{T}_{3i}^{\pm[*]} A_{1x_1}^{[*]}(x_1),$$
$$G_{31}^{\pm[*]} = \hat{G}_{31}^{\pm[*]} A_1^{[*]}(x_1), \quad \check{p}_1^{[*]} = \check{P}_1^{[*]} A_1^{[*]}(x_1),$$

and likewise for the terms $E_4^{[*]}$, $R_4^{[*]}$, $T_{4i}^{\pm[*]}$, $G_{41}^{\pm[*]}$, $\check{p}_4^{[*]}$. Combining all our information we finally have the amplitude equations,

$$\begin{aligned}
&- 4\beta^4 \frac{\rho_i}{\mu_i} \xi (1 - \frac{2\beta^2}{\gamma_1}) A_1^* \times \\
&\quad \left(\check{P}_1 \check{P}_{1c}^* \int_{-\infty}^{x_1} A_1 A_{1c}^* ds + 3\check{P}_2 \check{P}_{1c} \int_{-\infty}^{x_1} A_2 A_{1c} ds + 3\check{P}_1^* \check{P}_{2c}^* \int_{-\infty}^{x_1} A_1^* A_{2c}^* ds \right) \\
&- 4\beta^4 \frac{\rho_i}{\mu_i} \xi (1 - \frac{6\beta^2}{\gamma_2}) A_2 \times \\
&\quad \left(\check{P}_1^* \check{P}_{1c} \int_{-\infty}^{x_1} A_1^* A_{1c} ds + 3\check{P}_{1c}^* \check{P}_2^* \int_{-\infty}^{x_1} A_{1c}^* A_2^* ds + 3\check{P}_1 \check{P}_{2c} \int_{-\infty}^{x_1} A_1 A_{2c} ds \right) \\
&- 48\beta^4 \frac{\rho_i}{\mu_i} \xi (1 - \frac{12\beta^2}{\gamma_2}) A_2^* \times \\
&\quad \left(\check{P}_1 \check{P}_{2c}^* \int_{-\infty}^{x_1} A_1 A_{2c}^* ds + \check{P}_{1c}^* \check{P}_2 \int_{-\infty}^{x_1} A_{1c}^* A_2 ds \right) = M_1^{\pm} A_1 + L_1^{\pm} A_1', \quad \text{(3.3.24a)}
\end{aligned}$$

$$
\begin{aligned}
&-4\beta^4\frac{\rho_i}{\mu_i}\xi(1-\frac{2\beta^2}{\gamma_1})A_1\times\\
&\quad\left(\check{P}_1^*\check{P}_{1c}\int_{-\infty}^{x_1}A_1^*A_{1c}ds+3\check{P}_{1c}^*\check{P}_2^*\int_{-\infty}^{x_1}A_{1c}^*A_2^*ds+3\check{P}_1\check{P}_{2c}\int_{-\infty}^{x_1}A_1A_{2c}ds\right)\\
&\quad-48\beta^4\frac{\rho_i}{\mu_i}\xi(1-\frac{12\beta^2}{\gamma_2})A_2\left(\check{P}_1\check{P}_{2c}^*\int_{-\infty}^{x_1}A_1A_{2c}^*ds+\check{P}_{1c}^*\check{P}_2\int_{-\infty}^{x_1}A_{1c}^*A_2ds\right)\\
&-4\beta^4\frac{\rho_i}{\mu_i}\xi(1-\frac{6\beta^2}{\gamma_2})A_2^*\times\\
&\quad\left(\check{P}_1\check{P}_{1c}^*\int_{-\infty}^{x_1}A_1A_{1c}^*ds+3\check{P}_2\check{P}_{1c}\int_{-\infty}^{x_1}A_2A_{1c}ds+3\check{P}_1^*\check{P}_{2c}^*\int_{-\infty}^{x_1}A_1^*A_{2c}^*ds\right)\\
&\qquad\qquad=M_1^{\pm}A_1^*+L_1^{\pm}A_1^{*'},\quad(3.3.24b)
\end{aligned}
$$

$$
\begin{aligned}
&-4\beta^4\frac{\rho_i}{\mu_i}\xi(1+\frac{2\beta^2}{\gamma_1})A_1\times\\
&\quad\left(\check{P}_1\check{P}_{1c}^*\int_{-\infty}^{x_1}A_1A_{1c}^*ds+3\check{P}_2\check{P}_{1c}\int_{-\infty}^{x_1}A_2A_{1c}ds+3\check{P}_1^*\check{P}_{2c}^*\int_{-\infty}^{x_1}A_1^*A_{2c}^*ds\right)\\
&\quad-48\beta^4\frac{\rho_i}{\mu_i}\xi(1-\frac{4\beta^2}{\gamma_1})A_1^*\left(\check{P}_1\check{P}_{2c}^*\int_{-\infty}^{x_1}A_1A_{2c}^*ds+\check{P}_{1c}^*\check{P}_2\int_{-\infty}^{x_1}A_{1c}^*A_2ds\right)\\
&-324\beta^4\frac{\rho_i}{\mu_i}\xi(1-\frac{18\beta^2}{\gamma_2})A_2^*\left(\check{P}_2\check{P}_{2c}^*\int_{-\infty}^{x_1}A_2A_{2c}^*ds\right)=M_2^{\pm}A_2+L_2^{\pm}A_2^{'},\quad(3.3.24c)
\end{aligned}
$$

$$
\begin{aligned}
&-48\beta^4\frac{\rho_i}{\mu_i}\xi(1-\frac{4\beta^2}{\gamma_1})A_1\left(\check{P}_1\check{P}_{2c}^*\int_{-\infty}^{x_1}A_1A_{2c}^*ds+\check{P}_{1c}^*\check{P}_2\int_{-\infty}^{x_1}A_{1c}^*A_2ds\right)\\
&-4\beta^4\frac{\rho_i}{\mu_i}\xi(1+\frac{2\beta^2}{\gamma_1})A_1^*\times\\
&\quad\left(\check{P}_1^*\check{P}_{1c}\int_{-\infty}^{x_1}A_1^*A_{1c}ds+3\check{P}_{1c}^*\check{P}_2^*\int_{-\infty}^{x_1}A_{1c}^*A_2^*ds+3\check{P}_1\check{P}_{2c}\int_{-\infty}^{x_1}A_1A_{2c}ds\right)\\
&-324\beta^4\frac{\rho_i}{\mu_i}\xi(1-\frac{18\beta^2}{\gamma_2})A_2\left(\check{P}_2\check{P}_{2c}^*\int_{-\infty}^{x_1}A_2A_{2c}^*ds\right)=M_2^{\pm}A_2^*+L_2^{\pm}A_2^{*'},\quad(3.3.24d)
\end{aligned}
$$

where

$$
\xi=\left(\frac{\mu^{\pm}}{\alpha U_y(y_c)\rho^{\pm}}\right)^{\frac{5}{3}}\frac{\pi}{Fr^2\mu^{\pm 2}}\left(\frac{2}{3}\right)^{\frac{2}{3}}\Gamma\left(\frac{1}{3}\right),
$$

$$
\begin{aligned}
M_1^- &= +\frac{\gamma_1}{\sinh\gamma_1\left(\gamma_1 i\alpha U_s(\rho\cosh\gamma_1+\sinh\gamma_1)+Q_3\cosh\gamma_1\right)}\\
&\times\begin{pmatrix}\hat{R}_3+(Q_3+i\alpha U_s\gamma_1\rho)\frac{\hat{E}_3^+}{\sigma^+}(1-\rho)\\ +\hat{G}_{31}^-\left((\gamma_1 i\alpha U_s(\rho\cosh\gamma_1+\sinh\gamma_1)+Q_3\cosh\gamma_1)\right)\end{pmatrix},\qquad(3.3.25a)
\end{aligned}
$$

$$L_1^- = -\frac{\gamma_1}{\sinh\gamma_1\left(\gamma_1 i\alpha U_s(\rho\cosh\gamma_1+\sinh\gamma_1)+Q_3\cosh\gamma_1\right)}$$
$$\times\begin{pmatrix} P_3V_1(1)+Q_3\hat{T}_{31}^-(1)-i\alpha U_s(\rho\hat{T}_{32y}(1)-\hat{T}_{31y}(1)) \\ +i\alpha U_s\gamma_1\rho(\hat{T}_{31}^-(1)-\hat{T}_{32}^-(1)) \end{pmatrix}, \qquad (3.3.25b)$$

$$M_1^+ = -\frac{\gamma_1(\sinh\gamma_1 y_c+\cosh\gamma_1 y_c)}{i\alpha U_s(\rho\gamma_1\sinh\gamma_1-\frac{\gamma_1\cosh\gamma_1{}^2}{\sinh\gamma_1})-Q_3\cosh\gamma_1}$$
$$\times\begin{pmatrix} i\alpha U_s\gamma_1\left(\hat{G}_{31}^-\sinh\gamma_1-\frac{\cosh\gamma_1}{\sinh\gamma_1}\left(\frac{\hat{E}_3^+}{\sigma^+}(1-\rho)+\hat{G}_{31}^-\cosh\gamma_1\right)\right) \\ +\hat{R}_3 \end{pmatrix}, \qquad (3.3.26a)$$

$$L_1^+ = -\frac{\gamma_1(\sinh\gamma_1 y_c+\cosh\gamma_1 y_c)}{i\alpha U_s(\rho\gamma_1\sinh\gamma_1-\frac{\gamma_1\cosh\gamma_1{}^2}{\sinh\gamma_1})-Q_3\cosh\gamma_1}$$
$$\times\begin{pmatrix} \frac{P_3e^{\gamma_1(y_c-1)}}{i\alpha U_s}+Q_3\hat{T}_{32}^+(1)-i\alpha U_s\left(\rho\hat{T}_{32y}^+(1)-\hat{T}_{31y}^+(1)\right) \\ -\frac{i\alpha U_s\gamma_1\cosh\gamma_1}{\sinh\gamma_1}\left(\hat{T}_{31}^+(1)-\hat{T}_{32}^+(1)\right) \end{pmatrix}, \qquad (3.3.26b)$$

and for $L_2^\pm, M_2^\pm$ simply replace γ_1 by γ_2, and the subscripts 3 with the subscript 4.

The effect of four-wave resonance in the non-linear VWI is now obvious. We see that the nonlinearity in the amplitude equations supplies a coupling between the first and second pairs of waves. This coupling can be traced back to the mechanism of the vortex-production by waves. For example the $e^{i\beta z}$ wave term contributes to the $e^{2i\beta z}$ vortex components, which in self-interaction with the $e^{i\beta z}$ wave contributes both to that wave and to the second wave proportional to $e^{3i\beta z}$. The second pair of waves acts in a similar manner. For the four-wave interaction to be possible, however, the resonance conditions formulated at the start of this chapter must be satisfied. For non-resonant waves the amplitude equations simplify and the entire theory reduces to a special parallel-flow case of the VWI-theory developed in SBB.

Equations (3.3.24)-(3.3.26) were solved numerically using a second order accurate marching method. Figs 3:5 (a),(b) show the effect of the nonlinearity on the wave development in the flow, with the parameters taken from a resonant solution to (3.1.1.10). A number of different wave evolutions are possible, as in SBB, depending on the signs of $M_i^\pm, L_i^\pm$ and the β-dependent nonlinear coefficients. Due to the

large number of possible parameter values, with the four initial wave amplitudes also altering the flow development we present only a few example cases, all with symmetric initial conditions for the pairs of waves. Imposing the initial conditions $A_1 = A_1^* = 1, A_2 = A_2^* = 0$ at $x_1 = 0$, in fig 3:5(a) we see that a finite-distance blow-up of both pairs of waves occurs, with the second pair of waves, which are infinitesimally small at the initial station, captured by the nonlinearity. For the cases that were investigated, the non-linear growth of the initially infinitesimally small pair of waves was a typical phenomenon. In SBB this blow-up could be attributed to a ratio of the spanwise and streamwise wavenumbers and the equations could be reduced to a quadratic form for analysis, however in our case this reduction can not be done because of the interplay between modes. A comparison with the linear behaviour of the solution shows the dramatic effect of the nonlinear terms. A second resonant example, shown in fig 3:5(b), shows the nonlinearity stimulating growth in the second pair of waves and retarding the first pair before both are damped further downstream.

A Appendix A: The Critical layer

The critical layer has scalings governed by the balance

$$(U_0 - c)u \sim Re^{-1}u_{yy}, \tag{A.1a}$$

$$\Rightarrow (y - y_c)U_y(y_c)u \sim Re^{-1}u_{yy}. \tag{A.1b}$$

We introduce a new variable Y_1 where

$$y - y_c = \epsilon^2 Y_1 \tag{A.2}$$

and expand the velocities and pressure as

$$\begin{aligned} u &= U_0(y_c) + \epsilon^2 U_y(y_c)Y_1 + ... \\ &+\epsilon^5 \left(\begin{array}{l} (\breve{u}_1 e^{i\beta z} + \breve{u}_1^* e^{-i\beta z} + \breve{u}_2 e^{+i3\beta z} + \breve{u}_2^* e^{-i3\beta z})E + \\ (\breve{u}_{1c} e^{-i\beta z} + \breve{u}_{1c}^* e^{i\beta z} + \breve{u}_{2c} e^{-i3\beta z} + \breve{u}_{2c}^* e^{i3\beta z})E^{-1} + \\ \epsilon^3(\breve{u}_3 e^{i\beta z} + ...)E + ... + c.c., \end{array} \right) \end{aligned} \tag{A.3a}$$

$$v = \epsilon^5 \begin{pmatrix} (\breve{v}_1 e^{i\beta z} + \breve{v}_1^* e^{-i\beta z} + \breve{v}_2 e^{+i3\beta z} + \breve{v}_2^* e^{-i3\beta z})E + \\ (\breve{v}_{1c} e^{-i\beta z} + \breve{v}_{1c}^* e^{i\beta z} + \breve{v}_{2c} e^{-i3\beta z} + \breve{v}_{2c}^* e^{i3\beta z})E^{-1} + \\ \epsilon^3(\breve{v}_3 e^{i\beta z} + ...)E + ... + c.c. \end{pmatrix} + ..., \qquad \text{(A.3b)}$$

$$w = \epsilon^8 \begin{pmatrix} \breve{w}_{0m} + \breve{w}_{2m} e^{2i\beta z} + \breve{w}_{2m}^* e^{-2i\beta z} + \breve{w}_{4m} e^{4i\beta z} \\ + \breve{w}_{4m}^* e^{-4i\beta z} + \breve{w}_{6m} e^{6i\beta z} + \breve{w}_{6m}^* e^{-6i\beta z} \end{pmatrix} + ...$$

$$+\epsilon^5 \begin{pmatrix} (\breve{w}_1 e^{i\beta z} + \breve{w}_1^* e^{-i\beta z} + \breve{w}_2 e^{+i3\beta z} + \breve{w}_2^* e^{-i3\beta z})E + \\ (\breve{w}_{1c} e^{-i\beta z} + \breve{w}_{1c}^* e^{i\beta z} + \breve{w}_{2c} e^{-i3\beta z} + \breve{w}_{2c}^* e^{i3\beta z})E^{-1} + \\ \epsilon^3(\breve{w}_3 e^{i\beta z} + ...)E + ... + c.c. \end{pmatrix}, \qquad \text{(A.3c)}$$

$$p = P_0(y) + \epsilon^2 P_0{}'(y_c) + ...$$

$$+\epsilon^5 \begin{pmatrix} (\breve{p}_1 e^{i\beta z} + \breve{p}_1^* e^{-i\beta z} + \breve{p}_2 e^{+i3\beta z} + \breve{p}_2^* e^{-i3\beta z})E + \\ (\breve{p}_{1c} e^{-i\beta z} + \breve{p}_{1c}^* e^{i\beta z} + \breve{p}_{2c} e^{-i3\beta z} + \breve{p}_{2c}^* e^{i3\beta z})E^{-1} + \\ \epsilon^3(\breve{p}_3 e^{i\beta z} + ...)E + ... + c.c. \end{pmatrix} \qquad \text{(A.3d)}$$

where $\breve{w}_{nm}$ is, as will be demonstrated, the lowest order mean-flow correction generated by the jumps in the transverse shear stresses.

As in the other sections we proceed by substituting these expansions into our equations (3.1.1) and collecting terms of like magnitude in ϵ. From matching between the critical layer flow and the buffer layer we know that

$$\breve{v}_{iY_1}^{[*]} = 0 \text{ for } i = 1, 2, \qquad \text{(A.4)}$$

and obviously the conjugates are also constant with respect to Y_1. Turning to the continuity equation we obtain

$$\breve{u}_1 = -\frac{\beta}{\alpha}\breve{w}_1, \quad \breve{u}_1^* = \frac{\beta}{\alpha}\breve{w}_1^*, \quad \breve{u}_2 = -\frac{3\beta}{\alpha}\breve{w}_2, \quad \breve{u}_2^* = \frac{3\beta}{\alpha}\breve{w}_2^*,$$
$$\breve{u}_{1c} = -\frac{\beta}{\alpha}\breve{w}_{1c}, \quad \breve{u}_{1c}^* = \frac{\beta}{\alpha}\breve{w}_{1c}^*, \quad \breve{u}_{2c} = -\frac{3\beta}{\alpha}\breve{w}_{2c}, \quad \breve{u}_{2c}^* = \frac{3\beta}{\alpha}\breve{w}_{2c}^*. \qquad \text{(A.5)}$$

From the x-momentum we establish that

$$i\alpha U_y(y_c)Y_1\breve{u}_1 + U_y(y_c)\breve{v}_1 = -\frac{i\alpha\breve{p}_1}{Fr\rho^{\pm}} + \frac{\mu^{\pm}}{\rho^{\pm}}\breve{u}_{1Y_1Y_1}, \qquad \text{(A.6)}$$

and from the z-momentum balance we have

$$i\alpha U_y(y_c)Y_1\breve{w}_1 = -\frac{i\beta\breve{p}_1}{Fr\rho^{\pm}} + \frac{\mu^{\pm}}{\rho^{\pm}}\breve{w}_{1Y_1Y_1}. \qquad \text{(A.7)}$$

Together with the results from the y-momentum, that $\breve{p}_1^{[*]}, \breve{p}_2^{[*]}$ are Y_1- independent, and those of (A.5) we get

$$\breve{p}_1^{[*]} = \frac{U_y(y_c) i\alpha Fr \rho^{\pm} \breve{v}_1^{[*]}}{{\gamma_1}^2}, \tag{A.8a}$$

$$\breve{p}_2^{[*]} = \frac{U_y(y_c) i\alpha Fr \rho^{\pm} \breve{v}_2^{[*]}}{{\gamma_2}^2}, \tag{A.8b}$$

From the z-momentum equation we find, from the E independent terms that $\breve{w}_{0m} = 0$ and collecting terms in $e^{2i\beta z}$ of $O(\epsilon^{10})$ gives us

$$\begin{aligned} &-i\alpha(\breve{u}_1\breve{w}_{1c}^* + \breve{u}_1^*\breve{w}_{2c}^* + \breve{u}_2\breve{w}_{1c} + \breve{u}_{1c}\breve{w}_2 + \breve{u}_{1c}^*\breve{w}_1 + \breve{u}_{2c}^*\breve{w}_1^*) \\ &+\breve{v}_1\breve{w}_{1cY_1}^* + \breve{v}_1^*\breve{w}_{2cY_1}^* + \breve{v}_2\breve{w}_{1cY_1} + \breve{v}_{1c}\breve{w}_{2Y_1} + \breve{v}_{1c}^*\breve{w}_{1Y_1} + \breve{v}_{2c}^*\breve{w}_{1Y_1}^* \\ &+i\beta(\breve{w}_1\breve{w}_{1c}^* + 3\breve{w}_1^*\breve{w}_{2c}^* - \breve{w}_2\breve{w}_{1c} + 3\breve{w}_{1c}\breve{w}_2 + \breve{w}_{1c}^*\breve{w}_1 - \breve{w}_{2c}^*\breve{w}_1^*) \\ &= \frac{\mu^{\pm}}{\rho^{\pm}}\breve{w}_{2mY_1Y_1}, \end{aligned} \tag{A.9}$$

Substituting for $\breve{u}_i^{[*]}$ we have

$$\begin{aligned} &\breve{v}_1\breve{w}_{1cY_1}^* + \breve{v}_{1c}^*\breve{w}_{1Y_1} + \breve{v}_{1c}\breve{w}_{2Y_1} + \breve{v}_2\breve{w}_{1cY_1} + \breve{v}_{2c}^*\breve{w}_{1Y_1}^* + \breve{v}_1^*\breve{w}_{2cY_1}^* \\ &+4i\beta(\breve{w}_1\breve{w}_{1c}^* + \breve{w}_{1c}\breve{w}_2 + \breve{w}_1^*\breve{w}_{2c}^*) = \frac{\mu^{\pm}}{\rho^{\pm}}\breve{w}_{2mY_1Y_1}, \end{aligned} \tag{A.10}$$

and using equation (A.4) we obtain the relation

$$\begin{aligned} \int_{-\infty}^{\infty} \breve{w}_{2mY_1Y_1}\, dY_1 &= 4i\beta\frac{\rho^{\pm}}{\mu^{\pm}}\int_{-\infty}^{\infty}(\breve{w}_1\breve{w}_{1c}^* + \breve{w}_{1c}\breve{w}_2 + \breve{w}_1^*\breve{w}_{2c}^*)\, dY_1 \\ &+ \left[\begin{array}{l} \breve{v}_1\breve{w}_{1c}^* + \breve{v}_{1c}^*\breve{w}_1 + \breve{v}_{1c}\breve{w}_2 + \\ \breve{v}_2\breve{w}_{1c} + \breve{v}_{2c}^*\breve{w}_1^* + \breve{v}_1^*\breve{w}_{2c}^* \end{array}\right]_{-\infty}^{\infty}. \end{aligned} \tag{A.11}$$

where we have used the fact that $\breve{v}_{i(c)}^{[*]}$'s are Y_1 independent and since

$$\breve{w}_{i(c)}^{[*]} \sim \frac{1}{Y_1}, \text{ for } i = 1, 2, \tag{A.12}$$

this implies

$$\breve{w}_{i(c)}^{[*]} \to 0 \text{ as } \mid Y_1 \mid \to \infty \text{ for } i = 1, 2$$

and the term is square brackets in (A.11) does not contribute and we simply have

$$\int_{-\infty}^{\infty} \breve{w}_{2mY_1Y_1} dY_1 = 4i\beta\frac{\rho^{\pm}}{\mu^{\pm}} \int_{-\infty}^{\infty} \breve{w}_1\breve{w}_{1c}^* + \breve{w}_{1c}\breve{w}_2 + \breve{w}_1^*\breve{w}_{2c}^* dY_1. \quad \text{(A.13a)}$$

Similarly

$$\int_{-\infty}^{\infty} \breve{w}_{2mY_1Y_1}^* dY_1 = -4i\beta\frac{\rho^{\pm}}{\mu^{\pm}} \int_{-\infty}^{\infty} \breve{w}_1^*\breve{w}_{1c} + \breve{w}_{1c}^*\breve{w}_2^* + \breve{w}_1\breve{w}_{2c} dY_1, \quad \text{(A.13b)}$$

$$\int_{-\infty}^{\infty} \breve{w}_{4mY_1Y_1} dY_1 = 8i\beta\frac{\rho^{\pm}}{\mu^{\pm}} \int_{-\infty}^{\infty} \breve{w}_{2c}^*\breve{w}_1 + \breve{w}_{1c}^*\breve{w}_2 dY_1, \quad \text{(A.13c)}$$

$$\int_{-\infty}^{\infty} \breve{w}_{4mY_1Y_1}^* dY_1 = -8i\beta\frac{\rho^{\pm}}{\mu^{\pm}} \int_{-\infty}^{\infty} \breve{w}_{2c}\breve{w}_1^* + \breve{w}_{1c}\breve{w}_2^* dY_1, \quad \text{(A.13d)}$$

$$\int_{-\infty}^{\infty} \breve{w}_{6mY_1Y_1} dY_1 = 12i\beta\frac{\rho^{\pm}}{\mu^{\pm}} \int_{-\infty}^{\infty} \breve{w}_2\breve{w}_{2c}^* dY_1, \quad \text{(A.13e)}$$

$$\int_{-\infty}^{\infty} \breve{w}_{6mY_1Y_1}^* dY_1 = -12i\beta\frac{\rho^{\pm}}{\mu^{\pm}} \int_{-\infty}^{\infty} \breve{w}_2^*\breve{w}_{2c} dY_1. \quad \text{(A.13f)}$$

Now returning to the z-momentum equation and picking terms in $e^{i\beta z}$ of $O(\epsilon^7)$ we get

$$\breve{w}_{1Y_1Y_1} - i\alpha U_y(y_c)\frac{\rho^{\pm}}{\mu^{\pm}} Y_1\breve{w}_1 = -\frac{i\beta\breve{p}_1}{Fr\mu^{\pm}}, \quad \text{(A.14)}$$

which has the solution

$$\breve{w}_1 = -\frac{i\beta\breve{p}_1}{Fr\mu^{\pm}}\left(\frac{\mu^{\pm}}{\alpha U_y(y_c)\rho^{\pm}}\right)^{2/3} \int_0^{\infty} e^{i\left(\rho^{\pm}\alpha U_y(y_c)/\mu^{\pm}\right)^{1/3} Y_1 k - k^3/3} dk. \quad \text{(A.15)}$$

We combine this with the solution for the conjugate

$$\breve{w}_{1c} = +\frac{i\beta\breve{p}_{1c}}{Fr\mu^{\pm}}\left(\frac{\mu^{\pm}}{\alpha U_y(y_c)\rho^{\pm}}\right)^{2/3} \int_0^{\infty} e^{i\left(\rho^{\pm}\alpha U_y(y_c)/\mu^{\pm}\right)^{1/3} Y_1 k - k^3/3} dk, \quad \text{(A.16)}$$

to obtain

$$\int_{-\infty}^{\infty} \breve{w}_1\breve{w}_{1c}^* dY_1 = -\pi\left(\frac{\mu^{\pm}}{\alpha U_y(y_c)\rho^{\pm}}\right)^{5/3} \frac{\beta^2\breve{p}_1\breve{p}_{1c}^*}{Fr^2\mu^{\pm 2}}\left(\frac{2}{3}\right)^{2/3}\left(-\frac{2}{3}\right)!. \quad \text{(A.17)}$$

and in general we get

$$\int_{-\infty}^{\infty} \breve{w}_j^{[*]} \breve{w}_{kc}^{[*]} dY_1 = \xi(\breve{p}_j^{[*]}[\mp] li\beta)(-\breve{p}_{kc}^{[*]}[\mp]) ni\beta), \tag{A.18}$$

where

$$l, n = \begin{cases} 1 \text{ when } j, k = 1 \\ 3 \text{ when } j, k = 2 \end{cases}$$

and

$$\xi = \frac{\pi}{Fr^2 \mu^{\pm 2}} \left(\frac{\mu^{\pm}}{\alpha U_y(y_c) \rho^{\pm}} \right)^{5/3} \left(\frac{2}{3} \right)^{2/3} \left(-\frac{2}{3} \right)!$$

Combining equations (A.13) and (A.18) give us expressions for the jump in the transverse shear across the critical layer, e.g

$$\begin{aligned} [\breve{w}_{4mY_1}]_-^+ &= \frac{8i\beta\xi\rho^{\pm}}{\mu^{\pm}} ((i\beta\breve{p}_1)(-3i\beta\breve{p}_{2c}^*) + (3i\beta\breve{p}_2)(-i\beta\breve{p}_{1c}^*)) \\ &= 24i\beta^3 \frac{\rho^{\pm}}{\mu^{\pm}} (\breve{p}_1 \breve{p}_{2c}^* + \breve{p}_2 \breve{p}_{1c}^*) \end{aligned} \tag{A.19}$$

with similar expressions for w_{4m}^*, $w_{2m}^{[*]}$,$w_{6m}^{[*]}$.

3.2 Tables and figures

α	μ	Fr	B	ρ	ν	β	C
0.1	0.1	1000	0	0.2	0.5	2.6200	1.8376
0.1	0.1	1000	2	0.2	0.5	0.3800	2.7881
0.2	0.1	1000	2	0.2	0.5	0.6200	2.6058
0.3	0.1	1000	2	0.2	0.5	0.7900	2.4621
0.4	0.1	1000	2	0.2	0.5	0.9233	2.3519
0.5	0.1	1000	2	0.2	0.5	1.0300	2.2609
0.1	0.1	1000	2	0.3	0.33	0.6300	4.0701
0.2	0.1	1000	2	0.3	0.33	0.9400	3.5907
0.3	0.1	1000	2	0.3	0.33	1.1533	3.2909
0.4	0.1	1000	2	0.3	0.33	1.3167	3.0771
0.1	0.2	1000	6	0.3	0.67	0.1500	1.9468
0.1	0.3	1000	6	0.5	0.6	0.2100	2.1885
0.1	0.4	1000	6	0.5	0.8	0.2100	1.3853
0.2	0.1	10	0	0.2	0.5	0.2033	2.9240
0.3	0.1	10	0	0.2	0.5	0.7733	2.7032
0.4	0.1	10	0	0.2	0.5	1.1733	2.4715
0.5	0.1	10	0	0.2	0.5	1.4733	2.2923
0.2	0.3	10	2	0.5	0.6	0.0300	2.2484
0.3	0.3	10	2	0.5	0.6	0.0330	2.1981

Table 3:1 A few examples of resonant sets of parameters for which $c(\beta) = c(3\beta)$.

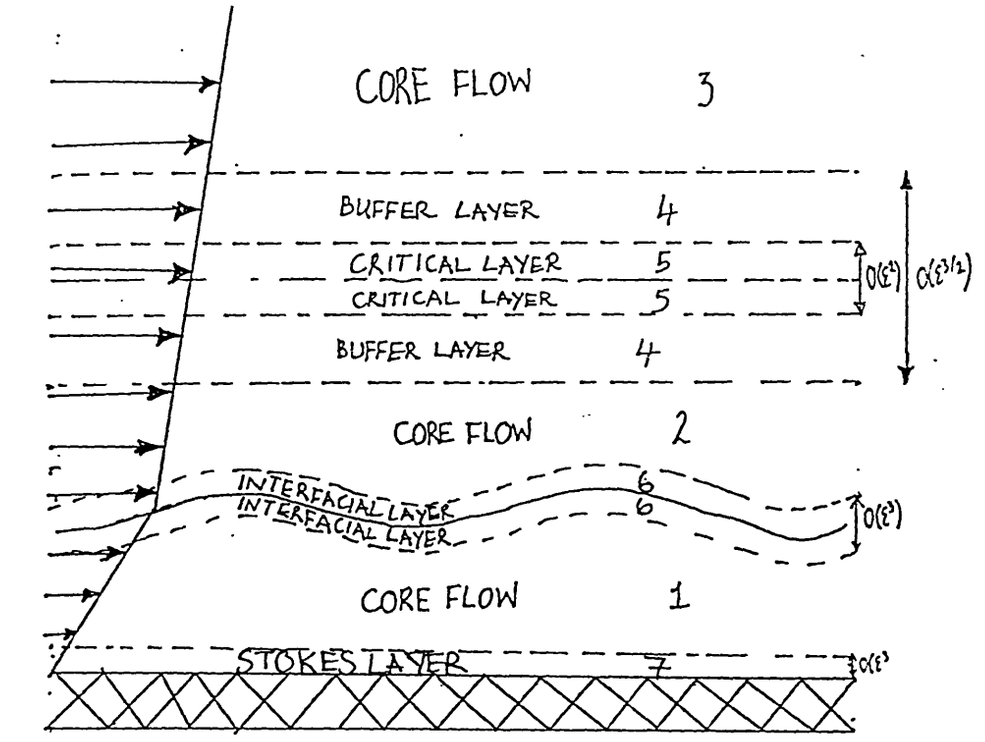

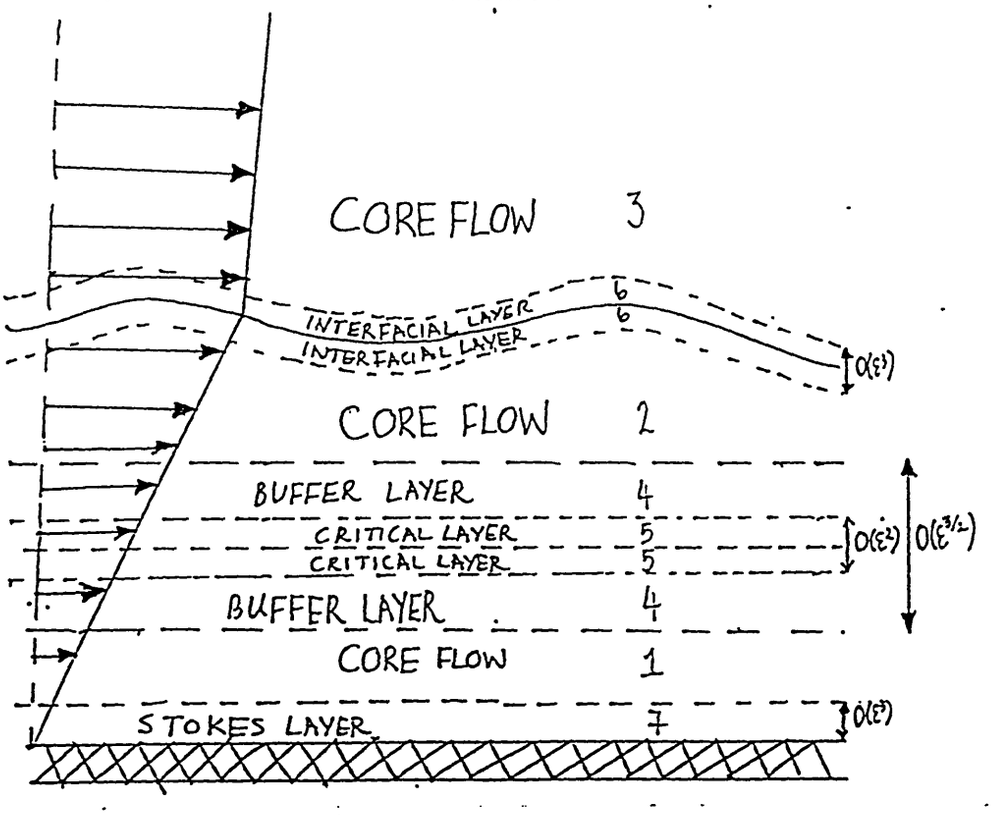

Figure 3:1 The base flow structure in the case when the critical layer occurs **(a)** above the interface and **(b)** below the interface

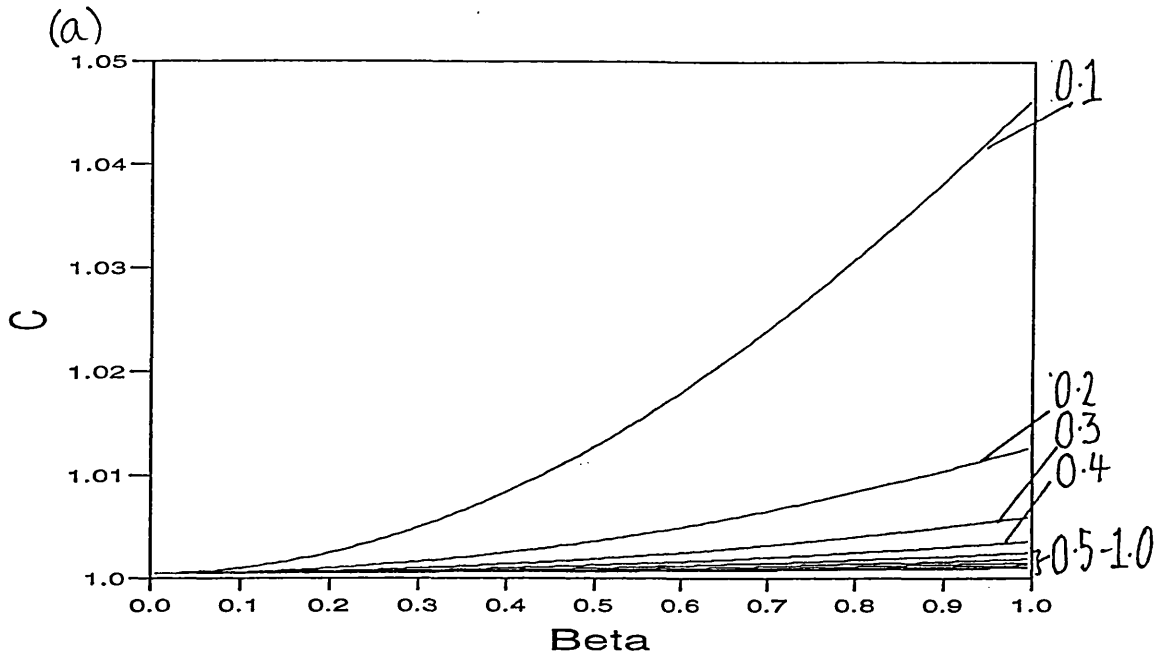

Froude no.=1000.0000 Bond/Fr= 0.0000 Alpha= 0.1000 Rho= 0.5000 Mu= 1.0000

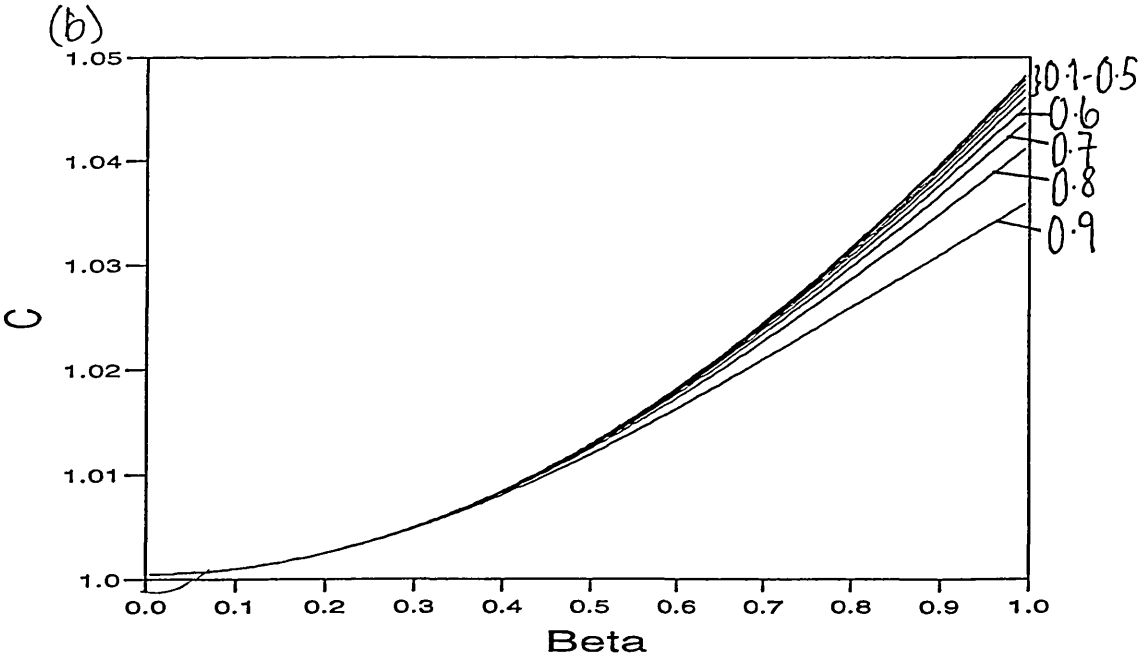

Froude no.=1000.0000 Bond/Fr= 0.0000 Alpha= 0.1000 Rho= 0.1000 Mu= 1.0000

Figure 3:2 Numerical solutions of (3.1.1.10), phase speed c plotted against β, with psrameters indicated below each figure (a) α varying, (b) ρ varying.

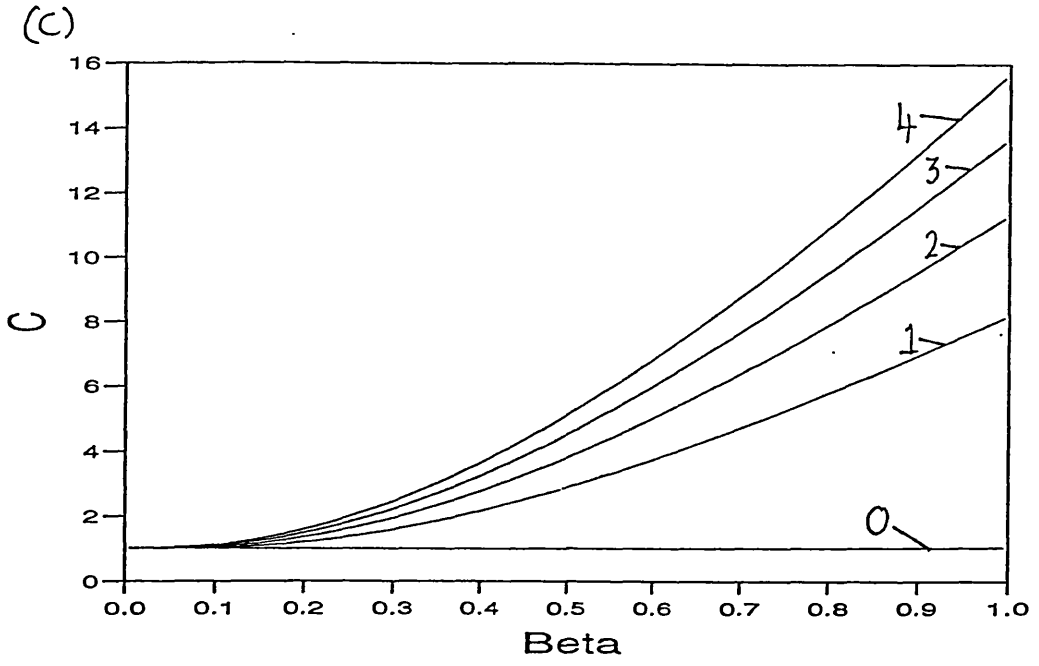

Froude no.=1000.0000 Bond/Fr= 0.0000 Alpha= 0.1000 Rho= 0.5000 Mu= 1.0000

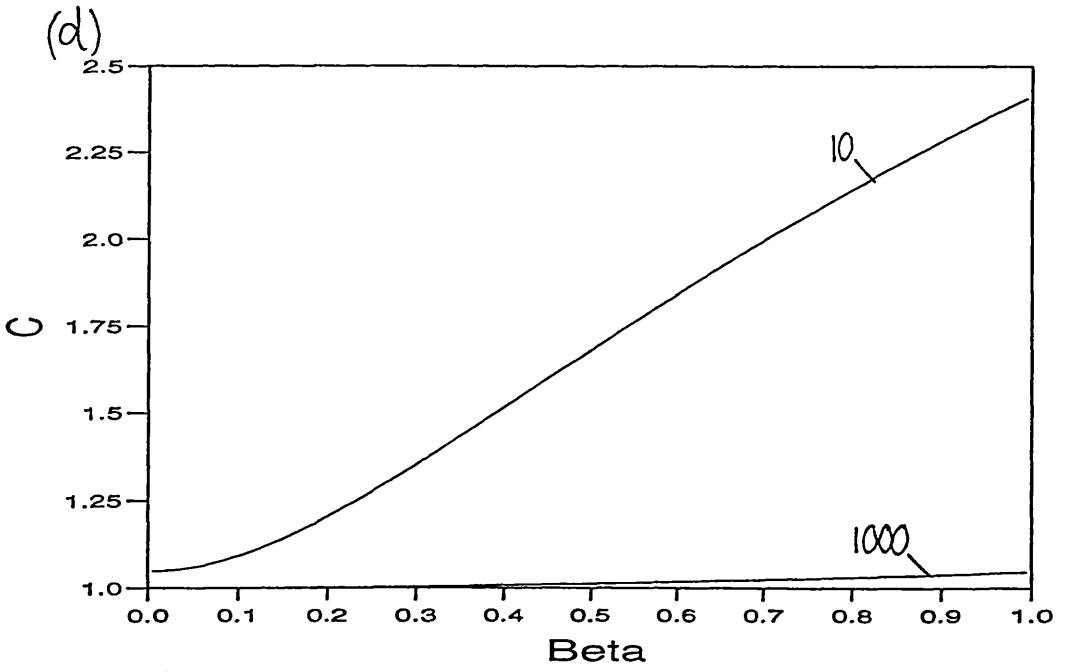

Froude no.=1000.0000 Bond/Fr= 0.0000 Alpha= 0.1000 Rho= 0.5000 Mu= 1.0000

Figure 3:2 As before, (c) $\tilde{B} = B/Fr$ varying, (d) Fr varying.

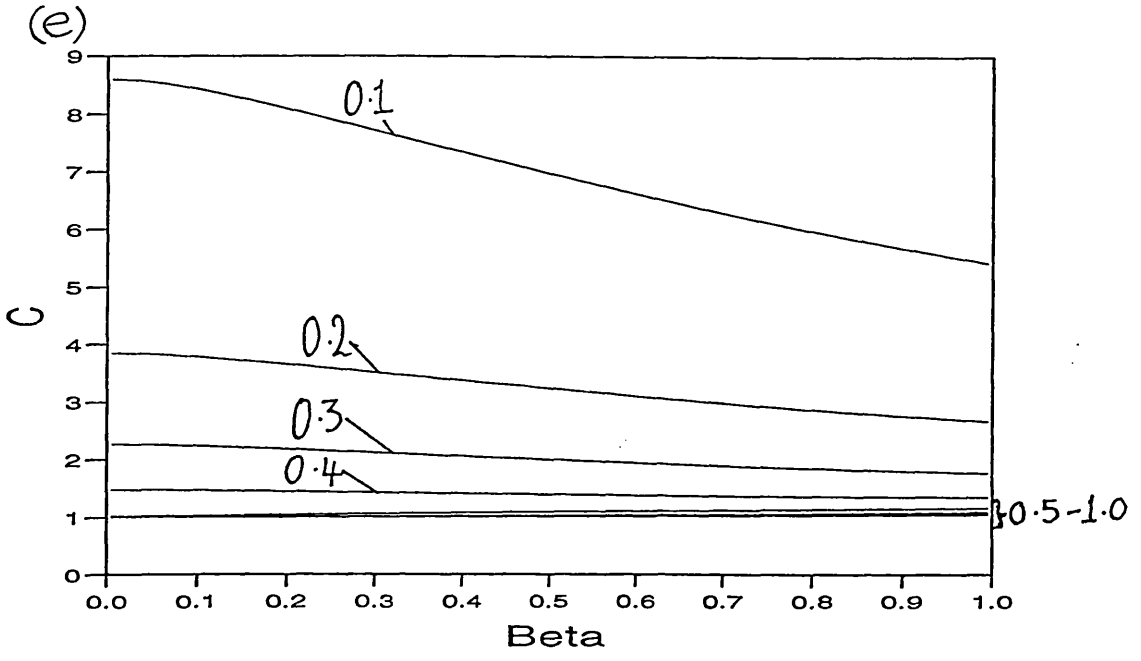

Froude no.=1000.0000 Bond/Fr= 0.0000 Alpha= 0.1000 Rho= 0.5000 Mu= 0.1000

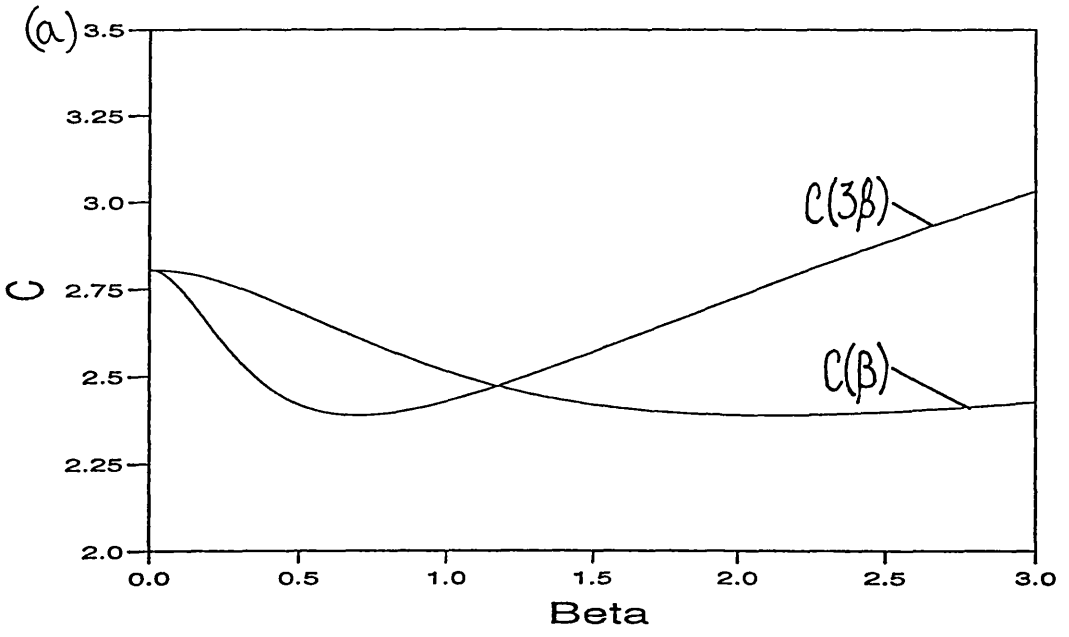

Froude no.= 10.00 Bond no.= 0.0000 Alpha= 0.4000 Rho= 0.2000 Mu= 0.1000

Figure 3:2 As before, (e) μ varying.

Figure 3:3 (a) Numerical solutions of (3.1.1.10), phase speed c plotted against α, for crosswise wavenumbers β and 3β, with parameters indicated underneath the figure.

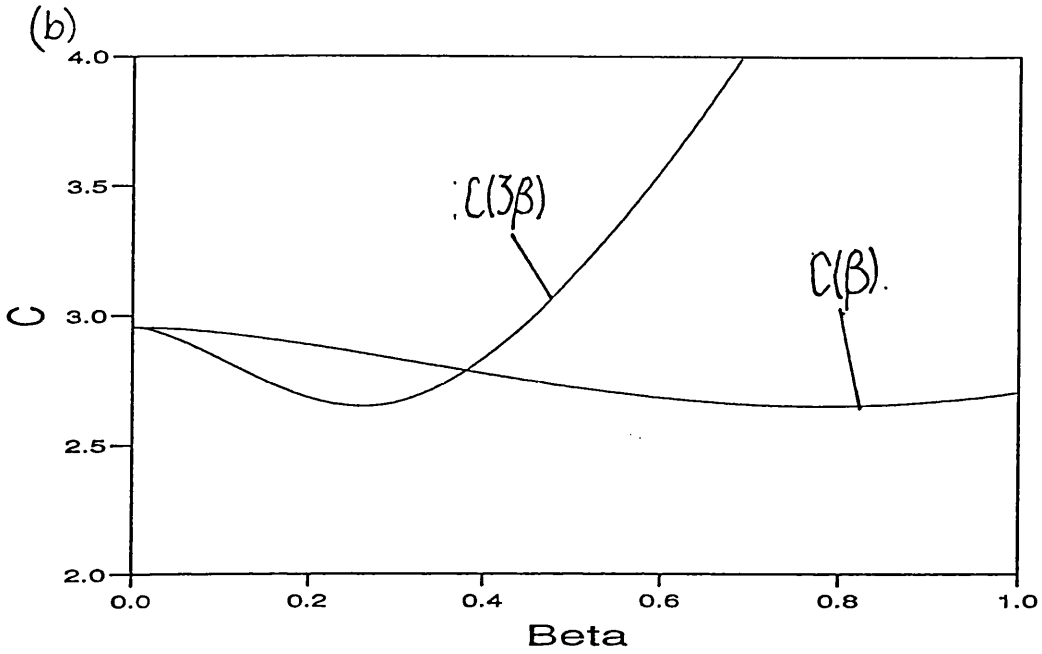

Froude no.=1000.00 Bond/Fr= 2.0000 Alpha= 0.1000 Rho= 0.2000 Mu= 0.1000

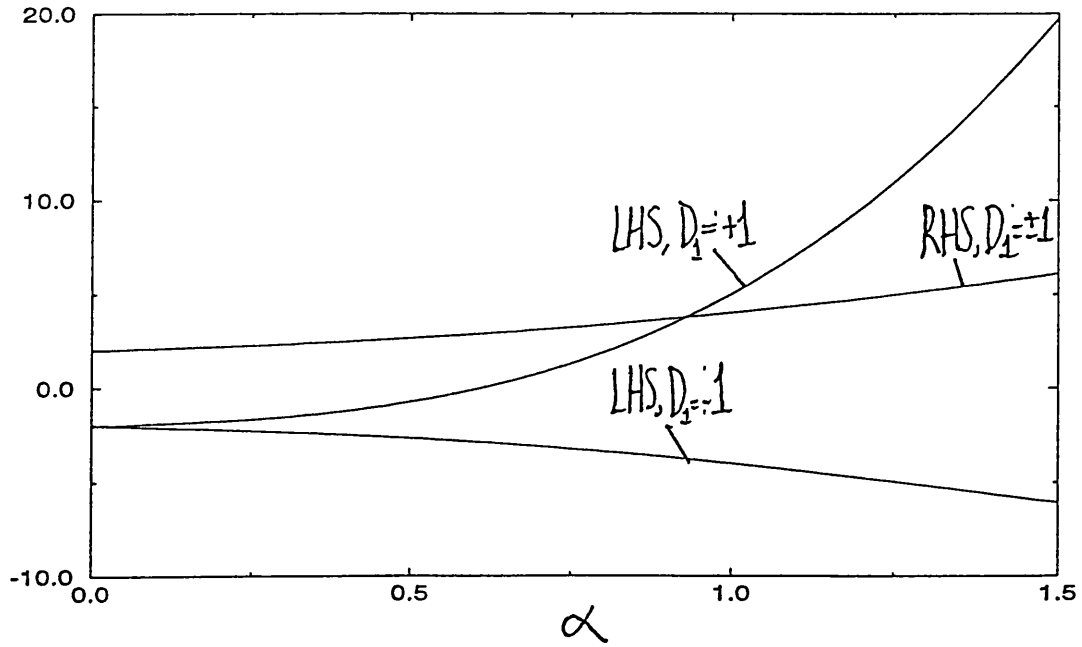

Figure 3:3(b) As before, with parameters indicated below the figure.

Figure 3:4 A plot of the left and right hand side of equation (3.1.2.7) against α with $D_2 = 1$, $D_3 = 2$, and various D_1.

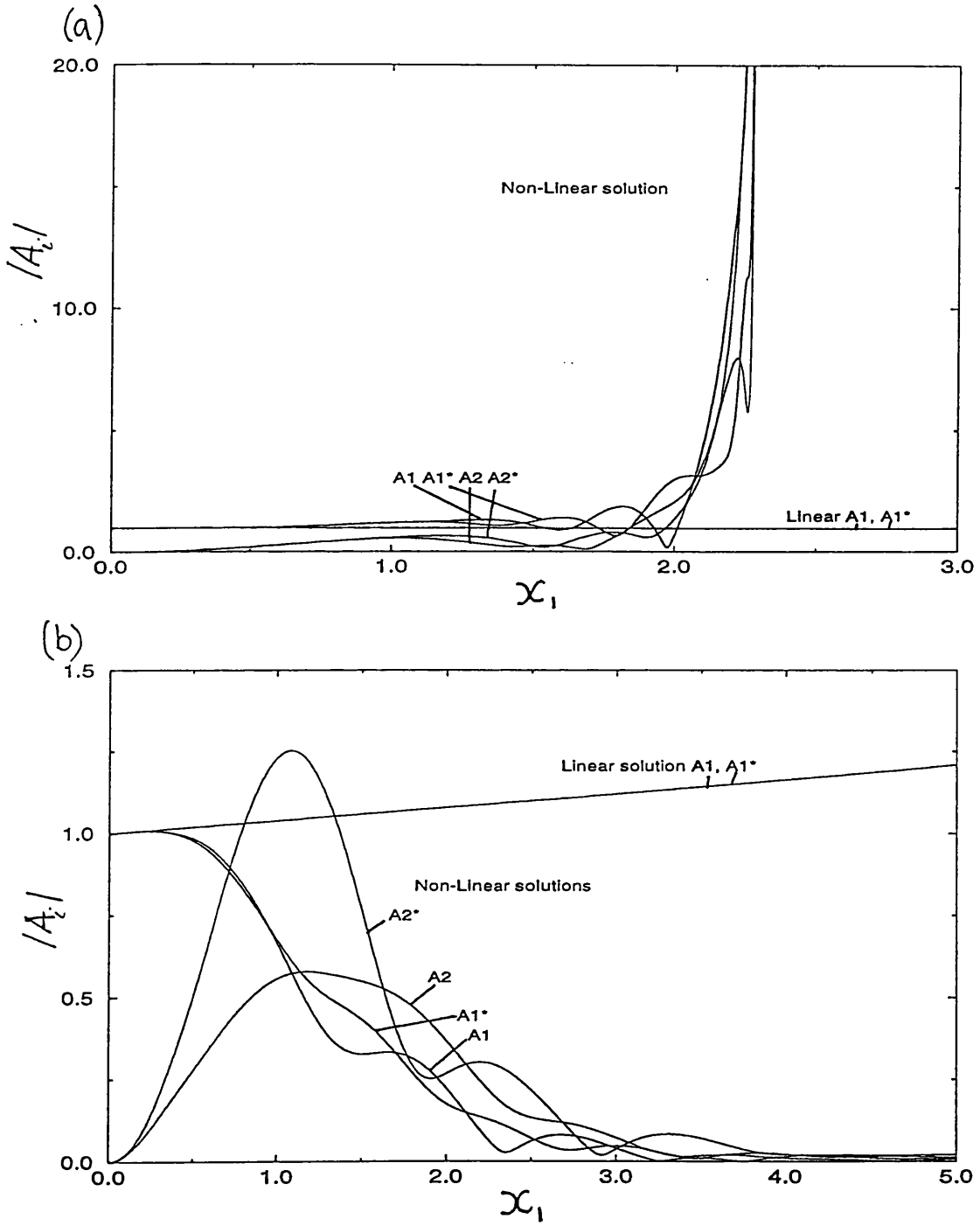

Figure 3:5 The solutions of (3.3.24) with modulus of the wave-amplitudes $|A_i^{[*]}|$ plotted against x_1 with initial conditions $A_1(-\infty) = A_1^*(-\infty) = 1$, $A_2(-\infty) = A_2^*(-\infty) = 0$ and parameters for figure (a) as in **3:3(a)**, and for figure (b) as in **3:3(b)**.

Chapter 4

Nonlinear short-wave TS instability

In this chapter we examine the weakly-nonlinear behaviour of Tollmien-Schlichting (TS) instability waves in a boundary layer on a liquid-film coated flat plate. The flow is entirely two dimensional and the problem will be tackled using a high Reynolds number, high-frequency triple-deck theory. The formulation used and some of the solutions found are similar to those in the single-fluid studies of Smith & Burggraf (1985), who investigated monochromatic small amplitude disturbances and their subsequent growth into fully nonlinear regimes, and Smith (1986) for the case of two-dimensional wave packets.

As mentioned in the introduction to the Thesis there are many different effects and mechanisms being observed during laminar-turbulent transition in film flows. We investigate the temporal development of two-dimensional waves with a fixed wavenumber along with, in one case, a longer-scale modulated disturbance. The high-Reynolds-number flow governed by the triple-deck equations introduced in §2.2 of Chapter 2 is taken as a starting point thus involving the interfacial effects whose influence on the TS modes we aim to investigate. The film-flow generation could be achieved by various means, for example by passing a moving plate through a stationary two-fluid system close to the interface between the fluids, or via injection

of a second fluid through the solid boundary, or through a slot as described in Chapter 2. Here we do not concern ourselves with the precise mechanism of the generation of disturbances or even the base film flow and require only that the instability is triggered in the fully developed part of the flow.

The single-fluid investigation carried out by Smith & Burggraf (1985) shows that the spatial development of finite amplitude disturbances are governed at the first weakly-nonlinear stage by an equation of the Stuart-Landau-Watson type but with an imaginary nonlinear coefficient. As a consequence the nonlinearity cannot influence the growth rate of the disturbance which continues to grow until the interaction becomes fully nonlinear, the near wall Stokes layer also becoming nonlinear and may then become prone to a Van Dommelen type singularity creating a finite-distance/ finite-time eruptive breakdown cf. Van Dommelen & Shen (1982). Smith (1986) examined short-wave packets of finite amplitude waves and obtained a controlling Schrodinger equation again with an imaginary nonlinear coefficient. In addition however there is also a second order spatial derivative which describes a 'spreading' of the disturbance amplitude due to wave dispersion.

We may apply the basic premises developed in the above papers to the two-fluid flow using the triple-deck framework of Chapter 2, §2.2. A linear stability analysis carried out by Timoshin (1997) shows that the leading neutral disturbance frequency for short TS waves of wavelength $O(k^{-1})$ is $\omega_r = O(k^2)$ whereas the growth rate ω_i is of $O(1)$. For such short waves the flow becomes essentially inviscid except for thin viscous layers near the wall and surrounding the interface. The instability mechanism for the TS waves is provided by the vertical velocity displacements produced in these viscous layers with the interface therefore heavily influencing instability. Stable short capillary waves also present in the flow become important under certain conditions. For whilst the leading-order TS growth rate remains independent of the wavelength, for a particular combination of the flow parameters the growth rate rises to $O(k^{\frac{3}{2}})$. This occurs by way of a linear resonance between the growing TS modes and decaying capillary waves substantially altering the characteristic flow scalings. This chapter represents a nonlinear extension of that work.

In section §4.2 we will formulate expansions for the weakly-nonlinear flow and derive a governing wave-amplitude equation for the leading-order disturbance. We will also derive equations governing the extra mean flow induced in viscous layers around the interface by means of the shear jump mechanism described in Longuet-Higgins (1953) and Dore (1970, 1975, 1976). We show that the presence of a second fluid leads to a stronger mean flow than in the homogeneous case. However, as in the single-fluid studies, the coefficient of the nonlinear term in the governing wave-amplitude equation is imaginary and so does not affect the exponential wave growth rate. Although the nonlinear terms do not affect the flow development here, the alterations to the shear profile by the interfacially generated mean flow allows the flow to be destabilized by shorter Rayleigh scale disturbances. These instabilities are examined in §4.3. The wave-amplitude equation of §4.2 again predicts the same linear resonance as in Timoshin (1997) and in §4.4 we explore this resonance at a nonlinear level. The amplitude equation changes from a first-order (as in Smith & Burggraf) to a second-order equation suggesting a strong wave coupling. The nonlinear coefficient is again imaginary but this time the nonlinearity appears in a differentiated form which, to this authors' best knowledge, has not been seen before. The wave development is examined and classified and then in §§4.5,4.5.5 two intermediate regimes are studied to try and form some sort of bridge between the two original cases with the apparently disparate forms of their governing amplitude equations.

Before starting the analysis, an outline of the typical scalings governing the temporal development of nonlinear TS waves is presented.

4.1 The triple-deck equations and scalings

We assume that disturbances are introduced in the triple-deck region located at some distance from the origin of the base boundary layer and the film source as shown in fig 4:1a. The disturbed motion in the viscous zone is governed by the equations derived in §2.2 which, on neglect of the wall roughness assumed in that

section can be written in the following non-dimensional and scaled form

$$\frac{\partial u^{\pm}}{\partial t} + u^{\pm}\frac{\partial u^{\pm}}{\partial x} + v^{\pm}\frac{\partial u^{\pm}}{\partial y} = -\frac{1}{\rho^{\pm}}\frac{\partial p^{\pm}}{\partial x} + \nu^{\pm}\frac{\partial^2 u^{\pm}}{\partial y^2}, \tag{4.1.1}$$

$$\frac{\partial u^{\pm}}{\partial x} + \frac{\partial v^{\pm}}{\partial y} = 0. \tag{4.1.2}$$

The boundary conditions for the equations (4.1.1), (4.1.2) are those of no-slip on the wall, and a match to the flow in the bulk of the boundary layer,

$$u^{-} = v^{-} = 0, \text{ on } y = 0, \tag{4.1.3}$$

$$u^{+} = y - a + u_s + A(x,t) + o(1), \text{ as } y \to \infty, \tag{4.1.4}$$

where a is the unperturbed film thickness and u_s is the interfacial streamwise velocity of the base flow. Since, in the base state, both are constants within the region we are investigating we may interpret the unknown function $A(x,t)$ as the negative disturbance displacement. The disturbance displacement is related to the pressure in the viscous sublayer above the interface by way of the principal value integral

$$p^{+}(x,t) = \frac{1}{\pi}\int_{-\infty}^{\infty}\frac{\partial A(s,t)}{\partial s}\frac{ds}{x-s}, \tag{4.1.5}$$

which reflects viscous/inviscid interaction. For our purposes in this chapter it proves convenient to replace (4.1.5) with the original formulation in the potential outer part of the triple-deck

$$\left(\frac{\partial^2}{\partial x^2} + \frac{\partial^2}{\partial y^2}\right)\phi = 0, \ \frac{\partial \phi}{\partial y}(0) = -\frac{\partial A}{\partial x}, \ -\frac{\partial \phi}{\partial x}(0) = p^{+}, \ \phi \to 0 \text{ as } x^2 + y^2 \to \infty, \tag{4.1.6}$$

where ϕ is the disturbance potential and A is the displacement function in (4.1.4).

At the interface between the two fluids at $y = f(x,t)$ we have the kinematic condition, with continuity of streamwise and normal velocities, the continuity of the tangential stresses and a pressure jump expressed in terms of the scaled surface tension coefficient, γ, and gravitational acceleration, $G = 1/Fr$. These are

$$u^{+} = u^{-}, \ \mu^{+}\frac{\partial u^{+}}{\partial y} = \mu^{-}\frac{\partial u^{-}}{\partial y}, \ v^{\pm} = \frac{\partial f}{\partial t} + u^{\pm}\frac{\partial f}{\partial x}, \tag{4.1.7}$$

$$p^+ - p^- = \left(\gamma \frac{\partial^2 f}{\partial x^2} + G(1-\rho^-)f\right). \tag{4.1.8}$$

As our base flow, in agreement with computations in Chapter 2, we take

$$u^+ = y - a + u_s,\ y > a, \tag{4.1.9a}$$

$$u^- = \lambda^- y,\ 0 \leq y < a, \tag{4.1.9b}$$

$$f = a, \tag{4.1.9c}$$

$$v^\pm = p^\pm = A = 0. \tag{4.1.9d}$$

Since $\mu^+ = \nu^+ = \rho^+ = 1$ this solution of the triple-deck equations is valid as long as $\lambda^- = 1/\mu^-$ and $u_s = a\lambda^-$.

4.1.1 The instability scalings

We focus on short (high-frequency) TS waves, choosing a small parameter $\epsilon \ll 1$ to represent their length. Such waves are governed by three time scales, a fast, neutral oscillation scale $O(\epsilon^2)$, an intermediary time scale of $O(\epsilon)$ which reflects the presence of an interface, and a slow scale of $O(1)$, which picks out linear wave growth driven by the viscosity, see Timoshin (1997). The fast scale can be seen from the estimates

$$\frac{\partial u^+}{\partial t} \sim \frac{\partial p^+}{\partial x},\ p^+ \sim \frac{A}{x},\ u^+ \sim A,\ \Rightarrow t \sim x^2, \tag{4.1.1.1}$$

modelling the inertia-pressure balance, the interaction condition and the wave displacement respectively. As usual in weakly-nonlinear theories, we suppose that the base flow (4.1.9) is perturbed by a small wave disturbance of a chosen wavenumber and with the streamwise velocity $u_w = O(\delta_1)$ where the subscript w indicates the wave. Non-linearity in the x-momentum equations (e.g. the term uu_x) generates a second harmonic and mean flow terms of $O({\delta_1}^2\epsilon)$ and then the fundamental correction, from the interaction of the leading disturbance with the second harmonic and mean flow terms, is of $O({\delta_1}^3\epsilon^2)$. The wave self-modulation starts when the fast temporal development of the fundamental correction is balanced with the slow-scale temporal development of the fundamental disturbance. This requires $\delta_1^2 = O(1)$, so the leading-order streamwise velocity in the wave is $O(1)$. Hence for the wave in the

film, for example, we can write

$$u^- = A_0(t)u_0^-(y)E + c.c., \text{ where } E = \exp[i(kX - \omega_0 T - \omega_1 t_1)], \qquad (4.1.1.2)$$

and we define $t_1 = \epsilon^{-1}t$, $T = \epsilon^{-2}t$, $X = \epsilon^{-1}x$ with the operator

$$\frac{\partial}{\partial t} = \frac{1}{\epsilon^2}\frac{\partial}{\partial T} + \frac{1}{\epsilon}\frac{\partial}{\partial t_1} + \frac{\partial}{\partial t}$$

of $O(1)$ and real parameters k, ω_0, ω_1.

The evolution equation for the amplitude $A_0(t)$ derived in the next section turns out to have the following structure:

$$\frac{dA_0}{dt} = (\sigma_r + i\sigma_i)A_0 + (\text{ imaginary const. }).(\text{non-linear terms}), \qquad (4.1.1.3)$$

where σ_r, σ_i denote the real and imaginary parts of the linear wave growth rate. The structure holds for a general choice of film parameters and is in some respects similar to that in Smith & Burggraf (1985).

As well as the wave amplitude and development scales, a second important area of interest in this study is an alteration in the mean flow forced by the Reynolds stresses. For short TS waves the lower deck of the flow field in fig 4:1(a) becomes essentially inviscid apart from inside thin layers of thickness $O(\epsilon)$ which form either side of the interface and on the wall (the latter being the well documented Stokes layer). This is illustrated in fig 4:1(b). For the mean velocity $u = u_m$ say, in these layers, we have the viscosity/Reynolds-stress balance of the form

$$\nu^- \frac{\partial^2 u_m}{\partial y^2} = \left\langle u_w \frac{\partial u_w}{\partial x} + v_w \frac{\partial u_w}{\partial y} \right\rangle, \qquad (4.1.1.4)$$

hence, with $u_w = O(1)$ and $(x, y) = O(\epsilon)$ we have

$$\frac{\partial u_m}{\partial y} = O(1). \qquad (4.1.1.5)$$

A subtle difference exists between the mean-flow generation near a solid wall and at a fluid/fluid boundary. In the first case the estimate (4.1.1.5) implies $u_m = O(\epsilon)$ outside this viscous layer (see Smith & Burggraf (1985)), whereas in the second case the relation $\partial u_m/\partial y = O(1)$ implies a shift in the shears outside this layer,

both above and below the interface (see Longuet-Higgins (1953), Dore (1970, 1975, 1976)). The mean flow then evolves on the slow temporal scale $t = O(1)$ and the diffusive balance

$$\frac{\partial u_m}{\partial t} = \frac{\partial^2 u_m}{\partial y^2}, \tag{4.1.1.6}$$

implies that the induced mean flow spreads over a region $y = O(1)$. We conclude that, in the case under examination here, the induced mean velocity is of the same order as the base-flow velocity, namely of $O(1)$.

The wave-amplitude evolution equation of the form (4.1.1.3) works for any order-one parameters of the film except at a resonance, described in the linear study by Timoshin (1997) as being between growing TS modes and decaying capillary modes, characterized by a certain relation between a, ρ^-, γ and G in the triple-deck formulation. At resonance the growth rate of short waves rises to $O(k^{3/2})$, as in the linear problem, and so the slow time scale governing the wave growth becomes $t = O(\epsilon^{3/2})$. We discuss the scalings for this and for two further intermediate regimes in the preambles to each section.

4.2 Short scale disturbances. The inviscid regions

For a general choice of the gravity and surface tension coefficients, we define the short streamwise coordinate to be $X = \epsilon^{-1}x$ where ϵ is an arbitrary small parameter. The other scaled variables involved, as outlined in §4.1.1, are

$$t_1 = \epsilon^{-1}t, \quad T = \epsilon^{-2}t, \quad x_1 = \epsilon x \tag{4.2.1}$$

with the operators

$$\frac{\partial}{\partial t} = \frac{1}{\epsilon^2}\frac{\partial}{\partial T} + \frac{1}{\epsilon}\frac{\partial}{\partial t_1} + \frac{\partial}{\partial t}, \quad \frac{\partial}{\partial x} = \frac{1}{\epsilon}\frac{\partial}{\partial X} + \frac{\partial}{\partial x} + \epsilon\frac{\partial}{\partial x_1}$$

of $O(1)$. The solution to the triple-deck equations in the region $y = O(1)$ is sought in the following form above $(+)$ and below $(-)$ the interface:

$$\begin{aligned} u^{\pm} &= u^{\pm}_{m0}(x_1, t, y) + (u^{\pm}_0 A_0(x_1, t)E + c.c.) + \epsilon(u^{\pm}_{20}E^2 + u^{\pm}_{10}E + c.c. + u^{\pm}_{m1}) \\ &\quad + \epsilon^2(u^{\pm}_{11}E + c.c.) + ..., \end{aligned} \tag{4.2.2}$$

$$v^{\pm} = \epsilon^{-1}(v_0^{\pm}A_0E + c.c.) + (v_{20}^{\pm}E^2 + v_{10}^{\pm}E + c.c.) + \epsilon(v_{11}^{\pm}E + c.c.) + ..., \quad (4.2.3)$$

$$p^{\pm} = \epsilon^{-1}(p_0^{\pm}A_0E + c.c.) + (p_{20}^{\pm}E^2 + p_{10}^{\pm}E + c.c.) + \epsilon(p_{11}^{\pm}E + c.c.) + ... \quad (4.2.4)$$

$$f = a + \epsilon(F_0A_0E + c.c.) + \epsilon^2(F_{20}E^2 + F_{10}E + c.c. + F_m) + \epsilon^3(F_{11}E + c.c.) + ..., \quad (4.2.5)$$

where we define $E = \exp[i(kX - \omega_0 T - \omega_1 t_1)]$, ω_0 and ω_1 are assumed to be real and $k > 0$ for definiteness. The terms without the E factor represent the mean flow which evolves on the slow scales.

Instead of using the interaction law (4.1.5), the lower-deck solution will be constructed simultaneously with the solution for the potential-flow equations (4.1.6). Taking the vertical co-ordinate for this region as $\bar{\eta} = \epsilon^{-1}y = O(1)$ the equations (4.1.6) become

$$\frac{1}{\epsilon^2}\frac{\partial^2\phi}{\partial X^2} + 2\frac{\partial^2\phi}{\partial X \partial x_1} + \epsilon^2\frac{\partial^2\phi}{\partial x_1^2} + \frac{1}{\epsilon^2}\frac{\partial^2\phi}{\partial \bar{\eta}^2} = 0, \quad (4.2.6)$$

$$\frac{\partial\phi}{\partial\bar{\eta}}(\bar{\eta} = 0) = -\frac{1}{\epsilon}\frac{\partial A}{\partial X} - \epsilon\frac{\partial A}{\partial x_1}, \; -\left(\frac{1}{\epsilon}\frac{\partial\phi}{\partial X} + \epsilon\frac{\partial\phi}{\partial x_1}\right)_{\bar{\eta}=0} = p^+. \quad (4.2.7)$$

The potential ϕ then expands in the form

$$\phi = (\bar{\phi}_0(\bar{\eta})E + c.c.) + \epsilon(\bar{\phi}_{10}E + \bar{\phi}_{20}E^2 + c.c.) + \epsilon^2(\bar{\phi}_{11}E + ...) + ... \quad (4.2.8)$$

Returning to the viscous sublayer we substitute (4.2.2)-(4.2.5) into the triple-deck equations (4.1.1), (4.1.2) to find, to leading order, that

$$-i\omega_0 u_0^{\pm} = -ik\frac{p_0^{\pm}}{\rho^{\pm}}, \; iku_0^{\pm} + \frac{\partial v_0^{\pm}}{\partial y} = 0. \quad (4.2.9)$$

We normalize the disturbance with respect to the leading streamwise wave component and note from the first equation in (4.2.9) that this velocity component is independent of the normal coordinate. Combining this fact with the leading-order solution for the potential (4.2.8), $\bar{\phi}_0 = iA_0\exp[-k\bar{\eta}]$, we find that $p_0^+ = ku_0^+$. The far field condition, which becomes $u_0^+(y \to \infty) \to 1$ (using the normalization) together with the upper-fluid momentum balance in (4.2.9) then provide the leading-order wave frequency $\omega_0 = k^2$.

The leading-order wave terms can now be found in the form

$$u_0^+ = 1, \quad p_0^+ = k, \quad v_0^+ = -ik(y - a + k\Delta), \quad F_0 = \Delta, \tag{4.2.10}$$

$$p_0^- = \frac{\rho^- k^2 \Delta}{a}, \quad u_0^- = \frac{k\Delta}{a}, \quad v_0^- = -\frac{ik^2\Delta}{a} y, \tag{4.2.11}$$

$$\Delta = \frac{k}{k^2(\rho^-/a - \gamma) + \bar{G}(1 - \rho^-)}. \tag{4.2.12}$$

In deriving (4.2.10)-(4.2.12) we have used the kinematic condition at the interface and the leading-order pressure jump,

$$v_0^\pm(a) = -i\omega_0 F_0 = -ik^2 F_0, \tag{4.2.13}$$

$$p_0^+ - p_0^- = -k^2 F_0 \gamma_0 + \bar{G}(1 - \rho^-) F_0, \tag{4.2.14}$$

and applied the no penetration wall condition $v_0^-(y = 0) = 0$. In order to keep the gravity effects at the main order we have also taken a larger value of G, $G = \epsilon^{-2}\bar{G}$ with $\bar{G} = O(1)$.

We remark here that it is obvious from the form of Δ in (4.2.12) that, given a particular combination of parameters, Δ may become infinite and the solution will become invalid. Subsequent sections will deal with this scenario and we will here only concentrate on the case of a finite Δ.

For the higher-order wave terms in (4.2.2)-(4.2.4) we have the following momentum and continuity balances,

$$-ik^2 u_{10}^\pm - i\omega_1 u_0^\pm A_0 + iku_0^\pm u_{m0}^\pm A_0 + A_0 v_0^\pm \frac{\partial u_{m0}^\pm}{\partial y} = -\frac{ikp_{10}^\pm}{\rho^\pm}, \tag{4.2.15}$$

$$-2ik^2 u_{20}^\pm + ik(u_0^\pm A_0)^2 = -\frac{2ikp_{20}^\pm}{\rho^\pm}, \tag{4.2.16}$$

$$iku_{10}^\pm + \frac{\partial v_{10}^\pm}{\partial y} = 0, \quad 2iku_{20}^\pm + \frac{\partial v_{20}^\pm}{\partial y} = 0, \tag{4.2.17}$$

$$u_0^\pm \frac{\partial A_0}{\partial t} - ik^2 u_{11}^\pm - i\omega_1 u_{10}^\pm + iku_{m0}^\pm u_{10}^\pm + iku_{20}^\pm u_0^{\pm *} A_0^* + A_0^* v_0^{\pm *} \frac{\partial u_{20}^\pm}{\partial y}$$
$$+ v_{10}^\pm \frac{\partial u_{m0}^\pm}{\partial y} + A_0 v_0^\pm \frac{\partial u_{m1}^\pm}{\partial y} + iku_0^\pm u_{m1}^\pm A_0 = -\frac{ikp_{11}^\pm}{\rho^\pm} - \frac{\partial A_0}{\partial x_1} p_0^\pm + \nu^\pm \frac{\partial^2 u_0^\pm}{\partial y^2}. \tag{4.2.18}$$

The equation (4.2.16) shows that the first harmonic terms $u_{20}^{\pm}$ are y-independent and we find from the potential-flow equation (4.2.6) that

$$\bar{\phi}_{20} = c_{20} \exp\left[-2k\bar{\eta}\right], \tag{4.2.19}$$

where $c_{20} = iu_{20}^{+}$ is fixed by the conditions (4.2.7). This leads to the relation

$$p_{20}^{+} = 2ku_{20}^{+}. \tag{4.2.20}$$

For the first harmonic terms this gives the solution

$$u_{20}^{+} = -\frac{A_0^2}{2k}, \quad p_{20}^{+} = -A_0^2, \quad v_{20}^{+} = i(y-a)A_0^2 + v_{20c}, \tag{4.2.21}$$

$$u_{20}^{-} = \frac{p_{20}^{-}}{k\rho^{-}} + \frac{A_0^2 F_0^2 k}{2a^2}, \quad v_{20}^{-} = -i\left(\frac{2p_{20}^{-}}{\rho^{-}} + \frac{k^2 A_0^2 F_0^2}{a^2}\right) y, \tag{4.2.22}$$

where we have used the condition of no-penetration at the wall. The constants p_{20}^{-} and v_{20c} can be found from the interfacial conditions but they are not required in the subsequent analysis.

Before the other wave terms are considered we need to state a very important assumption with regard to the properties of the mean flow. The $O(1)$ mean velocity in (4.2.2) is governed by the diffusion equation

$$\frac{\partial u_{m0}^{\pm}}{\partial t} = \nu^{-} \frac{\partial^2 u_{m0}^{\pm}}{\partial y^2}. \tag{4.2.23}$$

We shall assume (and we verify this in section §4.3) that the wave induced corrections to the base profile in (4.1.9) are confined to the layer $y = O(1)$, that is, the far-field boundary condition to (4.2.23) takes the form

$$u_{m0}^{+} \to y - a + u_s + o(1) \quad \text{as } y \to \infty. \tag{4.2.24}$$

Now we consider the first fundamental correction terms for the wave. The solution for the corresponding potential flow term in (4.2.8),
$\bar{\phi}_{10} = iu_{10}^{+}(y \to \infty) \exp\left[-k\bar{\eta}\right]$, gives the viscous/inviscid interaction condition

$$p_{10}^{+} = k \lim_{y \to \infty} u_{10}^{+}. \tag{4.2.25}$$

We apply this and the relation (4.2.24) to the far-field limit of equation (4.2.15) to find the real frequency correction ω_1,

$$\omega_1 = ku_s - k^2\Delta. \tag{4.2.26}$$

The velocities for the first fundamental correction are then written in the form

$$u_{10}^+ = \frac{p_{10}^+}{k} + \frac{A_0}{k}\left(u_{m0}^+ - u_s + k\Delta\right) - \frac{A_0}{k}(y - a + k\Delta)\frac{\partial u_{m0}^+}{\partial y}, \tag{4.2.27}$$

$$v_{10}^+ = -ip_{10}^+(y-a) - i(k\Delta - u_s)A_0(y-a) - iA_0\int_a^y \left[u_{m0}^+ - (s - a + k\Delta)\frac{\partial u_{m0}^+}{\partial s}\right] ds + iv_{10c}^+, \tag{4.2.28}$$

$$u_{10}^- = \frac{p_{10}^-}{k\rho^-} + \frac{A_0\Delta}{a}\left(-\frac{\omega_1}{k} - y\frac{\partial u_{m0}^-}{\partial y} + u_{m0}^-\right), \tag{4.2.29}$$

$$v_{10}^- = -i\left(\frac{p_{10}^-}{\rho^-} - \frac{A_0\Delta\omega_1}{a}\right)y + \frac{ikA_0\Delta}{a}\int_0^y \left[s\frac{\partial u_{m0}^-}{\partial s} - u_{m0}^-\right] ds + v_w, \tag{4.2.30}$$

where v_{10c}^+ is a constant which we will calculate presently and the constant v_w will be found from matching to the viscous Stokes layer on the wall. Before this however we will form the basis of the governing equation for the amplitude A_0 by taking the far-field limit $y \to \infty$ of equation (4.2.18) for the fundamental correction. Again we use the assumption that the mean flow occupies a region $y \sim O(1)$ and so $u_{m1}^+(y \to \infty) \to 0$ does not affect the limit equation which becomes

$$\frac{\partial A_0}{\partial t} + ip_{10}^+k\Delta + iv_{10c}^+ + iA_0\int_a^\infty U_{m0}^+ - (y - a + k\Delta)\frac{\partial U_{m0}^+}{\partial y}dy - \frac{i}{2}A_0|A_0|^2 = -ikp_{11}^+ + ik^2\lim_{y\to\infty} u_{11}^+ + k\frac{\partial A_0}{\partial x_1}, \tag{4.2.31}$$

where we have defined $U_{m0}^+ = u_{m0}^+ - (y - a + u_s)$ for the convergence of the integral. The potential equations (4.2.6), (4.2.7) and the far-field condition for the second wave fundamental show that

$$\bar{\phi}_{11} = (c_{11} - i\bar{\eta}\frac{\partial A_0}{\partial x_1})e^{-k\bar{\eta}}, \quad \frac{\partial\bar{\phi}_{11}}{\partial\bar{\eta}}(0) = \lim_{y\to\infty}\left(iku_{11}^+ + \frac{\partial A_0}{\partial x_1}\right), \tag{4.2.32}$$

where c_{11} is a constant, $c_{11} = -i\lim_{y\to\infty} u_{11} - 2/k\partial A_0/\partial X_1$, and the viscous/inviscid interaction condition becomes

$$p_{11}^+ = k\lim_{y\to\infty} u_{11}^+ - i\frac{\partial A_0}{\partial x_1}. \tag{4.2.33}$$

Substitution into (4.2.31) then gives us

$$\frac{\partial A_0}{\partial t} + 2k\frac{\partial A_0}{\partial x_1} + i(k\Delta p_{10}^+ + v_{10c}^+) + iA_0\int_a^\infty U_{m0}^+ - (y-a+k\Delta)\frac{\partial U_{m0}^+}{\partial y}dy - \frac{i}{2}A_0|A_0|^2 = 0. \tag{4.2.34}$$

4.2.1 The viscous Stokes layer on the wall

Close to the wall there is a thin viscous layer of thickness $O(\epsilon)$, the Stokes layer, which smoothes the inviscid velocity profiles so that the conditions of no-slip and no-penetration can be satisfied to all orders on the wall at $\eta = 0$, where $\eta = \epsilon^{-1}y = O(1)$ is the local normal coordinate. In this layer we take the following expansions

$$u^- = (\hat{u}_0^-(\eta)E + c.c.) + \epsilon(\hat{u}_{m0}(\eta) + ...) + ..., \; v^- = (\hat{v}_0^-(\eta)E + c.c.) + ... \tag{4.2.1.1}$$

Substituting into the triple-deck equations we obtain

$$\frac{\partial^2\hat{u}_0^-}{\partial\eta^2} + \frac{ik^2}{\nu^-}\hat{u}_0^- = \frac{ik}{\rho^-\nu^-}p_0^-A_0, \;\; ik\hat{u}_0^- + \frac{\partial\hat{v}_0^-}{\partial\eta} = 0, \tag{4.2.1.2}$$

$$\nu^-\frac{\partial^2\hat{u}_{m0}^-}{\partial\eta^2} = \hat{v}_0^-\frac{\partial\hat{u}_0^{-*}}{\partial\eta} + \hat{v}_0^{-*}\frac{\partial\hat{u}_0^-}{\partial\eta}. \tag{4.2.1.3}$$

Solutions for the leading wave terms are found to be

$$\hat{u}_0^- = \frac{p_0^-A_0}{\rho^-k}(1-e^{-\sigma^-\eta}), \; \hat{v}_0^- = -\frac{ip_0^-A_0}{\rho^-}(\eta + \frac{1}{\sigma^-}(e^{-\sigma^-\eta}-1)), \tag{4.2.1.4}$$

where $\sigma^- = \sqrt{-ik^2/\nu^-}$. Substituting these solutions into equation (4.2.1.3) and integrating twice we find

$$\hat{u}_{m0}^- = \frac{p_0^{-2}|A_0|^2}{\rho^{-2}k\nu^-}\left(i(2-\sigma^-\eta)\frac{e^{-\sigma^-\eta}}{(\sigma^-)^2} - \frac{e^{-\sigma^-\eta}}{(\sigma^-)^2} + \frac{2e^{-(\sigma^-+\sigma^{-*})\eta}}{(\sigma^-+\sigma^{-*})^2}\right) + C_1\eta + C_2, \tag{4.2.1.5}$$

where the constants C_1, C_2 are fixed by matching with the region $y = O(1)$ and the no-slip at the wall, respectively,

$$C_1 = \frac{\partial u_{m0}^-}{\partial y}(y=0), \;\; C_2 = -\frac{p_0^{-2}|A_0|^2}{\rho^{-2}k^3}(1-i). \tag{4.2.1.6}$$

A consequence of the form of $\hat{u}^-_{m0}$, the combined base and generated mean flow in this layer, is that, on matching ($\eta \to \infty$), we get the boundary condition of no-slip applying to the leading-order induced mean flow outside the viscous layer. From the matching condition for the normal velocities we also find the constant v_w in (4.2.30) to be

$$v_w = \frac{ip_0^- A_0}{\sigma^- \rho^-}. \tag{4.2.1.7}$$

4.2.2 The interfacial viscous layer

In the viscous layer about the interface we write our velocity components in terms of the shifted and stretched normal co-ordinate $\bar{z}$ defined by

$$y = f + \epsilon \bar{z}. \tag{4.2.2.1}$$

We also introduce the adjusted vertical velocity $w^\pm = v^\pm - \partial f/\partial t - u^\pm \partial f/\partial x$, and seek the solution in the form

$$u^\pm = (\bar{u}_0^\pm(\bar{z}) A_0 E + c.c.) + \bar{u}^\pm_{m0} + \epsilon(\bar{u}^\pm_{m1} + ...) + ..., \tag{4.2.2.2}$$

$$w^\pm = (\bar{w}_0^\pm(\bar{z}) A_0 E + c.c.) + ... \ . \tag{4.2.2.3}$$

The governing equations for the terms shown explicitly are

$$-ik^2 \bar{u}_0^\pm = -\frac{ik}{\rho^\pm} p_0^\pm + \nu^\pm \frac{\partial^2 \bar{u}_0^\pm}{\partial \bar{z}^2}, \tag{4.2.2.4}$$

$$ik\bar{u}_0^\pm + \frac{\partial \bar{w}_0^\pm}{\partial \bar{z}} = 0, \tag{4.2.2.5}$$

$$\frac{\partial^2 \bar{u}^\pm_{m0}}{\partial \bar{z}^2} = 0, \tag{4.2.2.6}$$

$$\nu^\pm \frac{\partial^2 \bar{u}_{m1}}{\partial \bar{z}^2} = |A_0|^2 (\bar{w}_0^\pm \frac{\partial \bar{u}_0^{\pm *}}{\partial \bar{z}} + \bar{w}_0^{\pm *} \frac{\partial \bar{u}_0^\pm}{\partial \bar{z}}). \tag{4.2.2.7}$$

with stars denoting the conjugate values. The solution of (4.2.2.5) is of the form

$$\bar{u}_0^\pm = Q^\pm e^{\mp \sigma^\pm \bar{z}} + \frac{\bar{p}_0^\pm}{\rho^\pm k}, \ \bar{w}_0^\pm = \pm \frac{ikQ^\pm}{\sigma^\pm}(e^{\mp \sigma^\pm \bar{z}} - 1) - \frac{i\bar{p}_0^\pm \bar{z}}{\rho^\pm} \tag{4.2.2.8}$$

where $\sigma^\pm = \sqrt{-ik^2/\nu^\pm}$, $\sigma_r^\pm > 0$; the constants $Q^\pm$ and a constant of integration in $\bar{w}_0^\pm$ are determined by the conditions of continuity of tangential stress and streamwise

velocity at the interface and the interfacial condition $\bar{w}_0^{\pm}(0) = 0$. With the expression for $p^{\pm}$ already given in (4.2.10), (4.2.11) we have

$$Q^- = \frac{1 - k\Delta/a}{1 + \rho^-\sqrt{\nu^-}}, \quad Q^+ = \frac{-\rho^-\sqrt{\nu^-}\,(1 - k\Delta/a)}{1 + \rho^-\sqrt{\nu^-}}. \tag{4.2.2.9}$$

The second formula in (4.2.2.8) shows that at large $\bar{z}$ the vertical velocity for the wave acquires a non-zero finite part. The effect of this is similar to the near-wall Stokes layer contribution to the wave solution and like the latter it affects the linear growth rate of the wave.

Returning to the mean-flow equations (4.2.2.6), (4.2.2.7), the first of these shows that the solution, on matching with the inviscid region, is
$\bar{u}_{m0}^{\pm} = U_m$ where U_m is a constant. We then substitute (4.2.2.8) into (4.2.2.7) and integrate to find

$$\nu^{\pm}\frac{\partial \bar{u}_{m1}^{\pm}}{\partial \bar{z}} = |A_0|^2 \left(\begin{array}{c} \left(\pm\dfrac{k|Q^{\pm}|^2}{\sigma^{\pm}} + \dfrac{iQ^{\pm}\bar{p}_0^{\pm}}{\rho^{\pm}}\left(\bar{z} \pm \dfrac{1}{\sigma^{\pm}}\right)\right) e^{\mp\sigma^{\pm}\bar{z}} \\ \pm\dfrac{2k|Q^{\pm}|^2}{(\sigma^{\pm} + \sigma^{\pm *})} e^{\mp(\sigma^{\pm}+\sigma^{\pm *})\bar{z}} + c.c. \end{array} \right) + \nu^- \Lambda_m^{\pm} \tag{4.2.2.10}$$

where $\Lambda_m^{\pm}$ are constants of integration. The stress continuity condition and the formula (4.2.2.9) then give us a relation for the wave-induced mean shear jump across the whole interfacial layer,

$$\Lambda_m^+ - \mu^-\Lambda_m^- = \sqrt{2}|A_0|^2 \left(\frac{\rho^-\sqrt{\nu^-}\,(k\Delta/a - 1)\left(1 + k\Delta a/\rho^{-2}\right)}{1 + \rho^-\sqrt{\nu^-}} \right), \tag{4.2.2.11}$$

where we have used the unit values for ρ^+, μ^+, ν^+. It is this jump in shears, as opposed to a velocity shift due to the Stokes layer, which causes the enhanced mean flow contribution.

4.2.3 The amplitude equation

We may now determine the governing equation for the wave amplitude $A_0(x_1, t)$. This is obtained from (4.2.34), by matching between the inviscid regions and the interfacial and near-wall viscous layers. The leading order match shows that the

mean profile $u^{\pm}_{m0}$ in the region $y = O(1)$ is continuous across the interface, hence $u^{\pm}_{m0}(a) = \bar{u}^{\pm}_{m0}$. Matching the first fundamental correction (of $O(1)$ in the normal velocity expansion (4.2.3)) with the solution in the viscous layers gives two relations,

$$iv^{+}_{10c} + i\Delta A_0(\omega_1 - ku^{\pm}_{m0}(a)) + ik^2F_{10} = -\frac{ikQ^{+}A_0}{\sigma^{+}}, \qquad (4.2.3.1)$$

$$-i\left(\frac{p^{-}_{10}a}{\rho^{-}}\right) - ik\Delta A_0(k\Delta - u_s) + \frac{ik\Delta A_0}{a}\int_0^a \left[y\frac{\partial u^{-}_{m0}}{\partial y} - u^{-}_{m0}\right]dy$$
$$+v_w + i\Delta A_0(\omega_1 - ku^{\pm}_{m0}(a)) + ik^2F_{10} = \frac{ikQ^{-}A_0}{\sigma^{-}}, \qquad (4.2.3.2)$$

and combining these with the pressure jump condition

$$p^{+}_{10} - p^{-}_{10} = -\left[\gamma k^2 + G(\rho^{-} - 1)\right]F_{10}, \qquad (4.2.3.3)$$

gives us p^{+}_{10} in terms of F_{10},

$$p^{+}_{10} = -\frac{k\Delta\rho^{-}A_0}{a}(k\Delta - u_s) + \frac{k\Delta A_0\rho^{-}}{a^2}\int_0^a \left[y\frac{\partial u^{-}_{m0}}{\partial y} - u^{-}_{m0}\right]dy - \frac{i\rho^{-}v_w}{a}$$
$$+\frac{\Delta\rho^{-}A_0}{a}(\omega_1 - ku^{\pm}_{m0}(a)) - \frac{k\rho^{-}Q^{-}A_0}{a\sigma^{-}} + \frac{k}{\Delta}F_{10}. \qquad (4.2.3.4)$$

If we now define the induced mean flow in the film as $U^{-}_{m0} = u^{-}_{m0} - \lambda^{-}y$ and substitute for v^{+}_{10c} from (4.2.3.1) and for p^{+}_{10} from (4.2.3.4), using (4.2.1.7), (4.2.2.9) and (4.2.25) then the relation (4.2.34) gives us the wave amplitude equation in its final form

$$\frac{\partial A_0}{\partial t} + 2k\frac{\partial A_0}{\partial x_1} = \frac{i}{2}A_0|A_0|^2 + (\beta_r + i\beta_i)A_0 +$$
$$iA_0\left(\begin{array}{l}\dfrac{k^2\Delta^2\rho^{-}}{a}\displaystyle\int_0^a\left[y\frac{\partial U^{-}_{m0}}{\partial y} - U^{-}_{m0}\right]dy - k\Delta\left(\frac{k\rho^{-}\Delta}{a} - 1\right)U^{\pm}_{m0}(a) \\ \displaystyle\int_a^{\infty}\left[U^{+}_{m0} - (y - a + k\Delta)\frac{\partial U^{+}_{m0}}{\partial y}\right]dy\end{array}\right) \qquad (4.2.3.5)$$

where

$$\beta_r = \frac{\rho^{-}\sqrt{\nu^{-}}}{\sqrt{2}a^2(1 + \rho^{-}\sqrt{\nu^{-}})}((k\Delta - a)^2 + k^2\Delta^2(1 + \rho^{-}\sqrt{\nu^{-}})), \qquad (4.2.3.6)$$

$$\beta_i = -\beta_r + k^2\Delta^2\left(1 + \frac{\rho^{-}}{a}(u_s - 2k\Delta)\right). \qquad (4.2.3.7)$$

The equation governing the wave-generated mean flow is found from (4.2.23) by subtracting the base flow and applying the no-slip wall condition (justified in §4.2.1), the decay condition in the far field and two interfacial conditions established in §4.2.2, those of continuity in the induced velocity and a prescribed jump in the shear (4.2.2.11). The final formulation for the induced mean flow is of the form

$$\frac{\partial U^{\pm}_{m0}}{\partial t} = \nu^{-}\frac{\partial^2 U^{\pm}_{m0}}{\partial y^2}, \tag{4.2.3.8a}$$

$$U^{-}_{m0} = 0 \text{ at } y = 0, \quad U^{+}_{m0} \to 0 \text{ as } y \to \infty, \tag{4.2.3.8b}$$

$$U^{+}_{m0} = U^{-}_{m0}, \quad \frac{\partial U^{+}_{m0}}{\partial y} - \mu^{-}\frac{\partial U^{-}_{m0}}{\partial y} = J \text{ at } y = a, \tag{4.2.3.8c}$$

$$J = -\frac{\rho^{-}\sqrt{2\nu^{-}}}{1+\rho^{-}\sqrt{\nu^{-}}}\left(1-\frac{k\Delta}{a}\right)^2 |A_0|^2. \tag{4.2.3.8d}$$

In the case of two fluids with identical properties ($\rho^{-} = \nu^{-} = 1$, $\gamma = \bar{G} = 0$) the equation (4.2.3.5) reduces to

$$\frac{\partial A_0}{\partial t} + 2k\frac{\partial A_0}{\partial x_1} = \frac{1-i}{\sqrt{2}}A_0 + \frac{i}{2}A_0|A_0|^2, \tag{4.2.3.9}$$

which is almost identical to the equation derived in study of spatial instability by Smith & Burggraf (1985) with the exception of the coefficient to the nonlinear term. The difference in non-linear coefficients is due to the different approach we took in calculating the wave-generated mean flow, allowing it to spread only through the diffusive layer $y = O(1)$ as opposed to the uninhibited mean-flow penetration across the entire boundary layer assumed in Smith & Burggraf (1985). Solutions presented in the next section verify the validity of our approach for the case of temporally developing waves but whether the same is true for spatial instability remains an open question. It is important to note however that in both (4.2.3.9) and (4.2.3.5) the nonlinear coefficient is always imaginary and therefore nonlinearity does not affect the growth rate of $|A_0|$. As a point of interest we also note that the homogeneous problem of Smith & Burggraf (1985) has very similar temporal ($\partial/\partial x_1 = 0$) and spatial ($\partial/\partial t = 0$) formulations. This is a quirk unassociated with the two-fluid case where the generated mean flow destroys spatio-temporal symmetry, see equation (4.2.3.8). However we see that for both the single- and two-fluid systems the linear growth rate β_r is positive for all choices of the flow parameters.

4.3 Solution properties and secondary instabilities

The absolute value of the wave amplitude $|A_0|$ governed by (4.2.3.5) is unaffected by the nonlinearity due to its purely imaginary coefficient. To illustrate, if we take the slow $x-$dependence in the form $\exp[ik_1x_1]$ with constant k_1 then

$$|A_0|^2 = A_{00}\exp(2\beta_r t), \quad A_{00} = constant. \tag{4.3.1}$$

This growing wave amplitude then creates stronger mean flow, as can be seen from (4.2.3.8) and due to the quadratic nature of the mean flow's dependence on $|A_0|$ it is growing faster than the base wave. The possible subsequent stages of the wave development are discussed in the final section, §4.6. Here we focus on properties of the induced mean flow which, as we aim to show, can become unstable to short-wavelength secondary disturbances which could be generated by, for example, the background noise of experimental equipment or external vibrations.

We begin by solving equations (4.2.3.8) with (4.3.1). Writing the total mean velocity, i.e. the sum of the induced and base components as

$$u^{\pm} = u^{\pm}_{m0} + O(\epsilon), \tag{4.3.2}$$

as in the expansions for $u^{\pm}$ in (4.2.2), we find

$$u^{+}_{m0} = y - a + u_s + A_m(t)\sinh(\xi^{-}a)e^{-\xi^{+}(y-a)} \text{ for } y \geq a, \tag{4.3.3}$$

$$u^{-}_{m0} = \lambda^{-}y + A_m(t)\sinh(\xi^{-}y) \text{ for } 0 \leq y \leq a, \tag{4.3.4}$$

where $\xi^{\pm} = \sqrt{2\beta_r/\nu^{\pm}}$, and

$$A_m(t) = \frac{A_{00}\rho^{-}\sqrt{2\nu^{-}}\,(1-k\Delta/a)^2\,e^{2\beta_r t}}{(1+\rho^{-}\sqrt{\nu^{-}})(\xi^{+}\sinh(\xi^{-}a)+\mu^{-}\xi^{-}\cosh(\xi^{-}a))}. \tag{4.3.5}$$

The secondary disturbances described in the following section are short compared with the primary TS waves and are heavily influenced by surface tension, whose effect is greater than that of gravity on short waves, as can be seen from the pressure jump condition (4.2.14). Therefore we assume that the primary wave is unaffected by surface tension but allow an influence on the secondary waves by a rescaling of the surface tension coefficient, and neglect gravity for both the primary and secondary disturbances for simplicity.

4.3.1 Intermediate secondary disturbances

In this subsection we consider secondary disturbances of wavelength $O(\hat{\delta})$ assumed to be smaller then the wavelength of the primary modes but larger then the film thickness whilst even shorter perturbations will be examined in §4.3.2. Here we take

$$Re^{-\frac{1}{4}} \ll \hat{\delta} \ll \epsilon, \tag{4.3.1.1}$$

and perturb the primary-wave solution of the governing triple-deck equations, (4.1.1), (4.1.2), in the following manner

$$u^{\pm} = (u_0 A_0 E + c.c + A_0 u^{\pm}_{m0}) + ... + \delta_a(\hat{u}\hat{E} + c.c.) + ..., \tag{4.3.1.2}$$

$$v^{\pm} = ... + \frac{\delta_a}{\hat{\delta}}(\hat{v}\hat{E} + c.c.) + ..., \tag{4.3.1.3}$$

$$p^{\pm} = ... + \delta_a(\hat{p}\hat{E} + c.c.) + ..., \tag{4.3.1.4}$$

$$f = a + ... + \delta_a(\hat{f}\hat{E} + c.c.) + ..., \tag{4.3.1.5}$$

where $\delta_a \ll \epsilon^n$ for all positive n, $\hat{E} = \exp[i\hat{k}(\hat{X} - \hat{c}\hat{T})]$ and the new temporal and spatial variables are defined as $\hat{X} = x\hat{\delta}^{-1}$, $\hat{T} = t\hat{\delta}^{-1}$. With regard to the temporal development of the mean flow we can treat $u^{\pm}_{m0}$ as frozen and the temporal development of the primary wave can also be ignored on these scales. We find, upon substitution into (4.1.1), (4.1.2) the equation

$$(u^{\pm}_{m0} - \hat{c})\frac{\partial^2 \hat{v}^{\pm}}{\partial y^2} = \hat{v}^{\pm}\frac{\partial^2 \hat{u}^{\pm}_{m0}}{\partial y^2} \tag{4.3.1.6}$$

Solving in the same manner as employed in Chapter 2 §2.4.1, by applying the inviscid interfacial and wall conditions and the decay of $\partial\hat{v}^{+}/\partial y$ at infinity, we arrive at the dispersion relation

$$\int_0^a \frac{dy}{(u^{-}_{m0} - \hat{c})^2} + \rho^{-}\left(1 - \frac{\hat{\gamma}\hat{k}^2}{\rho^{-}}\int_0^a \frac{dy}{(u^{-}_{m0} - \hat{c})^2}\right)\int_a^{\infty} \frac{dy}{(u^{+}_{m0} - \hat{c})^2} = 0, \tag{4.3.1.7}$$

for the disturbance phase speed $\hat{c} = \hat{c}(\hat{k})$ where, in order to keep surface tension in the equation, we take $\hat{\gamma} = \gamma\hat{\delta}^{-2}$ to be of $O(1)$. In the case $\rho^{-} = 1$, $\hat{\gamma} = 0$ the

equation (4.3.1.7) reduces to the relation

$$\int_0^a \frac{dy}{(u_{m0}^- - \hat{c})^2} + \int_a^\infty \frac{dy}{(u_{m0}^+ - \hat{c})^2} = 0, \qquad (4.3.1.8)$$

as derived earlier for a homogeneous flow by Smith & Bodonyi (1985), Tutty & Cowley(1986). In their studies of short waves in interactive boundary layers they showed that the appearance of secondary instability required a strong inflexional profile. In our case, however, the profiles are characterized by $\partial^2 u_{m0}^{\pm}/\partial y^2$ always being positive (see (4.3.3), (4.3.4)), but the shear $\partial u_{m0}^{\pm}/\partial y$ is discontinuous at the interface and this proves to be sufficient to provoke instability.

Solutions of (4.3.1.7) with (4.3.3)-(4.3.5) have been obtained numerically for the flow with $\rho^- = 1.087$ and $\nu^- = 0.484$, the water/oil mixture used in Chapter 2. We see that for the case of a fixed wavenumber $\hat{k} = 1$, fig 4:2(a), the instability is damped by increased surface tension as expected and that the maximum instability appears at a finite mean flow amplitude A_m. In fig 4:2(b) we examine the case of a fixed value of A_m, close to the instability maximum at $A_m = 0.5$, and vary the wavenumber $\hat{k}$. The maximum instability occurs as $\hat{k} \to 0$ which implies that in the case of the least stable generated mean flow amplitude the most unstable waves are long. Short waves are stabilized by surface tension and a plausible candidate for the neutral-wave solution is a stationary disturbance $\hat{c} = 0$. Indeed if $\hat{c} \to 0$ then the integral over the film region in (4.3.1.7) becomes large and (4.3.1.7) reduces to

$$1 - \hat{\gamma}\hat{k}^2 \int_a^\infty \frac{dy}{(u_{m0}^+)^2} = 0. \qquad (4.3.1.9)$$

This gives us a relation between the surface tension coefficient and the neutral wavenumber. For our example, with the mean flow set near its instability maximum at $A_m = 0.5$, the integral has the value 0.44256, hence, for $\hat{\gamma} = 0.1$ the neutral wavenumber is $\hat{k} = 4.75352$ and for $\hat{\gamma} = 0.2$, $\hat{k} = 3.36124$. These points shown in fig 4:2(b) seem to be in agreement with computations for the unstable waves.

4.3.2 Instability of weak primary waves

As in the stability analysis for two fluid flow over an obstacle tackled in §2.4.2, we can show analytically that instability will always be present as long as some alteration to

the shear profile takes place, no matter how small. Since the mean flow corrections are related to the slowly growing primary waves, instability of the former will also indicate secondary instability of the latter. When A_m is small the combined base and induced mean velocities can be written as

$$u_m^{\pm} = u_b^{\pm}(y) + A_m U_{m0}^{\pm} + ..., \quad A_m \to 0, \tag{4.3.2.1}$$

where

$$u_b^- = \lambda^- y, \text{ for } y < a, \tag{4.3.2.2}$$

$$u_b^+ = y - a + u_s \text{ for } y > a. \tag{4.3.2.3}$$

We proceed exactly as in §2.4.2, with $\bar{L} = Re^{-3/8}$, expanding the phase speed in the form $c = c_0 + A_m c_1 + ...$, which gives us, to the first order, a neutral solution for c_0 with the dispersion relation

$$(c_0 - u_s)(c_0 - \frac{a}{\rho^-}) = \frac{a\hat{\gamma}\hat{k}^2}{\rho^-}. \tag{4.3.2.4}$$

exactly analogous to equation (2.4.2.9) in the limit $k \to 0$. The root c_0 is such that either $c_0 > u_s$ and $c_0 > a/\rho^-$ or $c_0 < u_s$, $c_0 < a/\rho^-$. The growth rate c_{1i} at the next order depends on the location of the critical layer $y = y_c$, where $u_b^{\pm}(y_c) = c_0$. Again as in (2.4.2.21), (2.4.2.22) we find

$$c_{1i} = \frac{\pi a U_{m0}^{+''}(y_c)(u_s - c_0)^2}{\rho^-(u_s - a/\rho^-)}, \quad \text{if } y_c > a; \tag{4.3.2.5a}$$

$$c_{1i} = \frac{c_0^2 \pi U_{m0}^{-''}(y_c)(u_s - c_0)^2}{a\lambda^{-2}(u_s - a/\rho^-)}, \quad \text{if } y_c < a. \tag{4.3.2.5b}$$

with the difference in formulae due to the rescaled surface tension here. Equations (4.3.2.5) show that for instability to occur we need $U_{m0}^{+''}(y_c) < 0$ if the critical layer is above the interface and $U_{m0}^{-''}(y_c) > 0$ if it is below the interface. In the numerical solutions of the previous subsection we had $U_{m0}^{\pm''} > 0$ so only the second instability mode was found, i.e. the one with the critical layer in the lower fluid. From (4.3.2.4) we see that this instability will disappear if γ takes the value $\hat{\gamma} = u_s/\hat{k}^2$. A similar result holds for increased wavenumber k and fixed surface tension.

4.3.3 Weak surface tension

In flows with sufficiently reduced surface tension much shorter secondary waves can exist, with the typical wavelength (on triple-deck scales) of order $\delta = Re^{-\frac{1}{4}}$. Such waves are governed by the Rayleigh equation

$$(u_{m0}^{\pm} - \hat{c})\left(\frac{\partial^2 \hat{v}^{\pm}}{\partial y^2} - \hat{k}^2 \hat{v}^{\pm}\right) = \frac{\partial^2 u_{m0}^{\pm}}{\partial y^2}\hat{v}^{\pm}, \tag{4.3.3.1}$$

which, unlike the previously considered form (4.3.1.6) captures the pressure variation across the layer $y = O(1)$. The boundary conditions of no-penetration at the wall, decay at infinity and the usual inviscid interfacial conditions give us

$$\hat{v}^{+}(\infty) = 0, \quad \hat{v}^{-}(0) = 0, \quad \hat{v}^{+}(a) = \hat{v}^{-}(a), \tag{4.3.3.2}$$

$$(u_{00} - \hat{c})\begin{pmatrix} (u_{00} - \hat{c})\dfrac{\partial \hat{v}^{+}}{\partial y}(a) - \dfrac{\partial u_{m0}^{+}}{\partial y}(a)\hat{v}^{+}(a) \\ \rho^{-}\left((u_{00} - \hat{c})\dfrac{\partial \hat{v}^{-}}{\partial y}(a) - \dfrac{\partial u_{m0}^{-}}{\partial y}(a)\hat{v}^{-}(a)\right) \end{pmatrix} = -\hat{\gamma}\hat{k}^2 \hat{v}^{\pm}(a), \tag{4.3.3.3}$$

where $u_{00} = u_{m0}^{\pm}(a)$ denotes the interfacial speed. Solutions of (4.3.3.1)-(4.3.3.3) were obtained numerically using the method described in §2.4.3. In the case of small A_m, which corresponds to weak generated mean flow, the maximum growth rates occur as $k \to 0$ and hence long waves provide the fastest growing instability, see fig 4:3(a). For the stronger induced mean flow, in fig 4:3(a), the maximum growth rate increases and appears at a finite wavenumber. The inclusion of surface tension reduces instability and gives a short-wave neutral point, shown in fig 4:3(d), which is not present in the case of zero surface tension where we observe very short waves to have a small growth rate and a phase speed which approaches the interfacial velocity, see fig 4:3(c). We may show, however, that for any fixed $\hat{\gamma}$ the growth of the primary wave and hence the impact of A_m will eventually overcome the surface tension effect. The latter can be seen in the limit as $A_m \to \infty$, when the disturbance phase speed and the base profile can be written in the form

$$\hat{c} = A_m \sinh(\xi^{-} a)\tilde{c} + O(1), \tag{4.3.3.4}$$

$$u_{m0}^{\pm} = A_m \sinh(\xi^{-} a)\tilde{u}_{m0}^{\pm}(y) + O(1), \tag{4.3.3.5}$$

with $\hat{\gamma}$ rescaled as $\tilde{\gamma} = \hat{\gamma}/(A_m \sinh(\xi^- a))^2 = O(1)$, and

$$\tilde{u}^+_{m0} = \exp[-\xi^+(y-a)] \text{ if } y \geq a; \quad \tilde{u}^-_{m0} = \frac{\sinh \xi^- y}{\sinh \xi^- a} \text{ if } 0 \leq y \leq a \qquad (4.3.3.6)$$

We solve for $\tilde{c}$ using equations (4.3.3.1-4.3.3.3) by simply replacing $u^{\pm}_{m0}$, $\hat{c}$, $\hat{\gamma}$ with $\tilde{u}^{\pm}_{m0}$, $\tilde{c}$, $\tilde{\gamma}$, and note the increased surface tension required to provide an upper neutral point. The solutions for such strong induced mean flow are shown in fig 4:4 and again we see no neutral cut off for short waves in the flow without surface tension. Taking the short wave limit of the Rayleigh equation in these new variables, we find analytically that $\tilde{c} \to 1$ and $\hat{v}^{\pm} \to \exp[\mp \hat{k}(y-a)]$ as $\hat{k} \to \infty$.

In the case of surface tension still exerting an influence, which we remark requires relatively strong surface tension within the weak surface tension regime,(i.e. the unscaled tension is of $O(Re^{-1/2}A_m^2) \ll 1$), we again find the solution curves approaching neutral points at finite wavenumbers. As in the previous subsections we assume these neutral solutions to occur at zero phase speed $\tilde{c} = 0$, only this time the neutral wavenumber is determined by the full Rayleigh formulation of (4.3.3.1-4.3.3.3) with (4.3.3.4-4.3.3.6). The relation between the scaled surface tension $\tilde{\gamma}$ and the neutral wavenumber $\hat{k}$ is found to be of the form

$$\rho^- \left[\sqrt{(\xi^-)^2 + \hat{k}^2} \coth \left[a\sqrt{(\xi^-)^2 + \hat{k}^2} \right] - \xi^- \coth a\xi^- \right] + \xi^+ - \sqrt{(\xi^+)^2 + \hat{k}^2} + \tilde{\gamma}\hat{k}^2 = 0. \qquad (4.3.3.7)$$

From this we can now calculate, for example, the value of $\tilde{\gamma}$ for which $\hat{k} = 0$, that is the magnitude of surface tension required for complete stabilization of secondary modes in the flow with dominating induced mean component. So in the case of an equal mixture of silicone oil V2 and 1-2-3-4-tetrahydronaphtalene for the main fluid and water in the film as used in previous sections we have $\rho^- = 1.087$, $\nu^- = 0.484$, and for the critical value of $\tilde{\gamma}$, $\tilde{\gamma}_c = 0.81545$, see fig 4:5. In terms of the previous variables $\gamma > Re^{-\frac{1}{2}} \lambda_b A_m^2 \sinh^2(\xi^- a)\tilde{\gamma}_c$ is then the requirement for stabilization of the short secondary modes.

4.4 Nonlinear TS-capillary wave resonance

The general set of expansions (4.2.2)-(4.2.5) assumed in §4.2 fails when the constant Δ in (4.2.12) becomes infinite, which is described in Timoshin (1997) as corresponding to a crossing of the TS wave and a capillary mode. This extreme value of Δ can occur for a variety of combinations of the gravity and surface tension coefficients G and γ. We will, for definiteness, concentrate on the case of negligible gravity and a resonant value of the surface tension, $\gamma_0 = \rho^-/a$, see (4.2.12) .

It was shown that the resonant growth-rate for the linear counterpart to this study, Timsohin (1997), was $O(k^{3/2})$, so here we take the slow temporal scale to be $O(\epsilon^{3/2})$ and assume that γ is close to, and expand about, the critical value $\gamma = \gamma_0$, writing

$$\gamma = \gamma_0 + \epsilon^{\frac{1}{2}}\gamma_1, \ \gamma_1 = O(1). \tag{4.4.1}$$

4.4.1 Derivation of the amplitude equation

The fast and slow variables for the wave disturbance are now defined by the relations

$$X = \epsilon^{-1}x, \ T = \epsilon^{-2}t, \ t_1 = \epsilon^{-3/2}t, \ (X, T, t_1) = O(1). \tag{4.4.1.1}$$

The expansions for the disturbance above and below the interface have to be considered separately due to an increased amplitude in the film velocity terms, see (4.2.11). The same argument used for the non-resonant regime earlier in this Chapter, connecting the wave fundamental, harmonic/mean flow interaction and fundamental correction terms holds here but leads to a different non-linear wave amplitude,

namely $u_w = O(\epsilon^{-3/4})$ in the film, where we take

$$\begin{aligned} u^- &= \epsilon^{-\frac{3}{4}}(A_0(t_1)E + c.c) + \epsilon^{-\frac{1}{2}}(u_{20}^- E^2 + c.c.) + \\ &\quad \epsilon^{-\frac{1}{4}}(u_{10}^- E + u_{30}^- E^3 + c.c.) + ..., \qquad (4.4.1.2) \\ v^- &= \epsilon^{-\frac{7}{4}}(v_0^-(t_1)E + c.c.) + \epsilon^{-\frac{3}{2}}(v_{20}^- E^2 + c.c.) + \\ &\quad \epsilon^{-\frac{5}{4}}(v_{10}^- E + v_{30}^- E^3 + c.c.) + ..., \qquad (4.4.1.3) \\ p^- &= \epsilon^{-\frac{7}{4}}(A_0(t_1)E.k\rho^- + c.c.) + \epsilon^{-\frac{3}{2}}(p_{20}^- E^2 + c.c.) + \\ &\quad \epsilon^{-\frac{5}{4}}(p_{10}^- E + p_{30}^- E^3 + c.c.) + ..., \qquad (4.4.1.4) \end{aligned}$$

where $\epsilon \ll 1$ is measure of the TS wavelength, $E = \exp[i(kX - \omega_0 T)]$, with real k and ω_0 and the function describing the interface between the two fluids is expanded in the form

$$f = a + \epsilon^{\frac{1}{4}}(F_0 E + c.c.) + \epsilon^{\frac{1}{2}}(F_{20}E^2 + c.c.) + \epsilon^{\frac{3}{4}}(F_{10}E + F_{30}E^3 + c.c.) + ... \ . \qquad (4.4.1.5)$$

Substitution into the triple deck equations (4.1.1), (4.1.2) provides the momentum balances

$$\begin{aligned} -i\omega_0 A_0 &= -ik^2 A_0, \Rightarrow \omega_0 = k^2, \qquad (4.4.1.6) \\ -2i\omega_0 u_{20}^- + ikA_0^2 &= -\frac{2ik}{\rho^-} p_{20}^-, \qquad (4.4.1.7) \\ \frac{\partial A_0}{\partial t_1} - i\omega_0 u_{10}^- + ikA_0^* u_{20}^- &= -\frac{ik}{\rho^-} p_{10}^-, \qquad (4.4.1.8) \end{aligned}$$

and continuity balances

$$ikA_0 + \frac{\partial v_0^-}{\partial y} = 0, \ 2iku_{20}^- + \frac{\partial v_{20}^-}{\partial y} = 0, \ iku_{10}^- + \frac{\partial v_{10}^-}{\partial y} = 0, \qquad (4.4.1.9)$$

where, again, the superscript $(*)$ denotes the complex conjugate. The wall Stokes layer does not make a contribution to the normal velocity components until we reach the terms $O(\epsilon^{-\frac{3}{4}})$, so

$$v_0^-(0) = v_{20}^-(0) = v_{10}^-(0) = 0, \qquad (4.4.1.10)$$

and the solutions normalized on the streamwise velocity in the film (note a different normalization in §4.2) become

$$v_0^- = -iky \qquad (4.4.1.11)$$

$$u_{20}^{-} = \frac{p_{20}^{-}}{k\rho^{-}} + \frac{A_0^2}{2k}, \quad v_{20}^{-} = -2i\left(\frac{p_{20}^{-}}{\rho^{-}} + \frac{A_0^2}{2}\right)y, \tag{4.4.1.12}$$

$$u_{10}^{-} = \frac{1}{ik^2}\frac{\partial A_0}{\partial t_1} + \frac{p_{20}^{-}}{k^2\rho^{-}}A_0^* + \frac{1}{2k^2}A_0 \mid A_0 \mid^2 + \frac{1}{k\rho^{-}}p_{10}^{-}, \tag{4.4.1.13}$$

$$v_{10}^{-} = -\left(\frac{1}{ik}\frac{\partial A_0}{\partial t_1} + \frac{p_{20}^{-}}{k\rho^{-}}A_0^* + \frac{1}{2k}A_0 \mid A_0 \mid^2 + \frac{1}{\rho^{-}}p_{10}^{-}\right)iy. \tag{4.4.1.14}$$

In the expansions for the upper fluid

$$u^{+} = \epsilon^{-\frac{1}{4}}(u_{10}^{+}E + c.c.) + y - a + u_s + \epsilon^{\frac{1}{4}}(u_{11}^{+}E + c.c.) + ..., \tag{4.4.1.15}$$

$$v^{+} = \epsilon^{-\frac{7}{4}}(v_{10}^{+}E + c.c.) + ..., \tag{4.4.1.16}$$

$$p^{+} = \epsilon^{-\frac{5}{4}}(p_{10}^{+}E + c.c.) + \epsilon^{-\frac{3}{4}}(p_{11}^{+}E + c.c.) + ..., \tag{4.4.1.17}$$

with the orders of the leading velocity terms determined from the interfacial kinematic condition. Substituting these into the triple-deck equations we obtain

$$-i\omega_0 u_{10}^{+} = -ikp_{10}^{+}, \Rightarrow ku_{10}^{+} = p_{10}^{+}, \tag{4.4.1.18}$$

$$-i\omega_0 u_{11}^{+} + \frac{\partial u_{10}^{+}}{\partial t_1} + v_{10}^{+} = -ikp_{11}^{+}. \tag{4.4.1.19}$$

Then since u_{11}^{+} in (4.4.1.19) is y-independent the viscous-inviscid interaction law gives us

$$p_{11}^{+} = ku_{11}^{+}, \tag{4.4.1.20}$$

and substitution into (4.4.1.19) gives the relation

$$\frac{1}{k}\frac{\partial p_{10}^{+}}{\partial t_1} + v_{10}^{+} = 0. \tag{4.4.1.21}$$

We now turn our attention to the interfacial conditions. From the pressure jump condition (4.1.8) (with neglected gravity) we obtain the relations,

$$-k\rho^{-}A_0 = -\gamma_0 k^2 F_0, \tag{4.4.1.22}$$

$$p_{20}^{-} = 4k^2\gamma_0 F_{20}, \tag{4.4.1.23}$$

$$p_{10}^{+} - p_{10}^{-} = -\gamma_0 k^2 F_{10} - \gamma_1 k^2 F_0. \tag{4.4.1.24}$$

The kinematic condition leads us to another set of relations,

$$-ikaA_0 = -ik^2F_0, \tag{4.4.1.25}$$

$$-2ikA_0F_0 - \frac{2ia}{\rho^-}p_{20}^- - iaA_0^2 = -2i\omega_0F_{20}, \tag{4.4.1.26}$$

$$v_{10}^-(a) + ikA_0^*F_{20} - i(\frac{2p_{20}^-}{\rho^-} + A_0^2)F_0^* = -ikF_0^*u_{20}^- + 2ikA_0^*F_{20} + \frac{\partial F_0}{\partial t_1} - i\omega_0F_{10}. \tag{4.4.1.27}$$

and we note that the equations (4.4.1.22), (4.4.1.25) are simultaneously satisfied only if $\gamma_0 = \rho^-/a$, which was the condition for TS-capillary wave resonance in the linear approximation. Substituting this result back into (4.4.1.23), (4.4.1.26) we find

$$F_{20} = -\frac{a}{2k^2}A_0^2, \quad p_{20}^- = -2\rho^-A_0^2, \tag{4.4.1.28}$$

and then (4.4.1.24), (4.4.1.27) with (4.4.1.21) and the condition that, to the leading order, v is continuous across the viscous layers at the interface finally gives us the wave-amplitude equation for A_0

$$\frac{2\rho^-}{k}\frac{\partial^2A_0}{\partial t_1^2} + i\gamma_1ka\frac{\partial A_0}{\partial t_1} - k^2aA_0 = i\frac{7\rho^-}{2k}\frac{\partial}{\partial t_1}(A_0^2A_0^*). \tag{4.4.1.29}$$

There are, as in the non-resonant case §4.2 and as noted above, thin layers about the interface and a thin Stokes layer on the wall in which the viscous effects are dominant. The interfacial viscous layers are surrounded by a diffusion layer of thickness $O(\epsilon^{3/4})$ where the Reynolds-stress-generated mean profile adjusts to the outer conditions. We see that, unlike the non-resonant case, any induced mean flow does not spread througout the depth of the film due to the shortened slow time scale. These viscous layers are inactive in the present resonant regime as can be seen from the following argument. In the viscous interfacial layer we take

$$\bar{z} = \epsilon^{-1}(y - f(x,t)) = O(1), \quad w^\pm = \frac{\partial f}{\partial t} + u^\pm\frac{\partial f}{\partial x} - v^\pm, \tag{4.4.1.30}$$

where we may regard $w^\pm$ as representing viscous corrections to the inviscid outer

solution. The film-flow components in the layer $\bar{z} = O(1)$ below the interface are

$$u^- = \epsilon^{-\frac{3}{4}}(\bar{u}_0^-(\bar{z})A_0E + c.c. + \bar{u}_M) + \epsilon^{-\frac{1}{2}}(\bar{u}_{m0}^-(\bar{z}) + ...) \quad (4.4.1.31)$$

$$+..., \quad (4.4.1.32)$$

$$w^- = \epsilon^{-\frac{3}{4}}(\bar{w}_0(\bar{z})^- A_0E + c.c.) + ..., \quad (4.4.1.33)$$

$$p^- = \epsilon^{-\frac{3}{4}}(p_0^- A_0E + c.c.) + ... \ . \quad (4.4.1.34)$$

with $\bar{u}_M$ a constant relating to the mean flow in the diffusion layer. We see that the viscous contribution to the normal velocity is of $O(\epsilon^{-\frac{3}{4}})$ here and so does not enter the wave-amplitude equation derivation in the present resonant regime. The same order-of-magnitude estimate holds also for the corrections produced by the wall Stokes layer and the interfacial layer above the interface. The extra mean velocity anticipated in (4.4.1.32) is of $O(\epsilon^{-\frac{1}{2}})$ and the induced shear will then be of $O(\epsilon^{-\frac{3}{2}})$ at the edges of this layer. As in §4.2 the induced mean flow spreads across a layer in which the diffusive effects occur over the slow development time scale. In the resonant regime the slow time is of $O(\epsilon^{\frac{3}{2}})$, so the diffusion layer thickness is of $O(\epsilon^{\frac{3}{4}})$. The mean velocity correction, driven by the shear of $O(\epsilon^{-\frac{3}{2}})$, in the diffusive layer is then $u^{\pm}_{\text{mean}} = O(\epsilon^{-\frac{3}{4}})$ which, incidentally, is of the same order as the leading wave component in the film. Corresponding to this induced mean flow will be the induced streamwise and normal wave terms. An estimate for the mean-flow generated correction to this wave velocity, $u^- \sim \bar{u}^-_{\text{ind}}$, can be found from the balance $\partial \bar{u}^{\pm}_{\text{ind}}/\partial t \sim \bar{u}^{\pm}_{\text{mean}} \partial \bar{u}^{\pm}_{\text{wave}}/\partial x$ where x, t are the fast scales and $u^{\pm}_{\text{mean}} = O(\epsilon^{-3/4})$, $u^{\pm}_{\text{wave}} = O(\epsilon^{-3/4})$. Hence $u^{\pm}_{\text{ind}} = O(\epsilon^{-1/2})$ in the wave, and from incompressibility the corresponding normal component is $v^{\pm}_{\text{ind}} = O(\epsilon^{-3/4})$. Clearly the extra normal term of $O(\epsilon^{-\frac{3}{4}})$ plays no part in balances used in the derivation of the amplitude equation (4.4.1.29) and so can be neglected.

4.4.2 Analysis of the amplitude equation

Before beginning our analysis of the amplitude equation (4.4.1.29) we note the obvious dissimilarities with the form for the non-resonant case (4.2.3.5). Our new equation contains a second-order derivative of the wave amplitude which signifies

the presence of two wave modes coupled through the non-linear term. As has been noted in the prior sub-section, the equation contains no contributions from either the viscous interfacial, diffusion or Stokes wall layers. Again we see a purely imaginary nonlinear coefficient but this time, due to its differentiated form, the nonlinearity provides a strong phase-amplitude interaction as we will find in this subsection.

Second-order amplitude equations are well known in the theory of weakly nonlinear resonant interaction, see e.g. Drazin (1970), Akylas (1982), Akylas & Benney (1982), who examined the direct- and near-resonance between instability modes present for wind blowing over infinitely deep water. Weismann (1979), who looked at the stability of two- and three-dimensional wave packets in a two-fluid system of infinite depth, and Guckenheimer & Knobloch (1983), Dangelmayr & Knobloch (1987), for various problems, all encounter similar equations, which may be transformed into "energy" equations (see 4.4.2.9 below). However the particular combination of coefficients present in our equation (some of which are complex-valued) seems to be new and deserves investigation.

To ease analysis of the amplitude equation we make the change of variables

$$A_0 = \frac{2}{\sqrt{7}}\left(\frac{ak^3}{2\rho^-}\right)^{\frac{1}{4}}\bar{A},\quad t_1 = \left(\frac{2\rho^-}{ak^3}\right)^{\frac{1}{2}}\bar{t}, \tag{4.4.2.1}$$

which gives us

$$\frac{d^2\bar{A}}{d\bar{t}^2} + i\Gamma\frac{d\bar{A}}{d\bar{t}} - \bar{A} = i\frac{d\left(\bar{A}\mid\bar{A}\mid^2\right)}{d\bar{t}}, \tag{4.4.2.2}$$

where the coefficient Γ can be thought of as a "detuning parameter",

$$\Gamma = \frac{\gamma_1}{k}\left(\frac{ak^3}{2\rho^-}\right)^{\frac{1}{2}}. \tag{4.4.2.3}$$

Next we write

$$\bar{A} = \rho(\bar{t})\exp[i\phi(\bar{t})], \tag{4.4.2.4}$$

where ρ,ϕ are purely real functions of $\bar{t}$. The equation (4.4.2.2) then splits into two real equations for the magnitude ρ and phase ϕ of the wave amplitude,

$$\frac{d^2\rho}{d\bar{t}^2} - \rho u^2 - \Gamma\rho u - \rho = -\rho^3 u, \tag{4.4.2.5}$$

$$2\frac{d\rho}{d\bar{t}}u + \rho\frac{du}{d\bar{t}} + \Gamma\frac{d\rho}{d\bar{t}} = \frac{d(\rho^3)}{d\bar{t}}, \tag{4.4.2.6}$$

where $u = d\phi/d\bar{t}$. Integration of these two equations gives us

$$\left(\frac{d\rho}{d\bar{t}}\right)^2 = -\frac{1}{16}\rho^6 + \frac{\Gamma}{4}\rho^4 - \left(\frac{\Gamma^2}{4} - \frac{c_1}{8} - 1\right)\rho^2 - \frac{c_1^2}{32}\frac{1}{\rho^2} + c_2, \quad (4.4.2.7)$$

$$u = \frac{3}{4}\rho^2 - \frac{\Gamma}{2} + \frac{c_1}{4}\frac{1}{\rho^2}, \quad (4.4.2.8)$$

where c_1, c_2 are arbitrary constants, and we may think of (4.4.2.7) as being in the form of an "energy integral",

$$\left(\frac{d\rho}{d\bar{t}}\right)^2 = f(\rho) + c_2, \quad (4.4.2.9)$$

$$f(\rho) = -\frac{1}{16}\rho^6 + \frac{\Gamma}{4}\rho^4 - \left(\frac{\Gamma^2}{4} - \frac{c_1}{8} - 1\right)\rho^2 - \frac{c_1^2}{32}\frac{1}{\rho^2}, \quad (4.4.2.10)$$

with c_2 representing the "energy level" and $f(\rho)$ the "potential". We now analyze the solutions in the phase plane of the variables $\rho, d\rho/d\bar{t}$.

The solutions separate into two distinct instances depending on whether c_1 is zero or not. We begin with the special case $c_1 = 0$, see fig 4:6(a)-fig 4:6(g) and notice that for all values of the detuning parameter Γ the potential function $f(\rho)$ has the property that $f(0) = 0$ and so there exists a stationary point at the origin where $d\rho/d\bar{t} = \rho = 0$. As we vary the detuning parameter we uncover a number of typical solutions separated by the critical values of Γ, defined by $\Gamma^2 = 4$ (or in the earlier notation $\gamma_1^2 = 8\rho^-/ak$). If $\Gamma \leq -2$, fig 4:6(a), then the origin is the only stationary point surrounded by a family of periodic orbits which we obtain by varying the energy level parameter c_2. When $\Gamma = -2$, fig 4:6(b), the first of the critical values of Γ, we reach the limit of the single stagnation point solution. For values of Γ greater then this, see figs 4:6 (c)-(e), a second stagnation point bifurcates from the origin along the ρ axis giving rise to a separatrix solution along with a second set of periodic solutions. The solutions lying on the separatrix have orbits of infinite period, growing from infinitesimally small disturbances to a finite amplitude before eventually decaying. We can see this from the shape of the separatrix which approaches the origin linearly.

Our next value of interest for Γ is when it crosses the second critical value $\Gamma = 2$,

see fig 4:6(f). The phase-plane diagram now shows a saddle point separating two stable stationary points, one at the origin and one at a finite value of ρ.

The form of this diagram is typical for all values of $\Gamma > 2$, fig 4:6(g). We note that there are no solutions of (4.4.2.9), (4.4.2.10) with unbounded amplitude growth: all waves initiated at a small or finite amplitude remain bounded. This important property also holds in the second case of a non-zero value for c_1, see fig 4:7(a)-fig 4:7(c). Here we observe that the potential function $f(\rho) \to -\infty$ for both $\rho \to 0$ and $\rho \to \infty$ with either one of two maxima at finite positive ρ, depending on the values of the coefficients c_1, Γ. A numerical exploration was made using the Mathematica package and it was discovered that there exists a unique critical value of Γ, which we will denote as $\Gamma = \Gamma_c(c_1)$, as a boundary between the cases of one or two maxima see fig 4:7(d). For $\Gamma < \Gamma_c$, fig 4:7(a), there exists only one maximum and this translates to the existence of a single stagnation point at a finite non-zero value of ρ in the phase-plane diagram. For $\Gamma > \Gamma_c$, fig 4:7(c), there are two maxima and this gives a saddle point solution separating two stationary points in the phase plane. For the critical case of $\Gamma = \Gamma_c$, fig 4:7(b), the saddle point occurs at the same point on the ρ axis as the stationary point.

A comparison between the nonlinear wave behaviour and the corresponding linear wave properties reveals the important stabilizing role of the nonlinear effects. The linearized version of (4.4.2.2) gives us two solutions of the form $A = \exp(\bar{\sigma}\bar{t})$ where

$$\bar{\sigma} = -\frac{i\Gamma}{2} \pm \sqrt{1 - \frac{\Gamma^2}{4}}. \qquad (4.4.2.11)$$

We see that the linear solutions for the case when $\mid \Gamma \mid \geq 2$ are neutral and hence are similar to the nonlinear solutions. This is because away from the direct resonance the capillary and TS waves remain neutral on the timescale $t = O(\epsilon^{3/2})$, the slow growth only being felt on larger temporal scales (see below §§4.5 4.5.5). By contrast, when $\mid \Gamma \mid \leq 2$ the linear theory shows growing and decaying waves as described in Timoshin (1997). The non-linear effects for such waves therefore have a crucial, and indeed dominant, stabilizing role.

4.5 The near resonant regimes

Here and in §4.5.5 we bridge the gap between the two disparate regimes described in §§4.2,4.4. The weakly-nonlinear TS waves in §4.2 are essentially governed by a first-order differential equation with the growth-rate term associated with viscous effects but, in contrast, the resonant regime in §4.4 is governed by a second-order equation which relies on purely inviscid mechanisms. In order to elucidate the connection between these two regimes, in this section we consider an $O(\epsilon^{1/2})$ neighbourhood of the critical surface tension value $\gamma = \gamma_0$, as in §4.4, the difference being that the detuning parameter $\gamma_1 = \epsilon^{-1/2}(\gamma - \gamma_0)$ will be assumed outside the strong resonance , i.e. $\mid \gamma_1 \mid > \gamma_{1c}$, where $\gamma_{1c} = \sqrt{8\rho^-/(ak)}$ corresponding to $\Gamma = 2$ in the discussion in §4.4.2. Further, in comparison with the theory of strong interaction developed in §4.4, the wave amplitude will be taken sufficiently small to take into account the slow wave growth induced by viscous effects. This will take us back to the weakly-nonlinear modulation regimes typical for non-resonant wave development, as in §4.2. We will also show that the analysis along these lines becomes invalid in a refined vicinity of the critical detuning parameter $\gamma_1 - \gamma_{1c} = O(\epsilon)$, and the modifications in the theory required in that case will be given in the next section.

4.5.1 The first near-resonant regime

For the remainder of this Chapter the surface tension coefficient is taken in the form

$$\gamma = \gamma_0 + \epsilon^{1/2}\gamma_1 + \epsilon\gamma_2, \qquad (4.5.1.1)$$

where $\gamma_0 = \rho^-/a$ and γ_1, γ_2 are arbitrary except that $|\gamma_1| > \sqrt{8\rho^-/(ak)}$. The $O(\epsilon)$ correction in (4.5.1.1) is not strictly necessary, however its presence will help in evaluating the range of applicability of the theory in this section. The film-flow

components are written as

$$u^- = \epsilon^{-\frac{1}{2}}(A_0(\tau)u_0^- E + c.c.) + (u_{20}^- E^2 + u_{10}^- E + c.c.) + \epsilon^{\frac{1}{2}}(u_{11}^- E + c.c. + ...) + ... \quad (4.5.1.2)$$

$$v^- = \epsilon^{-\frac{3}{2}}(A_0(\tau)v_0^- E + c.c.) + \epsilon^{-1}(v_{20}^- E^2 + v_{10}^- E + c.c.) + \epsilon^{-\frac{1}{2}}(v_{11}^- E + c.c. + ...) + ... \quad (4.5.1.3)$$

$$p^- = \epsilon^{-\frac{3}{2}}(A_0(\tau)p_0^- E + c.c.) + \epsilon^{-1}(p_{20}^- E^2 + p_{10}^- E + c.c.) + \epsilon^{-\frac{1}{2}}(p_{11}^- E + c.c. + ...) + ... \quad (4.5.1.4)$$

where $E = \exp[i(kX - \omega_0 T - \omega_1 t_1)]$, $\tau = \epsilon^{-1}t$, $t_1 = \epsilon^{-\frac{3}{2}}t$, $T = \epsilon^{-2}t$, $k > 0$; ω_0, ω_1 are real and the interface position is described by

$$f = a + \epsilon^{\frac{1}{2}}(F_0 E + c.c.) + \epsilon(F_{10}E + F_{20}E^2 + c.c.) + \epsilon^{\frac{3}{2}}[F_{11}E + c.c. + ...] + ... \quad (4.5.1.5)$$

Upon substitution into (4.1.1),(4.1.2) we have the relations,

$$-i\omega_0 u_0^- = -\frac{ik}{\rho^-}p_0^-, \quad (4.5.1.6)$$

$$-2i\omega_0 u_{20}^- + ik(A_0 u_0^-)^2 = -\frac{2ik}{\rho^-}p_{20}^-, \quad (4.5.1.7)$$

$$-i\omega_0 u_{10}^- - i\omega_1 A_0 u_0^- = -\frac{ik}{\rho^-}p_{10}^-, \quad (4.5.1.8)$$

$$-i\omega_0 u_{11}^- - i\omega_1 u_{10}^- + u_0^- \frac{\partial A_0}{\partial \tau} + \lambda^- iky A_0 u_0^- + iku_{20}^- A_0^* u_0^{-*} + \lambda^- A_0 v_0^- = -\frac{ik}{\rho^-}p_{11}^-, \quad (4.5.1.9)$$

and

$$iku_0^- + \frac{\partial v_0^-}{\partial y} = 0, \quad 2iku_{20}^- + \frac{\partial v_{20}^-}{\partial y} = 0, \quad (4.5.1.10)$$

$$iku_{10}^- + \frac{\partial v_{10}^-}{\partial y} = 0, \quad iku_{11}^- + \frac{\partial v_{11}^-}{\partial y} = 0, \quad (4.5.1.11)$$

for the momentum and continuity balances respectively. The leading terms then,

after normalizing the streamwise component u_0^-, are found to be

$$u_0^- = 1,\ \omega_0 = k^2,\ p_0^- = k\rho^-,\ v_0^- = -iky, \tag{4.5.1.12}$$

$$u_{20}^- = \frac{p_{20}^-}{k\rho^-} + \frac{A_0^2}{2k},\ v_{20}^- = -i\left(\frac{2p_{20}^-}{\rho^-} + A_0^2\right)y, \tag{4.5.1.13}$$

$$u_{10}^- = \frac{p_{10}^-}{k\rho^-} - \frac{\omega_1}{k^2}A_0,\ v_{10}^- = -i\left(\frac{p_{10}^-}{\rho^-} - \frac{\omega_1}{k}A_0\right)y, \tag{4.5.1.14}$$

$$u_{11}^- = \frac{p_{11}^-}{k\rho^-} - \frac{\omega_1}{k^2}\left(\frac{p_{10}^-}{k\rho^-} - \frac{\omega_1}{k^2}A_0\right) - \frac{i}{k^2}\frac{\partial A_0}{\partial\tau} + \frac{1}{k^2}A_0^*\left(\frac{p_{20}^-}{\rho^-} + \frac{A_0^2}{2}\right), \tag{4.5.1.15}$$

$$v_{11}^- = v_w - i\left[\frac{p_{11}^-}{\rho^-} - \frac{\omega_1}{k^2}\left(\frac{p_{10}^-}{\rho^-} - \frac{\omega_1}{k}A_0\right) + \frac{1}{k}A_0^*\left(\frac{p_{20}^-}{\rho^-} + \frac{A_0^2}{2}\right)\right]y - \frac{y}{k}\frac{\partial A_0}{\partial\tau}, \tag{4.5.1.16}$$

where v_w represents the effect of the wall and is given by (4.2.1.7). For the flow above the interface in the region $y = O(1)$ the expansions are,

$$\begin{aligned} u^+ &= y - a + u_s + (u_{10}^+E + c.c.) + \epsilon^{\frac{1}{2}}(u_{11}^+E + c.c.) \\ &\quad +\epsilon(u_{12}^+E + u_{20}^+E^2 + c.c.) + ..., \end{aligned} \tag{4.5.1.17}$$

$$v^+ = \epsilon^{-\frac{3}{2}}(v_0^+E + c.c.) + \epsilon^{-1}(v_{10}^+E + v_{20}^+E^2 + c.c.) + ..., \tag{4.5.1.18}$$

$$p^+ = \epsilon^{-1}(p_{10}^+E + c.c.) + \epsilon^{-\frac{1}{2}}(p_{11}^+E + c.c.) + (p_{12}^+E + p_{20}^+E^2 + c.c.) + ..., \tag{4.5.1.19}$$

and the coefficients are governed by the equations

$$-ik^2u_{10}^+ = -ikp_{10}^+, \tag{4.5.1.20}$$

$$-ik^2u_{11}^+ - i\omega_1u_{10}^+ + v_0^+ = -ikp_{11}^+, \tag{4.5.1.21}$$

$$-2ik^2u_{20}^+ + ik(u_{10}^+)^2 + v_{20}^+ + v_0^+\frac{\partial u_{11}^+}{\partial y} = -2ikp_{20}^+, \tag{4.5.1.22}$$

$$-ik^2u_{12}^+ - i\omega_1u_{11}^+ + \frac{\partial u_{10}^+}{\partial\tau} + (y - a + u_s)iku_{10}^+ + v_{10}^+ = -ikp_{12}^+, \tag{4.5.1.23}$$

$$\frac{\partial v_0^+}{\partial y} = 0,\ iku_{10}^+ + \frac{\partial v_{10}^+}{\partial y} = 0,\ \frac{\partial v_{20}^+}{\partial y} = 0. \tag{4.5.1.24}$$

The velocity components here can be expressed via the pressure contributions,

$$v_0^+ = \frac{i\omega_1}{k}p_{10}^+,\ u_{10}^+ = \frac{p_{10}^+}{k},\ u_{11}^+ = \frac{p_{11}^+}{k},\ u_{20}^+ = \frac{p_{20}^+}{2k}, \tag{4.5.1.25}$$

$$v_{20}^+ = -\frac{i}{k}(p_{10}^+)^2 - ikp_{20}^+, \tag{4.5.1.26}$$

$$v_{10}^+ = -i(y-a)p_{10}^+ + \frac{i\omega_1}{k}p_{11}^+ - \frac{1}{k}\frac{\partial p_{10}^+}{\partial \tau} - iu_s p_{10}^+. \tag{4.5.1.27}$$

where the viscous-inviscid interaction condition has already been taken into account.

4.5.2 The viscous diffusion layer

The thickness of this layer, based on the slow time scale, is $O(\epsilon^{\frac{1}{2}})$ and so we construct a new local normal co-ordinate $\tilde{z}$ along with a new velocity component $w^{\pm}$,

$$y = f + \epsilon^{\frac{1}{2}}\tilde{z},\ v^{\pm} = \frac{\partial f}{\partial t} + u^{\pm}\frac{\partial f}{\partial x} + w^{\pm}. \tag{4.5.2.1}$$

For the flow above the interface the velocities expand as

$$u^+ = \epsilon^{-\frac{1}{2}}\tilde{u}_{m0}^+(\tilde{z},\tau) + (u_{10}^+E + c.c. + \tilde{u}_{m1}) + ..., \tag{4.5.2.2}$$

$$w^+ = \epsilon^{-\frac{1}{2}}[(-iu_{10}^+\tilde{z} + \tilde{w}_{vu})E + c.c.] + ..., \tag{4.5.2.3}$$

where the mean-flow terms are necessary for the subsequent match with an even thinner interfacial layer and w_{vu} is a constant of integration which represents the effect of the inner layer on the wave.

In the diffusion layer in the film we take

$$u^- = \epsilon^{-\frac{1}{2}}(\tilde{u}_{m0}^- + A_0E + c.c.) + (\tilde{u}_{m1}^- + \tilde{u}_{10}^-E + \tilde{u}_{20}^-E^2 + c.c.) + ..., \tag{4.5.2.4}$$

$$w^- = \epsilon^{-1}(\tilde{w}_0^-E + c.c.) + \epsilon^{-\frac{1}{2}}(\tilde{w}_{10}^-E + \tilde{w}_{20}^-E^2 + c.c.) + ..., \tag{4.5.2.5}$$

with the pressure, which is a constant with respect to y across the entire boundary layer, represented by the inviscid solution. The governing equations for the wave terms are of the form

$$ikA_0 + \frac{\partial \tilde{w}_0^-}{\partial \tilde{z}} = 0,\ -2ik^2\tilde{u}_{20}^- + ikA_0^2 = -\frac{2ik}{\rho^-}p_{20}^- \tag{4.5.2.6}$$

$$2ik\tilde{u}_{20} + \frac{\partial \tilde{w}_{20}}{\partial \tilde{z}} = 0 \tag{4.5.2.7}$$

$$-ik^2\tilde{u}_{10}^- - i\omega_1 A_0 + ikA_0\tilde{u}_{m0}^- + \tilde{w}_0^- \frac{\partial \tilde{u}_{m0}^-}{\partial \tilde{z}} = -\frac{ik}{\rho^-}p_{10}^-, \tag{4.5.2.8}$$

$$ik\tilde{u}_{10}^- + \frac{\partial \tilde{w}_{10}^-}{\partial \tilde{z}} = 0, \tag{4.5.2.9}$$

$$\frac{\partial \tilde{u}_{m0}^-}{\partial \tau} + (\tilde{w}_0^- \frac{\partial \tilde{u}_{10}^{-*}}{\partial \tilde{z}} + \tilde{w}_0^{-*}\frac{\partial \tilde{u}_{10}^-}{\partial \tilde{z}}) = \nu^- \frac{\partial^2 \tilde{u}_{m0}^-}{\partial \tilde{z}^2}. \tag{4.5.2.10}$$

Solving for $\tilde{w}_0^-, \tilde{u}_{20}^-, \tilde{w}_{20}^-, \tilde{u}_{10}^-, \tilde{w}_{10}^-$ we obtain

$$\tilde{w}_0^- = -ikA_0\tilde{z}, \tag{4.5.2.11}$$

$$\tilde{u}_{20} = \frac{A_0^2}{2k} + \frac{p_{20}^-}{k\rho^-}, \quad \tilde{w}_{20} = -i\left(A_0^2 + \frac{p_{20}^-}{k\rho^-}\right)\tilde{z}, \tag{4.5.2.12}$$

$$\tilde{u}_{10}^- = -\frac{\omega_1}{k^2}A_0 + \frac{A_0}{k}\left(\tilde{u}_{m0}^- - \tilde{z}\frac{\partial \tilde{u}_{m0}^-}{\partial \tilde{z}}\right) + \frac{p_{10}^-}{k\rho^-}, \tag{4.5.2.13}$$

$$\tilde{w}_{10}^- = w_{vl} - i\left[\frac{\omega_1}{k}A_0\tilde{z} + A_0\int_0^{\tilde{z}}\left(\tilde{u}_{m0}^- - s\frac{\partial \tilde{u}_{m0}^-}{\partial s}\right)ds + \frac{p_{10}^-}{\rho^-}\tilde{z}\right], \tag{4.5.2.14}$$

where the constant w_{vl} will be found in the next subsection. The mean flow in the diffusion layer is governed by

$$\frac{\partial \tilde{u}_{m0}^{\pm}}{\partial t} = \nu^- \frac{\partial^2 \tilde{u}_{m0}^{\pm}}{\partial \tilde{z}^2}, \tag{4.5.2.15}$$

with the boundary conditions

$$\tilde{u}_{m0}^+(\tilde{z} = \infty) = 0,\ \tilde{u}_{m0}^-(\tilde{z} = -\infty) = 0,\ \tilde{u}_{m0}^-(\tilde{z} = 0) = \tilde{u}_{m0}^+(\tilde{z} = 0), v \tag{4.5.2.16}$$

and the shear jump relation of the form

$$\frac{\partial \tilde{u}_{m0}^+}{\partial \tilde{z}} - \mu^- \frac{\partial \tilde{u}_{m0}^-}{\partial \tilde{z}} = J, \tag{4.5.2.17}$$

where J is determined in the next subsection.

4.5.3 The interfacial viscous layer

As in the non-resonant case in §4.2, viscosity affects the wave components in a thinner interfacial layer defined as

$$y = f + \epsilon\bar{z}, \quad \bar{z} = O(1). \tag{4.5.3.1}$$

We take the following expansions in this region both above and below the interface:

$$u^{\pm} = \epsilon^{-\frac{1}{2}}(\bar{u}_0^{\pm} A_0 E + c.c + \bar{u}_{m0}) + (\bar{u}_{m1}^{\pm} + ...), \tag{4.5.3.2}$$

$$w^{\pm} = \epsilon^{-\frac{1}{2}}(\bar{w}_0^{\pm} A_0 E + c.c.) + ... \ . \tag{4.5.3.3}$$

In a similar manner to the non-resonant regime, §4.2.2, we have

$$\bar{u}_0^{\pm} = Q^{\pm} e^{\mp\sigma^{\pm}\bar{z}} + \frac{p_0^{\pm}}{\rho^{\pm} k}, \ \bar{w}_0^{\pm} = \pm\frac{ikQ^{\pm}}{\sigma^{\pm}}(e^{\mp\sigma^{\pm}\bar{z}} - 1) - \frac{ip_0^{\pm}\bar{z}}{\rho^{\pm}}, \tag{4.5.3.4}$$

where $\sigma^{\pm} = \sqrt{-ik^2/\nu^{\pm}}$, $Real(\sigma^{\pm}) > 0$, $Q^{\pm}$ are found to be

$$Q^{-} = \frac{-1}{1 + \rho^{-}\sqrt{\nu^{-}}}, \ Q^{+} = \frac{\rho^{-}\sqrt{\nu^{-}}}{1 + \rho^{-}\sqrt{\nu^{-}}}. \tag{4.5.3.5}$$

and matching (4.5.3.4) to the outer diffusion-layer solution we find that

$$w_{vl} = \frac{e^{\frac{-i\pi}{4}}\sqrt{\nu^{-}}}{1 + \rho^{-}\sqrt{\nu^{-}}} A_0. \tag{4.5.3.6}$$

The jump condition for the generated mean flow across the interface is then found to be

$$J = \Lambda_m^{+} - \mu^{-}\Lambda_m^{-} \ = \ -\frac{\sqrt{2}|A_0|^2}{k}\left(\frac{\sqrt{\nu^{-}}k\rho^{-}}{1 + \rho^{-}\sqrt{\nu^{-}}}\right). \tag{4.5.3.7}$$

This last equation, combined with (4.5.2.15), (4.5.2.16) and (4.5.2.17) completes the set of relations governing the mean flow in the diffusion layer.

4.5.4 The amplitude equation

With the exception of the jumps in pressure across the interface, which we will calculate first, we now have enough information about the jumps in shears and velocities to derive the wave amplitude equation and the generated mean flow. The interfacial pressure jump condition (4.1.8) provides the relations

$$\rho^{-} A_0 = \gamma_0 k F_0, \tag{4.5.4.1}$$

$$p_{20}^{-} = 4\gamma_0 k^2 F_{20}, \tag{4.5.4.2}$$

$$p_{10}^{+} - p_{10}^{-} = -\gamma_0 k^2 F_{10} - \gamma_1 k^2 F_0, \tag{4.5.4.3}$$

$$p_{11}^{+} - p_{11}^{-} = -\gamma_0 k^2 F_{11} - \gamma_1 k^2 F_{10} - \gamma_2 k^2 F_0. \tag{4.5.4.4}$$

Armed with these relations all that is left to do is match the viscous and inviscid flow regions. The normal velocity match between the viscous diffusion layer and inviscid region in the boundary-layer fluid shows that

$$v_0^{+} = -ik^2 F_0, \;\; v_{20}^{+} = -2ik^2 F_{20}, \tag{4.5.4.5}$$

and also

$$v_{10}^{+}(a) = \frac{i\omega_1}{k} p_{11}^{+} - \frac{1}{k}\frac{\partial p_{10}^{+}}{\partial \tau} - iu_s p_{10}^{+} = -ik^2 F_{10} - i\omega_1 F_0. \tag{4.5.4.6}$$

Substituting these relations into equations (4.5.1.25), (4.5.1.26) we have

$$\frac{i\omega_1}{k} p_{10}^{+} = -ik^2 F_0, \tag{4.5.4.7}$$

$$-ik\left(\frac{p_{10}^{+}}{k}\right)^2 - ikp_{20}^{+} = -2ik^2 F_{20}, \tag{4.5.4.8}$$

$$\frac{i\omega_1}{k} p_{11}^{+} - \frac{1}{k}\frac{\partial p_{10}^{+}}{\partial \tau} - iu_s p_{10}^{+} = -ik^2 F_{10} - i\omega_1 F_0. \tag{4.5.4.9}$$

We note that the constant w_{vu} does not enter the solution as it appears at $O(\epsilon^{-\frac{1}{2}})$.

Next we match the diffusion layer in the film to the lower inviscid layer, which yields the relations

$$A_0 = \frac{k}{a} F_0, \tag{4.5.4.10}$$

$$-ikA_0 F_0 - ia\left(\frac{2p_{20}^{-}}{\rho^{-}} + A_0^2\right) = -2ik^2 F_{20} + ikF_0 A_0, \tag{4.5.4.11}$$

$$-ia\left(\frac{p_{10}^{-}}{\rho^{-}} - \frac{\omega_1}{k} A_0\right) = -ik^2 F_{10} - i\omega_1 F_0, \tag{4.5.4.12}$$

$$ikA_0^*F_{20} - i\left(\frac{2p_{20}^-}{\rho^-} + A_0^2\right)F_0^* + v_w - \frac{a}{k}\frac{\partial A_0}{\partial \tau}$$
$$-ia\left[\frac{p_{11}^-}{\rho^-} - \frac{\omega_1}{k^2}\left(\frac{p_{10}^-}{\rho^-} - \frac{\omega_1}{k}A_0\right) + \frac{A_0^*}{k}\left(\frac{p_{20}^-}{\rho^-} + \frac{A_0^2}{2}\right)\right]$$
$$= -ik^2F_{11} - i\omega_1 F_{10} + \frac{\partial F_0}{\partial \tau} + 2ikF_{20}A_0^* + u_s ikF_0$$
$$-ikF_0^*\left(\frac{A_0^2}{2k} + \frac{p_{20}^-}{k\rho^-}\right) + w_{vl} - iA_0\int_0^{-\infty}\left(\tilde{u}_{m0}^- - \tilde{z}\frac{\partial \tilde{u}_{m0}^-}{\partial \tilde{z}}\right)d\tilde{z}. \tag{4.5.4.13}$$

Combining (4.5.4.10) with (4.5.4.1) shows that $\gamma_0 = \rho^-/a$, the condition of resonance in §4.2. Then (4.5.4.12), (4.5.4.7) and the relation between them, the jump condition (4.5.4.3), provide an equation for ω_1,

$$\frac{2\rho^-}{k}\omega_1^2 - \gamma_1 ak\omega_1 + ak^2 = 0, \tag{4.5.4.14}$$

and the pressure components $p_{10}^{\pm}$ in terms of A_0 and F_{10}:

$$p_{10}^+ = -\frac{ak^2}{\omega_1}A_0, \quad p_{10}^- = 2\frac{\rho^-\omega_1}{k}A_0 + \frac{\rho^- k^2}{a}F_{10}. \tag{4.5.4.15}$$

Repeating a similar combination, the equations (4.5.4.13), (4.5.4.8) and the pressure jump (4.5.4.2) give us

$$F_{20} = -\frac{a}{2k^2}A_0, \quad p_{20}^- = -2\rho^- A_0^2, \tag{4.5.4.16}$$

$$p_{20}^+ = -A_0^2\left(\frac{a}{k} + \frac{a^2k^2}{\omega_1^2}\right). \tag{4.5.4.17}$$

Substituting these results into the remaining triplet of relations (4.5.4.13), (4.5.4.4) and (4.5.4.9) we obtain the following equation for the wave amplitude:

$$\left(\frac{2a}{k} - \frac{a^2k^2}{\rho^-\omega_1^2}\right)\frac{dA_0}{d\tau} + iA_0\int_0^{-\infty}\left(u_{m0}^- - z\frac{\partial u_{m0}^-}{\partial z}\right)dz +$$
$$\frac{e^{-i\pi/4}\sqrt{\nu^-}}{1+\rho^-\sqrt{\nu^-}}A_0 = \frac{7a}{2k}iA_0|A_0|^2 + i\left(\frac{a\omega_1^2}{k^3} - au_s\right)A_0$$
$$-i\frac{a}{\rho^-}\left[\gamma_2 ak - a\left(1 + \frac{k^3u_s}{\omega_1^2}\right)\right]A_0 + \frac{ikA_0}{\sigma^-}, \tag{4.5.4.18}$$

where w_{vl} was determined in (4.5.3.6).

The form of the equation, with purely imaginary non-linear co-efficients and first-order differentiation shows that the growth rate will be dependent only on the viscous terms w_{vl}, v_w. The non-linear terms will cause only rapid phase changes and the equation and solution properties are therefore similar to those for the non-resonant regime in §4.2.3.

Since ω_1 above was assumed to be real, this imposes a restriction on the values of γ_1 permissible. The validity of the calculation leading to (4.5.4.18) breaks down if the coefficient of the derivative in the amplitude equation becomes zero which occurs when

$$\omega_1^2 = \frac{ak^3}{2\rho^-}. \tag{4.5.4.19}$$

This critical value of ω_1 is exactly that at which the roots of (4.5.4.14) coalesce and corresponds to the value $\Gamma = 2$ in the resonant regime, section §4.4. It is in this region of γ where ω_1 becomes complex and we must alter the assumed development time scales.

4.5.5 The second near-resonant regime

We begin this section by analyzing the region in γ where the previous intermediary regime fails, and then outline the structure for one further regime to link the behaviours of the solutions in §4.4 and §4.5. In the previous section we found a wave-amplitude evolution equation, (4.5.4.18), which was governed by the balance

$$\alpha \frac{dA_0}{d\tau} \sim \text{linear growth rate terms} \tag{4.5.5.1}$$

where $\alpha = \alpha(\gamma_1)$ and the linear growth rate terms come from the viscous wall and interfacial layers. As $\alpha \to 0$, the solution to the quadratic equation, (4.5.4.14), governing ω_1 in terms of γ_1, approaches a double root. We see that, as $\gamma_1 \to \gamma_{1c}$

$$\omega_1 \to \omega_{1c} + O(\sqrt{\gamma_1 - \gamma_{1c}}), \quad \alpha \to O(\sqrt{\gamma_1 - \gamma_{1c}}) \tag{4.5.5.2}$$

Therefore, writing $A_0 = e^{\sigma_r \tau}\bar{A}(\tau)$, to maintain the growth-rate contributions from the viscous layers, the growth rate becomes $\sigma_r \sim (\gamma_1 - \gamma_{1c})^{-\frac{1}{2}}$. We can see

that the scalings used in §4.5 become invalid when,

$$\epsilon^{-1}\frac{1}{\sqrt{\gamma_1-\gamma_{1c}}} \sim \epsilon^{-\frac{3}{2}}(\omega_{1c}+\sqrt{\gamma_1-\gamma_{1c}}) \text{ as } \gamma_1 \to \gamma_{1c}. \tag{4.5.5.3}$$

Growth then occurs over the same time scale as neutral development when $\epsilon^{\frac{1}{2}} \sim \gamma_1 - \gamma_{1c}$, so we now concentrate on the role of the second correction to γ, namely γ_2, when $\gamma_1 = \gamma_{1c}$.

4.5.6 The flow expansions

For the surface tension and flow parameters in the film we take the expansions of the form

$$\gamma = \gamma_0 + \epsilon^{1/2}\gamma_1 + \epsilon\gamma_2 \tag{4.5.6.1}$$

$$\begin{aligned} u^- = {} & \epsilon^{-1/2}(A_0(t_2)E + c.c.) + (u^-_{20}E^2 + u^-_{10}E + c.c. + \lambda^- y) \\ & + \epsilon^{1/4}(u^-_{11}E + c.c.) + \epsilon^{1/2}(u^-_{12}E + u^-_{21}E^2 + u^-_{30}E^3 + c.c.) + \ldots \end{aligned} \tag{4.5.6.2}$$

$$\begin{aligned} v^- = {} & \epsilon^{-3/2}(-iky A_0(t_2) + c.c.) + \epsilon^{-1}(v^-_{20}E^2 + v^-_{10}E + c.c.) \\ & + \epsilon^{-3/4}(v^-_{11}E + c.c.) + \epsilon^{-1/2}(v^-_{12}E + \ldots + c.c.) \end{aligned} \tag{4.5.6.3}$$

$$\begin{aligned} p^- = {} & \epsilon^{-3/2}(k\rho^- A_0(t_2)E + c.c.) + \epsilon^{-1}(p^-_{20}E^2 + p^-_{10}E + c.c.) \\ & + \epsilon^{-3/4}(p^-_{11}E + c.c.) + \epsilon^{-1/2}(p^-_{12}E + \ldots + c.c.) + \ldots, \end{aligned} \tag{4.5.6.4}$$

where $E = \exp[i(kX - \omega_0 T - \omega_1 t_1)]$, $t_2 = \epsilon^{-5/4}t$, $t_1 = \epsilon^{-3/2}t$, $T = \epsilon^{-2}t$. Again we have normalized the leading- order streamwise velocity in the film.

Note that the slow time-scale has been shortened to $O(\epsilon^{-5/4})$ whilst the wave amplitude remains at the same order as in §4.5. Substituting these expansions into the triple-deck equations we obtain the following relations, from the momentum conservation

$$-ik^2 u^-_{10} - i\omega_1 A_0 = -\frac{ik}{\rho^-}p^-_{10}, \tag{4.5.6.5}$$

$$-2ik^2 u^-_{20} + ikA_0^2 = -\frac{2ik}{\rho^-}p^-_{20}, \tag{4.5.6.6}$$

$$-ik^2u_{11}^- + \frac{\partial A_0}{\partial t_2} = -\frac{ik}{\rho^-}p_{11}^-, \tag{4.5.6.7}$$

$$-ik^2u_{12}^- - i\omega_1 u_{10}^- + iku_{20}^- A_0^* + iky\frac{\partial u_{20}^-}{\partial y}A_0 = -2ikp_{12}^-, \tag{4.5.6.8}$$

and from the continuity,

$$iku_{10}^- + \frac{\partial v_{10}^-}{\partial y} = 0, \quad 2iku_{20}^- + \frac{\partial v_{20}^-}{\partial y} = 0, \tag{4.5.6.9}$$

$$iku_{11}^- + \frac{\partial v_{11}^-}{\partial y} = 0, \quad iku_{12}^- + \frac{\partial v_{12}^-}{\partial y} = 0. \tag{4.5.6.10}$$

The solutions for the leading terms here are

$$u_{10}^- = \frac{p_{10}^-}{k\rho^-} - \frac{\omega_1}{k^2}A_0, \quad v_{10}^- = -i\left(\frac{p_{10}^-}{\rho^-} - \frac{\omega_1}{k}A_0\right)y, \tag{4.5.6.11}$$

$$u_{20}^- = \frac{p_{20}^-}{k\rho^-} + \frac{A_0^2}{2k}, \quad v_{20}^- = -i\left(\frac{2p_{20}^-}{\rho^-} + A_0^2\right)y, \tag{4.5.6.12}$$

$$u_{11}^- = \frac{p_{11}^-}{\rho^- k} + \frac{1}{ik^2}\frac{\partial A_0}{\partial t_2}, \tag{4.5.6.13}$$

$$v_{11}^- = -i\left(\frac{p_{11}^-}{\rho^-} + \frac{1}{ik}\frac{\partial A_0}{\partial t_2}\right)y. \tag{4.5.6.14}$$

The next-order terms include the first viscous effects felt in the film

$$u_{12}^- = \frac{p_{12}^-}{k\rho^-} - \frac{\omega_1}{k^2}\left(\frac{p_{10}^-}{k\rho^-} - \frac{\omega_1}{k^2}A_0\right) + \frac{A_0^*}{k}\left(\frac{p_{20}^-}{k\rho^-} + \frac{A_0^2}{2k}\right), \tag{4.5.6.15}$$

$$v_{12}^- = v_w - \frac{ip_{12}^- y}{\rho^-} + \frac{i\omega_1}{k}\left(\frac{p_{10}^-}{k\rho^-} - \frac{\omega_1}{k^2}A_0\right)y - iA_0^*\left(\frac{p_{20}^-}{k\rho^-} + \frac{A_0^2}{2k}\right)y, \tag{4.5.6.16}$$

where v_w is the wall contribution from the Stokes layer given by (4.2.1.7).

We now turn to the flow above the interface. Here we take the expansions

$$u^+ = y - a + u_s + (u_{10}^+E + c.c.) + \epsilon^{1/4}(u_{11}^+E + c.c.) + \epsilon^{1/2}(u_{12}^+E + c.c.) + ..., \tag{4.5.6.17}$$

$$v^+ = \epsilon^{-3/2}(v_0^+ E + c.c.) + \epsilon^{-1}(v_{20}^+ E^2 + v_{10}^+ E + c.c.) + ..., \tag{4.5.6.18}$$

$$p^+ = \epsilon^{-1}(p_{10}^+ E + c.c.) + \epsilon^{-3/4}(p_{11}^+ E + c.c.) + \epsilon^{-1/2}(p_{12}^+ E + c.c.) + ... \ . \tag{4.5.6.19}$$

Then along with the viscous-inviscid interaction condition, which gives

$$ku_{10}^+(y \to \infty) = p_{10}^+, \ \ ku_{11}^+(y \to \infty) = p_{11}^+, \ \ ku_{12}^+(y \to \infty) = p_{12}^+, \tag{4.5.6.20}$$

we obtain, firstly, the momentum balances,

$$-i\omega_1 u_{10}^+ + v_0^+ = 0, \tag{4.5.6.21}$$

$$\frac{\partial u_{10}^+}{\partial t_2} = \frac{i\omega_1}{k} p_{11}^+, \tag{4.5.6.22}$$

$$\frac{\partial u_{11}^+}{\partial t_2} - i\omega_1 u_{12}^+ + (y - a + u_s)iku_{10}^+ + v_{10}^+ = 0, \tag{4.5.6.23}$$

and secondly the continuity balances,

$$iku_{10}^+ + \frac{\partial v_{10}^+}{\partial y} = 0, \tag{4.5.6.24}$$

$$\frac{\partial v_0^+}{\partial y} = 0, \quad \frac{\partial v_{20}^+}{\partial y} = 0. \tag{4.5.6.25}$$

From (4.5.6.20), (4.5.6.22) and (4.5.6.21) we find that

$$p_{11}^+ = \frac{1}{\omega_1}\frac{\partial p_{10}^+}{\partial t_2}, \ \ v_0^+ = \frac{i\omega_1}{k} p_{10}^+. \tag{4.5.6.26}$$

Also from (4.5.6.24), (4.5.6.25) we have

$$v_{10}^+ = -iku_{10}^+(y - a) + B^+, \tag{4.5.6.27}$$

where, on substituting into (4.5.6.23),

$$B^+ = -iu_s p_{10}^+ + \frac{i\omega_1}{k} p_{12}^+ - \frac{1}{k}\frac{\partial p_{11}^+}{\partial t_2}. \tag{4.5.6.28}$$

Before we turn to the viscous layer of thickness $O(\epsilon)$ and the diffusion layer of $O(\epsilon^{5/8})$ at the interface we express the shape of the interface as

$$\begin{aligned} f &= a + \epsilon^{1/2}(F_0 E + c.c.) + \epsilon(F_{20}E^2 + F_{10}E + c.c.) + \epsilon^{5/4}(F_{11}E + c.c.) \\ &\quad + \epsilon^{3/2}(F_{12}E + c.c.) + ..., \end{aligned} \tag{4.5.6.29}$$

and calculate the pressure jumps at the successive orders of ϵ. We find the relations:

$$A_0 = \frac{\gamma_0 k}{\rho^-} F_0, \tag{4.5.6.30}$$

$$p_{10}^+ - p_{10}^- = -k^2\gamma_0 F_{10} - k^2\gamma_1 F_0, \tag{4.5.6.31}$$

$$p_{20}^- = 4\gamma_0 k^2 F_{20}, \tag{4.5.6.32}$$

$$p_{11}^+ - p_{11}^- = -\gamma_0 k^2 F_{11}, \tag{4.5.6.33}$$

$$p_{12}^+ - p_{12}^- = -k^2\gamma_0 F_{12} - \gamma_1 k^2 F_{10} - \gamma_2 k^2 F_0. \tag{4.5.6.34}$$

4.5.7 The interfacial viscous layers

First we tackle the $O(\epsilon)$ viscous layer about the interface. The result is, to the leading order, the same as in the previous intermediary case, as can be deduced from the velocity expansions

$$u^\pm = \epsilon^{-1/2}(\bar{u}_0^\pm A_0 E + c.c. + \bar{u}_{m0}^\pm) + ..., \tag{4.5.7.1}$$

$$w^\pm = \epsilon^{-1/2}(\bar{w}_0^\pm E + c.c.) + ..., \tag{4.5.7.2}$$

which are valid when $\bar{z} = \epsilon^{-1}(y-f) = O(1)$, and where $w^\pm = v^\pm - \partial f/\partial t - u^\pm \partial f/\partial x$. The leading disturbance terms are given by (4.5.3.2),(4.5.3.3) of the previous section.

As in the other regimes there are diffusive layers about the interface. The thickness of this layer in the current regime is of $O(\epsilon^{5/8})$, and the normal adjusted components $w^\pm$, in terms of the vertical coordinate $\tilde{z} = \epsilon^{-5/8}(y-f) = O(1)$, along with

the streamwise velocities $u^{\pm}$ are taken as

$$u^+ = u_s + (\tilde{u}_0^+ E + c.c.) + ..., \tag{4.5.7.3}$$

$$w^+ = \epsilon^{-1/2}(\tilde{w}_{vu} A_0 E + c.c.) + O(\epsilon^{-3/8}). \tag{4.5.7.4}$$

$$u^- = \epsilon^{-1/2}(\tilde{u}_0^+ E + c.c.) + O(1), \tag{4.5.7.5}$$

$$w^- = \epsilon^{-7/8}(-ip_0^- \tilde{z}\sigma^- A_0 E + c.c.) + \epsilon^{-1/2}(w_{vl} A_0 E + c.c.) + O(\epsilon^{-3/8}). \tag{4.5.7.6}$$

where, from matching to the interfacial viscous layer, of thickness $O(\epsilon)$, we find

$$w_{vu} = \frac{1}{2} e^{-i\pi/4}, \quad w_{vl} = -\frac{\sqrt{\nu^-}}{1 + \rho^- \sqrt{\nu^-}} e^{-i\pi/4}. \tag{4.5.7.7}$$

The wave terms will be matched to the inviscid flow above and below the interface in the next section. It only remains to be noted here that the induced mean flow in this region does not contribute in any way to the wave amplitude equation.

The final layer of interest is the viscous Stokes layer on the wall, which can be tackled in exactly the same manner as in §4.2.1. The only result required here is the value of the constant

$$v_w = \frac{ikA_0}{\sigma^-} = e^{3\pi i/4} \sqrt{\nu^-} A_0 \text{ with } \sigma^- = \sqrt{-ik^2/\nu^-}, \tag{4.5.7.8}$$

which enters (4.5.6.16).

4.5.8 The amplitude equation

We match the inviscid and viscous layers to obtain the amplitude equation, starting with the inviscid upper flow and viscous diffusion layer. This gives

$$v_0^+(y = a) = -ik^2 F_0, \tag{4.5.8.1}$$

$$v_{10}^+ = -ik^2 F_{10} - i\omega_1 F_0, \tag{4.5.8.2}$$

and then combining equation (4.5.8.1) with (4.5.6.26) we find that

$$p_{10}^+ = -\frac{k^3}{\omega_1} F_0. \tag{4.5.8.3}$$

Similarly the result of (4.5.8.2) and (4.5.6.27), (4.5.6.28) is

$$\frac{i\omega_1}{k}p_{12}^{+} - \frac{1}{k}\frac{\partial p_{11}^{+}}{\partial t_2} - iu_s p_{10}^{+} = -ik^2 F_{11} - i\omega_1 F_0. \tag{4.5.8.4}$$

We now turn to the flow in the film and, matching between the inviscid and diffusion layers, find the relations

$$A_0 = \frac{k}{a}F_0, \tag{4.5.8.5}$$

$$-ia\left(\frac{p_{10}^{-}}{\rho^{-}} - \frac{\omega_1}{k}A_0\right) = -ik^2 F_{10} - i\omega_1 F_0, \tag{4.5.8.6}$$

$$-ia\left(\frac{2p_{20}^{-}}{\rho^{-}} + A_0^2\right) = -2ik^2 F_{20} + 2ikF_0 A_0, \tag{4.5.8.7}$$

$$-ia\left(\frac{p_{11}^{-}}{\rho^{-}} + \frac{1}{ik}\frac{\partial A_0}{\partial t_2}\right) = \frac{\partial F_0}{\partial t_2} - ik^2 F_{12}, \tag{4.5.8.8}$$

$$v_{21}^{-} = -2ik^2 F_{21} \tag{4.5.8.9}$$

$$\begin{aligned} -ia\left(\frac{p_{12}^{-}}{\rho^{-}} - \frac{\omega_1}{k}\left(\frac{p_{10}^{-}}{k\rho^{-}} - \frac{\omega_1}{k^2}A_0\right) + A_0^{*}\left(\frac{p_{20}^{-}}{k\rho^{-}} + \frac{A_0^2}{2k}\right)\right) \\ + v_w + ikA_0^{*}F_{20} - i\left(\frac{2p_{20}^{-}}{\rho^{-}} + A_0^2\right)F_0^{*} = \\ -ik^2 F_{12} - i\omega_1 F_{10} + ika\lambda^{-}F_0 - iku_{20}^{-}F_0^{*} + \bar{w}_{vl} + 2ikA_0^{*}F_{20}. \end{aligned} \tag{4.5.8.10}$$

Eventually (4.5.8.10) will provide us with the amplitude equation. First, however, we must write all the terms as functions of A_0.

We begin by combining condition (4.5.6.30) with (4.5.8.5) to find $\gamma_0 = \rho^{-}/a$ as the leading-order resonance condition. Substituting this into (4.5.8.6) gives

$$F_{10} = -\frac{2a\omega_1}{k^3}A_0 + \frac{a}{k^2\rho^{-}}p_{10}^{-}, \tag{4.5.8.11}$$

and then the pressure jump condition (4.5.6.31) becomes

$$p_{10}^{+} = \left(\frac{2\omega_1\rho^{-}}{k} - ka\gamma_1\right)A_0, \tag{4.5.8.12}$$

whilst we leave p_{10}^- written as

$$p_{10}^- = \frac{2\rho^- k\omega_1}{k} A_0 + \frac{k^2\rho^-}{a} F_{10}. \tag{4.5.8.13}$$

Combining these with the relation (4.5.8.3) again, as in §4.5, we find the relation (4.5.4.19) for ω_1 which we will apply later,

$$\omega_1^2 - \frac{k^2 a\gamma_1}{2\rho^-}\omega_1 + \frac{k^3 a}{2\rho^-} = 0. \tag{4.5.8.14}$$

Next we combine (4.5.8.7) with (4.5.6.32), and obtain

$$F_{20} = -\frac{a}{2k^2} A_0^2, \quad p_{20}^- = -2\rho^- A_0^2. \tag{4.5.8.15}$$

Then from (4.5.8.8) and (4.5.6.33) we have

$$p_{11}^- = \frac{2i\rho^-}{k}\frac{\partial A_0}{\partial t_2} + \frac{\rho^- k^2}{a} F_{11}, \quad p_{11}^+ = \frac{2i\rho^-}{k}\frac{\partial A_0}{\partial t_2}, \tag{4.5.8.16}$$

and placing this solution back into (4.5.6.26) with (4.5.8.12) gives us

$$\omega_1 = \frac{k^2 a\gamma_1}{4\rho^-}. \tag{4.5.8.17}$$

The last formula coupled with (4.5.8.14) specifies the values of γ_1, ω_1, to be

$$\gamma_1 = \pm 2\sqrt{\frac{2\rho^-}{ka}}, \quad \omega_1 = \frac{2k}{\gamma_1}. \tag{4.5.8.18}$$

which are exactly the critical values encountered in the previous intermediary regime.

All that remains is to calculate p_{12}^- in terms of A_0 and substitute the result into (4.5.8.10). We can now rewrite (4.5.8.4) in terms of A_0

$$\begin{aligned} p_{12}^+ \;=\; & \frac{k}{i\omega_1}\left(iu_s\left(\frac{2\omega_1\rho^-}{k} - ka\gamma_1\right) - \frac{i\omega_1 a}{k}\right) A_0 \\ & + \frac{k}{i\omega_1}\left(\frac{2\rho^-}{ik^2} - \frac{a\gamma_1}{i\omega_1}\right)\frac{\partial^2 A_0}{\partial t_2^2} - \frac{k^3}{\omega_1} F_{10}, \end{aligned} \tag{4.5.8.19}$$

and then the pressure-jump condition (4.5.6.34) gives us

$$\begin{aligned} p_{12}^- \;=\; & \frac{k}{i\omega_1}\left(\frac{2\rho^-}{ik^2} - \frac{a\gamma_1}{i\omega_1}\right)\frac{\partial^2 A_0}{\partial t_2^2} + \frac{k}{i\omega_1}\left(iu_s\left(\frac{2\omega_1\rho^-}{k} - ka\gamma_1\right) - \frac{i\omega_1 a}{k}\right) A_0 \\ & + \frac{k^2\rho^-}{a} F_{12} + \left(\gamma_1 k^2 - \frac{k^3}{\omega_1}\right) F_{10} + \gamma_2 ka A_0. \end{aligned} \tag{4.5.8.20}$$

Substituting (4.5.8.20), (4.5.8.15), (4.5.8.13) and (4.5.8.18) back into (4.5.8.10) we obtain the required wave-amplitude equation for $A_0(t_2)$:

$$-sign(\omega_1)\frac{2}{k^2}\sqrt{\frac{2\rho^-}{ka}}\frac{d^2A_0}{dt_2^2}$$
$$+\left(\frac{3a}{2\rho^-}+\frac{2u_s}{a}-\frac{\gamma_2 k}{\rho^-}-\lambda^- a+e^{i\pi/4}\left(\frac{\rho^-\nu^-}{a(1+\rho^-\sqrt{\nu^-})}\right)\right)A_0 \;=-\frac{7}{2}A_0|A_0|^2. \tag{4.5.8.21}$$

We can transform this equation into a simpler form by writing

$$t_2=\beta\bar{T},\quad A_0=\beta_1\bar{A}, \tag{4.5.8.22}$$

where both β,β_1 are real and define β, β_1 as

$$\beta=\frac{2}{k}\sqrt{\frac{(1+\rho^-\sqrt{\nu^-})\sqrt{a}}{\sqrt{k\rho^-}\nu^-}},\quad \beta_1=\sqrt{\frac{\sqrt{2}\rho^-\nu^-}{7a(1+\rho^-\sqrt{\nu^-})}}, \tag{4.5.8.23}$$

to leave us with the transformed amplitude equation

$$sign(\omega_1)\frac{\partial^2\bar{A}}{\partial\bar{T}^2}=(\Gamma_1+i)\bar{A}+\bar{A}|\bar{A}|^2, \tag{4.5.8.24}$$

where the coefficient Γ_1 is defined as

$$\Gamma_1=\left(\frac{3a}{2\rho^-}+\frac{2u_s}{a}-\frac{\gamma_2 k}{\rho^-}-\lambda^- a+\frac{1}{a\sqrt{2}}\left(\frac{\rho^-\nu^-}{1+\rho^-\sqrt{\nu^-}}\right)\right)\left(\frac{a\sqrt{2}(1+\rho^-\sqrt{\nu^-})}{\rho^-\sqrt{\nu^-}}\right) \tag{4.5.8.25}$$

The solution to (4.5.8.24) now only depends on the sign of ω_1, the initial conditions for $\bar{A}$ and the real parameter Γ_1. Examples of the behaviour for various Γ_1 are shown in Figs 4:8(a) & (b). As we see from (4.5.8.18) there are two possible values of the frequency correction ω_1, corresponding to the two admissible values of the surface tension correction γ_1. These specific values mark the critical conditions at the coalescence of real eigenvalues of the linearized resonant amplitude equation in §4.4. The next-order correction term γ_2 contained in the parameter Γ_1 represents a measure of the deviation from the exact mode crossing. By taking the limit $\gamma_2\to-\infty$ if $\gamma_1>0$ or conversely $\gamma_2\to\infty$ if $\gamma_1<0$ we can establish a continuation of the present flow regime into the resonant regime governed by (4.4.1.29) where

we need to take Γ close to ± 2 and make the appropriate adjustments in the wave amplitude and slow time scales. In (4.4.1.29) we rewrite $\bar{A}$ as

$$\bar{A} = \delta_a B(\delta_t \bar{T}) e^{i\omega \bar{T}}, \tag{4.5.8.26}$$

and take $\Gamma = \pm 2 + \bar{\delta}\bar{\Gamma}$. This gives us the equation

$$\delta_a \left(\delta_t^2 \frac{d^2 B}{d\bar{T}^2} + 2i\omega\delta_t \frac{dB}{d\bar{T}} - \omega^2 B + i(2 + \delta\bar{\Gamma} \left(\delta_t \frac{dB}{\partial \bar{T}} + i\omega B \right) - B \right)$$
$$= \delta_a^3 i(i\omega A|A|^2 + o(\delta_t)). \tag{4.5.8.27}$$

Picking out terms of $O(\delta_a \delta_t)$ gives us the relation $\omega = \mp 1$. Then if we let $\delta_a^2 \sim \delta_t^2 \sim \delta$ we find

$$\frac{d^2 B}{d\bar{T}^2} = -\omega(-\bar{\Gamma} B + B|B|^2). \tag{4.5.8.28}$$

Hence if $\Gamma = +2$ (or $\Gamma = -2$), with $\bar{\Gamma} > 0$, ($\bar{\Gamma} < 0$) respectively, then $\omega = -1$ ($\omega = +1$) and (4.5.8.28) corresponds to the limit $\gamma_2 \to -\infty$ ($\gamma_2 \to \infty$) in (4.5.8.24).

A continuation from the flow regime in this section to that in §4.2 can be seen by taking the limit as $\gamma_2 \to \pm\infty$ in (4.5.8.24), i.e. moving away from resonance. We let $\gamma_2 \to \infty$ (or $\gamma_2 \to -\infty$) if $\gamma_1 > 0$ ($\gamma_1 < 0$) respectively and write $\bar{A}$ in (4.5.8.24) as

$$\bar{A} = e^{\pm i\sqrt{|\Gamma_1|}\bar{T}} B(\delta_t \bar{T}). \tag{4.5.8.29}$$

Taking $\delta_t = 1/\sqrt{|\Gamma_1|}$, the equation (4.5.8.24) becomes

$$\pm 2\frac{dB}{d\bar{\tau}} + B = -iB|B|^2 \tag{4.5.8.30}$$

at the leading order where $\tau = t/\sqrt{|\Gamma_1|}$,.

For $O(1)$ values of γ_2 the wave behaviour in equation (4.5.8.24) is strongly affected by the term iA_0. This non-conservative term can be regarded as an extra energy supply in the system and comes from the viscous interfacial and wall layers. The response of the wave to the supplied energy depends on the sign of ω_1. If $\omega_1 < 0$ then at large time $|\bar{A}|$ grows linearly with a rapid quadratic phase growth,

$$\bar{A} \sim 2te^{it^2}. \tag{4.5.8.31}$$

By contrast, in the case $\omega_1 > 0$ we find a finite-distance blow-up singularity in the wave development at some instance t_c with

$$|\bar{A}| \sim \sqrt{2}(t - t_c)^{-1}. \tag{4.5.8.32}$$

The value $\omega_1 = +1$ (or $\omega_1 = -1$) corresponds to the critical value $\Gamma = +2$ ($\Gamma = -2$) in terms of the analysis for the resonant regime in §4.4. The increased amplitudes produced during this intermediary stage will lead to a strongly nonlinear flow.

4.6 Concluding remarks

We will use a graph of the scaled primary disturbance amplitude A_0 plotted against the surface tension coefficient γ, fig 4:9, to illustrate the different regimes which have been examined in this chapter. The wave-amplitude A in the film will be measured in powers of ϵ, the disturbance wavelength. We saw in §4.2, the non-resonant regime, that the TS disturbance required an amplitude $O(1)$ to initiate self-modulation. However, on solution of the governing equation, this modulation affected only the phase and not the size of the disturbance. We find similar 'passive' nonlinearities in the homogeneous-fluid cases that were examined by Smith & Burggraf (1985) and also in Van Duin (1996) for a water-wave problem. Where our system differs is in the stronger interfacially generated mean flow in comparison with the single-fluid cases where the mean-flow generation is restricted to the Stokes wall layer as discussed in the general introduction in Chapter 1. The increased mean current exposes the flow to background or secondary short-wave disturbances to which, in the case of weak surface tension, they are potentially unstable. The magnitude of the interfacial tension is important here. Whilst we note that increased surface tension stabilizes the mean profiles to secondary disturbances, if the surface tension coefficient is close to a certain critical value γ_0 (defined in §4.4), then resonance between decaying capillary waves and growing TS modes can occur. This resonant regime is examined in §4.4 and is illustrated by region (II). In an $O(\epsilon^{\frac{1}{2}})$ neighborhood of the resonant range of γ we find an increased initial amplitude $O(\epsilon^{-\frac{3}{4}})$ required for self-modulation and hence faster time scales. The flow becomes essentially inviscid

and the nonlinearity stabilizes the flow with two potential outcomes of either finite-amplitude wave oscillations or eventual decay. The two intermediate regimes studied in section §§4.5,4.5.5 are shown in the sketch by (III) and (IV). These regimes serve as a bridge between the non-resonant, viscous regime and the essentially inviscid, resonant case with its non-linear ceiling on the disturbance growth.

We will now consider what may happen to the weakly non-linear modes over longer time periods. As has just been discussed, the resonant case is clearest for large times. Infinitesimally small growing disturbances eventually decay due to the non-linear effects in (4.4.1.29). We cannot tell however if finite amplitude disturbances will remain either periodic or bounded on larger temporal scales. In the non-resonant case, on the other hand, it is clear from the form of the non-linearity, which affects the phase alone, that the disturbance will continue to grow unchecked until it becomes strongly non-linear. In Smith & Burggraf's single-fluid study short waves continue to grow until they reach the largest magnitude of $O(\epsilon^{-1})$ for a weakly non-linear theory. At this stage the Stokes layer becomes non-linear as does the waves dispersion relation which is governed by a Benjamin-Ono equation with initial conditions which take into account longer scale, non-linear events.

In the two-fluid flow examined here however we have a different scheme developing. Because of the stronger generation of mean flow at the interface as opposed to the viscous wall layer the entire flow scheme may be altered before these large wave amplitudes of $O(\epsilon^{-1})$ are reached. Whilst the linear growth rate of the disturbance is of the form $\mid A \mid \sim \exp[\beta_r t]$, the generated mean flow is growing like $\mid u^{\pm}_{m0} \mid \sim \exp[2\beta_r t]$ due to the quadratic nature of the Reynolds-stress terms driving the mean flow in the interfacial layer, see §4.2.2. When the disturbance amplitude reaches $O(\epsilon^{-\frac{1}{2}})$ the mean velocity becomes of $O(\epsilon^{-1})$, and the generated mean flow will enter the leading-order wave solutions in equations (4.2.10), (4.2.11). Investigation of this later stage has been carried out by S N Timoshin recently.

4.4 Figures

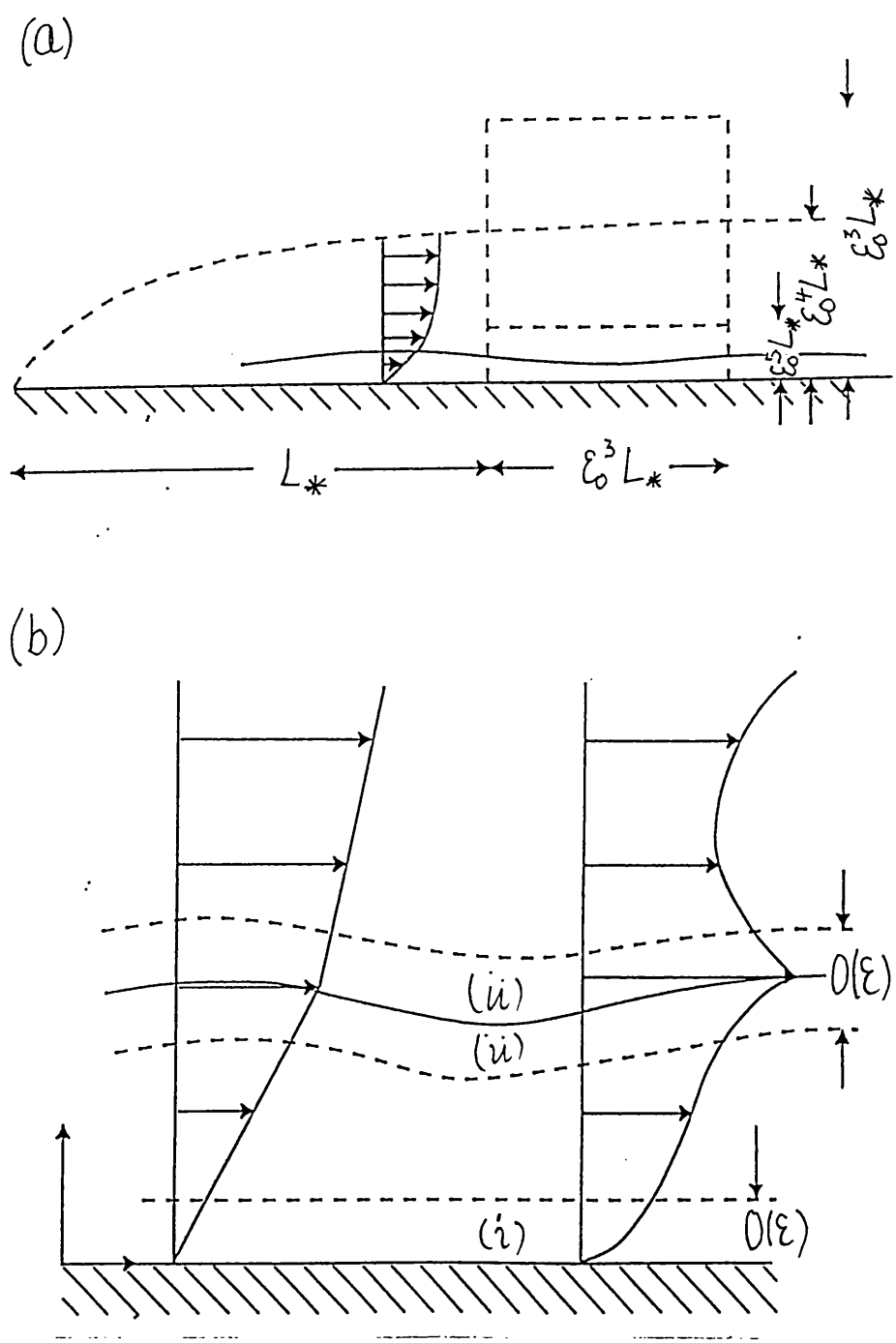

Figure 4:1. (a) The Triple deck structure for the boundary layer flow on a film coated wall (b) The additional layers which appear within the viscous sublayer, (i) The Stokes layer, (ii) the interfacial layer. Also shown is the base profile (on the left) and the profile as altered by Reynolds stresses (on the right).

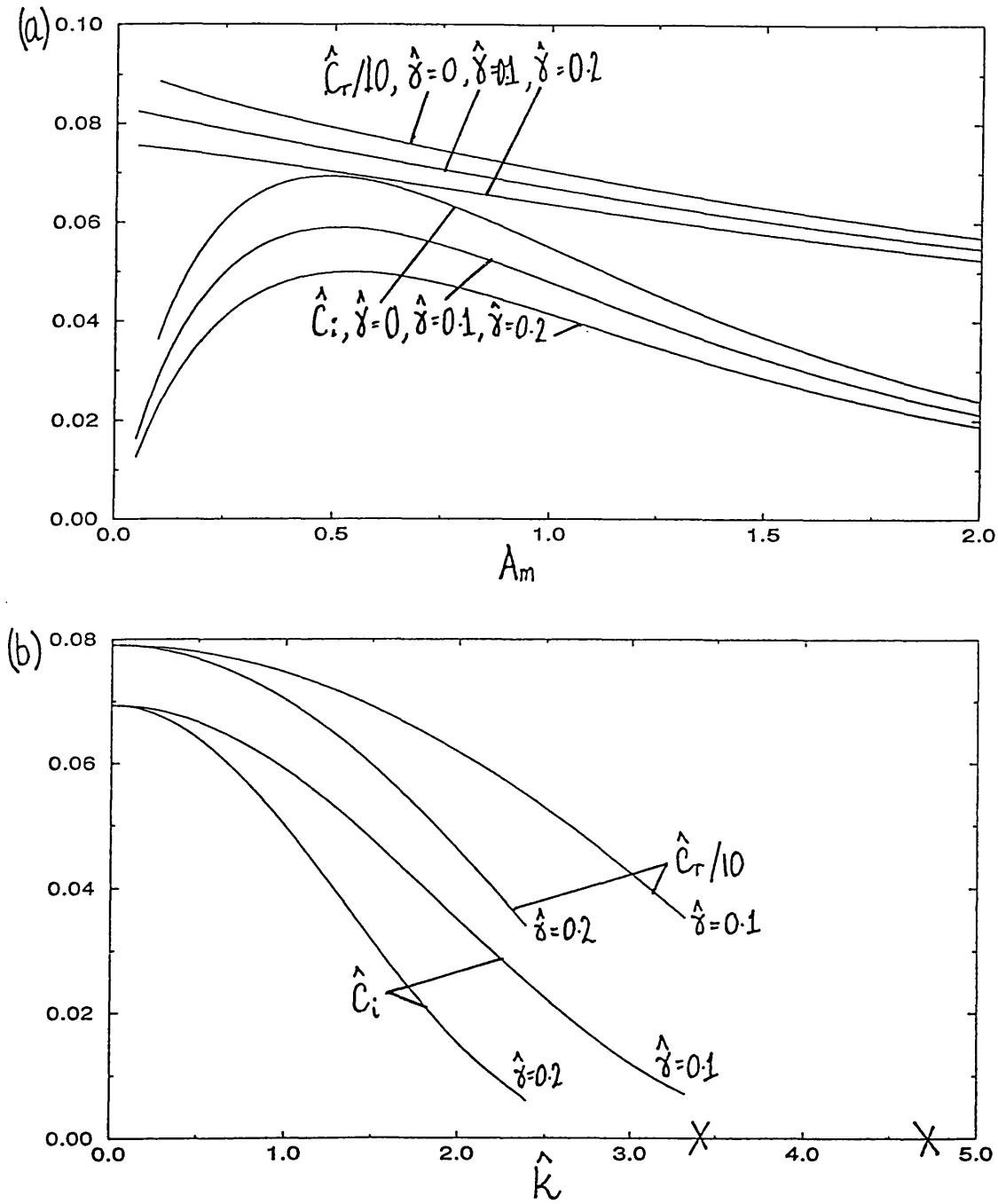

Figure 4:2. Numerical solutions of (4.3.1.7) with $y_i = 5, \rho^- = 1.087, \nu^- = 0.484$, (a) For $\hat{k} = 1$ the imaginary ($\hat{c}_i$), and scaled real ($\hat{c}_r/10$) parts of the complex phase speed $\hat{c}$ versus A_m for different $\hat{\gamma}$, (b) $\hat{c}_r/10$, $\hat{c}_i$ versus wavenumber $\hat{k}$ for $A_m = 0.5$. The neutral points predicted by (4.3.1.9) at $\hat{k} = 4.75352$, and $\hat{k} = 3.36124$ are indicated with crosses.

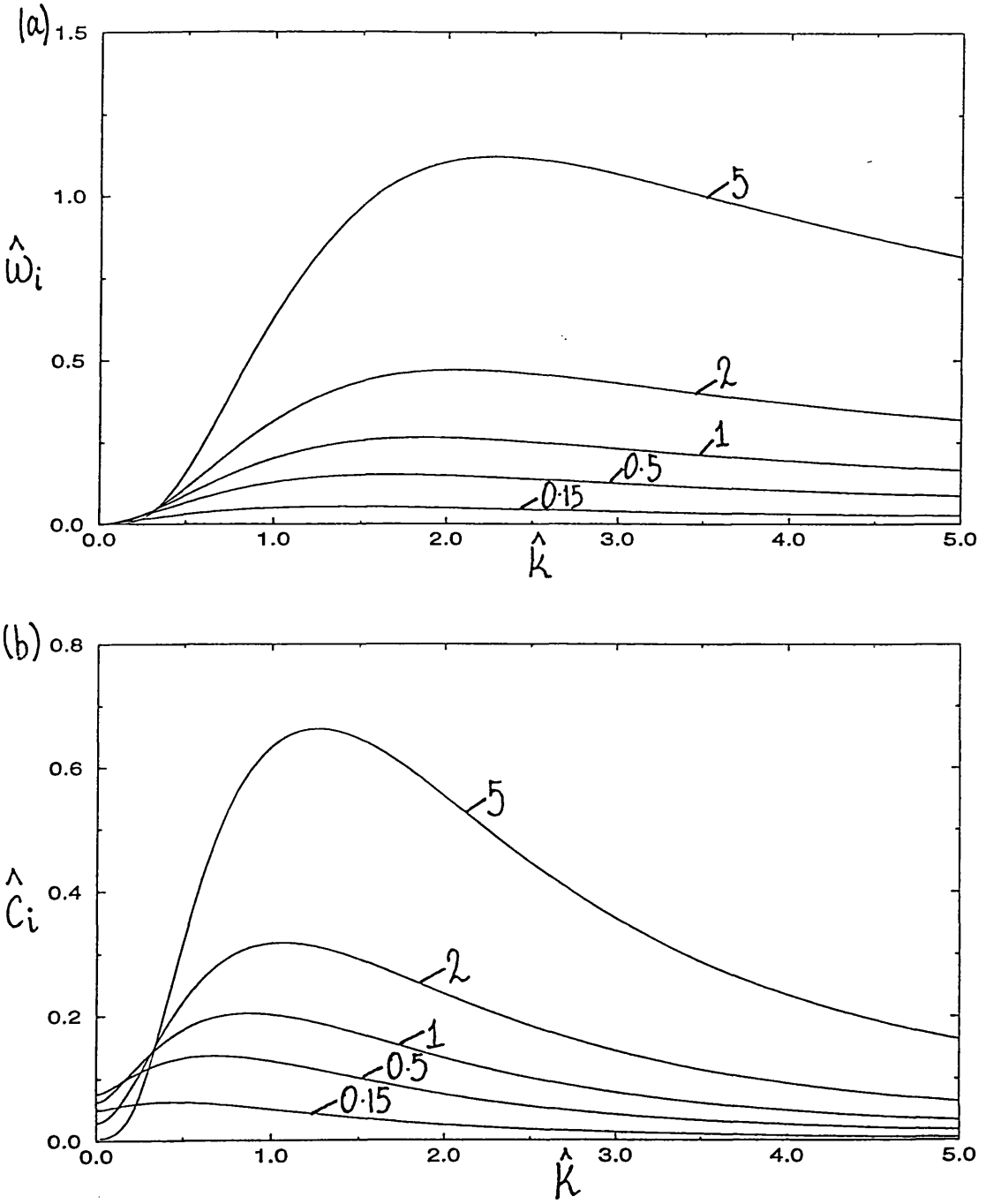

Figure 4:3. The unstable eigenvalues of (4.3.3.1)- (4.3.3.3) with $y_i = 5, \rho^- = 1.087, \nu^- = 0.484$.(a) The growth rate $\hat{\omega}_i = \hat{c}_i\hat{k}$ versus the wavenumber $\hat{k}$ with $\hat{\gamma} = 0$ for increasing induced mean flow amplitude A_m. (b) The imaginary phase speed $\hat{c}_i$ versus $\hat{k}$ for various A_m.

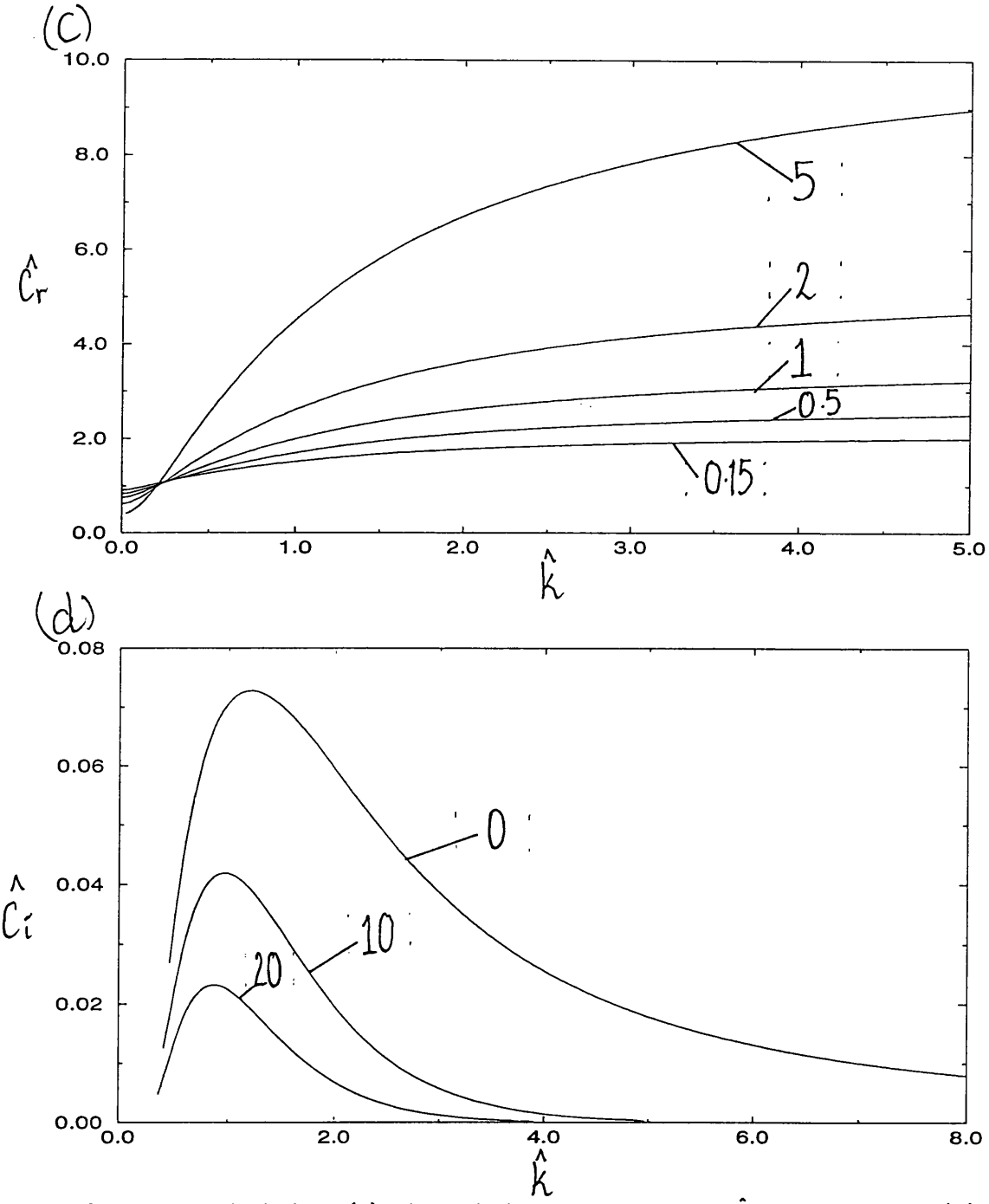

Figure 4:3. As before, (c) The real phase speed $\hat{c}_r$ versus $\hat{k}$ for various A_m, (d) The imaginary phase speed $\hat{c}_i$ versus $\hat{k}$, with $A_m = 5$ for various $\hat{\gamma}$.

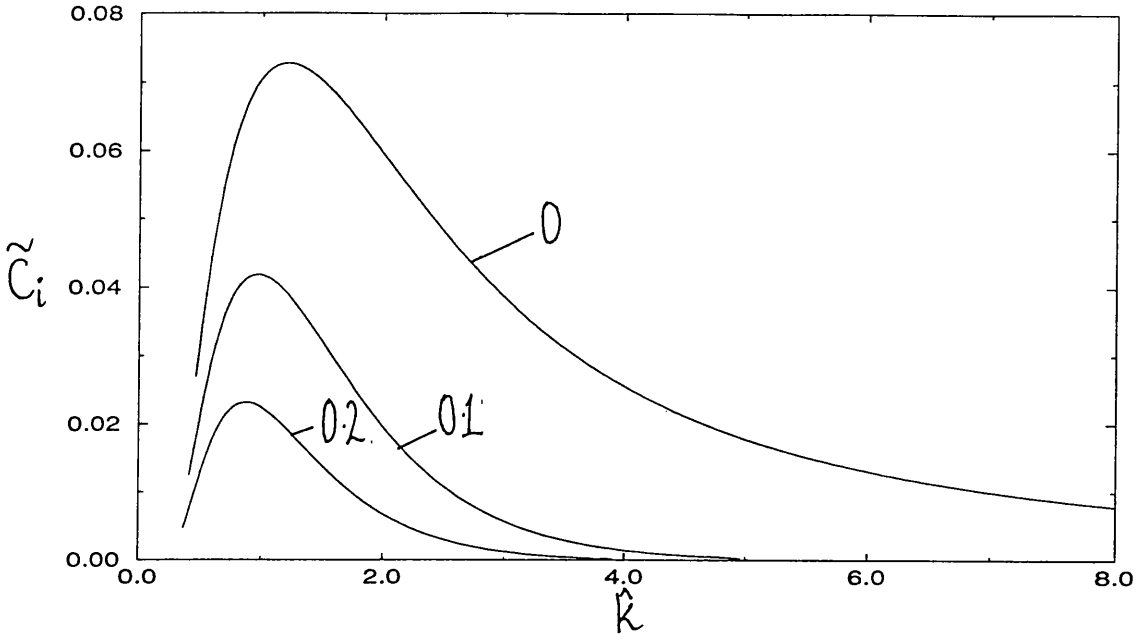

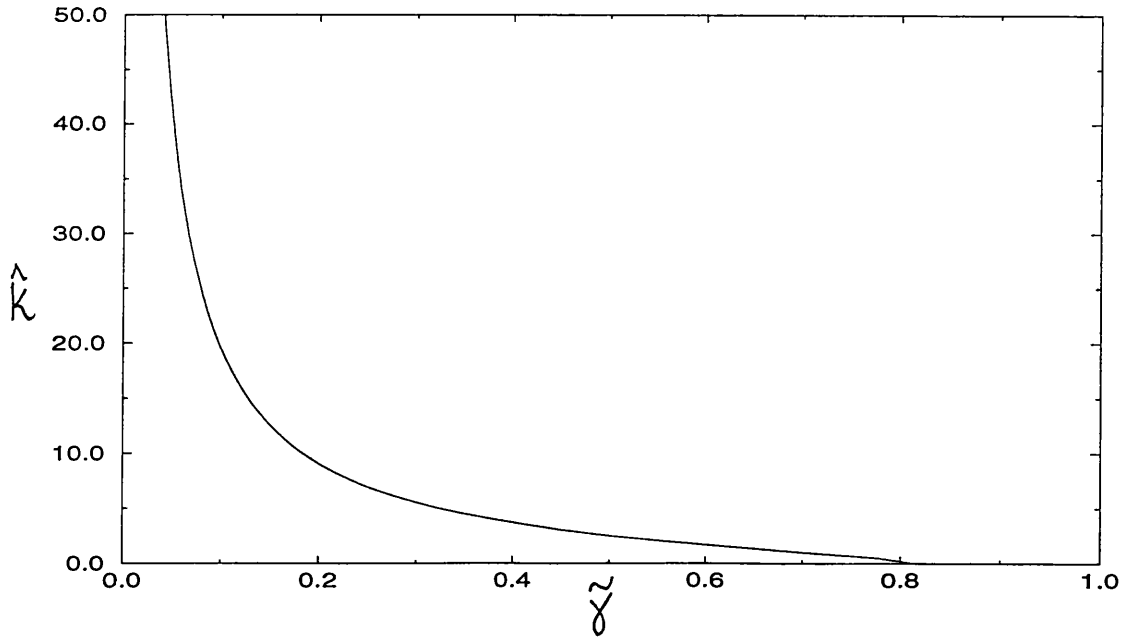

Figure 4:4. Strong induced mean flow. The Rayleigh instability of the induced mean profiles (4.3.3.6), imaginary phase speed $\tilde{c}_i$ versus wavenumber $\hat{k}$ with $y_i = 5, \rho^- = 1.087, \nu^- = 0.484$ for various $\tilde{\gamma}$.

Figure 4:5. The numerical solution of (4.3.3.7) showing neutral wavenumber $\hat{k}$ against $\tilde{\gamma}$ for $y_i = 5, \rho^- = 1.087, \nu^- = 0.484$.

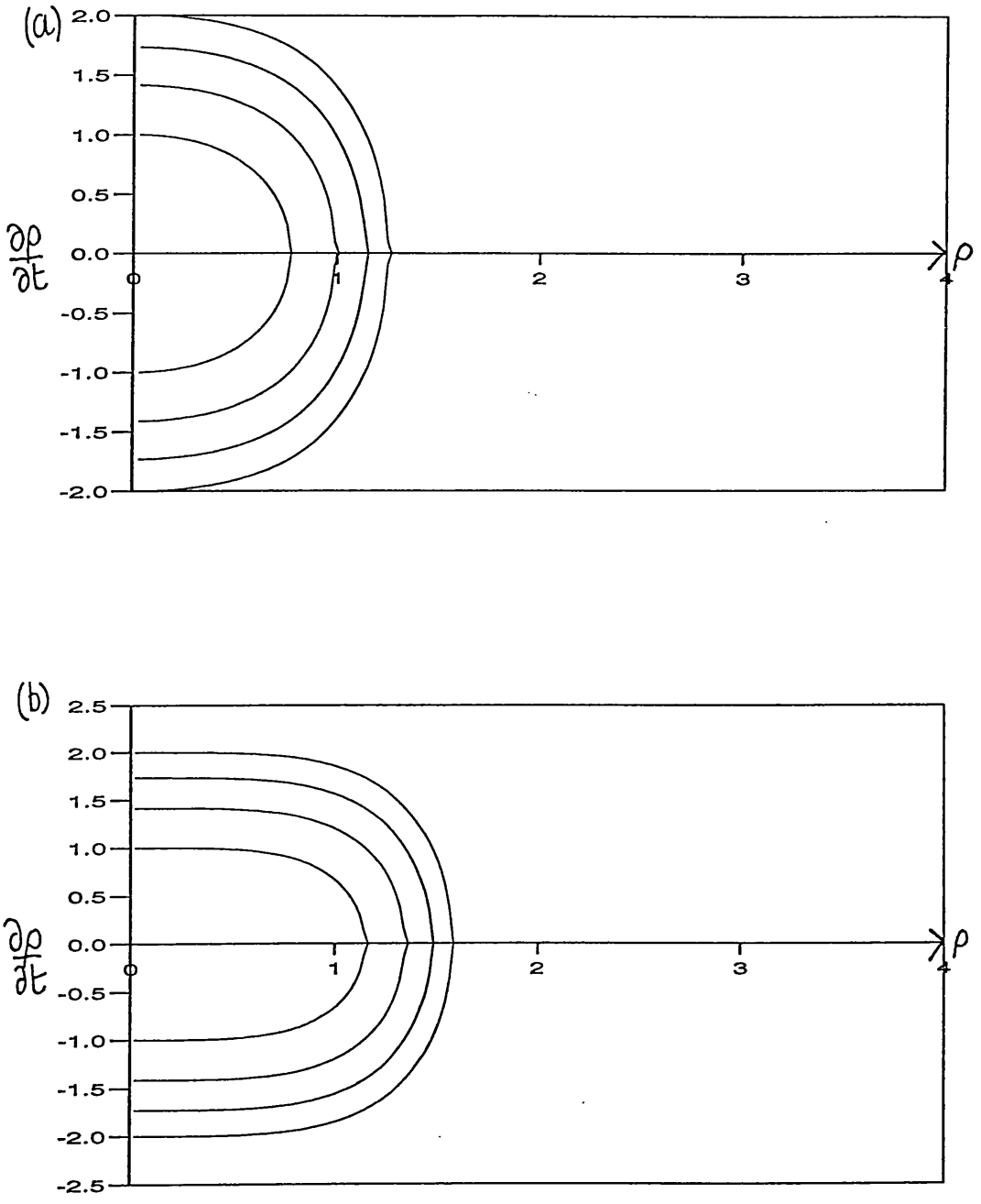

Figure 4:6. The phase plane of equations (4.4.2.9) & (4.4.2.10), when $c_1 = 0$. (a) $\Gamma = -3$, (b) $\Gamma = -2$.

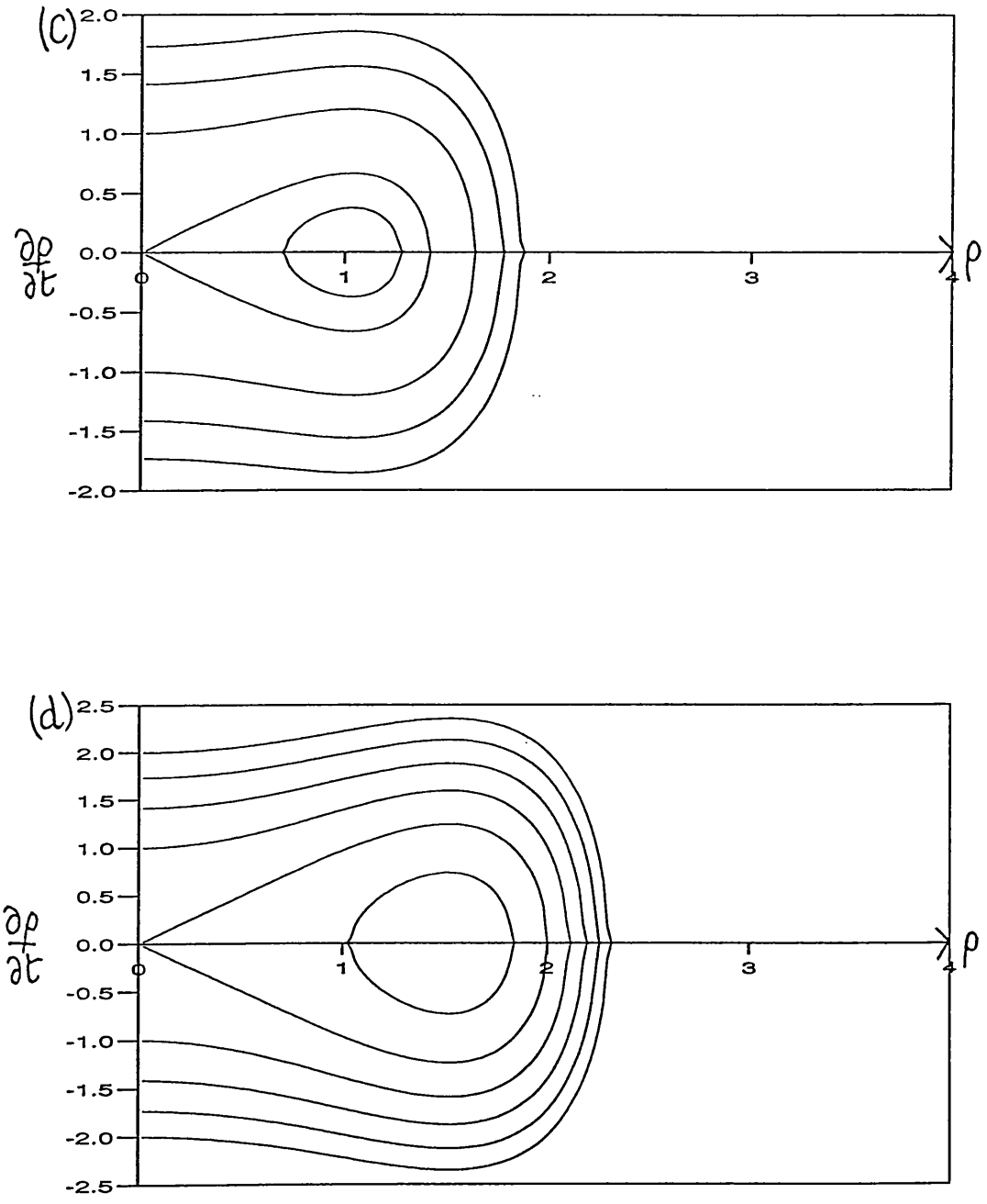

Figure 4:6. As before **(c)** $\Gamma = -1$, **(d)** $\Gamma = 0$.

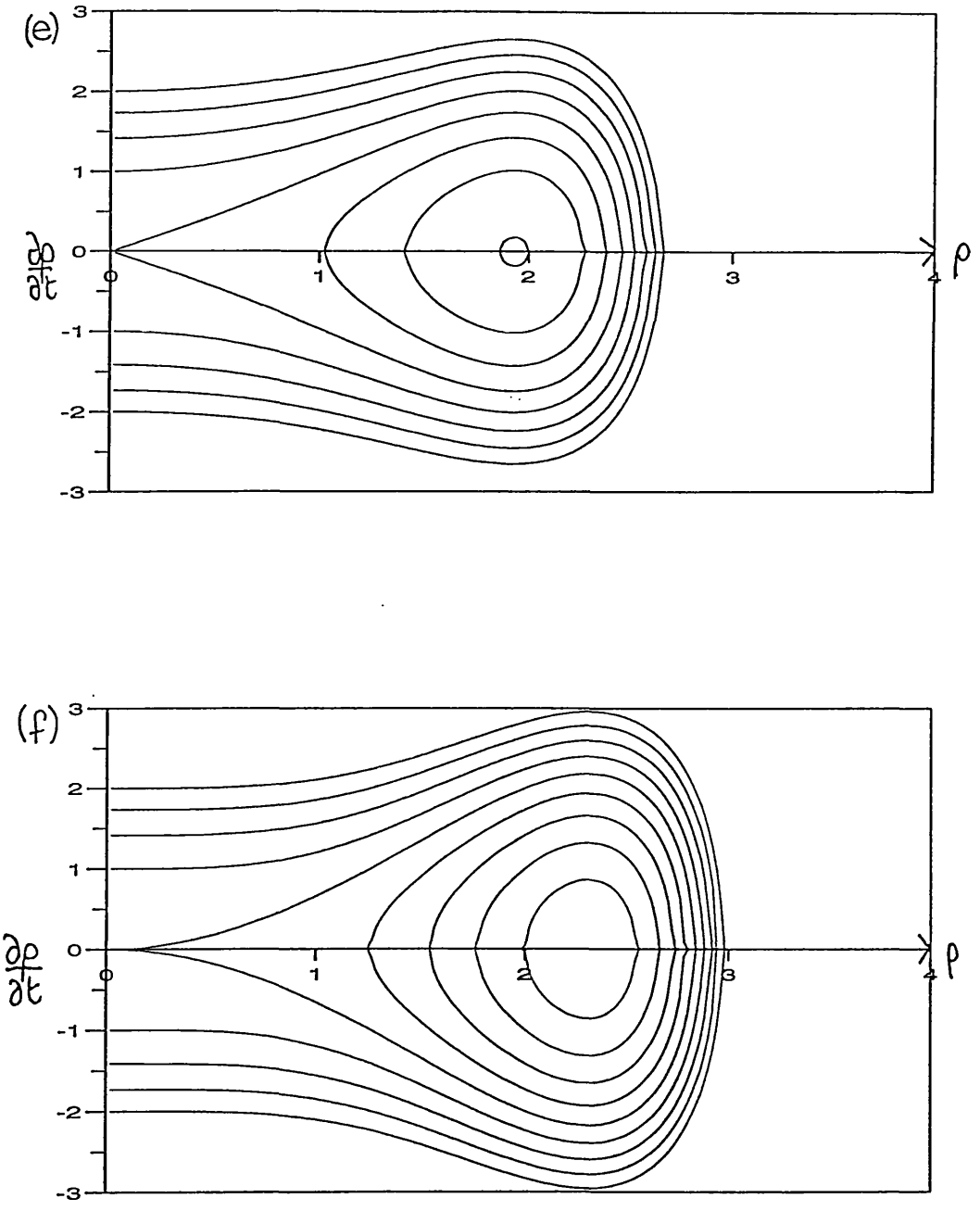

Figure 4:6. As before (e) $\Gamma = 1$, (f) $\Gamma = 2$.

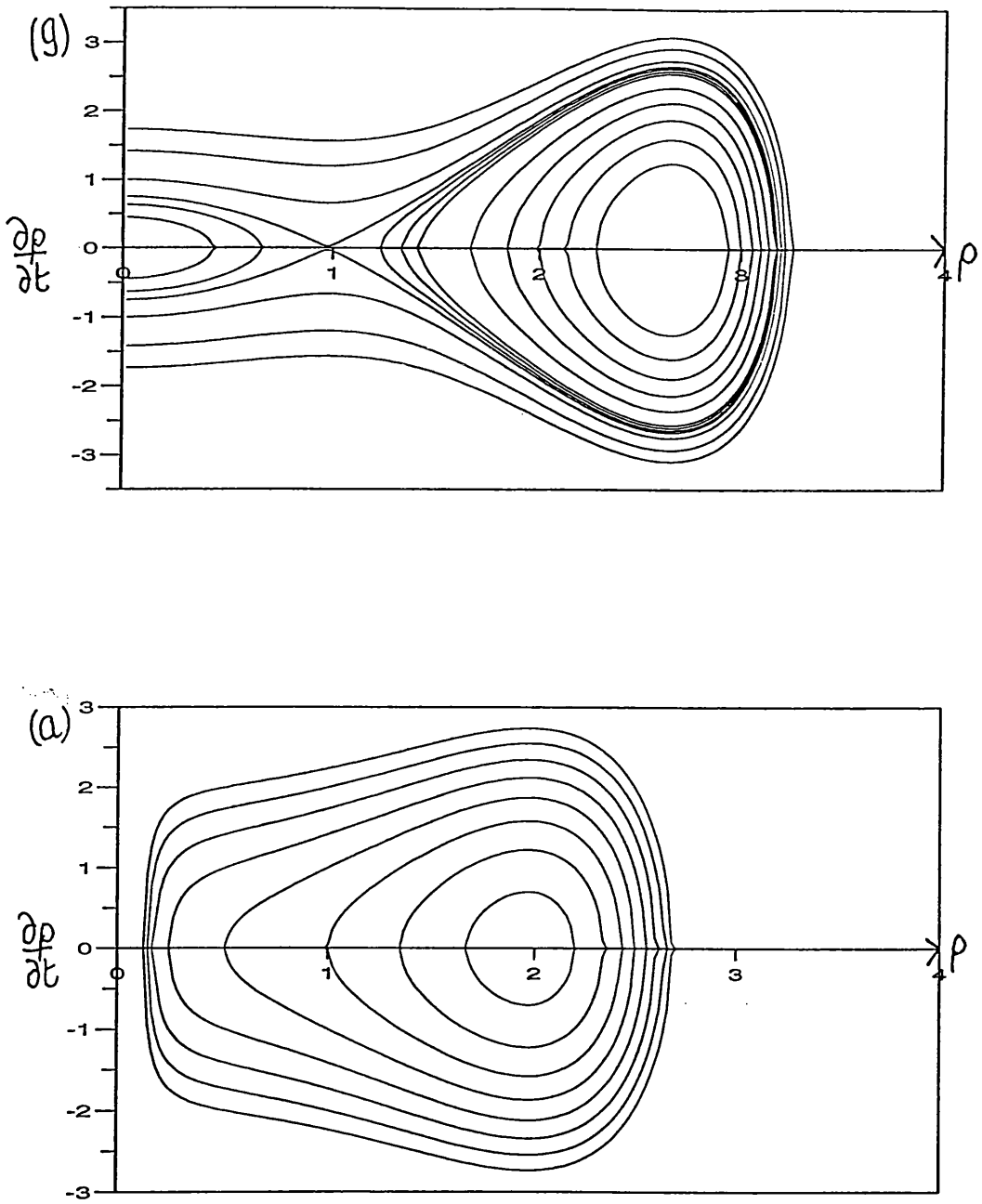

Figure 4:6. As before (g) $\Gamma = 1$.

Figure 4:7. The phase plane of equations (4.4.2.9) & (4.4.2.10), for $c_1 = 1$ with the critical $\Gamma_c = 2.85461$, (a) $\Gamma < \Gamma_c$.

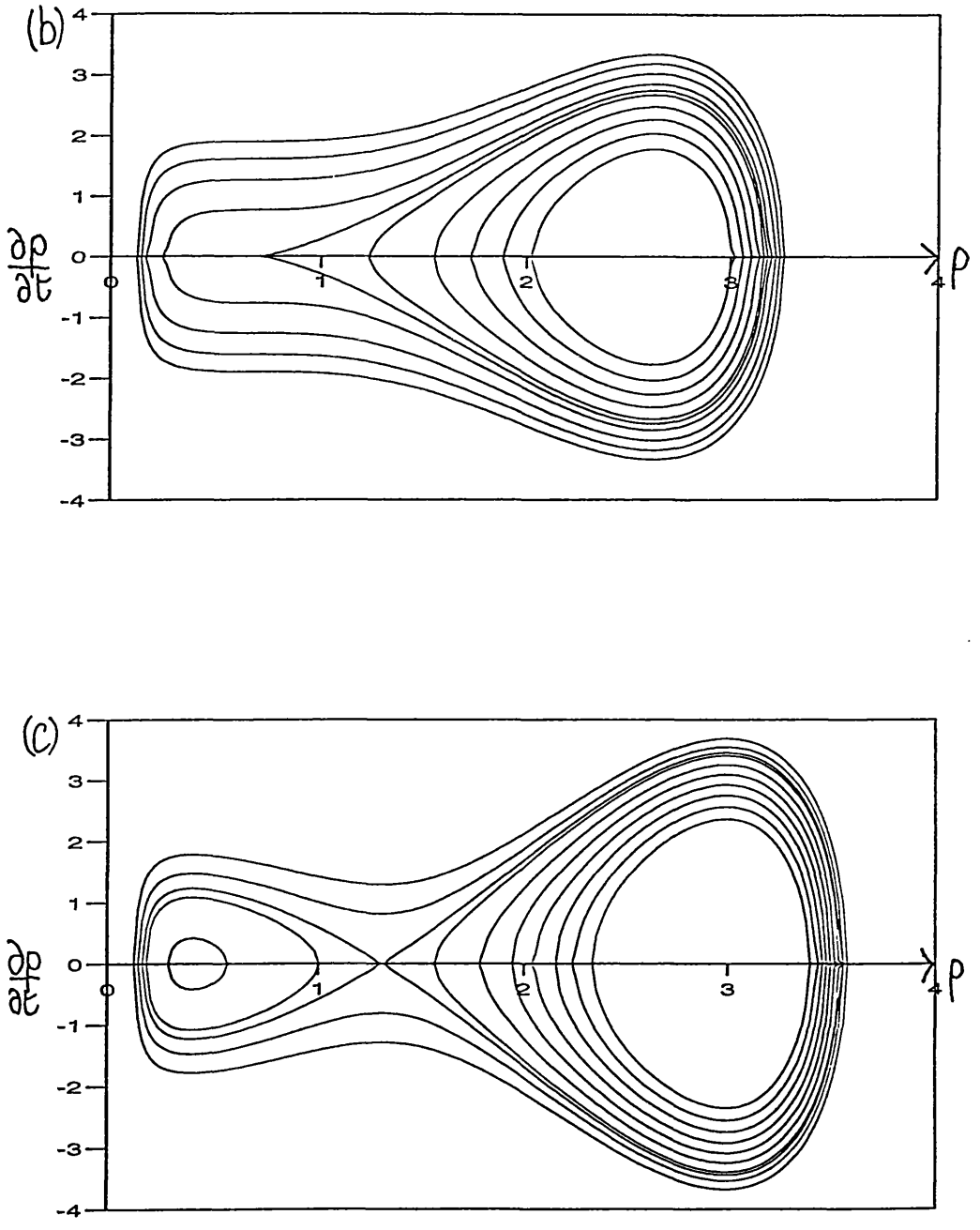

Figure 4:7 As before, (b) $\Gamma = \Gamma_c$, (c) $\Gamma > \Gamma_c$.

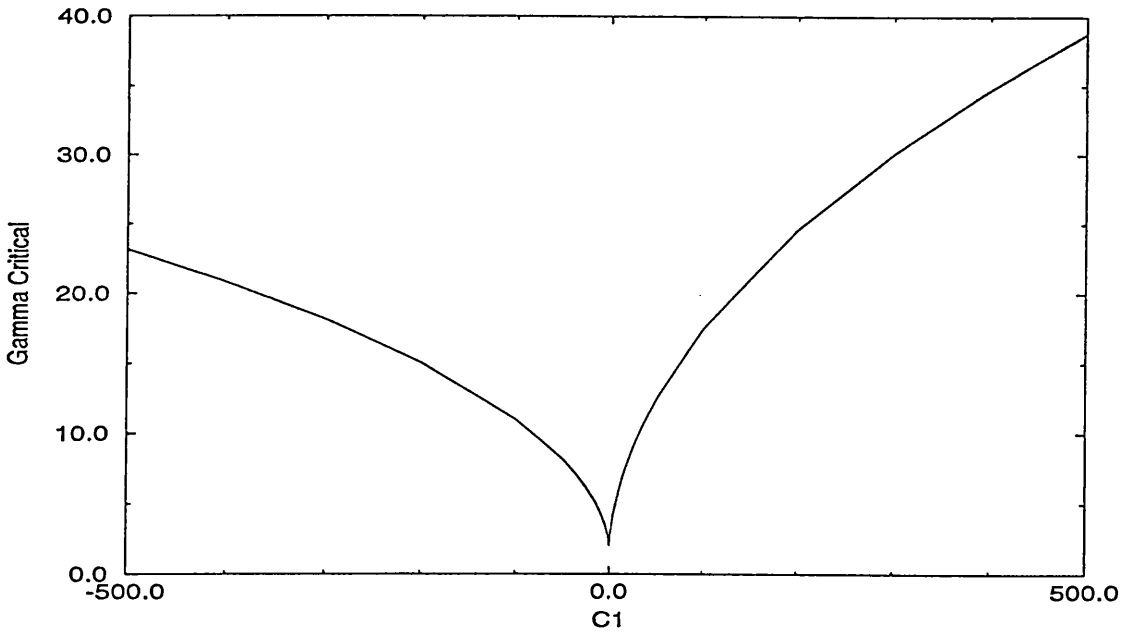

Figure 4:7. As before, (d) the critical Γ_c against c_1.

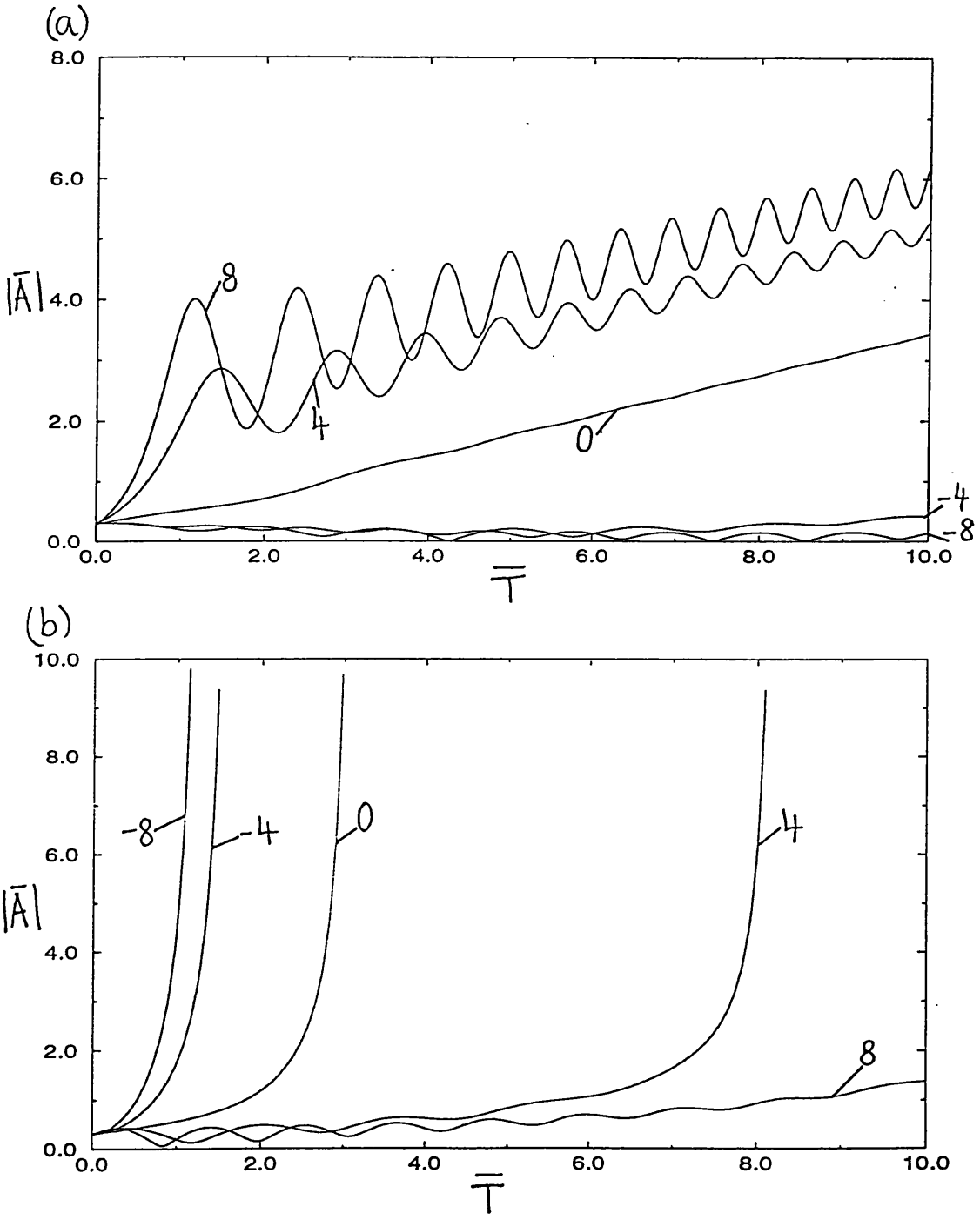

Figure 4:8. Numerical solutions of (4.5.8.24) with the initial conditions $\bar{A}(0) = 0.3$ with the value of $\bar{A}'(0)$ determined by the growing mode solution of the linearised equation $sign(\omega_1)\bar{A}'' = (\Gamma_1 + i)\bar{A}$. (a) $\mid \bar{A} \mid$ against $\bar{T}$ with $\omega_1 < 0$ for various Γ_1. (b) As in (a), but with $\omega_1 > 0$.

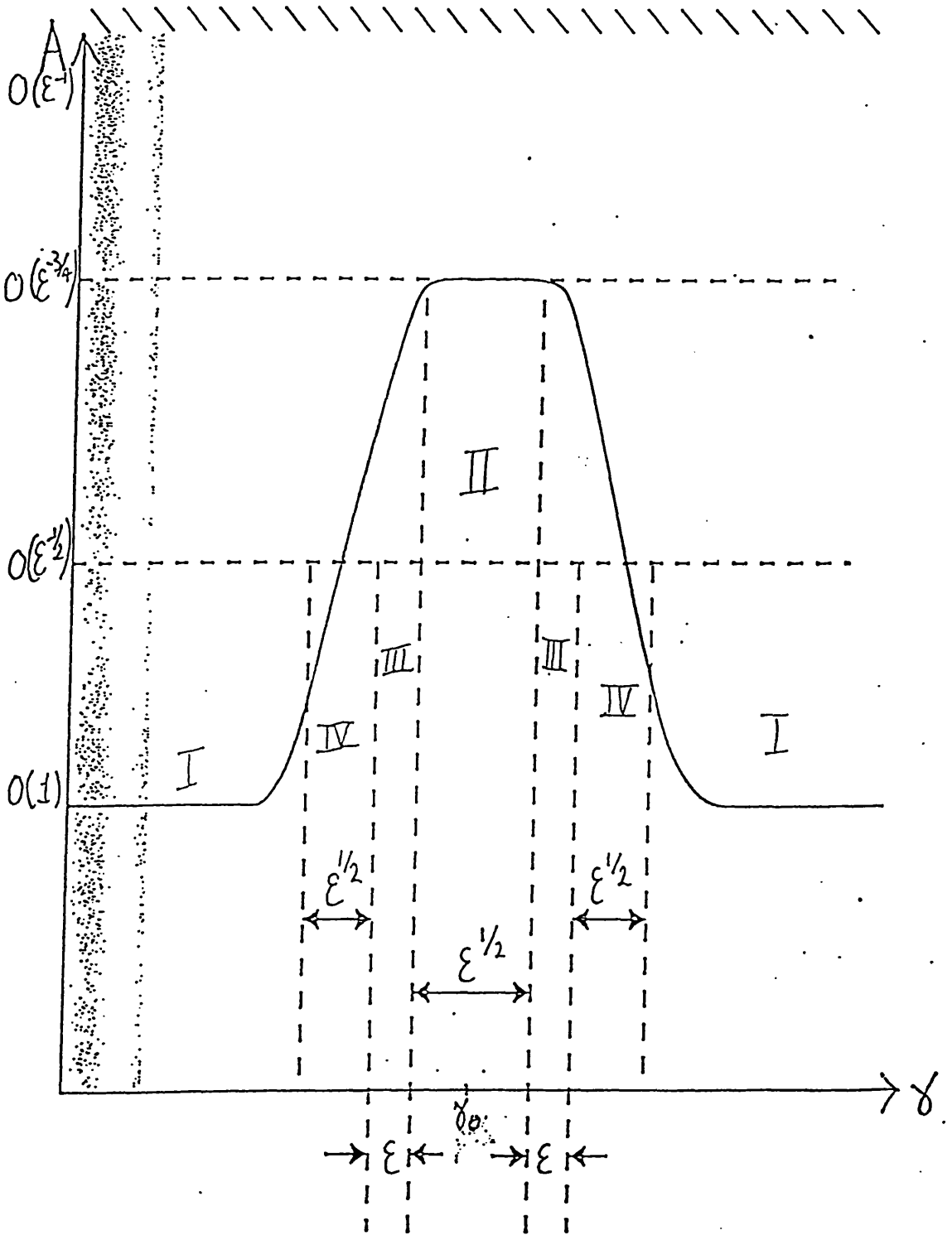

Figure 4:9 The scaled disturbance amplitude A sketched against the scaled suface tension coefficient γ for the different regimes examined in this chapter, with the shaded region denoting the range of secondary instability.

Chapter 5

Instability of flow on a very viscous film

5.1 Introduction

The Kelvin-Helmholtz (K-H) instability is a model of inviscid instability in irrotational flow. It can occur when two uniform horizontal currents, with velocities U_*^+, U_*^- and densities ρ_*^+, ρ_*^-, are in contact. As before, the superscripts $+/-$ refer to the upper/lower fluids. If the contact surface possesses interfacial tension and the flow is subject to gravity, then the growth rate ω_{i*} of a small planar disturbance in a travelling-wave form $\exp[i(k_*x_* - \omega_* t_*)]$ is given by the well known formula (e.g. see Landau & Lifshitz (1959) p241)

$$\omega_{i*} = \sqrt{\frac{k_*^2\rho_*^+\rho_*^-(U_*^- - U_*^+)^2}{(\rho_*^- + \rho_*^-)^2} - \frac{k_* g_*(\rho_*^- - \rho_*^+) + \gamma_* k^3}{\rho_*^- + \rho_*^+}}, \qquad (5.1.1)$$

where γ_*, g_* are the surface tension coefficient and gravitational acceleration respectively. In a stably stratified flow we see that long waves (small k_*) are neutral in the presence of gravity whilst short waves (large k_*) are stabilized by surface tension. The K-H instability relies on the discontinuity in streamwise velocities which can only be admitted in a purely inviscid analysis. In the case of viscous fluids, the velocity field (for both the disturbance and the base flow) is continuous therefore this instability is not present in the usual sense (see, however, below in §5.3) and

instabilities are governed by either the full Orr-Sommerfeld or Rayleigh equation for viscous or inviscid disturbances respectively.

The outcome of such generalizations becomes rather non-trivial, for more subtle mechanisms which rely on the curvature distribution in the base velocity profile, the presence of viscosity and a solid boundary in the flow or on the strength of the interfacial forces which may come into play and modify the simple formula (5.1.1) or completely replace it with new instabilities. Some of the most relevant results for the investigation undertaken here, in particular the three-fold classification by Benjamin (1960), Landahl (1962), have already been quoted in the introduction to the Thesis, Chapter 1.

It should be emphasized, however, that Benjamin-Landahl's classification and many related studies into the physics of various types of instabilities (e.g. Baines & Mitsudera (1994), Baines, Mahjumdar & Mitsudera (1996), Craik & Adams (1979), Cairns (1979)) often rely on quasi-neutral arguments. To what extent and how such models can be applied to the stability calculations for a particular flow obviously depends on the nature of that flow.

Our aim in this chapter is to examine the instability of a laminar boundary layer developing, in contrast with previous chapters, on a relatively thick coat of a very viscous fluid covering the solid wall. The flow is entirely two-dimensional and its geometry is shown in fig 5:1. The main boundary layer and the film are assumed to have comparable thickness, and the disturbance length scales are then taken of the same order, i.e. $O(Re^{-1/2})$, in a suitably non-dimensionalized form with Re ($\gg 1$) denoting the Reynolds number based on the global flow parameters. We take these to be the development length of the boundary layer, the free-stream speed far from the wall and viscosity and density of the boundary-layer fluid. The assumption of large film viscosity is crucial here: on one hand it simplifies the treatment of the base flow allowing us to neglect the flow rate in the film, but on the other hand it makes calculation of the disturbance in the film more tedious since we intend to treat perturbations in the lower fluid as fully viscous. In the upper fluid the perturbed motion is naturally inviscid, on account of the large Reynolds number.

Instability in this flow may arise for various reasons. The inflexional Rayleigh instability could appear if an adverse pressure gradient is acting on the boundary layer. Below we eliminate this possibility by taking model non-inflexional profiles in the upper fluid (mostly the Blasius, or, to illustrate one theoretical point, an artificial exponential profile). The K-H instability can be expected when the film is somewhat thicker than the boundary layer, viscosity in the film is not very large and the disturbance wavelength is large.

The Miles (1957) mechanism of water-wave generation by wind (Class B waves in the Benjamin-Landahl classification) and the TS modes (Class A waves) are of relevance to the problem, the former for sufficiently strong gravity and the latter for thicker films.

In the solutions presented below all these classes of instabilities appear as special limits of a more general instability formulation. Numerical solutions for the full formulation establishes connections between the various growing modes and clarifies the conditions for their appearance.

5.2 The problem formulation

The flow is governed by the Navier-Stokes equations, as given in the general introduction §1.1, and we assume a non-dimensionalization with respect to the characteristic length of the solid body L_*, the free stream speed U_* and the viscosity and density in the upper fluid, with the $+/-$ sign convention applied to upper/lower fluids with respect to the interface. Hence the base flow is characterized by the non-dimensional velocities $(u^{\pm}, v^{\pm})$ in the $(\hat{x}, \hat{y})$-directions, the pressures $p^{\pm}$ in the two fluids, the time $\hat{t}$, the Reynolds number Re ($\gg 1$), the Froude number $\hat{Fr} = {U_*}^2/g_* L_*$, g_* being the gravitational acceleration, surface tension coefficient $\hat{\gamma} = \gamma_*/\rho_* U_*^2 L_*$, density ρ^- and viscosity ν^- in the film (note we have taken $\rho^+ = \nu^+ = 1$). The key assumption in this chapter is that μ^- is large, and we take

$$\mu^- = Re^{1/2}\mu_0^-, \text{with } \mu_0^- = O(1). \tag{5.2.1}$$

The film density is of $O(1)$.

For our instability calculation we adopt a quasi-parallel approximation in which the base velocity at a chosen station ($\hat{x} = \hat{x}_0$ in fig 5:1) is treated as unidirectional with the undisturbed interface at $\hat{y} = \hat{a}$ parallel to the wall and the pressure varying with $\hat{y}$ on account of gravity. The film thickness is of $O(Re^{-1/2})$, i.e. of the same order as the main boundary layer. Then the tangential stress continuity at the interface, $\partial u^+/\partial \hat{y} = \mu^- \partial u^-/\partial \hat{y}$, shows that, for the film viscosity given in (5.2.1), the film velocity is of $O(Re^{-1/2})$. This leads to the following representation of the base-flow components:

$$f = \bar{a} \tag{5.2.2}$$

$$\bar{y} > 0: \qquad u^+ = U_0^+(\bar{y}), \ , v^+ = 0, \ p^+ = P_0^+(\bar{y}) = -\bar{y}/Fr; \tag{5.2.3}$$

$$-\bar{a} < \bar{y} < 0: \quad u^- = O(Re^{-1/2}), \ v^- = 0, \ p^- = P_0^-(\bar{y}) = -\bar{y}\rho^-/Fr, \tag{5.2.4}$$

where the vertical coordinate has been shifted onto the interface and scaled $\bar{y} = Re^{1/2}(\hat{y} - \hat{a})$, $\bar{a} = Re^{1/2}\hat{a}$ and the Froude number is taken small, $\hat{Fr} = Fr/\sqrt{Re}$ with $Fr = O(1)$, in order to retain gravitational effects in the formulation for disturbances. The base flow (5.2.3), (5.2.4) is perturbed by a travelling-wave disturbance of small amplitude δ, where $\delta > Re^{-1/2}$,

$$(u^+, v^+, p^+) = (U_0^+, 0, P_0^+) + \delta(\bar{u}^+, \bar{v}^+, \bar{p}^+)E + ..., \tag{5.2.5}$$

$$(u^-, v^-, p^-) = (0, 0, P_0^-) + \delta(\bar{u}^-, \bar{v}^-, \bar{p}^-)E + ..., \tag{5.2.6}$$

where the leading film velocity has been neglected, and $E = \exp[ik(x - ct)]$ is the wave-factor written in terms of fast Rayleigh-scale variables

$$(\hat{x} - \hat{x}_0, \hat{t}) = Re^{-1/2}(x, t). \tag{5.2.7}$$

The interface shape is written as $\bar{y} = \delta\eta E$ with η a perturbation to the base interface

position $\bar{y} = 0$. For the disturbance above the interface we find the relations

$$ik(U_0^+ - c)\bar{u}^+ + \frac{dU_0^+}{d\bar{y}}\bar{v}^+ = -ik\bar{p}^+, \tag{5.2.8}$$

$$ik(U_0^+ - c)\bar{v}^+ = -\frac{d\bar{p}^+}{d\bar{y}}, \tag{5.2.9}$$

$$ik\bar{u}^+ + \frac{d\bar{v}^+}{d\bar{y}} = 0. \tag{5.2.10}$$

and from these obtain the Rayleigh equation,

$$(U_0^+ - c)(\frac{d^2\bar{v}^+}{d\bar{y}^2} - k^2\bar{v}^+) = \frac{d^2U_0^+}{d\bar{y}^2}\bar{v}^+. \tag{5.2.11}$$

In the film the disturbance equations are

$$\frac{d^2\bar{u}^-}{d\bar{y}^2} - (k^2 - \frac{i\omega\rho^-}{\mu_0^-})\bar{u}^- = \frac{ik\bar{p}^-}{\mu_0^-}, \tag{5.2.12}$$

$$\frac{d^2\bar{v}^-}{d\bar{y}^2} - (k^2 - \frac{i\omega\rho^-}{\mu_0^-})\bar{v}^- = \frac{1}{\mu_0^-}\frac{d\bar{p}^-}{d\bar{y}}, \tag{5.2.13}$$

$$ik\bar{u}^- + \frac{d\bar{v}^-}{d\bar{y}} = 0, \tag{5.2.14}$$

with $\omega = ck$, and these give us the general solution,

$$\bar{v}^- = A\cosh\lambda^+\bar{y} + B\sinh\lambda^+\bar{y} + C\cosh\lambda^-\bar{y} + D\sinh\lambda^-\bar{y}, \tag{5.2.15}$$

where $\lambda^+ = k$ and $\lambda^- = \sqrt{k^2 - i\omega\rho^-/\mu_0^-}$. We normalize the solution as $\bar{v}^-(0) = 1$ and apply the no-slip boundary conditions on the wall,

$$\bar{v}^-(-\bar{a}) = 0, \quad \frac{d\bar{v}^-}{d\bar{y}}(-\bar{a}) = 0. \tag{5.2.16}$$

One more boundary condition needed to solve completely for $\bar{v}^-$ follows from the requirement of tangential stress continuity at the interface. Above the interface there is a thin layer of thickness $O(Re^{-1/4})$ in which viscous effects become important in the upper fluid. We write $\bar{y} = Re^{-1/4}Y$ and expand the velocity and pressure components as

$$u^+ = U_0^+(0) + Re^{-\frac{1}{4}}Y\frac{dU_0^+}{d\bar{y}}(0) + Re^{-\frac{1}{2}}\frac{Y^2}{2}\frac{d^2U_0^+}{d\bar{y}^2}(0) + \ldots + \delta(\tilde{u}^+(Y)E + c.c.) + \ldots, \tag{5.2.17}$$

$$v^+ = \delta(\tilde{v}^+(Y)E + c.c.) + \ldots, \tag{5.2.18}$$

$$p^+ = \tilde{P_0}^+ + \delta(\tilde{p}^+(Y)E + c.c.) + \ldots . \tag{5.2.19}$$

Substituting these expansions along with those for the lower flow into the interfacial conditions we obtain the relations

$$\frac{d\bar{u}^-}{d\bar{y}}(0) + ik\bar{v}^-(0) = 0, \tag{5.2.20}$$

$$\bar{p}^+(0) - \bar{p}^-(0) = \eta\frac{(1-\rho^-)}{Fr} - 2\mu_0^-\frac{d\bar{v}^-}{d\bar{y}}(0) - k^2\eta\gamma, \tag{5.2.21}$$

where $\gamma = \hat{\gamma}\sqrt{Re}$ is the scaled surface tension coefficient and $\tilde{p}^+ = \bar{p}^+(0)$. Combining (5.2.14) with (5.2.20) we obtain the fourth condition for $\bar{v}^-$:

$$\frac{d^2\bar{v}^-}{d\bar{y}^2}(0) + k^2\bar{v}^-(0) = 0. \tag{5.2.22}$$

The constants in (5.2.15) are then found to be

$$C = -\frac{2k^2}{\lambda^{-2}+k^2}, \quad A = 1 - C, \tag{5.2.23}$$

$$B = \frac{A(\lambda^-\cosh\lambda^-\bar{a}\cosh\lambda^+\bar{a} - \lambda^+\sinh\lambda^+\bar{a}\sinh\lambda^-\bar{a}) + C\lambda^-}{\lambda^-\cosh\lambda^-\bar{a}\sinh\lambda^+\bar{a} - \lambda^+\sinh\lambda^-\bar{a}\cosh\lambda^+\bar{a}}, \tag{5.2.24}$$

$$D = \frac{A\lambda^+ + C(\lambda^+\cosh\lambda^-\bar{a}\cosh\lambda^+\bar{a} - \lambda^-\sinh\lambda^+\bar{a}\sinh\lambda^-\bar{a})}{\lambda^-\cosh\lambda^-\bar{a}\sinh\lambda^+\bar{a} - \lambda^+\sinh\lambda^-\bar{a}\cosh\lambda^+\bar{a}}. \tag{5.2.25}$$

In order to couple the film and boundary-layer disturbances, we use (5.2.8), (5.2.10) (5.2.21) and the kinematic condition at the interface $-i\omega\eta = \bar{v}^{\pm}(0)$. This gives

$$\frac{d\bar{v}^+}{d\bar{y}}(0) = \bar{v}^+(0)\left[\left(-\frac{\lambda_b}{c} + \frac{(1-\rho^-)}{Frc^2} - \frac{\gamma k^2}{c^2}\right) - \frac{i\mu_0^-}{kc}\left(\frac{(i\omega\rho^-/\mu_0^- - 2k^2)\lambda^+B - 2k^2\lambda^-D}{A+C}\right)\right] \tag{5.2.26}$$

where $\lambda_b = dU_0^+/d\bar{y}(0)$. Thus, the disturbance phase speed $c = c(k)$ is an eigenvalue of the Rayleigh equation (5.2.11) with the usual boundary condition

$$\bar{v}^+(\infty) = 0, \tag{5.2.27}$$

and the interfacial condition (5.2.26). Numerical and asymptotic solution of this problem are discussed below. Unless specified otherwise U_0^+ is taken as the Blasius profile, in particular $\lambda_b = 0.33206$.

5.3 The thick inviscid film limit

First of all we would like to demonstrate how some of the known instabilities can be derived from the formulation (5.2.11), (5.2.26), (5.2.27). This will also link our work with previous studies such as those undertaken by Shrira (1993), Morland, Saffman and Yuen (1991), Morland & Saffman (1993), Miles (1957) and others.

In the limit of inviscid disturbance in the film, $\mu_0^- \to 0$, the boundary condition (5.2.26) reduces to

$$\frac{d\bar{v}^+}{d\bar{y}}(0) = \left(-\frac{\lambda_b}{c} + \frac{k\rho^-}{\tanh k\bar{a}} + \frac{(1-\rho^-)}{Frc^2} - \frac{k^2\gamma}{c^2}\right)\bar{v}^+(0). \tag{5.3.1}$$

If, next, film thickness is large, $\bar{a} \to \infty$, then this relation becomes

$$\frac{d\bar{v}^+}{d\bar{y}}(0) = \left(-\frac{\lambda_b}{c} + k\rho^- + \frac{(1-\rho^-)}{Frc^2} - \frac{k^2\gamma}{c^2}\right)\bar{v}^+(0). \tag{5.3.2}$$

This last form was used by Miles (1957), Morland, Saffman & Yuen (1991), Morland & Saffman (1993) in their study of wind-induced water waves. If in (5.3.2) we put $\rho^- = 0$, and write $Fr = -\bar{F}r$ that is for the case of heavy fluid in the boundary layer and gravity pointing upward, the boundary condition becomes of the form used in Shrira (1993) who investigated instability of a current with a free surface.

Let us consider in more detail the flow with inviscid disturbances on thick films (5.3.2). The disturbance phase speeds, obtained numerically with the use of the method described in §5.4, for the Blasius profile in the boundary layer, with several values of the Froude number and negligible surface tension, are illustrated in Fig 5:2(a). The solutions for small ($Fr = \infty$) and finite ($Fr \neq \infty$) gravity are clearly distinct. In the first case, $Fr = \infty$, $\gamma = 0$, $\bar{a} \to \infty$, we can expand the solution of the Rayleigh equation (5.2.11) in the form

$$\bar{v}^+ = \bar{v}_0^+ + k\bar{v}_1^+, \quad c = \bar{c}_0 + k\bar{c}_1, \text{as } k \to 0. \tag{5.3.3}$$

Substituting into the governing equation (5.2.11) and matching to the potential flow

region where $y = O(1/k)$ we find

$$\bar{v}_0^+ = U_0^+ - c_0 \tag{5.3.4}$$

$$\bar{v}_1^+ = -c_1 + Q_1(U_0^+ - c_0) - (U_0^+ - c_0)\int_0^\infty \frac{(1-c_0)^2}{(U_0^+ - c_0)^2} d\bar{y}, \tag{5.3.5}$$

$$c_0 \frac{d\bar{v}_1^+}{dy}(0) + c_1\lambda_b = -\rho^- c_0^2 - \lambda_b \bar{v}_1^+(0), \tag{5.3.6}$$

where surface tension and gravitational influence have been neglected, and Q_1 is an undefined constant. We find that the unstable wave is governed by the relation

$$c_0 = \frac{1 + i\sqrt{\rho^-}}{1 + \rho^-}. \tag{5.3.7}$$

The imaginary part of c_0 corresponds to the K-H growth rate given by the formula (5.1.1). Hence we found that KH instability arises as the long-wave limit of our formulation in the case of inviscid perturbations on a thick film. A comparison of the numerical solution with the limit formula (5.3.7) is made in fig 5:2(b). Note that the condition of negligible gravity is vital for the K-H type limit solution, we see that even a small amount of gravity eliminates the eigenmode at sufficiently small wavenumbers, see fig 5:2(a), $Fr = 10, 20$.

Consider next short waves. First, neglecting gravity and surface tension ($Fr = \infty, \gamma = 0$), we observe that short-wave instability persists for all wavenumbers. The growth rate, derived by Timoshin, is found to be

$$c_i = \frac{12\lambda_1 e^{(\rho^-+1)^{-1}}}{k^4(\rho^-+1)^4} \cosh(\rho^-+1)^{-1}(\tanh(\rho^-+1)^{-1} - 1), \quad \text{as } k \to \infty, \tag{5.3.8}$$

for this case, where $\lambda_1 = -\lambda_b^2/48$. Gravity enhances short-wave instability, as is seen in fig 5:2(a). This connects with Miles (1957) suggestion that water waves are destabilized by a boundary-layer type flow in the air. We find that in fig 5:2(a) the phase speed at $k = 0.4$ is $c_r = 0.4449$ for $Fr = 10$, and this is close to a pure water-wave with phase speed $c_r = (kFr)^{-1/2} = 0.5$.

We can illustrate this connection analytically in the limit $\rho^- \to \infty$ (strong grav-

itational influence) for an inviscid thick film. Writing the solution in the form

$$c = c_0 + \frac{1}{\rho^-}c_1 + ..., \tag{5.3.9}$$

$$\bar{v}^+ = \phi_0 + \frac{1}{\rho^-}\phi_1 + ..., \tag{5.3.10}$$

at the leading order we find immediately that

$$c_0 = \frac{1}{\sqrt{kFr}}, \tag{5.3.11}$$

which is the phase speed of deep water waves, and then from (5.3.2) we have

$$c_1 = \frac{c_0(c_0\phi_0'(0) + \lambda_b) + k^2\gamma - 1/Fr}{2c_0k}. \tag{5.3.12}$$

Since c_0 is real the solution for ϕ_0 will have a critical layer at the point $\bar{y} = \bar{y}_c$ where $U_0^+(\bar{y}_c) = c_0$. The effect of this critical layer is most easy to evaluate for short waves $k \to \infty$, and we write ϕ_0, U_0^+ as functions of the shorter-scale vertical co-ordinate $z = k^{1/2}\bar{y}$,

$$\phi_0 = \bar{\phi}_0(z) + \frac{1}{k^{\frac{1}{2}}}\bar{\phi}_1(z) + ... \ . \tag{5.3.13}$$

$$U_0^+ = \frac{\lambda_b}{k^{\frac{1}{2}}}z + \frac{\lambda_1}{4!k^2}z^4 + ..., \ \lambda_1 = -\frac{\lambda_b^2}{48}, \ c_0 = k^{-\frac{1}{2}}\bar{c}_0. \tag{5.3.14}$$

Substitution into (5.2.11) and application of the normalization $\bar{v}^+(0) = 1$ gives the solution

$$\bar{\phi}_0 = e^{-z}, \tag{5.3.15}$$

$$\bar{\phi}_1^{\pm} = -\frac{\lambda_1}{2\lambda_b}\left(\frac{z^2}{4} + \frac{z}{4} + \frac{1}{8} + \frac{\bar{c}_0}{2\lambda_b}\left(z + \frac{1}{2}\right)\right)e^{-z}$$
$$-Q^{\pm}e^{-z} + P^{\pm}e^{z} + \frac{\lambda_1\bar{c}_0^2}{2\lambda_b^3}e^{z}\int_{y_1^{\pm}}^{y_2^{\pm}} \ln|\, z - z_c\,|e^{-2z}dz, \tag{5.3.16}$$

where $z_c = c_0/\lambda_b$ is the critical layer position, the superscripts $+/-$ refer to regions above and below $z = z_c$ respectively and $y_1^+ = z_c$, $y_2^+ = \infty$, $y_1^- = 0$, $y_2^- = z_c$. We apply the boundary conditions (5.3.2) and find that

$$P^+ = 0, \quad P^- = Q^- + \frac{\lambda_1}{2\lambda_b}\left(\frac{1}{8} + \frac{bc_0}{4\lambda_b}\right). \tag{5.3.17}$$

At the critical layer, $\bar{\phi}_1^{\pm}$ must be continuous whereas the derivative is singular and must satisfy the usual logarithmic jump condition

$$\frac{d\bar{\phi}_1^+}{dz}(z=z_c) - \frac{d\bar{\phi}_1^-}{dz}(z=z_c) = i\pi \frac{\lambda_1 \bar{c}_0^2 e^{-z_c}}{2\lambda_b^3}. \tag{5.3.18}$$

These constraints lead to the solutions

$$Q^+ = \frac{\lambda_1 \bar{c}_0^2 e^{-2z_c}}{2\lambda_b^3}\left(\int_{z_c}^{\infty} \ln \mid z - z_c \mid e^{-2z} dz - \int_0^{z_c} \ln \mid z - z_c \mid e^{-2z} dz\right) - \frac{\lambda_1}{2\lambda_b}\left(\frac{1}{8} + \frac{\bar{c}_0}{4\lambda_b}\right) e^{2z_c} - Q^-(e^{2z_c} - 1), \tag{5.3.19}$$

$$Q_i^- = -\frac{\lambda_1 \bar{c}_0^2 e^{-2z_c}\pi}{4\lambda_b^3}, \tag{5.3.20}$$

where the subscript i denotes the imaginary part. Substituting this result back into (5.3.12) using (5.3.13) we find

$$c_{1i} = -\frac{\lambda_1 \pi e^{-2/\lambda_b\sqrt{Fr}}}{2(Fr^{\frac{1}{2}} k^{\frac{1}{2}} \lambda_b)^3}. \tag{5.3.21}$$

We observe that the instability here is dependent on the existence of a critical level where the curvature of the base profile must be negative. This is exactly the mechanism investigated by Miles and others and which was defined in Benjamin (1963) as Class B instability.

5.4 The numerical solution

In the full formulation the equation (5.2.11) was solved numerically with the boundary conditions (5.2.26), (5.2.27) and the normalization condition $\bar{v}^+(0) = 1$. The method (a second order accurate discretization with Newton iterations to improve on the value of c for a given k) is a minor modification of the method described in Chapter 2. The results for the complex frequency $\omega = kc = \omega_r + i\omega_i$ and various combinations of the flow parameters are shown in figs 5:3(a)-(e). First we examine the effect of viscosity variations in the film with no interfacial effects, i.e. at $Fr = \infty$, $\gamma = 0$. We see in fig 5:3(a) that stronger film viscosity reduces growth rates, with

the maximum in $\omega_i(k)$ always around a finite wave number. In fig 5:3(b) we see that even without gravity the density variation strongly affects the instability as it alters the momentum/pressure balance in the film part of the disturbance. For increasingly dense films the maximum instability decreases and occurs for longer waves. The loss of this instability for very large values of ρ^- shows that very viscous and heavy films act like a solid wall, in effect turning the flow into that of a single fluid. The introduction of surface tension, $\gamma \neq 0$, damps the instability at all wavenumbers, particularly affecting short waves, the growth rate maximum is decreased for increased γ, occuring for longer waves, see fig 5:3(c). Gravity also stabilizes the flow, fig 5:3(d), although the wavenumber of the most unstable disturbance is only weakly dependent on the Froude number. A rather interesting non-monotonic behaviour under the Froude number variation is observed on short waves, however, since the short waves are completely stabilized by viscosity we do not see here the strong destabilizing influence of gravity noted for inviscid disturbances in §5.3. The effect of the film thickness is quite obvious from fig 5:3(e). As the film thickness decreases for $Fr = \infty$, $\gamma = 0$, the growth rate maximum decreases and the unstable spectrum moves towards longer waves. Increasing the film thickness on the other hand leads to saturation of the solution as the wall effect becomes weak.

5.4.1 Long-wave limit

In this section we analytically obtain a long-wave limit solution to the full problem. We approach this by assuming $k \ll 1$ and expand both above and below the interface in powers of k. Starting with the flow in the film we expand the perturbations $\bar{u}^-$, $\bar{v}^-$, $\bar{p}^-$ and frequency as follows

$$\bar{u}^- = k\bar{u}_1^-(\bar{y}) + k^2\bar{u}_2^- + ..., \tag{5.4.1.1}$$

$$\bar{v}^- = k^2\bar{v}_1^-(\bar{y}) + k^3\bar{v}_2^- + ..., \tag{5.4.1.2}$$

$$\bar{p}^- = \bar{p}_0^-(\bar{y}) + k\bar{p}_1^- + ..., \tag{5.4.1.3}$$

$$\omega = k^2\omega_0 + k^3\omega_1 + ... \ . \tag{5.4.1.4}$$

Substituting these expansions into the governing equations (5.2.12)-(5.2.14) and applying the boundary conditions

$$\bar{u}_1^-(-\bar{a}) = 0, \quad \frac{d\bar{u}_1^-}{d\bar{y}}(0) = 0, \quad \bar{v}_1(-\bar{a}) = 0, \quad \bar{v}_1^-(0) = 1, \tag{5.4.1.5}$$

where the last of these is a normalization of our choosing, we find that

$$\bar{v}_1^- = \frac{3}{2\bar{a}^3}\left(\bar{a}^2\bar{y} - \frac{\bar{y}^3}{3} + \frac{2\bar{a}^3}{3}\right), \quad \bar{p}_0^- = -\frac{3\mu_0^-}{\bar{a}^3}. \tag{5.4.1.6}$$

Likewise, in the upper flow we expand the perturbations in $\bar{u}^+, \bar{v}^+, \bar{p}^+$, writing

$$\bar{p}^+ = \bar{p}_0^+ + k\bar{p}_1^+ + k^2\bar{p}_2^+ + ..., \tag{5.4.1.7}$$

$$\bar{v}^+ = \bar{v}_0^+ + k\bar{v}_1^+ + k^2\bar{v}_2^+ + ..., \tag{5.4.1.8}$$

$$\bar{u}^+ = \frac{1}{k}\bar{u}_0^+ + \bar{u}_1^+ + k\bar{u}_2^+ + ..., \tag{5.4.1.9}$$

and upon substitution into (5.2.8)-(5.2.10) we obtain the solutions

$$\bar{v}_0^+ = Q_0 U_0^+, \tag{5.4.1.10}$$

$$\bar{v}_1^+ = U_0^+\left(Q_1 - \int_{\bar{y}}^{\infty} \frac{r}{U_0^{+2}}dy\right); \tag{5.4.1.11}$$

$$\text{As } \bar{y} \to 0, \qquad \bar{v}_1^+ \to \frac{r(0)}{\lambda_b}, \tag{5.4.1.12}$$

$$\bar{p}_1^+ = \bar{p}_{1c} + Q_0 i\left(\bar{y} + \int_{\bar{y}}^{\infty}\left\{(U_0^+)^2 - 1\right\}dy\right). \tag{5.4.1.13}$$

$$\bar{v}_2^+ = U_0^+\left(Q_2 - \int_{\bar{y}}^{\infty} \frac{s}{U_0^{+2}}dy\right); \tag{5.4.1.14}$$

$$\text{As } \bar{y} \to 0, \qquad \bar{v}_2^+ \to \frac{s(0)}{\lambda_b}, \tag{5.4.1.15}$$

where

$$r = -Q_0\omega_0\frac{dU_0^+}{d\bar{y}} - i\bar{p}_0^+, \tag{5.4.1.16}$$

$$s = -i\bar{p}_1^+ - \omega_0\frac{d\bar{v}_1^+}{d\bar{y}} - Q_0\omega_1\frac{dU_0^+}{d\bar{y}}, \tag{5.4.1.17}$$

Q_0, Q_1, Q_2, p_{1c} are constants of integration and, without loss of generality, we set $Q_1 = Q_2 = 0$.

From the definitions of r, s we see that

$$\omega_0 = -\frac{i\bar{p}_0^+}{Q_0\lambda_b}, \tag{5.4.1.18}$$

$$\omega_1 = -\frac{s(0)+i\bar{p}_1^+(0)}{\lambda_b Q_0}, \tag{5.4.1.19}$$

and from the kinematic condition, along with the jump in pressures we find

$$s(0)=\lambda_b, \quad Q_0=\frac{3\mu_0 i}{\bar{a}^3}+\frac{\Gamma}{\omega_0}, \tag{5.4.1.20}$$

where $\Gamma=-\tilde{\gamma}+(\rho^- -1)/Fr$ and we have rescaled the surface tension to keep it in the problem by writing $\gamma=\tilde{\gamma}/k^2$.

The expansions in the far field where $Y=k\bar{y}=O(1)$ are written as

$$u_1^+ = \hat{u}_1^+(Y)+k\hat{u}_2^+..., \tag{5.4.1.21}$$

$$v_1^+ = \hat{v}_1^+(Y)+k\hat{v}_2^+..., \tag{5.4.1.22}$$

$$p_1^+ = \hat{p}_1^+(Y)+k\hat{p}_2^+..., \tag{5.4.1.23}$$

and substitution into (5.2.8)-(5.2.10) gives the solutions

$$\hat{p}_1^+ = ic_1e^{-Y}, \quad \hat{v}_1^+ = c_1e^{-Y}, \tag{5.4.1.24}$$

$$\hat{p}_2^+ = ic_2e^{-Y}, \quad \hat{v}_2^+ = c_2e^{-Y}, \tag{5.4.1.25}$$

where c_1, c_2 are constants of integration. Then the match with the region $\bar{y}=O(1)$ gives

$$c_1 = Q_0, \qquad \bar{p}_0^+ = iQ_0, \tag{5.4.1.26}$$

$$c_2 = -L_1Q_0, \quad \bar{p}_{1c} = -iQ_0(L_2-L_1) \tag{5.4.1.27}$$

where

$$L_1 = \lim_{\bar{y}\to 0}\left[-1+\int_{\bar{y}}^{\infty}\frac{1-\omega_0 U_0^{+\prime}(y)}{(U_0^+(y))^2}dy\right], \tag{5.4.1.28}$$

$$L_2 = \lim_{\bar{y}\to 0}\int_{\bar{y}}^{\infty}\left((U_0^+(y))^2-1\right)dy. \tag{5.4.1.29}$$

Therefore $\omega_0 = 1/\lambda_b$ is real and the growth rate is given by ω_1 which is found by combining (5.4.1.20), (5.4.1.27) and (5.4.1.19). Numerical integration of L_1, L_2 gives

the values $L_1 = -2.21428$, $L_2 = -2.38489$ and since $\bar{p}_1^+(0) = p_{1c}$ we find that

$$\omega_1 = -\frac{1}{Q_0} + \frac{L_1 + L_2}{\lambda_b}. \tag{5.4.1.30}$$

We note here that neither surface tension nor gravity affect the growth rate at this order. We show in fig 5:4 a graphical comparison of the asymptotic solution (5.4.1.4) with c_r, c_i computed for the full problem.

5.5 The thin-film limit case

In this subsection we describe various instabilities arising on thin films. Simultaneously with the film thickness the viscosity μ_0^- will also be taken small to capture the most typical flow regimes. Our numerical solutions in §5.4 show that thin-film instability tends to be moved towards smaller wavenumbers, hence we take $k \ll 1$ as well.

5.5.1 TS instability on a viscous thin film

Suppose first that k and $\bar{a}$ are of the same order, $(k, \bar{a}) = O(\epsilon)$ say, where $\epsilon \ll 1$. We take the film viscosity $\mu_0^- = O(\epsilon^4)$ and we will justify this choice later. So we write

$$k = \epsilon K, \;\; \bar{a} = \epsilon \tilde{a}, \;\; \mu_0^- = \epsilon^4 \bar{\mu}_0^-, \;\; (K, \tilde{a}, \bar{\mu}_0^-) = O(1). \tag{5.5.1}$$

The disturbance components in the film are sought in the form

$$\bar{u}^- = \epsilon U^-(Y), \;\; \bar{v}^- = \epsilon^3 V^-(Y), \;\; \bar{p}^- = \epsilon^2 P^-(Y), \tag{5.5.2}$$

to leading order, with $Y = \bar{y}/\epsilon = O(1)$ and the frequency and interfacial displacement written as

$$\omega = \epsilon^2 \Omega + \ldots, \;\; \eta = \epsilon \bar{\eta} + \ldots . \tag{5.5.3}$$

Substitution into (5.2.12)-(5.2.14) and the use of the boundary conditions $U^-(-\tilde{a}) = V^-(-\tilde{a}) = 0$, $dU^-/dY(0) = 0$ lead to the solutions

$$U^- = \frac{KP^-}{\Omega\rho^-}\left(\tilde{a} - \frac{\cosh\sigma Y}{\cosh\sigma\tilde{a}}\right), \tag{5.5.4}$$

$$V^- = -\frac{iK^2P^-}{\Omega\rho^-}\left(\tilde{a} + Y - \frac{\sinh\sigma\tilde{a} + \sinh\sigma Y}{\sigma\cosh\sigma\tilde{a}}\right). \tag{5.5.5}$$

where $\sigma = \sqrt{-i\omega\rho^-/\bar{\mu}_0^-}$. The interfacial kinematic condition then becomes

$$\bar{\eta} = \frac{K^2P_1^-}{\Omega^2\rho^-}\left(\tilde{a} - \frac{\tanh\sigma\tilde{a}}{\sigma}\right). \tag{5.5.6}$$

The disturbance in the upper fluid takes a three-layer structure. In the region $\bar{y} \sim O(1)$, we have

$$\bar{u}^+ = \epsilon A U_0^{+'}(\bar{y}) + \ldots, \quad \bar{v}^+ = \epsilon^2(-iKAU_0^+(\bar{y})) + \ldots, \tag{5.5.7}$$

$$\bar{p}^+ = \epsilon^2 P^+ E + c.c. + \ldots, \tag{5.5.8}$$

and we find, matching in the usual way to the outer potential flow where $\bar{y} \sim O(\epsilon^{-1})$ that

$$P^+ = |K|A. \tag{5.5.9}$$

Then in the region $Y \sim O(1)$, $Y > 0$ the solution takes the form

$$\bar{u}^+ = \epsilon\lambda_b A + O(\epsilon), \quad \bar{v}^+ = \epsilon^2(BY - iK\lambda_b A), \tag{5.5.10}$$

with the same pressure (5.5.8) and the constant B given by the relation

$$\lambda_b B = -iKP^+ + i\Omega\lambda_b A. \tag{5.5.11}$$

The kinematic condition for the upper flow, $B = -i\Omega\bar{\eta}$, along with (5.5.9) and the interfacial condition,

$$P^+ - P^- + K^2\tilde{\gamma}\bar{\eta} + \frac{(\rho^- - 1)\bar{\eta}}{\tilde{Fr}} = 0, \tag{5.5.12}$$

with the surface tension coefficient and the Froude number adjusted to the present regime by $\gamma = \tilde{\gamma}\epsilon$ and $Fr = \epsilon^{-1}\tilde{Fr}$, lead eventually to the dispersion relation for

$\Omega = \Omega(K)$

$$(\lambda_b\Omega - K|K|)\left(\Omega^2 - \frac{K^2}{\rho^-}\left(\tilde{\gamma}K^2 + \frac{\rho^- - 1}{\tilde{F}r}\right)\left(\tilde{a} - \frac{\tanh\sigma\tilde{a}}{\sigma}\right)\right) + \frac{\lambda_b K^2|K|}{\rho^-}\left(\tilde{a} - \frac{\tanh\sigma\tilde{a}}{\sigma}\right)\Omega = 0, \qquad (5.5.13)$$

with $\sigma = \sqrt{-i\Omega\rho^-/\bar{\mu}_0^-}$. Figures 5:5(a)-(c) illustrate the growth rate Ω_i obtained numerically from (5.5.13). The effect of gravity in fig 5:5(a) is rather complex, as we see that long waves are damped whilst short waves are not affected, and the range of wavenumbers in the middle is destabilized. On the other hand, the influence of surface tension, shown in fig 5:5(b), does not affect long waves, but destabilizes short waves. A most remarkable behaviour is observed for reduced film viscosity with an island of instability arising in a fixed wavenumber interval as $\bar{\mu}_0^- \to 0$, see fig 5:5(c). These properties are explored in more detail in the next subsection whilst here we comment on the connection of the present regime with the solutions derived in the previous subsections and elsewhere. At small wavenumber $K \to 0$, the solution of (5.5.13) has the limit properties

$$\Omega_r = \frac{K|K|}{\lambda_b} + O(K^3), \qquad (5.5.14)$$

$$\Omega_i = \frac{3\tilde{a}^3\bar{\mu}_0^- K^2|K|}{(\bar{\mu}_0^-)^2 + 9(\rho^- - 1)^2\tilde{a}^6\lambda_b^2/\tilde{F}r^2} + O(K^4) \qquad (5.5.15)$$

which for large $\tilde{F}r$ coincide with the long-wave result (5.4.1.4). The gravity term explicitly included in (5.5.15) confirms the stabilizing influence on long waves observed in all our numerical solutions in this chapter. If, next, $\tilde{\gamma} = 0, \tilde{F}r = \infty$ and $\rho^- \to \infty$, $\bar{\mu}_0^- \to \infty$ with $\bar{\mu}_0 \sim \rho^-$ then

$$\Omega = \frac{K|K|}{\lambda_b} + \frac{1}{\rho^-}K\lambda_b\left(\frac{\tanh\sigma_0\tilde{a}}{\sigma_0} - \tilde{a}\right) + O(\frac{1}{\rho^{-2}}), \qquad (5.5.16)$$

where $\sigma_0 = \sqrt{-iK|K|\rho^-/\mu_0^-}$. The solution of the form (5.5.16) was derived by Timoshin (1997), in his §5.4, as a special limit of the TS instability governed by the triple-deck equations, see Chapter 4. The destabilizing effects of surface tension, which caused a resonance between capillary and TS waves in Chapter 4, appear to also be present here and we discuss this possibility in the next section.

5.5.2 Thin films of smaller viscosity

The formation of an isolated range of instability at a reduced film viscosity in fig 5:5(c) could have been explained by simply taking the limit $\bar{\mu}_0^- \to 0$ in (5.5.13), however far more interesting results are obtained if we assume much smaller values of the film viscosity,

$$\mu_0^- = \epsilon^{10}\tilde{\mu}_0^-, \text{ with } \tilde{\mu}_0^- = O(1). \tag{5.5.1}$$

We keep the other parameters (i.e. $K, \rho^-, \tilde{a}$) scaled as in §5.5.1 and expand the complex wave speed c as

$$c = \epsilon(c_0 + \epsilon c_1 + \epsilon^2 c_2 + \epsilon^3 c_3 + ...). \tag{5.5.2}$$

As in §5.5.1, the upper fluid has three distinct regions with $\bar{y}$ of $O(\epsilon), O(1)$ and $O(\epsilon^{-1})$. A new feature here is that the film also becomes multi layered, due to the reduced viscosity, splitting into three regions for $\bar{y} < 0$, $Y + \tilde{a} \sim O(\epsilon^3)$, $Y \sim O(1)$ and $Y \sim O(\epsilon^3)$ where we recall $\bar{y} = \epsilon Y$. The viscous effects are contained within wall and interfacial layers, with the interfacial viscous layer remaining inactive for our purposes. As the calculations for the limit solution below are both long and tedious we present the expansions along with solutions for their coefficients but reserve comment only for the most significant steps.

In the region $\bar{y} \sim O(\epsilon)$ above the interface we take $\bar{y} = \epsilon Y$, expand the base Blasius profile U_0^+ and the solution of the Rayleigh equation (5.2.11) in the form

$$U_0^+ = \epsilon\lambda_b Y + \epsilon^4\lambda_1 Y^4 + ..., \text{ with } \lambda_1 = -\lambda_b^2/48, \tag{5.5.3}$$

$$\bar{v}^+ = \epsilon^2(V_0^+ + \epsilon V_1^+ + \epsilon^2 V_2^+ + \epsilon^3 V_3^+ + \epsilon^4 V_4^+ + ...), \tag{5.5.4}$$

$$c = \epsilon(c_0 + \epsilon c_1 + \epsilon^2 c_2 + \epsilon^3 c_3 + ...), \tag{5.5.5}$$

where the leading coefficients are found to be

$$V_0^+ = \lambda_b Y + B_0, \;\; V_1^+ = A_1 Y + B_1, \;\; V_2^+ = A_2 Y + B_2, \tag{5.5.6}$$

$$V_3^+ = V_{3w}^+ + Q_3^{\pm}(Y - Y_c) + 12\lambda_1\left(\frac{Y^4}{4!} + Y_c\frac{Y^3}{3!} + {Y_c}^2\frac{Y^2}{2!}\right)$$
$$+12\lambda_1({Y_c}^3 + B_0 Y_c^2)((Y - Y_c)\ln|Y - Y_c| - (Y - Y_c)) + d^{\pm}, \tag{5.5.7}$$

with constants A_j, B_j, V_{3w}^+, $Q_3^\pm$ and $d^\pm$. The superscript $\pm$ refers to the value of V_3^+ above or below the critical level $Y = Y_c = c_0/\lambda_b$. In the layer $\bar{y} = O(1)$ the solution expands as

$$\bar{v}^+ = \epsilon(\tilde{V}_0^+ + \epsilon\tilde{V}_1^+ + \epsilon^2\tilde{V}_2^+ + \epsilon^3\tilde{V}_3^+ + \epsilon^4\tilde{V}_4^+ + ...), \tag{5.5.8}$$

whereas in the outer region $\bar{Y} = \epsilon\bar{y} = O(1)$ we have

$$\bar{v}^+ = \bar{V}_0^+(\bar{Y}) + ... \tag{5.5.9}$$

For the terms shown in (5.5.8) we obtain the solutions

$$\tilde{V}_0^+ = U_0^+, \;\; \tilde{V}_1^+ = c_0(U_0^+ - 1) + |K|\Phi_1, \tag{5.5.10}$$

$$\tilde{V}_2^+ = c_1 + c_0^2(U_0^+ - 1) - \theta_{20}U_0^+ - \theta_{21}U_0^+\left(\int_\infty^{\bar{y}} \left\{ \frac{1}{U_0^+(s)^2} - 1 \right\} ds - \bar{y}\right) + \Phi_2, \tag{5.5.11}$$

$$\begin{aligned} \tilde{V}_3^+ = {} & (c_0^3 - c_0K^2 - c_1c_0 - \theta_{20}c_0 + c_2)(U_0^+ - 1) - \theta_{30}U_0^+ \\ & -\theta_{31}\left(\int_\infty^{\bar{y}} \left\{ \frac{1}{(U_0^+(s))^2} - 1 \right\} ds - Y_1\right) + \Phi_3, \end{aligned} \tag{5.5.12}$$

where θ_{ij} are real constants and the functions $\Phi_j(\bar{y})$ have the following properties:

$$\Phi_1 = U_0^+\left(\int_\infty^{\bar{y}} \left\{ \frac{1}{(U_0^+(s))^2} - 1 \right\} ds - \bar{y}\right), \tag{5.5.13}$$

$$\Phi_2 = U_0^+\left(\int_0^{\bar{y}} \frac{1}{(U_0^+)^2}\left(\int_0^s \left\{ K^2(U_0^+)^2 - |K|\Phi_1'' \right\} d\tau\right) ds\right), \tag{5.5.14}$$

$$\Phi_3 = U_0^+\left(\int_1^{\bar{y}} \frac{1}{(U_0^+)^2}\left(\int_0^s r_3(\tau)d\tau\right) ds\right), \tag{5.5.15}$$

$$r_3 = K^2U_0^+\left((U_0^+ - 1)c_0 - |K|\Phi_1\right) + c_0\Phi_2'' - (\theta_{21}c_0 - |K|c_1)\Phi_1'', \tag{5.5.16}$$

$$\text{As } \bar{y} \to \infty: \qquad \Phi_2 \to \frac{|K|^2}{2}\bar{y}^2 + \theta_{21}\bar{y} + \theta_{20} + t.s.t., \tag{5.5.17}$$

$$\text{As } \bar{y} \to 0: \qquad \Phi_2 \to \frac{6\lambda_1 c_0}{\lambda_b^2}(c_0 + B_0)\bar{y}^2 + O(\bar{y}^3), \tag{5.5.18}$$

$$\text{As } \bar{y} \to \infty: \qquad \Phi_3 \to -\frac{|K|K^2}{6}\bar{y}^3 + \theta_{31}\bar{y} + \theta_{30} + t.s.t., \tag{5.5.19}$$

$$\text{As } \bar{y} \to 0: \qquad \Phi_3 \to \frac{\Phi_2''(0)c_0}{\lambda_b}\bar{y}\ln\bar{y} + \theta_{33}\bar{y} + \theta_{32}\bar{y}^2 + t.s.t. \;\; . \tag{5.5.20}$$

Here the letters *t.s.t.* denotes transcendentally small terms. Matching to the solution in layers $\bar{y} = O(1)$ and $\bar{y} = O(\epsilon)$ shows that

$$B_0 = -c_0 + \frac{|K|}{\lambda_b}, \tag{5.5.21}$$

$$B_1 = -c_1 - c_0^2 + \frac{\theta_{21}}{\lambda_b}, \tag{5.5.22}$$

$$B_2 = c_0 K^2 + c_1 c_0 - c_0^3 - \theta_{20} c_0 - c_2 + \frac{\theta_{31}}{\lambda_b}. \tag{5.5.23}$$

Provided that c_0, c_1, c_2 are real, the growth rate is contained in the next term $c_3 = c_{3r} + ic_{3i}$. To determine c_{3i} we only need to look at the imaginary part of $\tilde{V}_4^+$,

$$\tilde{V}_{4i}^+ = (U_0^+ - 1)c_{3i}. \tag{5.5.24}$$

Then, from matching to the region $\bar{y} = O(\epsilon)$, we find that

$$c_{3i} = -Im(V_{3w} + d^+) = -V_{3wi} + \frac{12\lambda_1 c_0^3 |K|\pi}{\lambda_b^5} \tag{5.5.25}$$

with the value of d^+ related to the logarithmic phase jump across the critical layer in the region $\bar{y} = O(\epsilon)$, $\bar{y} > 0$. In the film, $\bar{y} < 0$, in the wall Stokes layer, we write $Y + \tilde{a} = \epsilon^3 \hat{Y}$. The leading terms in the disturbance expansions are

$$\bar{u}^- = \hat{U}_0^-(\hat{Y}), \quad \bar{v}^- = \epsilon^5 \hat{V}_0^-(\hat{Y}), \quad \bar{p}^- = \epsilon \hat{P}_0^-, \tag{5.5.26}$$

and we obtain the result

$$\hat{V}_0^- = \frac{iK\hat{P}_0^-}{c_0\rho^-}\left(\frac{1 - e^{-\hat{\sigma}\hat{Y}}}{\hat{\sigma}} - \hat{Y}\right), \tag{5.5.27}$$

where $\hat{\sigma} = \sqrt{-iKc_0/\nu^-}$. In the main part of the film, where $\bar{y} = \epsilon Y$, $Y = O(1)$, $Y < 0$ the expansions are

$$\bar{u}^- = \hat{u}_0^- + \epsilon\hat{u}_1^- + \epsilon^2\hat{u}_2^- + \epsilon^3\hat{u}_3^- + ..., \tag{5.5.28}$$

$$\bar{v}^- = \epsilon^2\hat{v}_0^- + \epsilon^3\hat{v}_1^- + \epsilon^4\hat{v}_2^- + \epsilon^5\hat{v}_3^- + ..., \tag{5.5.29}$$

$$\bar{p}^- = \epsilon\hat{p}_0^- + \epsilon^2\hat{p}_1^- + \epsilon^3\hat{p}_2^- + \epsilon^4\hat{p}_3^- + ..., \tag{5.5.30}$$

and for the normal velocity terms (for example), in terms of the pressures, we have the following relations

$$\hat{v}_0^- = -\frac{iK\hat{p}_0^-}{c_0\rho^-}(Y + \tilde{a}), \quad \hat{v}_1^- = -\frac{iK}{c_0\rho^-}\left(-\frac{c_1\hat{p}_0^-}{c_0} + \hat{p}_1^-\right)(Y + \tilde{a}), \tag{5.5.31}$$

$$\hat{v}_2^- = -\frac{iK}{c_0\rho^-}\left(\left(-\frac{c_2}{c_0} + \frac{c_1^2}{c_0^2}\right)\hat{p}_0^- - \frac{c_1}{c_0}\hat{p}_1^- + \hat{p}_2^-\right)(Y + \tilde{a}), \tag{5.5.32}$$

$$\hat{v}_3^- = -\frac{iK}{c_0\rho^-}\left(\left(\frac{2c_1c_2}{c_0^2}-\frac{c_1^3}{c_0^3}-\frac{c_3}{c_0}\right)\hat{p}_0^- + \left(-\frac{c_2}{c_0}+\frac{c_1^2}{c_0^2}\right)\hat{p}_1^- - \frac{c_1}{c_0}\hat{p}_2^- + \hat{p}_3^-\right) \times(Y+\tilde{a}). \tag{5.5.33}$$

Then the interfacial pressure jump condition and the kinematic condition lead, first of all, to an equation for the leading-order phase speed,

$$|K| = \left(\frac{|K|}{\lambda_b}-c_0\right)\left(\frac{c_0\rho^-}{\tilde{a}}-\frac{\Gamma}{c_0}\right), \tag{5.5.34}$$

where $\Gamma = \tilde{\gamma}K^2 + (\rho^- - 1)/\tilde{F}r$, and then to the sequence of corrections to the phase speed

$$c_1 = \frac{K^2\lambda_b^{-1}\theta_{20}\,(c_0+1/\tilde{a}+\Gamma/c_0) - c_0^3\,(1-\rho^-/\tilde{a}) - c_0(\Gamma - A_1)}{\rho^-/\tilde{a}\,(|K|/\lambda_b - 2c_0) + \Gamma/c_0\,(1+\lambda_b/c_0)}, \tag{5.5.35}$$

$$c_2 = \left[\left(1-\frac{c_0\rho^-}{\tilde{a}}+\frac{\Gamma}{c_0}\right)\left(K^2c_0 + c_1c_0 - c_0^3 - c_0\theta_{20} + \frac{\theta_{31}}{\lambda_b}\right) - \frac{c_1}{c_0}\left(B_1 - \frac{c_0\rho^-}{\tilde{a}}\left(B_1 + \frac{2c_1}{c_0}B_0\right)\right)\right]\left(\frac{\Gamma}{c_0}(1+\frac{\lambda_b}{c_0}) - \frac{B_0}{\tilde{a}} - \frac{c_0}{\rho^-}\tilde{a}\right)^{-1}. \tag{5.5.36}$$

We note that if c_0 in (5.5.34) is complex-valued then this formula provides the leading order growth rate so the rest of the analysis is not necessary. The first bracketed expression in (5.5.34) can be thought of as relating to TS waves, and the second is related to gravity-capillary waves. The instability governed by (5.5.34) can thus be interpreted as a resonance between the two classes of neutral waves, very similar to the K-H mechanism in (5.1.1). We saw in fig 5:5(b) that an increase in surface tension destabilized a wider band of wavenumbers, indicating a resonance of this kind. However when c_0 is real we see that so are c_1, c_2, but c_3 is not and $c_{3i} = Im(c_3)$ is found to be

$$c_{3i} = \left[\frac{1}{\tilde{a}}\left(c_0 - \frac{|K|}{\lambda_b}\right)\sqrt{\frac{\nu^- c_0}{2K}} - \left(\frac{\Gamma}{c_0} - \frac{\rho^- c_0}{\tilde{a}}\right)\frac{12\tilde{a}\lambda_1 c_0^3|K|\pi}{\rho^-\lambda_b^5}\right] \times\left(2c_0 - \frac{|K|}{\lambda_b} - \frac{\tilde{a}\Gamma|K|}{\rho^- c_0^2\lambda_b}\right)^{-1}. \tag{5.5.37}$$

Numerical results for the leading order instability and its corrections in this regime are shown in figures 5:6(a)-(c) and figs 5:7(a),(b). Two distinct modes can be seen

in Fig 5:6(a) corresponding to Class A (TS) and Class B modes of the Benjamin-Landahl classification. We see, for the long-wave limit $K \ll 1$ that when no gravitational influence is present c_0 fully describes the leading order instability. However with a gravitational effect, in our example $Fr = 10$, the leading instability is given by c_{3i}, see fig 5:6 (c), $K < 0.02$. Class B waves remain stable, whilst for TS (Class A) waves a slight broadening of the unstable wave spectrum is seen. For short waves, on the other hand, we see that there appears to be a critical value of the Froude number, $\tilde{Fr}_c$, below which the presence of gravity provides a positive imaginary correction to c, increasing the destabilizing role of the curvature for Class B waves but stabilizing TS modes, see fig 5:6 (b). For $\tilde{Fr} > \tilde{Fr}_c$ the curvature plays an (almost negligible) contrary, i.e. stabilizing, role over a small wavenumber range. An analysis of the influence of both curvature and viscosity on the instabilities present shows curvature to be the dominant force. However if we take $\tilde{\mu}_0^- \gg 1$, linking with the previous regime, we see in fig 5:7(a), that the effect of viscosity overcomes that of curvature and a wider range of K becomes unstable for Class A waves. We clearly see the destabilizing role of viscosity for TS waves both here and in fig 5:5(c). Strong viscosity, within this regime, can stabilize bands of wavenumber for Class B modes even in the presence of gravity or surface tension but we observe in fig 5:7(b) that surface tension will become the dominant effect as K becomes large and a second range of wavenumbers will become unstable.

5.6 Discussion

Through analytical investigation of limiting regimes of the Rayleigh problem (given by (5.2.11), (5.2.26), $v^+(\infty) = 0$ and $v^+(0) = 1$) we have been able to see how different flow parameters affect the instability mechanisms. The K-H, Tollmien-Schlichting, and Miles mechanisms as well as a capillary/TS wave resonance are found to operate in special limits of the full formulation, however in order to determine full instability ranges, especially the range of the growth rate maximum, numerical solution of the problem is necessary in general. We have also shown that

the various special cases tackled in previous papers are continuously connected in the parameter space of the Rayleigh problem considered here.

There are some apparent discrepancies between the behaviours of the full numerical and limiting solutions which require clarification. We do not observe a short-wave instability in the full solution whilst one is present in limiting solutions in §5.5. This means that an alternative limit theory is required to describe the short-wave cut-off of the curves in figs 5:3, for example. It is also clear that the shape of the growth-rate curves in figs 5:5, 5:6 and 5:7 with a pronounced hump in the middle surrounded by broad ranges of weakly growing modes, has nothing in common with computational solutions shown in fig 5:3, with perhaps the exception of one curve in fig 5:3(a). One reason for this difference is of a technical nature: full numerical solutions were difficult to obtain for thinner films due to very small growth rates. The small growth rates are in agreement with our predictions in §5.5, where it is shown that this is related to the small curvature of the Blasius profile near the interface. We can expect that a better agreement between thin film theory and numerical solutions can be obtained for a base profile with larger curvature. To verify this idea we have computed a few solutions in the full formulation using the exponential base-velocity distribution $U_0^+ = 1 - \exp[-y]$. The results are shown in fig 5:8, and we can see an agreement with the properties of the limiting solution (note that the theory in §5.5 can be easily adjusted to the case with an exponential profile).

Finally we comment on the validity of our numerical solutions for very long waves. The growth rate calculations at very small wavenumbers were difficult since the solutions obtained by the Rayleigh solver require a far field condition to be imposed at $\bar{y} = \bar{y}_{max}$ of inverse proportion to the wavelength for small wavenumbers. Via accuracy tests a relation $\bar{y}_{max} = 5/k$ was settled on as a satisfactory numerical depth for the upper fluid. Values smaller than this meant that the solution for $\bar{v}^+$ struggled to decay as $\bar{y} \to \bar{y}_{max}$. Because of this restriction calculations became very slow for $k < 0.02$ and so this was taken as the longest wavelength to be examined. The stepsize $d\bar{y}$ was chosen to be $d\bar{y} = 0.005$ for the full Rayleigh solutions. For the

parameters $k = 0.1$, $\rho^- = 2$, $\mu_0^- = 0.1$, $\bar{a} = 5$, $\Gamma = 0$ with 64001 steps and varying stepsize $d\bar{y}$ the following results were obtained:

$$\begin{aligned} d\bar{y} &= 0.01,\ c = 0.2283496 + 0.0951937i \\ d\bar{y} &= 0.005\ c = 0.2283497 + 0.0951939i \\ d\bar{y} &= 0.0025,\ c = 0.2283497 + 0.0951939i \end{aligned} \tag{5.6.1}$$

A doubling of stepsize and halving of $\bar{y}_{max}$ gave exactly the same answer.

5.7 Figures

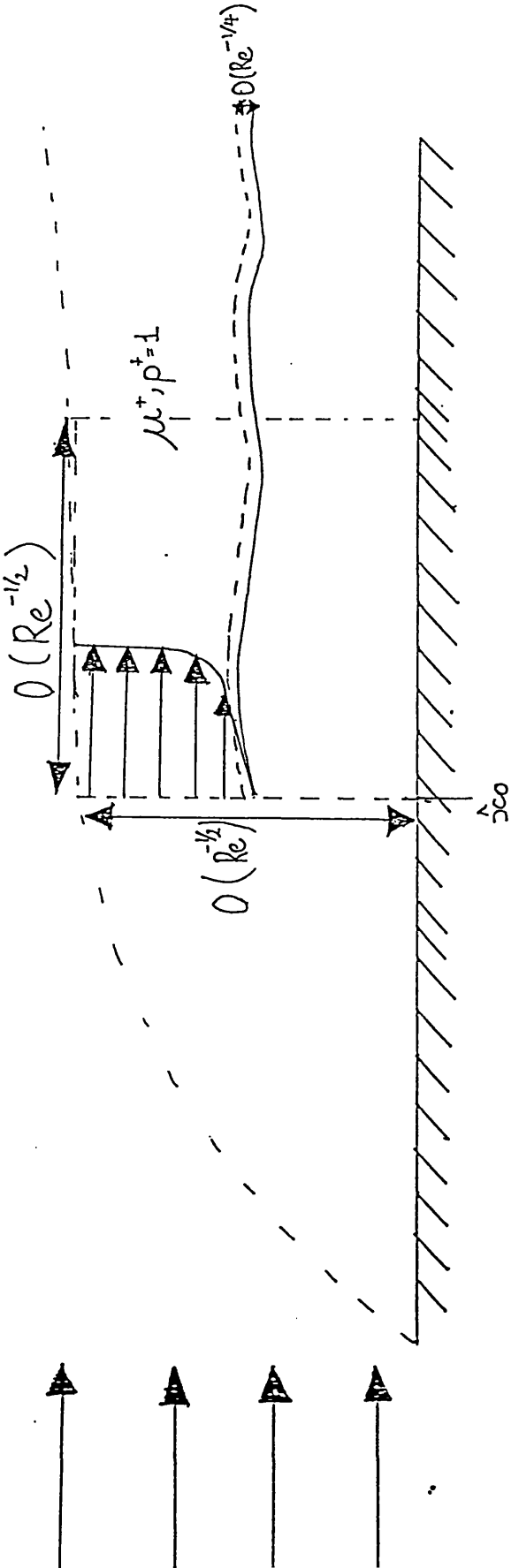

Figure 5:1 The boundary layer flow on a film coated wall.

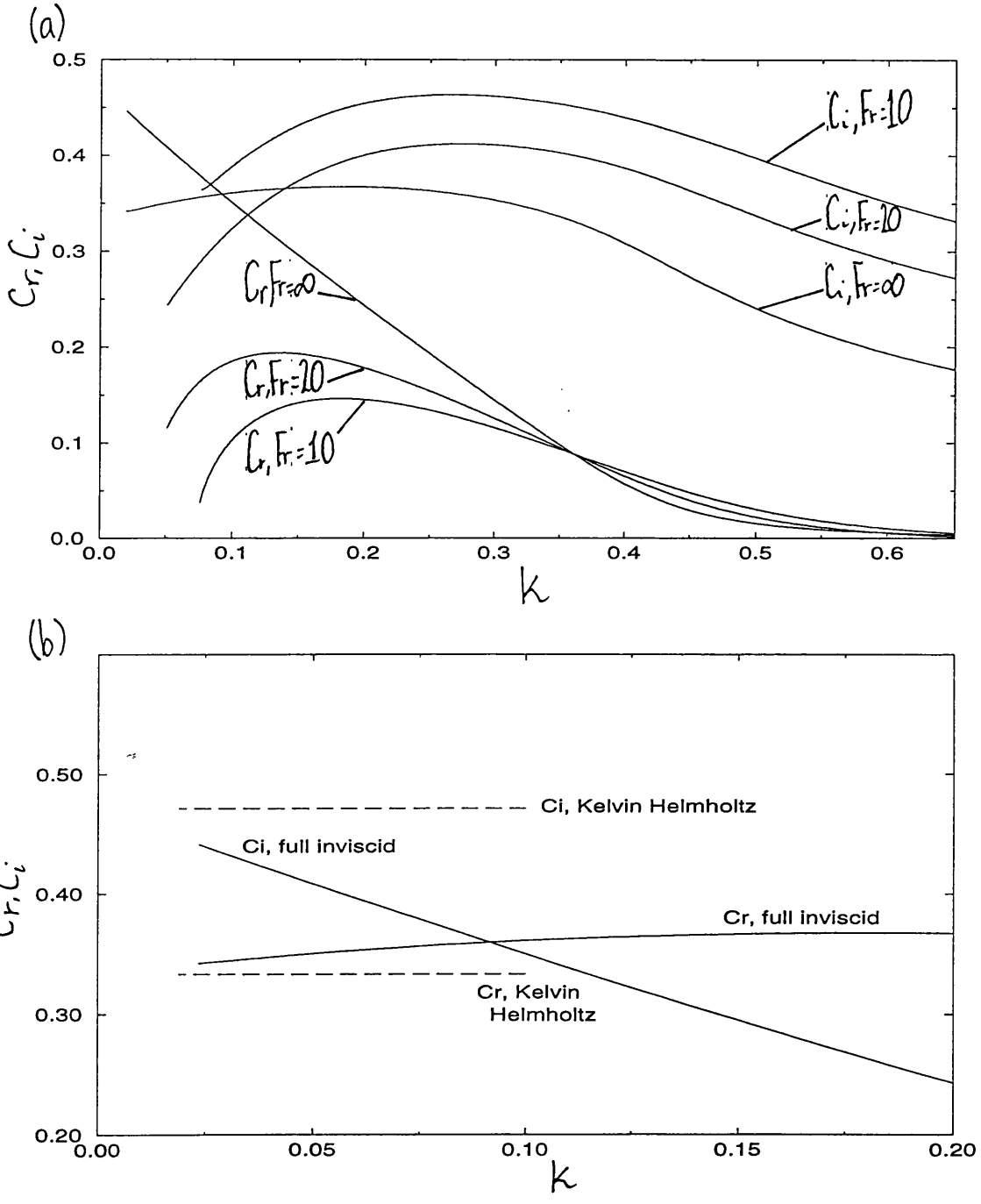

Figure 5:2(a) Numerical solutions of (5.2.11), with the boundary conditions (5.3.2), (5.2.27) and $\bar{a} = 5, \rho^- = 2.0, \mu_0^- = 1.0, \gamma_{st} = 0$, real and imaginary c plotted against wavenumber k for various Fr. (b) a comparison of the solution when $Fr = \infty$ with (5.3.7).

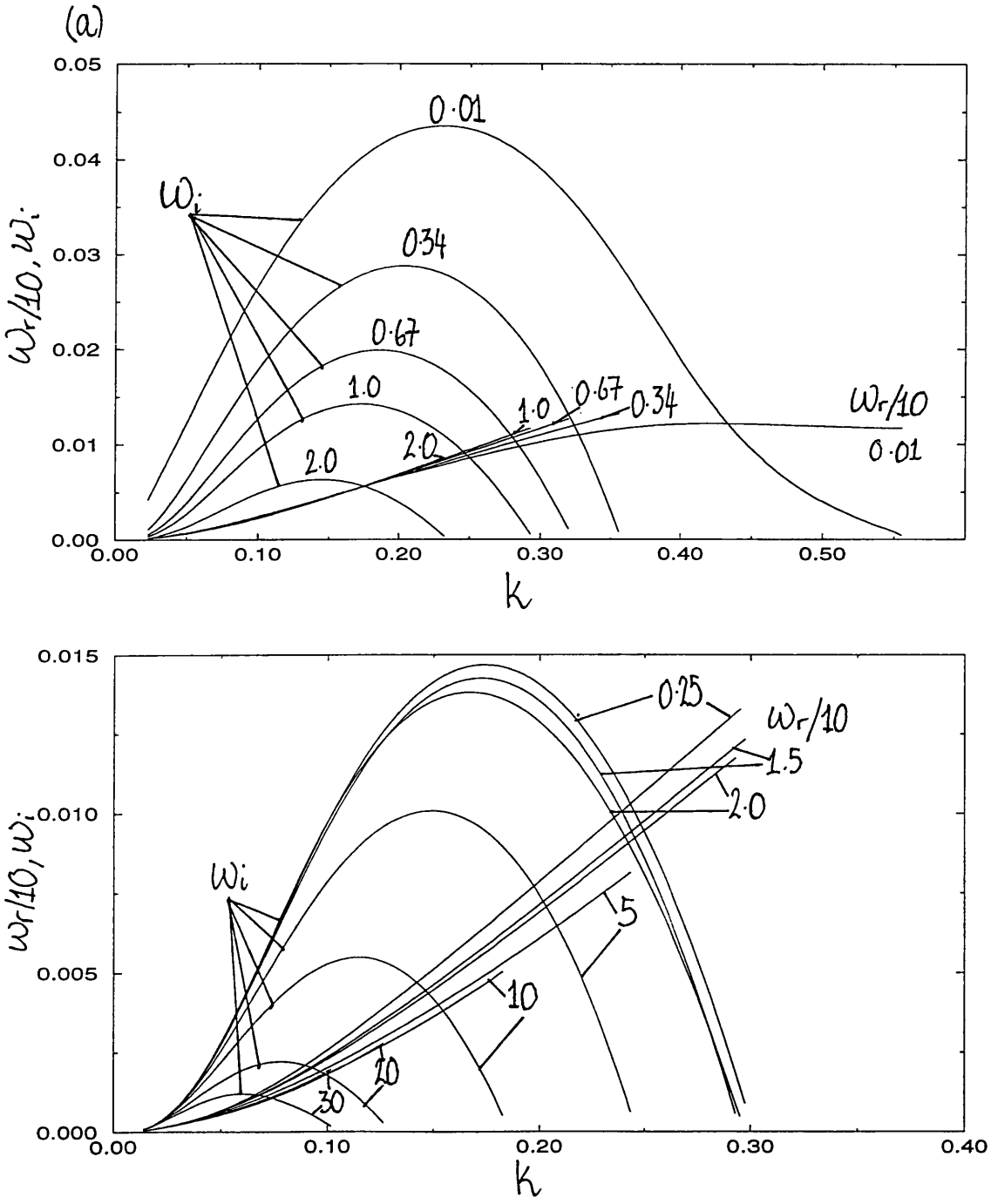

Figure 5:3 The full Rayleigh problem. Unstable eigenvalues of (5.2.11), (5.2.26) and (5.2.27); $\omega_r/10$ and growth rate ω_i versus wavenumber k for (a) $\bar{a} = 5, \rho^- = 2.0, \gamma_{st} = 0, Fr = \infty$ and μ_0^- varying, (b) $\bar{a} = 5, \mu_0^- = 1.0, \gamma_{st} = 0, Fr = \infty$ and ρ^- varying.

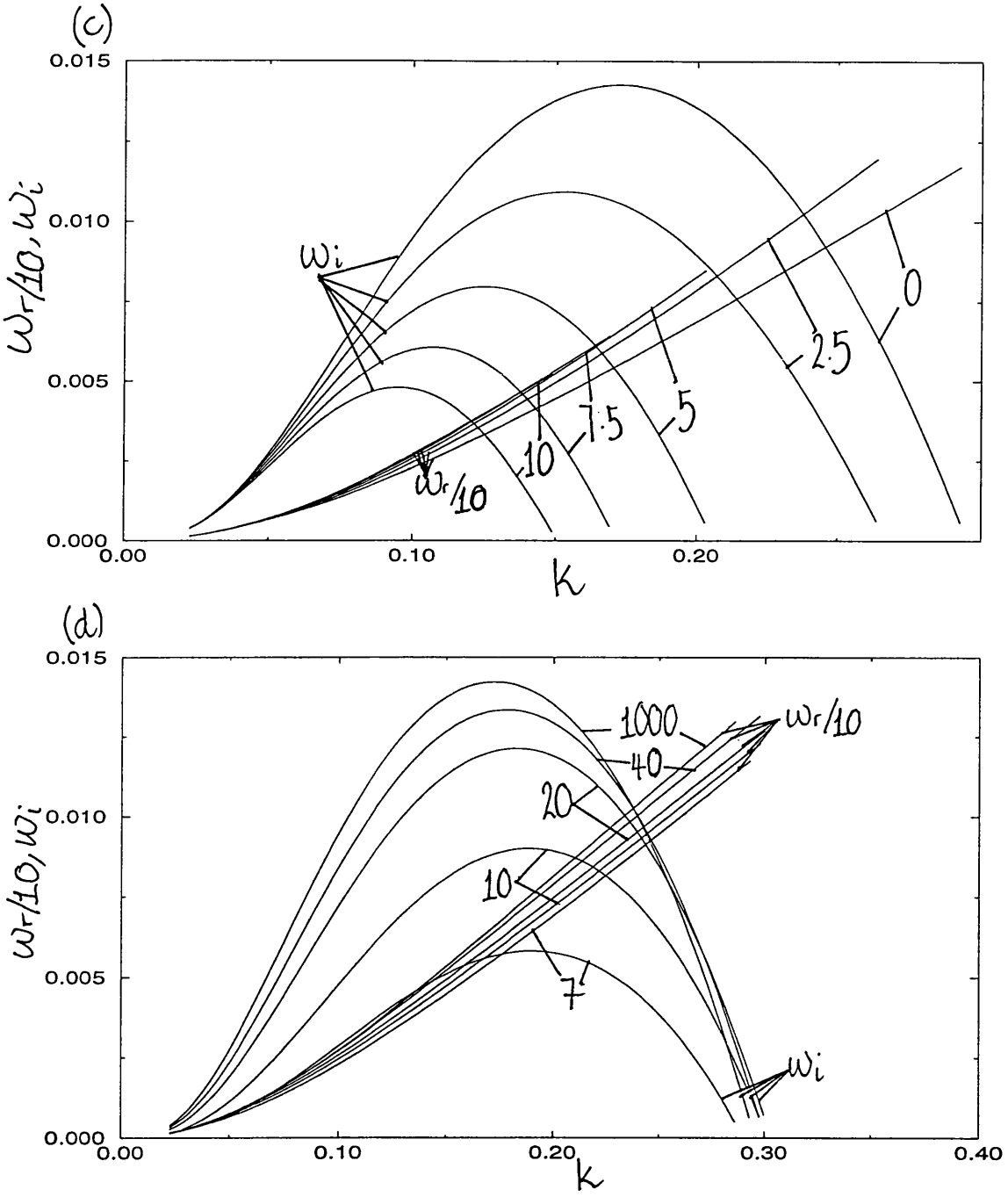

Figure 5:3 As before, **(c)** $\bar{a} = 5, \rho^- = 2.0, \mu_0^- = 1.0, Fr = \infty$ and γ_{st} varying, **(d)** $\bar{a} = 5, \rho^- = 2.0, \mu_0^- = 1.0, \gamma_{st} = 0$, and Fr varying.

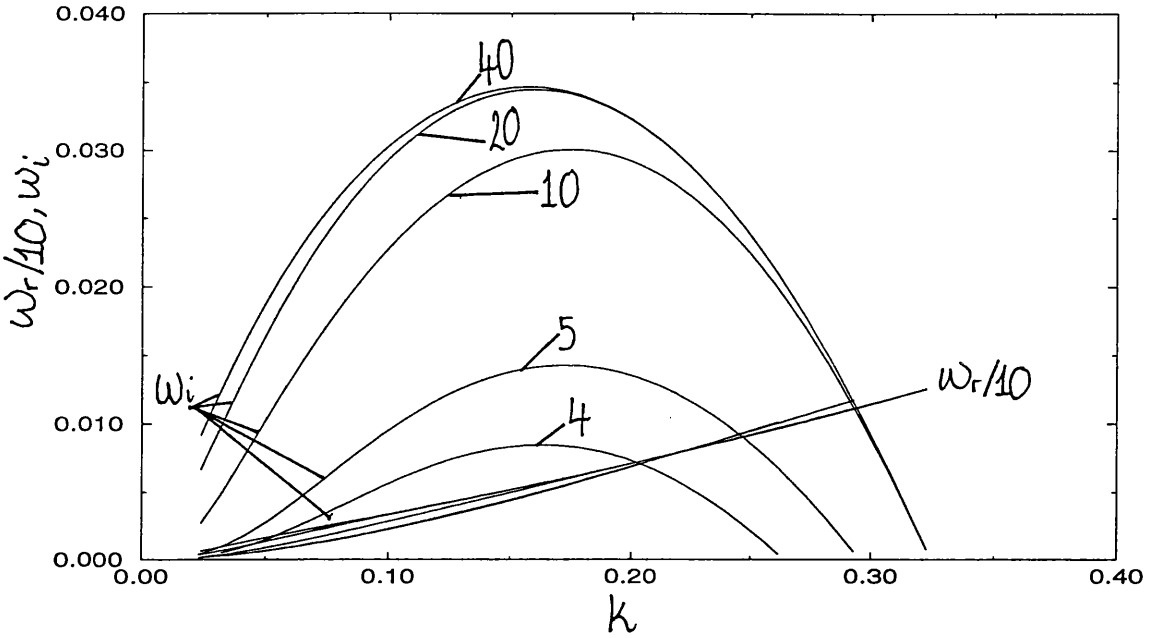

Figure 5:3(e) As before, (e) $\rho^- = 2.0$, $\mu_0^- = 1.0$, $\gamma_{st} = 0$, $Fr = \infty$ and $\bar{a}$ varying.

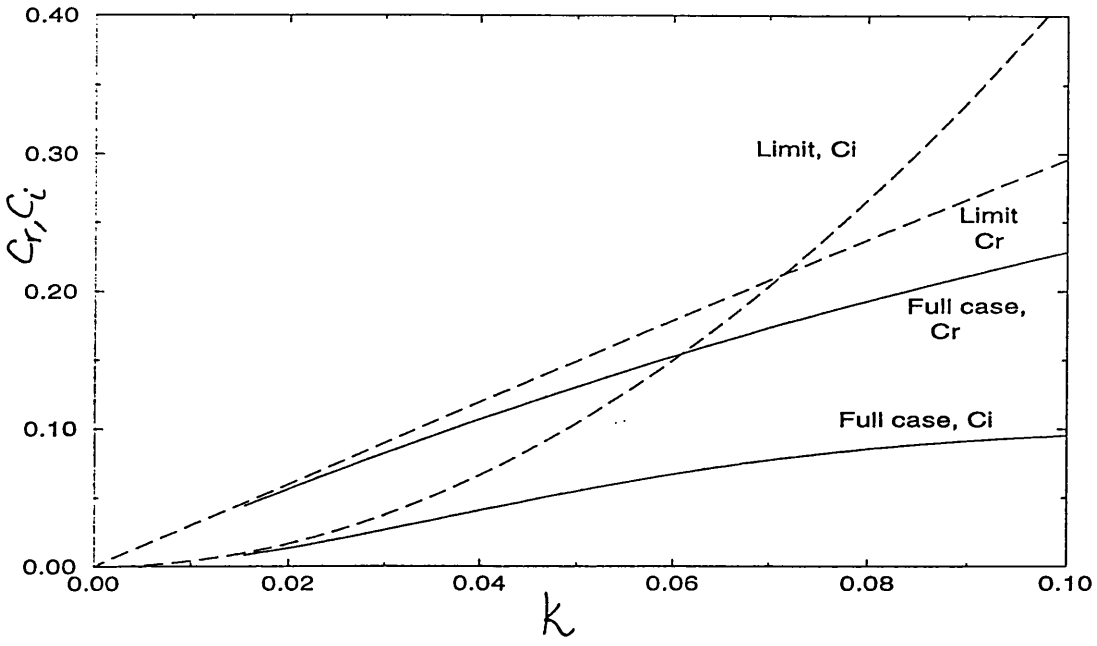

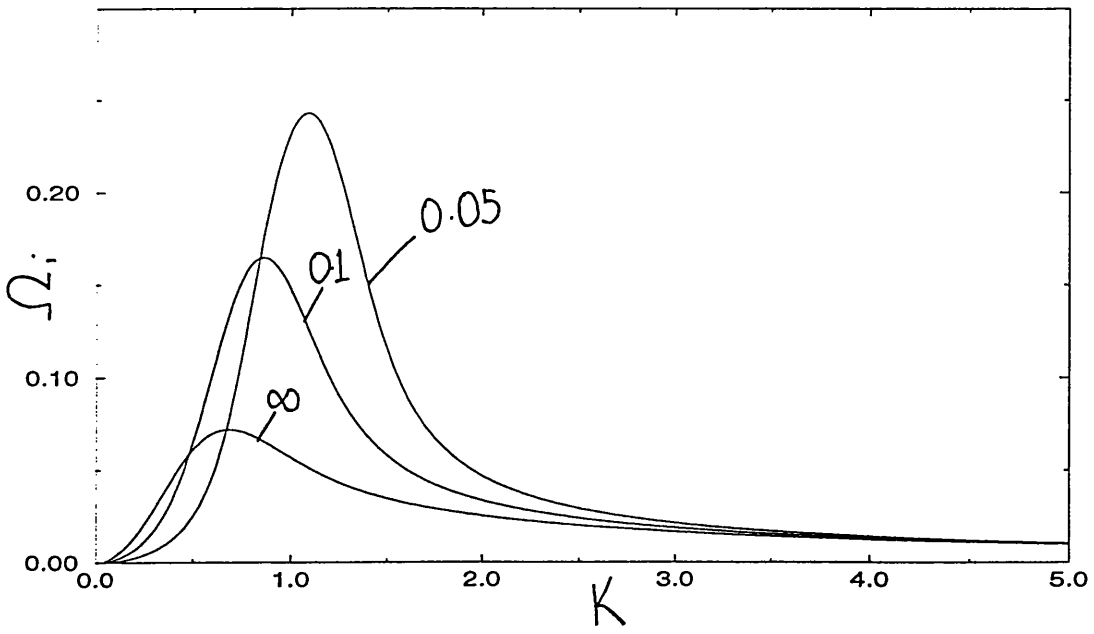

Figure 5:4. Comparison of the complex phase speed $c = \omega/k = c_r + ic_i$ versus the wavenumber k, calculated from (5.2.11), (5.2.26) and (5.2.27), with the limit formula (5.4.1.4), (5.4.1.18), (5.4.1.30) for $\bar{a} = 5, \mu_0^- = 1.0, \rho^- = 2.0, \gamma_{st} = \gamma = 0, Fr = \infty$.

Figure 5:5. The numerical solution of (5.5.13), with $\tilde{a} = 1, \rho^- = 2.0$. The growth rate Ω_i plotted against K, (a) $\tilde{\gamma} = 0, \bar{\mu}_0^- = 1$ for various $\tilde{Fr}$,

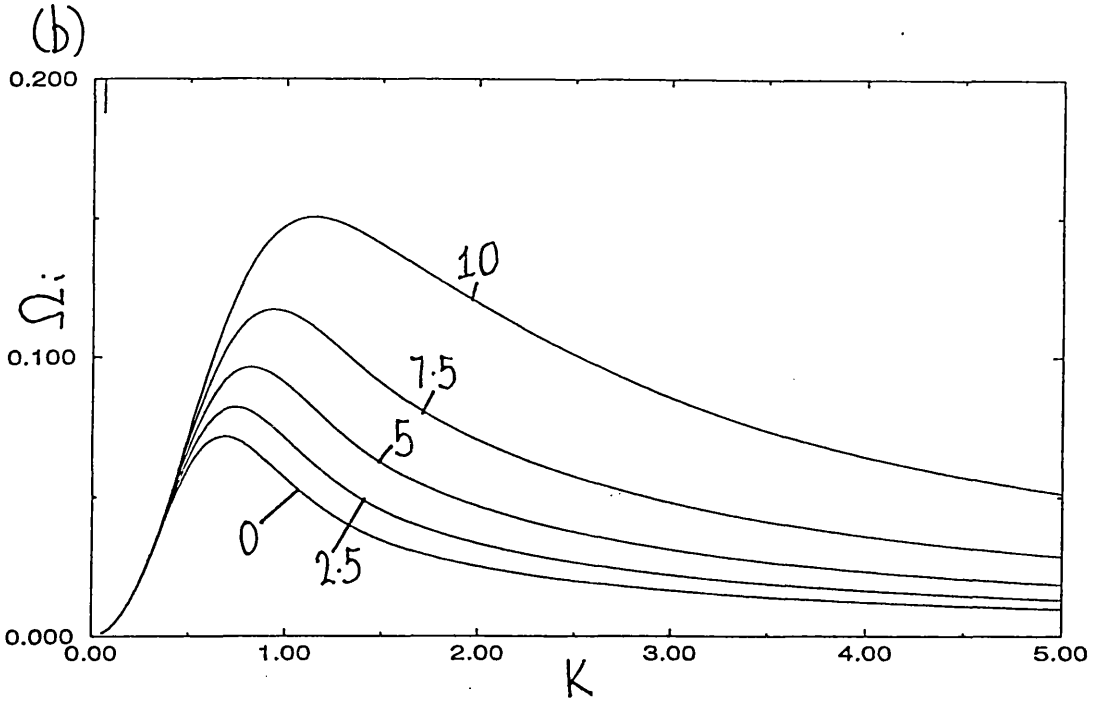

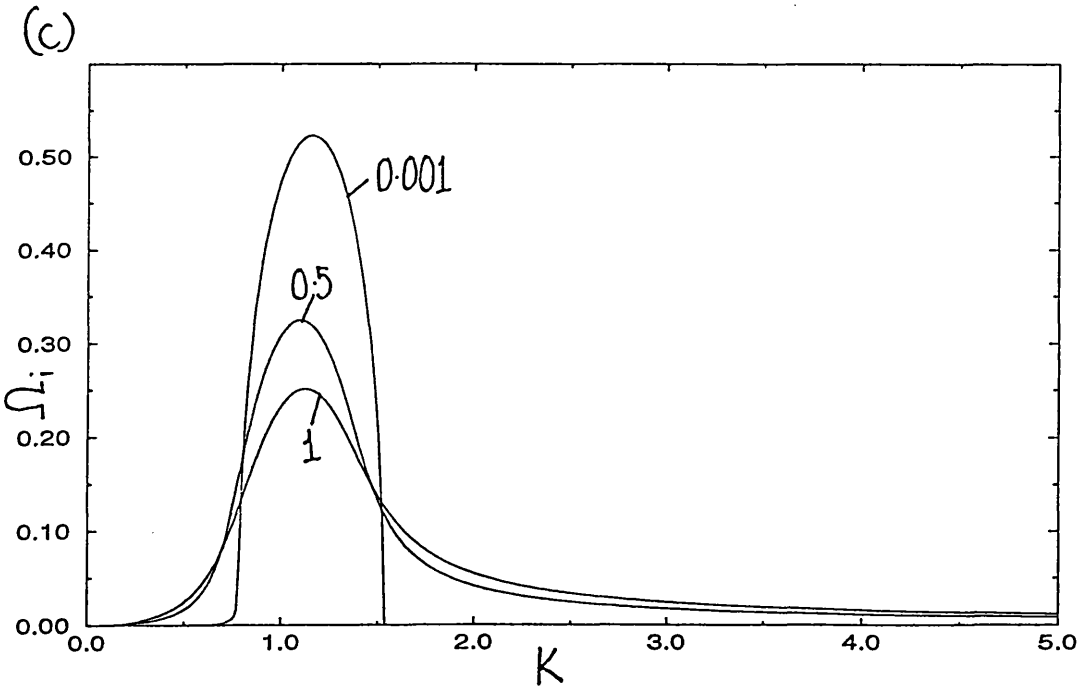

Figure 5:5. As before, (b) $\tilde{Fr} = \infty$, $\bar{\mu}_0^- = 1$, various $\tilde{\gamma}$

(c) as before, $\tilde{Fr} = 0.05$, $\tilde{\gamma} = 1$, various $\bar{\mu}_0^-$.

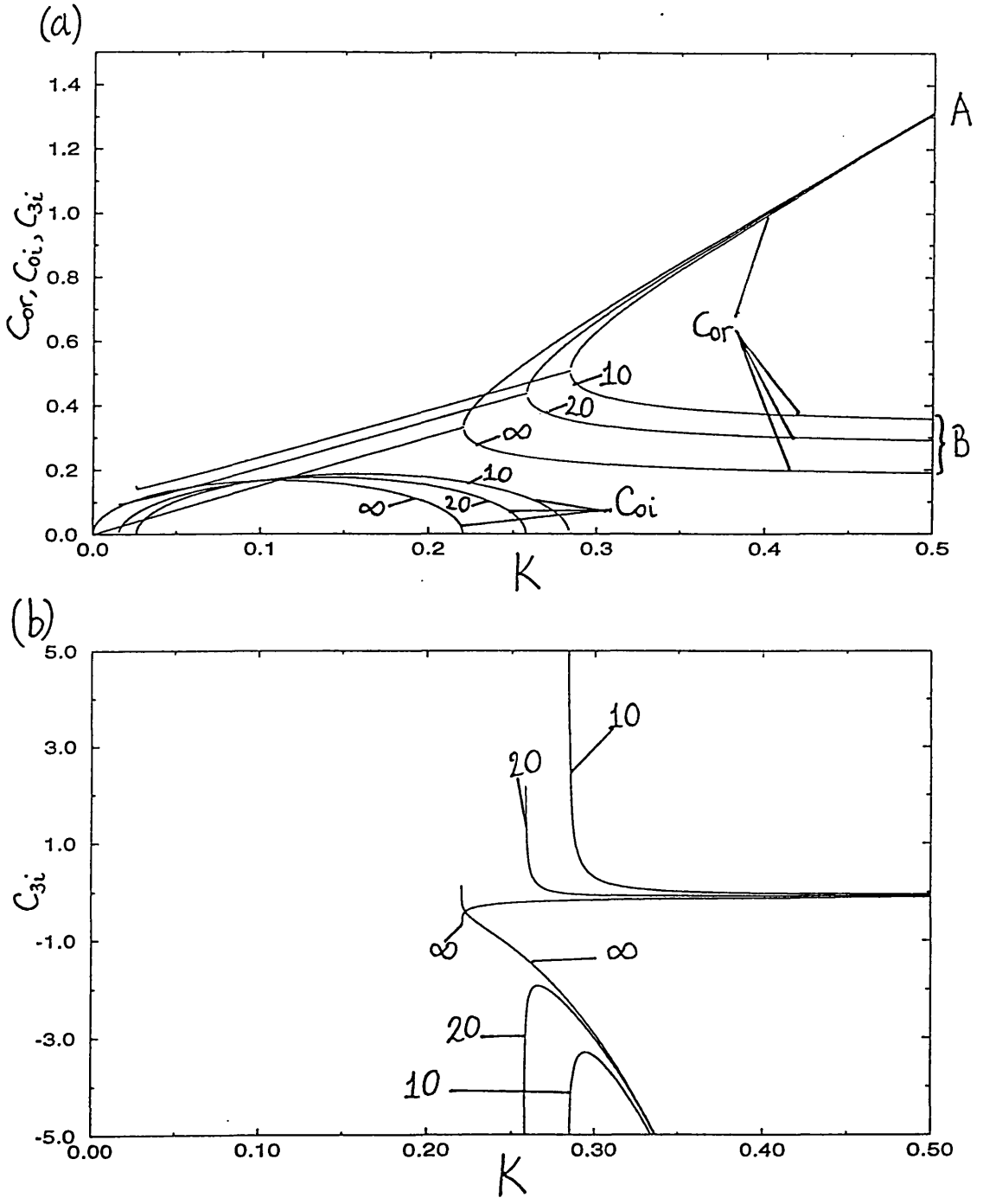

Figure 5:6. Numerical values for the complex phase speed components c_{0r}, c_{0i}, c_{3i}, with $\tilde{\mu}_0^- = .1, \rho^- = 2, \tilde{a} = 1, \tilde{\gamma} = 0$ given by (5.5.34), (5.5.37). Letters A, B denote the Benjamin-Landahl wave class; (a) c_0 against wavenumber K varying $\tilde{Fr}$ (b) c_{3i} against wavenumber K varying $\tilde{Fr}$,

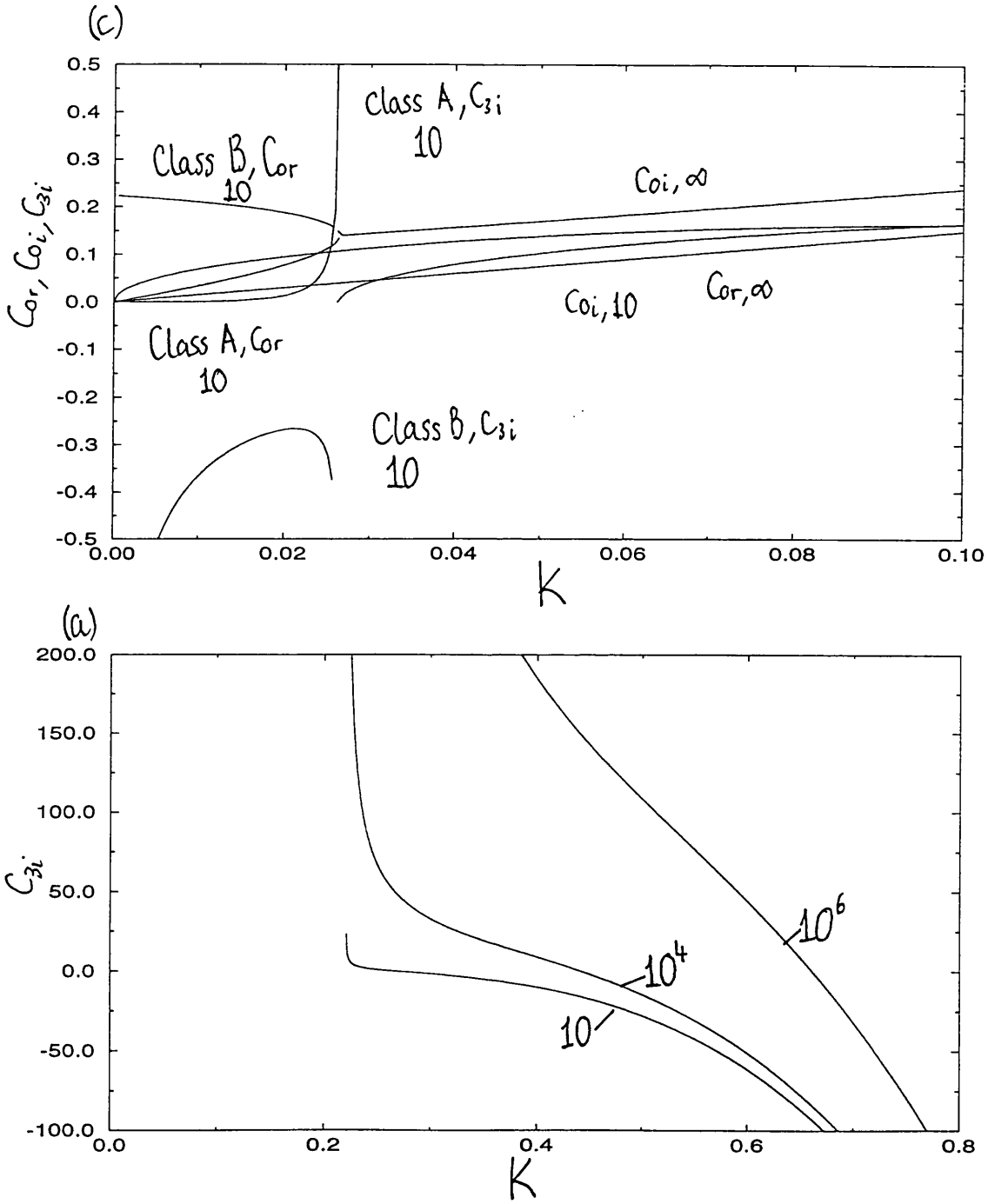

Figure 5:6. As before, (c) c_{3i}, c_{0r}, c_{0i} against wavenumber K, with varying $\tilde{F}r$.

Figure 5:7. Numerical values for the complex phase speed component c_{3i}, plotted against wavenumber K, with $\rho^- = 2$, $\tilde{a} = 1$. (a) Class A wave, $\tilde{\gamma} = 0$, $\tilde{F}r = \infty$ various $\tilde{\mu}$.

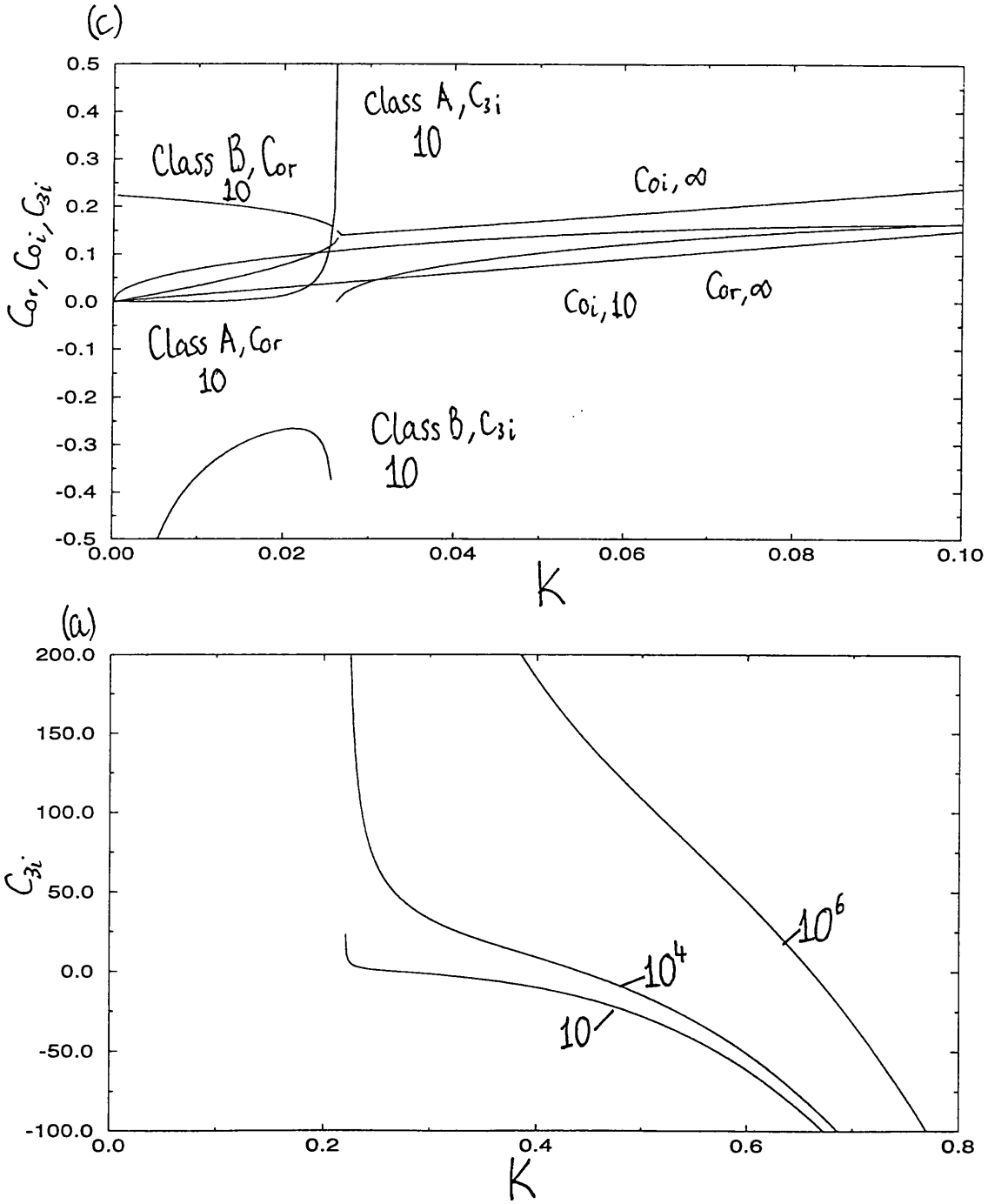

Figure 5:6. As before, (c) c_{3i}, c_{0r}, c_{0i} against wavenumber K, with varying $\tilde{F}r$.

Figure 5:7. Numerical values for the complex phase speed component c_{3i}, plotted against wavenumber K, with $\rho^- = 2$, $\tilde{a} = 1$. (a) Class A wave, $\tilde{\gamma} = 0$, $\tilde{F}r = \infty$ various $\tilde{\mu}$.

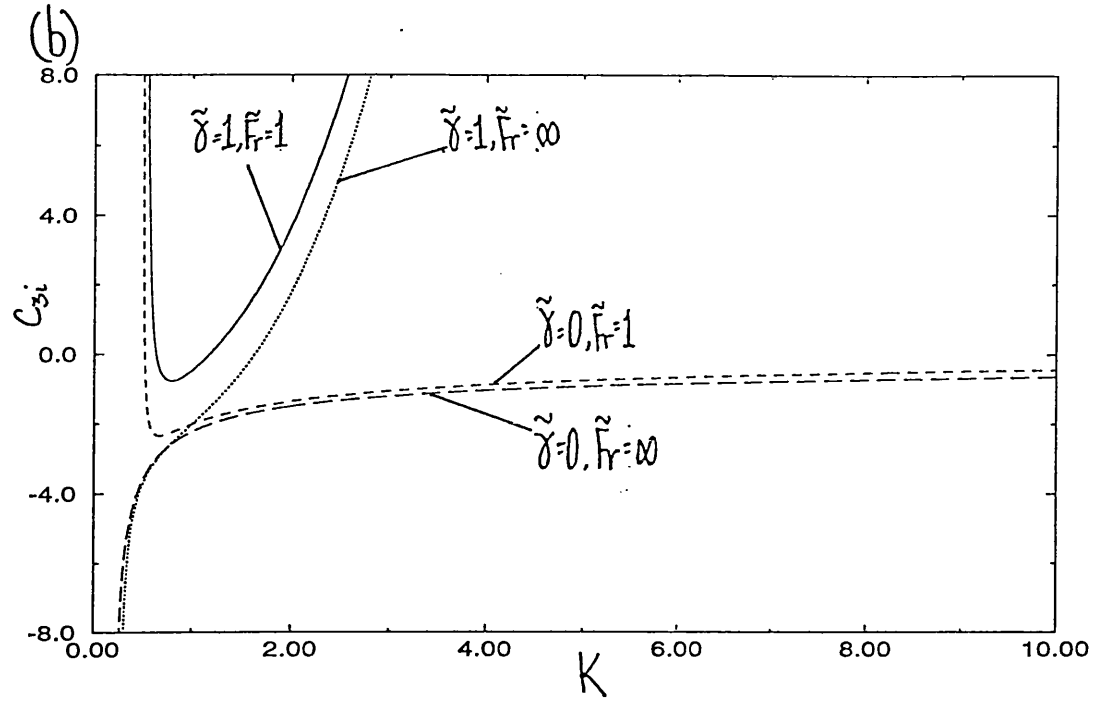

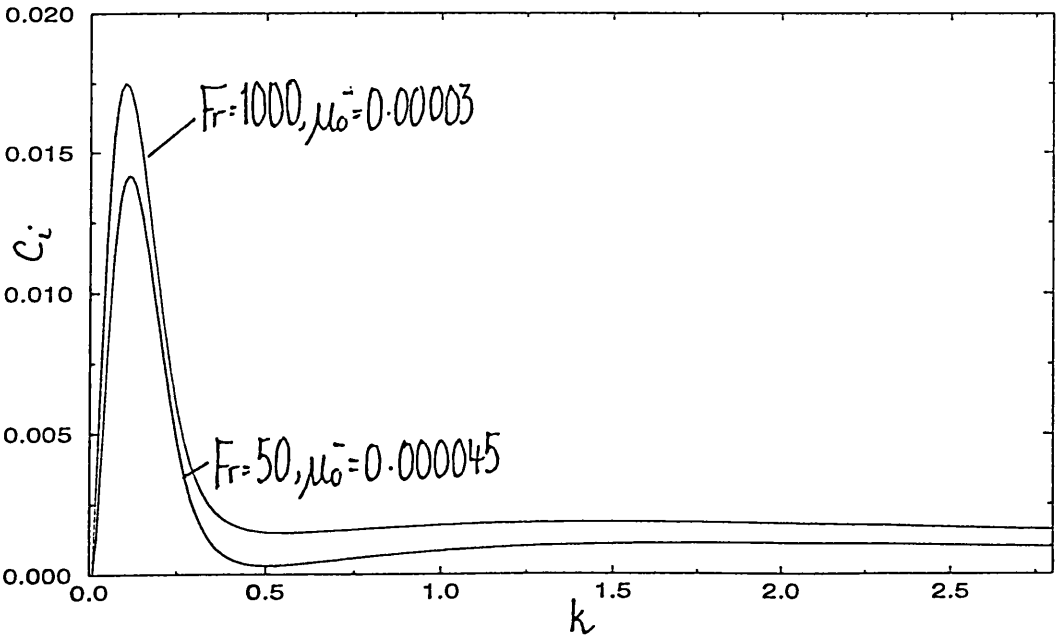

Figure 5:7. As before, (b) Class B waves, $\tilde{\mu} = 100$, various $\tilde{\gamma}$, $\tilde{Fr}$.

Figure 5:8. The full Rayleigh problem with $U_0^+ = 1 - \exp[-\bar{y}]$. Unstable eigenvalues of (5.2.11), (5.2.26) and (5.2.27), with growth rate $c_i = \omega_i/k$ versus wavenumber k for $\rho^- = 2.0$, $\gamma_{st} = 0$, $\bar{a} = 0.1$, for various Fr, μ_0^-.

Chapter 6

Conclusions

To conclude this Thesis we summarize here the new results obtained in Chapters 2-5.

First and foremost we showed in Chapter 2 that a two shear profile was indeed a valid initial approximation for triple-deck studies of two-fluid flow when the film lies completely within the viscous sublayer. We then went on to investigate the stability properties of two-fluid flow over an elongated obstacle and found that the presence of a thin film greatly enhanced inviscid instability. The discontinuity in material properties at the interface was seen to provide an important mechanism for instability. A study of the condensed flow problem, for short obstacles, then allowed us to calculate separated profiles for two fluid flow and we showed that the presence of a film could retard or enhance flow separation, depending on the film thickness and the ratio of film and boundary layer fluid viscosities and densities.

In Chapter 3 we derived wave-amplitude equations governing the resonant interaction of two pairs of oblique waves traveling with the same phase speed and their interaction with a three-dimensional vortex which develops in a unidirectional piecewise shear flow. The wave-amplitude equations were found to reduce to those of Smith, Brown & Brown (1993) in the non-resonant limit. We showed that the presence of this second pair of waves could lead to finite-distance wave-amplitude blow-up, which may lead to stronger nonlinear regimes or to transition.

The linear stability study of Tollmien-Schlichting disturbances in film flows by Timoshin (1997) was extended to cover weakly-nonlinear temporal TS instabilities. The governing wave-amplitude equation was derived along with equations for strong Reynolds-stress induced mean flow in the interfacial layers. The stability properties of the altered base profile to secondary disturbances were examined within these layers and Rayleigh instability was found. In the absence of such background disturbances it was found that, for a particular combination of the surface tension, gravity, film thickness and density ratios, a resonance could take place which was attributed to the interaction of growing TS modes and decaying capillary modes. Analysis of the wave-amplitude equation showed non-linear effects forcing a saturation in magnitude of the disturbances. The disparate natures of the two regimes were connected via two intermediate regimes and a smooth analytic transition between the regimes confirmed the expansion structures.

In the final chapter we studied the instability of disturbances of a comparable wavelength to the lower layer thickness in flow on a very viscous film. We showed that disturbances previously categorized distinctly, namely the Class A, Class B and KH modes in the Benjamin-Landahl classification, exist as special limiting cases of our general formulation. Investigation of the thin film case revealed the presence of a similar resonance mechanism to that of Chapter 4.

6.1 Bibliography

ANDREUSSI P., ASALI, J.C. & HANRATTY, T.J. 1985 Initiation of roll waves in gas-liquid flows.*AIchE J.* **31**, 119-126.

AKYLAS, T.R. 1982 A nonlinear theory for the generation of water waves by wind. *Stud. Appl. Math.* **67**, 1-24.

AKYLAS, T.R. & BENNEY, D.J. 1982 The evolution of waves near direct resonance conditions. *Stud. Appl. Math.* **67**, 107-123.

BAINES, P.G. & MITSUDERA, H. 1994 On the mechanism of shear flow instabilities. *J. Fluid Mech.* **276** , 327-342.

BAINES, P.G., MAHJUMDAR, S.J. & MITSUDERA, H. 1996 The mechanics of the Tollmien-Schlichting wave. *J. Fluid Mech.* **312**, 107-124.

BENJAMIN, T. BROOKE 1960 Effects of a flexible boundary on hydrodynamic stability. *J. Fluid Mech.* 9, 513.

BENJAMIN, T. BROOKE 1963 The threefold classification of unstable disturbances in flexible surface bounding inviscid flows. *J. Fluid Mech.* **16**, 436-450.

BLACKABY, N.D. 1991 On viscous, inviscid and centrifugal instability mechanisms in compressible boundary layers, including non-linear vortex/wave interactions and the effects of large Mach number on transition. *Ph. D Thesis, University of London.*

BODONYI, R.J., SMITH, F.T. 1985 On the short-scale inviscid instabilities in flow past surface-mounted obstacles and other non-parallel motions. *Aero. J.* June/July, 205-212

BOWLES, R.I., CAPORN, P.A., TIMOSHIN, S.N. 1998 Nonlinear short-wave Tollmein-Schlichting instability in a boundary layer on a film-coated wall. *Proc. Roy. Soc.* To appear.

BROWN P.G., BROWN S.N., SMITH F.T., TIMOSHIN S.N. 1993 On the starting process of strongly nonlinear vortex/Rayleigh wave interactions, *Mathematika* **40**, 7-29.

BROWN, P.G. 1993 High Reynolds number vortex flows: Vortex/Rayleigh wave interaction and the compressible leading-edge vortex. *Ph. D. Thesis, University of London.*

BROTHERTON-RATCLIFFE, R.V. 1986 Boundary-layer effects in liquid layer flows. *Ph. D. Thesis, University of London.*

CAIRNS, R.A. 1979 The role of negative energy waves in some instabilities of parallel flows. *J. Fluid Mech.* **92**, 15-33.

CHARLES, M.E., LILLELEHT, L.U. 1965 An experimental investigation of stability and interfacial waves in co-current flow of two liquids. *J. Fluid Mech.* **22**, 217-224.

CRAIK, A.D.D. & ADAMS, J.A. 1979 'Explosive' resonant wave interactions in a three layer fluid flow. *J. Fluid Mech.* **92**, 1-14.

CRAIK, A.D.D. 1981 The drift velocity of water waves. *J. Fluid Mech.* **116**, 187-205.

COWARD, A.V., HALL, P. 1996 The stability of two-phase flow over a swept wing. *J. Fluid Mech.* **329**, 247-273.

COWLEY, S.J.,& WU, X. 1993 Asymptotic approaches to transition modelling. *AGARD Rep.* 793.

DANGELMAYR, G. & KNOBLOCH, E. 1987 The Takens-Bogdanov bifurcation with O(2)-symmetry. *Phil. Trans. R. Soc. Lond. A* **322**, 243-279.

DIMAS, A.A. & TRIANTAFYLLOU, G.S. 1994 Nonlinear interaction of shear flow with a surface. *J. Fluid Mech.* **260**, 211-246.

DORE, B.D. 1970 Mass transport in layered fluid systems. *J. Fluid Mech.* **40**, 113-126.

DORE, B.D. 1976 Double boundary layers in standing interfacial waves. *J. Fluid Mech.* **76**, 819-828.

DORE, B.D. 1977 On mass transport velocity due to progressive wave. *Quart. J. Mech. Appl. Math.*, **30**, 157-173.

DRAZIN, P.G. 1970 Kelvin-Helmholtz instability of finite amplitude. *J. Fluid Mech.* **42**, 321-335.

DRAZIN, P.G., & REID, W.H. 1981 Hydrodynamic stability. *Cambridge Uni. Press.*

ELLIOT, J.W., SMITH, F.T., & COWLEY, S.J. 1983 Breakdown of boundary layers (i) on moving surfaces; (ii) in semi-similar unsteady flow; (iii) in fully unsteady flow. *Geophys. Astrophys. Fluid Dyn.* **25**, 77-138.

FELDMAN, S. 1957 On the hydrodynamic stability of two viscous incompressible fluids in parallel uniform shearing motion. *J. Fluid Mech.* **2**, 343-370.

GOLDSTEIN, S. 1930 Concerning some solutions of the boundary layer equations in hydrodynamics. *Proc. Cam. Phil. Soc.* **26**, 1-30.

GOLDSTEIN, S. 1948 On laminar boundary-layer flow near a position of separation. *Phil. Trans. R. Soc. Lond. A* **333**, 343-378.

GUCKENHEIMER, J. & KNOBLOCH, E. 1983 Nonlinear convection in a rotating

layer: Amplitude expansions and normal forms. *Geophys. Astrophys. Fluid Dynamics* **23**, 247-272.

HALL, P. & SMITH, F.T. 1988 The nonlinear interaction of Tollmien Schlichting waves and Taylor-Görtler vortices in curved channel flows. *Proc. Roy. Soc. Lond.* **A417**, 255-282.

HALL, P. & SMITH, F.T. 1989 Nonlinear Tollmien-Schlichting wave/vortex interaction in boundary layers. *Eur. J. Mech.* **8**, 179-205.

HALL, P. & SMITH, F.T. 1990 Theory on instability and transition. *Proc. ICASE workshop on instability and transition Vol II, edited by M. Y. Hussiani and R.G. Voigt*, 5-39.

HALL, P., SMITH, F.T. 1991 On strongly nonlinear vortex/ wave interactions in boundary-layer transition. *J. Fluid Mech.*, **227**, 641-666.

HALL, P. 1991 Görtler vortices in growing boundary layers: The leading-edge receptivity problem, linear growth and the nonlinear breakdown stage. *Mathematika* **37**, 151-189.

HANRATTY, T.J. & ENGEN, J.M. 1957 Interaction between a turbulent air stream and a moving water surface. *AIChE J.* **3**, 299-304.

HOOPER, A.P. & BOYD, W.G.C. 1986 Shear-flow instability due to a wall and a viscosity discontinuity at the interface. *J. Fluid Mech.* **179**, 201-225.

ITOH, N. 1974 Spatial growth of finite wave disturbances in parallel and nearly parallel flows. Part 2, The numerical results for the flat plate boundary layer. *Trans. Japan Soc. Aero. Space Sci.* **17**, 175-86.

KAO, T.W. & PARK, C. 1972 Experimental investigations of the stability of channel flows. Part 2. Two-layered co-current flow in a rectangular channel. *J. Fluid Mech.* **52**, 401-423.

LANDAHL, M.T. 1962 On the stability of a laminar incompressible boundary layer over a flexible surface. *J. Fluid. Mech.* **13**, 609-632.

LANDAU, L.D. & LIFSHITZ, E.M. 1959 Fluid mechanics. Pergamon Press.

LIN, C.C. 1955 The theory of hydrodynamic stability. *Cambridge Uni. Press.*

LOCK, R.C. 1954 Hydrodynamic stability of flow in the laminar boundary layer

between parallel streams. *Proc. Camb. Phil. Soc.* **50**, 105-124.

LONGUET-HIGGINS, M.S., 1953 Mass transport in water waves. *Phil. Trans. R. Soc. Lond. A* **245**, 535-581.

LUDWIEG, H. & HORNUNG, H. 1989 The instability of a liquid film on a wall exposed to an air flow. *J. Fluid Mech.* **200**,217-233.

MESSITER, A.F. 1970 Boundary layer flow near the trailing edge of a flat plate. *SIAM J. Appl. Math.* **18**, 241-257.

MESSITER, A.F. 1975 Laminar separation-a local asymptotic flow description for constant pressure downstream. *AGARD Conf. Proc. Nº 168, Flow separation paper 4.*

MESSITER, A.F. 1979 Boundary layer separation. *Proc. 8th U.S. Navy. Appl. Math. Congr.*, Los Angeles, California, U.S.A.

MILES, J.W. 1957 On the generation of surface waves by shear flows. *J. Fluid Mech.* **3**, 185-204.

MILES, J.W. 1959 On the generation of surface waves by shear flows. Part 2. *J. Fluid Mech.* **6**, 568-582.

MILES, J.W. 1960 The hydrodynamic stability of a thin film of liquid in uniform shearing motion. *J. Fluid. Mech.* **8**, 593-610.

MILES, J.W. 1962 On the generation of surface waves by shear flows. Part 4. *J. Fluid Mech.* **13**, 433-448.

MORLAND, L.C., SAFFMAN, P.G. & YUEN, H.C. 1991 Waves generated by shear layer instabilities. *Proc. Roy. Soc. Lond. A* **433**, 441-450.

MORLAND, L.C. & SAFFMAN, P.G. 1993 Effect of wind profile on the instability of wind blowing over water. *J. Fluid Mech.* **252**, 383-398

NEILAND, V. Y. 1969 Towards a theory of separation of the laminar boundary layer in a supersonic stream. *Izv. Akad. Nauk. SSSR, Mehk. Zhidk. i Gaza* **4**.

NELSON, J.J, ALVING, A.E. & JOSEPH, D.D. 1995 Boundary layer flow of air over water on a flat plate. *J. Fluid Mech.* **284**, 159-169.

POULIQUEN, O., CHOMAZ, J.M. & HUERRE, P. 1994 Propagating Holmboe waves at the interface between two immiscible fluid. *J. Fluid Mech.* **266**, 277-302.

REYHNER, T.A. & FLÜUGGE-LOTZ, I. 1968 *Int. J. Nonlinear Mech.* **3**, 173.

RILEY, N. 1965 Oscillating viscous flows. *Mathematika* **12**, 161-175.

RUBAN, A.I. 1981 Singular solution of the boundary-layer equations which can be extended continuously through the point of zero surface tension. *Izv. Akad. Nauk. SSSR, Mehk. Zhidk. i Gaza* 6, 42-52.

RUBAN, A.I. 1982 Asymptotic theory of short separation regions on the leading edge of a slender airfoil. *Izv. Akad. Nauk. SSSR, Mehk. Zhidk. i Gaza* **1**, 42-51.

SEDDOUGUI, S.O. & BASSOM, A.P. 1991 On the instability of Görtler vortices to nonlinear travelling waves. *IMA Journal of Applied Mathematics* **46**, 269-296.

SHRIRA, V.I. 1993 Surface waves on shear currents: solution of the boundary-value problem. *J. Fluid Mech.* **252**, 565-584.

SMITH, F.T. 1977 The laminar separation of an incompressible fluid streaming past a smooth surface. *Proc. Roy. Soc. Lond. A* **356**, 433-463.

SMITH, F.T. 1979a On the non-parallel flow stability of the Blasius boundary layer. *Proc. Roy. Soc. Lond. A* **366**, 91-109.

SMITH, F.T., 1979b, Nonlinear stability of boundary layers for disturbances of various sizes. *Proc. Roy. Soc. Lond. A* **368**, 573-589. (and corrections 1980 *A* **371**, 439.)

SMITH F.T., & DANIELS, P.G. 1981 Removal of Goldstein's singularity at separation in the flow past obstacles in wall layers *J. Fluid Mech.* **110**, 1-37.

SMITH, F.T., BRIGHTON, P.W.M., JACKSON, P.S. & HUNT, J.C.R. 1981 On boundary layer flow past two-dimensional obstacles. *J. Fluid Mech.* **113**, 123-152.

SMITH, F.T. 1982 On the high Reynolds number theory of laminar flows. *IMA Journal of Applied Mathematics* **28**, 207-281.

SMITH, F.T., BURGGRAF, O.R. 1985 On the development of large-sized short-scale disturbances in boundary layers. *Proc. Roy. Soc. Lond. A* **399**, 25-55.

SMITH, F.T. 1986 Two-dimensional disturbance travel, growth and spreading in boundary layers. *J. Fluid Mech.* **169**, 353-377.

SMITH F.T., & WALTON, A.G. 1989 Nonlinear interaction of near-planar TS waves and longitudinal vortices in boundary layer transition. *Mathematika* **36**, 262-289.

SMITH, F.T. & BLENNERHASSETT, P. 1992 Nonlinear interaction of oblique three-dimensional Tollmien-Schlichting waves and longitudinal vortices in channel flows and boundary layers. *Proc. Roy. Soc. Lond. A 436*, 585.

SMITH, F.T. 1993 Theoretical aspects of transition and turbulence in boundary layers. *AIAA Journal* **31**, N°12, 2220-2226.

SMITH, F.T., BROWN, S.N., BROWN, P.G. 1993 Initiation of three dimensional transition paths from an inflexional profile. *Eur. J. Mech., B/Fluids* **12**, N°4, 447-473.

SMITH, F.T. 1996 Weak and strong nonlinearity in boundary layer transition. *Nonlinear mathematics and its applications edited by Philip J Aston*

STEWARTSON, K. & WILLIAMS, P.G. 1969 Self-induced separation. *Proc. R. Soc. Lond. A* **312**, 181-206.

STEWARTSON, K. 1970 Is the singularity at separation removable? *J. Fluid Mech.* 44, 347-364.

STEWARTSON, K., SMITH, F.T. & KAUPS, K. 1982 Marginal separation. *Stud. Appl. Maths* **67**, 45-61.

STUART, J.T. 1960 On the nonlinear mechanics of wave disturbances in stable and unstable parallel flows. Part 1. The basic behaviour in plane Poiseuille flow. *J. Fluid. Mech.* **9**, 353-370.

STUART, J.T. 1966 Double boundary layers in oscillating viscous flow. *J. Fluid Mech.* **24**, 673-687.

SYCHEV, V.V. 1972 On laminar separation. *Izv. Akad. Nauk. SSSR, Mehk. Zhidk. i Gaza* **3**, 47. Translated in *Fluid Mechanics* 407-419. Plenum Pub. Corp. 1974.

SYCHEV, V.V. 1980 On certain singularities in solutions of the equations of boundary layers on a moving surface. *Prikl. Matem. Mekh.* 44, 831-838.

TIMOSHIN, S.N. 1996 Concerning marginal singularities in the boundary-layer flow on a downstream-moving surface. *J Fluid Mech.* **308**, 171-194.

TIMOSHIN, S.N. & SMITH, F.T. 1997 Vortex/inflexional-wave interactions with weakly. three-dimensional input *J. Fluid Mech.* **248**, 247-294.

TIMOSHIN, S.N. 1997 Instabilities in a high-Reynolds-number boundary layer on

a film-coated surface. *J. Fluid Mech.* **353**, 163-195.

TSAO, J.C. ROTHMAYER, A.P. & RUBAN A.I. 1996 Stability of air flow past thin liquid films on airfoils. *AIAA Paper 96-2155.*

TUTTY, O.R., COWLEY S.J. 1986 On the stability and the numerical solution of the unsteady interactive boundary-layer equation. *J. Fluid Mech.* **168**, 431-456.

VAN DUIN, C.A. 1996 An asymptotic theory for the generation of nonlinear surface gravity waves by turbulent air flow. *J. Fluid Mech.* **320**, 287-304.

VAN DOMMELEN, L.L. & SHEN, S.F. 1982 The genesis of separation. *Numerical Methods and Physical Aspects of Aerodynamic Flows (ed. T. Cebeci)*, 293-311. Springer-Verlag.

WALTON, A.G. & SMITH, F.T. 1992 Properties of strongly nonlinear vortex/Tollmien Schlichting wave interactions *J. Fluid Mech.* **244**, 649-676.

WATSON, J. 1960 On the nonlinear mechanics of wave disturbances in stable and unstable parallel flows. Part 2. The development of a solution for plane Poiseuille flow and for plane Couette flow. *J. Fluid Mech.* **9**, 371-389.

WEISSMAN, M.A. 1979 Nonlinear wave packets in the Kelvin-Helmholtz instability **290. A 1377**, 639-681.